Report No. FAA-RD-74-119, II

ILS GLIDE SLOPE STANDARDS

Part II: Validation of Proposed Flight Inspection Filter Systems and Responses of Simulated Aircraft on Coupled Approaches

Lee Gregor Hofmann
John J. Shanahan
Dunstan Graham

October 1975
Final Report

Document is available to the public through the National Technical Information Service, Springfield, Virginia 22161.

Prepared for

U.S. DEPARTMENT OF TRANSPORTATION
FEDERAL AVIATION ADMINISTRATION
Systems Research & Development Service
Washington, D.C. 20590

NOTICE

This document is disseminated under the sponsorship of the Department of Transportation in the interest of information exchange. The United States Government assumes no liability for its contents or use thereof.

(12) 254 p.

(18) (19)

Technical Report Documentation Page

1. Report No.	2. Government Accession No.	3. Recipient's Catalog No.
FAA-RD-74-119-II		(11)

4. Title and Subtitle (6)

ILS GLIDE SLOPE STANDARDS. PART II: VALIDATION OF PROPOSED FLIGHT INSPECTION FILTER SYSTEMS, AND RESPONSES OF SIMULATED AIRCRAFT ON COUPLED APPROACHES.

5. Report Date: Oct 1975

6. Performing Organization Code: (14)

7. Author(s) (10)

Lee Gregor Hofmann, John J. Shanahan, Dunstan Graham

8. Performing Organization Report No.: SYT-TR-1043-1-II

9. Performing Organization Name and Address

Systems Technology, Inc.
13766 South Hawthorne Boulevard
Hawthorne, California 90250

10. Work Unit No. (TRAIS): 071-313-013

11. Contract or Grant No.: (15) DOT-FA74WA-3340

12. Sponsoring Agency Name and Address

Federal Aviation Administration
Systems Research and Development Service
800 Independence Avenue, S. W.
Washington, D. C. 20591

13. Type of Report and Period Covered: Final, Phase II, [redacted], 10/29/74 to 9/29/75

14. Sponsoring Agency Code: FAA/ARD-322

15. Supplementary Notes (9)

Final report. 29 Oct 74 - 29 Sep 75 on Phase 2, [redacted]

16. Abstract

This report contains the data base for validation of the longitudinal approach and landing models used in Phase I of Contract No. DOT-FA74WA-3340. The simulation models include: Convair 880 in combination with the Lear Siegler, Inc. (LSI) Automatic Landing System, an inertially augmented version of the LSI System, or a manual flight director version of the LSI System; and Piper PA-30 with an inverted coupler and autothrottle system. Simplified simulation models include an aircraft with perfect pitch attitude and airspeed control and a proportional coupler model (Filter System No. 1) and an aircraft with perfect rate-of-climb and airspeed control and a proportional-plus-integral coupler model (Filter System No. 2). The first four models cover a range of aircraft and Glide Slope coupling techniques. The latter two models represent the dynamics of the aircraft-coupler system in a highly simplified way which is useful for estimating indicated and actual glide path deviation and actual glide path deviation rate responses to glide slope "bends" or structure.

The simulation models' responses to 9 prototype Glide Slope faults (steps, sinusoids, and specially configured waveforms) and to actual flight inspection differential trace records for 16 ILS Glide Slope facilities are documented. A total of 24 response records for selected simulation models in response to all Glide Slope inputs, and all simulation models in response to selected Glide Slope inputs are given. In addition, 8 response records document response standard deviations which arise because of random wind and wind shear variability from one approach to another and from turbulence. Results show:

- More accurate estimates of indicated and actual glide path deviation and glide path deviation rate are provided by Filter System No. 2 (aircraft with perfect rate-of-climb and airspeed control and proportional-plus-integral coupler model) than by Filter System No. 1.
- There is substantial similarity in the gross nature of the responses for all aircraft and Glide Slope coupling techniques among themselves and with respect to the responses estimated using Filter Systems No. 1 and 2.
- The inertially augmented coupler has substantially attenuated responses to "high" frequency ILS Glide Slope structure for all variables except indicated glide path deviation (as one would expect). This is the principal feature differentiating the aircraft/control system combinations simulated. The inertially augmented coupler also results in a modest reduction in longitudinal touchdown dispersion.
- The simulation techniques reported in Phase I of Contract No. DOT-FA74WA-3340 can be used to predict a typical mean longitudinal touchdown point using flight inspection data for a specific ILS Glide Slope facility and can predict the typical longitudinal dimension of the 2σ touchdown dispersion footprint arising from winds, wind shear and turbulence.
- Disturbances arising from facility-to-facility variability in ILS Glide Slope structure and winds, wind shear and turbulence combine in a synergistic way which causes longitudinal touchdown dispersion for the combination of all disturbances to greatly exceed the root-sum-square dispersions for each disturbance acting separately.
- The 2σ tolerances (developed in Phase I of Contract No. DOT-FA74WA-3340) applied to the corresponding responses of Filter System No. 2 are successful in discriminating against those ILS Glide Slope facilities which produce out-of-specification approaches and landings.

17. Key Words	18. Distribution Statement
Instrumentation Landing System (ILS) Automatic Landing System Flight Control System Flight Inspection Standards	Document is available to the public through the National Technical Information Service, Springfield, Virginia 22161.

19. Security Classif. (of this report)	20. Security Classif. (of this page)	21. No. of Pages	22. Price
Unclassified	Unclassified	252	

Form DOT F 1700.7 (8-72) Reproduction of completed page authorized

340 435

mt

METRIC CONVERSION FACTORS

Approximate Conversions to Metric Measures

Symbol	When You Know	Multiply by	To Find	Symbol
	LENGTH			
in	inches	*2.5	centimeters	cm
ft	feet	30	centimeters	cm
yd	yards	0.9	meters	m
mi	miles	1.6	kilometers	km
	AREA			
in^2	square inches	6.5	square centimeters	cm^2
ft^2	square feet	0.09	square meters	m^2
yd^2	square yards	0.8	square meters	m^2
mi^2	square miles	2.6	square kilometers	km^2
	acres	0.4	hectares	ha
	MASS (weight)			
oz	ounces	28	grams	g
lb	pounds	0.45	kilograms	kg
	short tons (2000 lb)	0.9	tonnes	t
	VOLUME			
tsp	teaspoons	5	milliliters	ml
Tbsp	tablespoons	15	milliliters	ml
fl oz	fluid ounces	30	milliliters	ml
c	cups	0.24	liters	l
pt	pints	0.47	liters	l
qt	quarts	0.96	liters	l
gal	gallons	3.8	liters	l
ft^3	cubic feet	0.03	cubic meters	m^3
yd^3	cubic yards	0.76	cubic meters	m^3
	TEMPERATURE (exact)			
°F	Fahrenheit temperature	5/9 (after subtracting 32)	Celsius temperature	°C

*1 in = 2.54 (exactly). For other exact conversions and more detailed tables, see NBS Misc. Publ. 286, Units of Weights and Measures, Price $2.25, SD Catalog No. C13.10:286.

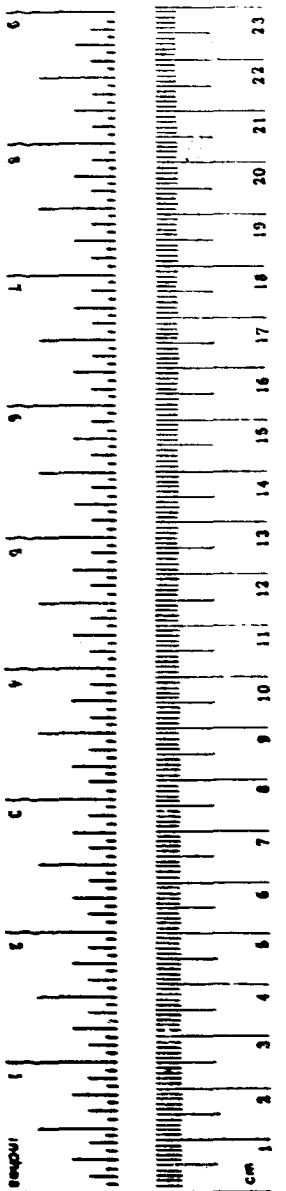

Approximate Conversions from Metric Measures

Symbol	When You Know	Multiply by	To Find	Symbol
	LENGTH			
mm	millimeters	0.04	inches	in
cm	centimeters	0.4	inches	in
m	meters	3.3	feet	ft
m	meters	1.1	yards	yd
km	kilometers	0.6	miles	mi
	AREA			
cm^2	square centimeters	0.16	square inches	in^2
m^2	square meters	1.2	square yards	yd^2
km^2	square kilometers	0.4	square miles	mi^2
ha	hectares (10,000 m^2)	2.5	acres	
	MASS (weight)			
g	grams	0.035	ounces	oz
kg	kilograms	2.2	pounds	lb
t	tonnes (1000 kg)	1.1	short tons	
	VOLUME			
ml	milliliters	0.03	fluid ounces	fl oz
l	liters	2.1	pints	pt
l	liters	1.06	quarts	qt
l	liters	0.26	gallons	gal
m^3	cubic meters	35	cubic feet	ft^3
m^3	cubic meters	1.3	cubic yards	yd^3
	TEMPERATURE (exact)			
°C	Celsius temperature	9/5 (then add 32)	Fahrenheit temperature	°F

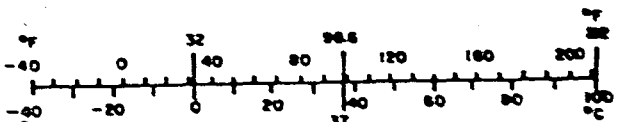

FOREWORD

The research reported here was accomplished for the United States Department of Transportation by Systems Technology, Inc., Hawthorne, California, under Phase II of Contract DOT-FA74WA-3340. The program was sponsored by the Federal Aviation Administration (FAA), Systems Research and Development Service, Washington, D. C.

This research, conducted from December 1974 to April 1975, was accomplished under the general direction of Mr. Dunstan Graham at Systems Technology, Inc. Mr. John F. Hendrickson served as Technical Officer for the FAA. Valuable guidance throughout the course of this research was provided by Messrs. Henry H. Butts, Richard D. Munnikhuysen and John F. Hendrickson of the FAA.

The manuscript was released by the authors in October 1975.

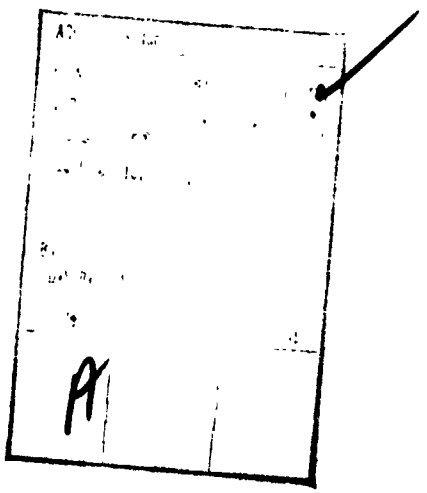

TABLE OF CONTENTS

LIST OF FIGURES

LIST OF TABLES

ABBREVIATIONS, SYMBOLS AND SPECIAL NOTATION

Abbreviations

DDM	Difference in depth of modulation
FAA	Federal Aviation Administration
ICAO	International Civil Aviation Organization
ILS	Instrument Landing System
ILS Point "B"	An imaginary point on the glide path/localizer course measured along the runway centerline extended, in the approach direction, 3500 feet from the runway threshold
ILS Point "C"	A point through which the downward extended straight portion of the glide path (at the commissioned angle) passes at a height of 100 feet above the horizontal plane containing the runway threshold
ILS Approach Zone 3	The distance from Point "B" to Point "C" for evaluations of Category I and Category II training systems. The distance from Point "B" to the runway threshold for evaluations of Category II operational systems
RTT	Radio telemetering theodolite

Symbols

C	Covariance for variables indicated by subscripts
d or D	Actual glide path deviation in linear units (ft)
$\bar{d}_c$ or DCB	Distance between the 0 DDM locus and the straight-line asymptote at the commissioned angle as measured in the vertical plane containing the runway centerline, measured normal to the straight-line asymptote (ft)
d_e or DE	Indicated glide path deviation in linear units (ft)
H	Total altitude of aircraft wheels above GPIP on runway (ft)
$\dot{H}$ or HD	Actual rate of climb (ft/sec)
K_{I_u}	Integral of airspeed error feedback gain in autothrottle (lb/ft)

K_θ'	Pitch attitude gain in autothrottle (lb-thrust/rad)
t or T	Time (sec)
X	Total horizontal displacement of aircraft center of gravity from GPIP on the runway in the direction of the centerline, or longitudinal force applied to aircraft (ft or lb)
δ_e or DEL E	Elevator deflection angle (rad)
δ_T or DEL T	Engine thrust perturbation (lb)
$\bar{\eta}_c$ or ETACB	Differential trace referenced to the ideal 0 DDM locus for the commissioned angle, in angular units (μA)
η_e or ETAE	Indicated glide path deviation in angular units (μA)
η_p or ETAP	Actual glide path deviation from the ideal 0 DDM locus for the commissioned angle in angular units (μA)
$\dot{\eta}_p$ or ETAPD	Actual glide path deviation rate in angular units at fixed range (μA/sec)
θ or THETA	Pitch attitude perturbation (rad)
ρ	Correlation coefficient for variables indicated by subscripts
σ	Denotes one standard deviation in general; may be particulariz by subscript
τ_u	Airspeed low-pass filter time constant (sec)
τ_θ	Pitch attitude low-pass filter time constant (sec)

Special Notation

$E[\cdot]$	Expected value of $[\cdot]$
$(\cdot)_{TD}$	Touchdown-related value of $(\cdot)$
$(\bar{\cdot})$	Denotes mean or expected value of $(\cdot)$
$(\dot{\cdot})$	Derivative with respect to time of $(\cdot)$

SECTION I

INTRODUCTION

The standard aid to low visibility approach and landing in commercial aviation is the Instrument Landing System (ILS). Two radio beams (the "Glide Slope" and the "Localizer") are formed to guide an aircraft on the proper approach glide path and along the extended runway centerline in the landing direction. Part I of this report documents the results of using system simulation and analysis techniques to determine maximum levels for ILS Glide Slope beam structure characteristics which still result in acceptable approach and landing outcomes. These results, in turn, led to recommendations for revision of the flight inspection procedure which is used to assure the accuracy of ILS Glide Slope facility guidance. The recommended procedure proposes that limits be applied to indicated glide path deviation, actual glide path deviation, and actual glide path deviation rate responses for typical aircraft/control system combinations. This is in addition to the current practice of applying limits to the "differential trace" generated in the course of flight inspection. These additional limits would be upon variables which are directly relevant to the approach and landing outcome. This is in distinction to limits placed upon the "differential trace" variable alone since the differential trace relates only indirectly to approach and landing performance. It is proposed that the required responses for "typical aircraft/control system combinations" be generated by a filter system having as its input the "differential trace" signal in the revised flight inspection procedure. The filter system would be part of the airborne flight inspection equipment. The filter system, in effect, is a highly simplified, but representative, simulation of any aircraft executing automatically or manually coupled approaches.

Here in Part II of the report, validation of assumptions and in-depth exercise of the aircraft/control system simulations and filter systems is the central purpose. The objective is to identify the filter system which generates responses most representative of typical aircraft/control system responses, and to provide deterministic response data for the aircraft/control system combinations simulated.

ORGANIZATION OF FILTER SYSTEM AND AIRCRAFT/ CONTROL SYSTEM SIMULATION DATA

The nature of this validation task requires a substantial data base. The required data base is included in this report in the form of numerous computer-drawn plots. The fact that several different types of comparisons must be made precludes organizing the data in a universally suitable way. Therefore an organization which facilitates reference has been chosen.

The data base is organized primarily by type of input (prototype Glide Slope fault or Glide Slope flight inspection record with or without stochastic atmospheric disturbances). The secondary level of organization is by the particular dynamic system generating the responses (the particular proposed flight inspection filter system or aircraft/control system combination simulated).

ORGANIZATION OF THE REPORT

Section II is concerned with selection and validation of a filter system representation of typical aircraft/control system dynamics during coupled approaches.

In Section III, simulated aircraft/control system responses to actual ILS Glide Slope facility flight inspection data are evaluated for acceptability of approach and landing performance. This evaluation is made by examining touchdown sink rate and location, and by examining the responses for exceedances of their critical 2σ levels (developed in Ref. 1) for acceptable approach and landing outcomes. Simulated flight inspections using the filter system concept are used to evaluate the same ILS Glide Slope flight inspection data using the 2σ tolerance levels developed for the recommended revised flight inspection procedure in Ref. 1. Section III also presents a comparison of ILS Glide Slope facility acceptability results as determined by simulated approach and landing and as determined by simulated flight inspection. In addition, touchdown dispersion arising from wind, wind shear and turbulence effects is presented for approaches and landings simulated for several different ILS Glide Slope facilities.

A final section, Section IV, summarizes the principal conclusions derived from this simulation effort.

The filter system and aircraft/control system response plots for the prototype Glide Slope fault inputs are contained in Appendix A, and the response plots for actual ILS Glide Slope flight inspection data inputs are contained in Appendix B.

SECTION II

SELECTION AND VALIDATION OF A FILTER SYSTEM REPRESENTATION OF TYPICAL AIRCRAFT/CONTROL SYSTEM DYNAMICS ON COUPLED APPROACHES

Two filter systems have been proposed in Ref. 1 for the processing of ILS Glide Slope flight inspection data. Filter System No. 1 is a highly simplified simulation of typical aircraft/control system combinations. It assumes perfect pitch attitude and airspeed control, and a proportional control representation of the approach coupler. Figure 1 is a block diagram for Filter System No. 1. The essential dynamic behavior of the aircraft in this simplification is the first-order lag in rate-of-climb response to pitch attitude changes.

Filter System No. 2 is an alternative highly simplified simulation of typical aircraft/control system combinations. It assumes perfect rate-of-climb and airspeed control, and a proportional-plus-integral representation of the approach coupler. Figure 2 is a block diagram for Filter System No. 2. The dynamic behavior of this simplified simulation is independent of all aircraft dynamic characteristics. It depends only upon the coupler dynamic characteristics and kinematic relationships.

The responses of these two filter systems will be compared with the responses of the four simulated aircraft/control system combinations in order to select the one filter system which provides the best general representation of all simulated aircraft/control system combinations. The nature of the response comparison is qualitative. Reproduction of response features without particular regard for magnitude is the main criterion. Differences in response magnitude are calibrated out by the procedure used to evolve the permissible tolerance levels for flight inspection in Ref. 1.

FINAL SELECTION AND VALIDATION OF A FILTER SYSTEM

Table 1 lists figure numbers for comparable responses of the filter systems and aircraft/control system combinations on each line. Actual comparison shows that:

ω_{RC} Typical aircraft rate of climb response bandwidth, 0.2 (rad/sec)

K_o Conversion constant 12,278. (μA/rad)

K_1 Course softening gain function; $K_1 = 1.0$, $H \geq 600$ ft; decreasing linearly to zero at $H = 0$; $K_1 = 0$, $H \leq 0$ ft

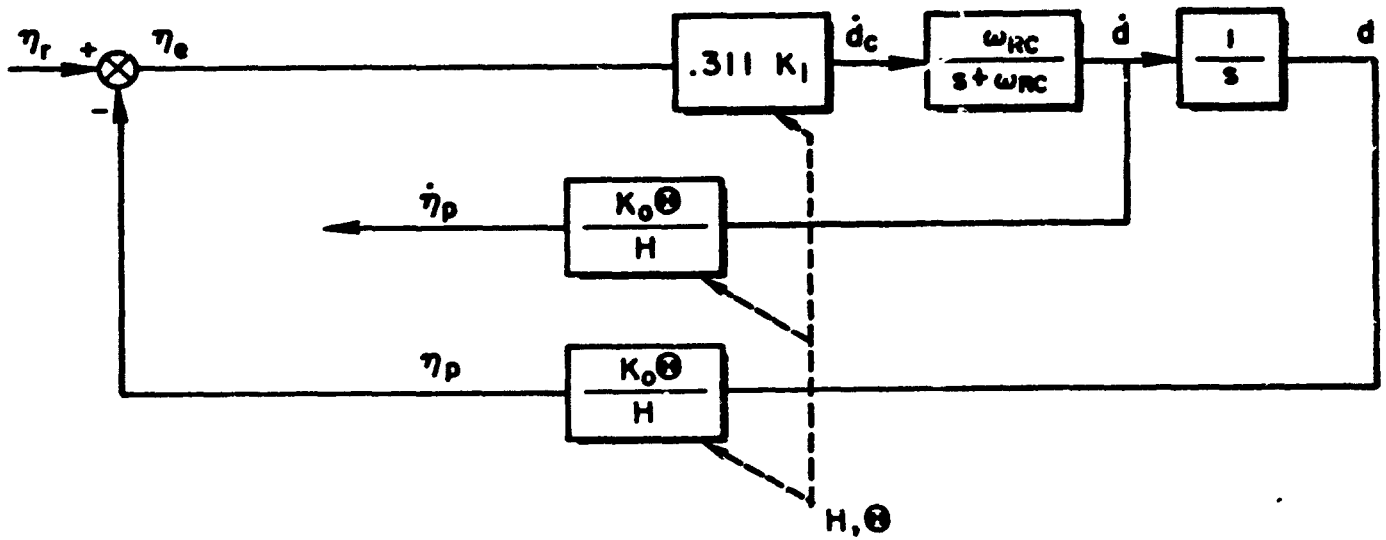

Figure 1. Block Diagram for Filter System Which Generates Typical Aircraft Indicated Deviation and Actual Path Deviation and Actual Path Deviation Rate Responses (Filter System No. 1)

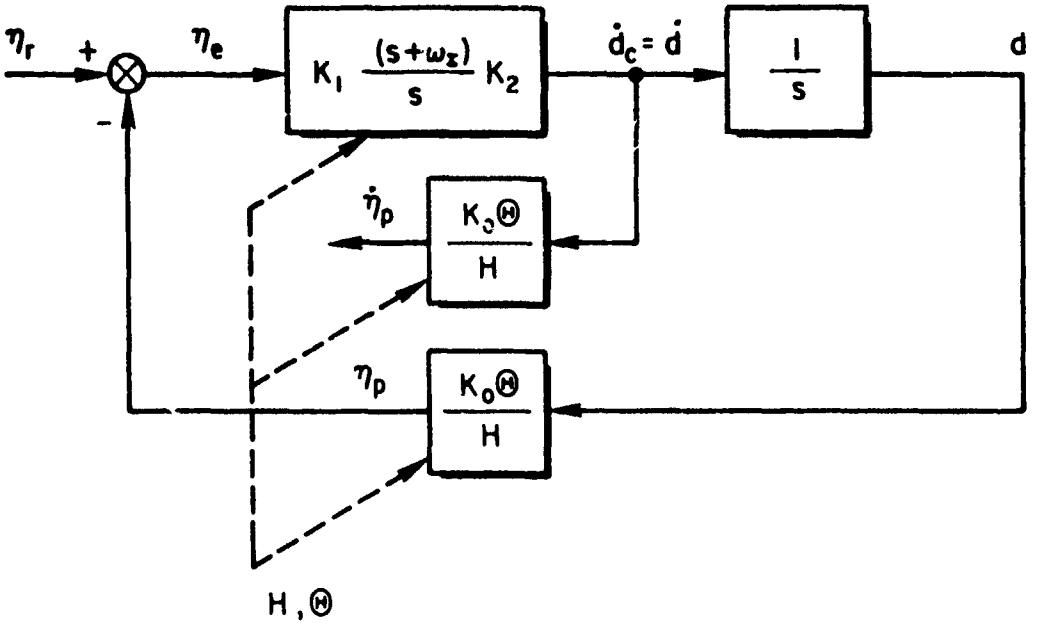

ω_I Typical Glide Slope coupler integral path gain, 0.20 rad/sec

K_0 Conversion constant 12,278. (μA/rad)

K_1 Course softening gain function; K_1 = 1.0, H ≥ 600 ft; decreasing linearly to zero at H = 0; K_1 = 0, H ≤ 0 ft

K_2 Typical Glide Slope coupler gain, 0.2918 (ft/sec)/μA

Figure 7. Block Diagram for Alternative Filter System Which Generates Typical Aircraft Indicated Deviation, Actual Path Deviation, and Actual Path Deviation Rate Responses (Filter System No. 2)

- **Filter System No. 2 is slightly superior to Filter System No. 1 in its ability to reproduce qualitatively the response characteristics of the aircraft/control system combinations.**

- **The response characteristics of all aircraft/control system combinations simulated with the exception of the inertially augmented system are similar.**

- **Responses of the inertially augmented system in actual path deviation, D, and actual path deviation rate, DD, are considerably smoothed and attenuated, respectively. The indicated path deviation response, DE, for the inertially augmented system approximates the Glide Slope forcing function, DCB.**

The first point above is the basis for selection of Filter System No. 2 for representing typical aircraft/control system dynamic behavior. The fact that Filter System No. 2 does not represent the inertially augmented system responses accurately is of little importance because of the third point above. Namely, since DE is approximately DCB for inertially augmented systems, and because it has been shown in Ref. 1 that the limiting factor for inertially augmented systems is the missed approach rate (which in turn has its source in large indicated path deviation), tolerances placed upon DCB alone are sufficient to assure adequate performance from inertially augmented systems. Of course, it would also be possible to consider a third filter system which would be a highly simplified simulation of inertially augmented systems, but this does not appear to be warranted.

The second point above is the basis for not specifically considering manually controlled flight director systems further. The manually controlled flight director system responses are very similar to the LSI automatic landing system responses in Figs. A-14 and A-16 and in Figs. A-25 and A-27. Additional manually controlled flight director runs therefore are unnecessary.

Table 2 lists figure numbers for comparable responses of Filter System No. 2 and the CV-880/LSI automatic landing system for all nine prototype Glide Slope fault inputs. Actual comparison shows good qualitative agreement in response shape and phase for all prototype Glide Slope inputs. This validates selection of Filter System No. 2.

TABLE 1

RESPONSE COMPARISON FOR FILTER SYSTEMS NO. 1 AND NO. 2
ACROSS AIRCRAFT/CONTROL SYSTEM COMBINATIONS FOR
GIVEN PROTOTYPE GLIDE SLOPE FAULTS

PROTOTYPE GLIDE SLOPE FAULT NO.	FILTER SYSTEM FIGURE NUMBER NO. 1 / NO. 2		AIRCRAFT/CONTROL SYSTEM FIGURE NUMBER LSI / IS / FD / PA-30			
2	A-2	A-3	A-14	A-15	A-16	A-17
3	A-4	A-5	A-18	A-19		
9	A-11	A-12	A-25	A-26	A-27	A-28

TABLE 2

RESPONSE COMPARISON FOR FILTER SYSTEM NO. 2 WITH THE
CV-880/LSI SIMULATION ACROSS PROTOTYPE
GLIDE SLOPE FAULT INPUTS

PROTOTYPE GLIDE SLOPE FAULT NO.	FILTER SYSTEM NO. 2 FIGURE NUMBER	CV-880/LSI FIGURE NUMBER
1	A-1	A-13
2	A-3	A-14
3	A-5	A-18
4	A-6	A-20
5	A-7	A-21
6	A-8	A-22
7	A-9	A-23
8	A-10	A-24
9	A-12	A-25

SECTION III

SIMULATED AIRCRAFT/CONTROL SYSTEM PERFORMANCE WITH ACTUAL ILS GLIDE SLOPE DATA INPUT

In this section the performance prediction capability of the aircraft/control system simulation model will be presented. In addition, the key flight inspection tolerances developed in Ref. 1 will be applied to the responses of Filter System 2 to illustrate their effectiveness in discriminating against ILS Glide Slope facilities which would induce out-of-specification approach and landing performance.

LANDING PERFORMANCE

Table 3 summarizes the landing performance data for the simulated aircraft/control system combinations in response to actual Glide Slope data inputs. Data for 22 runs in response to 16 different Glide Slope facilities covering all categories of service is given. Among these, 8 runs are given which include calculation of the dispersive effects of wind, wind shear and turbulence upon landing performance.

The mean sink rate at touchdown and the mean location of the touchdown point with respect to the Glide Path Initial Point (GPIP) in Table 3 may be regarded either as the average values at touchdown in the presence of atmospheric disturbances, or as the values which would occur in the complete absence of atmospheric disturbances. The mean sink rates resulting at touchdown are reasonable, but are slightly on the high side, for all runs. (No special attempt was made to tune up the flare computer in the simulations to achieve the more usual nominal sink rate at touchdown of 2 ft/sec.) The mean touchdown point location is acceptable for all cases except

No. 14 CV-880 LSI

No. 16 CV-880 LSI

and the following cases are near the borderline but are nevertheless within specification:

TABLE 3. LANDING PERFORMANCE FOR ACTUAL GLIDE SLOPE FLIGHT INSPECTION DATA INPUTS

GLIDE SLOPE ID. NO.	ILS FACILITY CATEGORY	AIRCRAFT	CONTROL SYSTEM	MISSED APPROACH PROBABILITY	STANDARD DEVIATION			MEAN TOUCHDOWN		±2σ TOUCHDOWN FOOTPRINT DIMENSION (ft)
					PITCH (deg)	ACCELERATION (g's)	TOUCHDOWN SINK RATE (ft/sec)	SINK RATE (ft/sec)	LOCATION (ft)	
1	III	CV-880	LSI					3.56	247	
2	↓	CV-880	LSI	0.000	0.619	0.0287	0.341	3.35	426	193
2		PA-30	INVENTED†	0.054	0.779	0.0383	0.576	3.01	356	640
3		CV-880	LSI					3.32	433	
3	III	PA-30	INVENTED†					2.71	373	
4	II	CV-880	LSI					3.28	521	
5	↓	↓	↓					3.46	298	
6								3.16	466	
7	II							3.20	520	
9	I		↓	NA*				3.91	289	
10	↓		LSI	NA	0.619	0.0287	0.340	3.34	426	191
10			IS*	0.93×10^{-3}	0.625	0.0294	0.340	3.18	517	164
11			LSI	NA				3.30	436	
12		↓	↓	↓				3.30	529	
13		CV-880	LSI					3.28	548	
13		PA-30	INVENTED					2.53	442	
14		CV-880	LSI	NA				2.77	905	
15		↓	↓					4.08	315	
16	↓		LSI	NA	0.619	0.0287	0.342	3.09	606	196
16	I		IS*	0.000	0.625	0.0294	0.340	3.20	344	163
24	II	↓	LSI	0.15×10^{-7}	0.619	0.0287	0.340	3.53	213	194
24	II	CV-880	IS*	0.15×10^{-7}	0.625	0.0294	0.339	3.45	389	159
Critical Value(s)				0.05	2.00	0.170	$p(0 \leq \dot{h}_{TD} \leq 8) \geq 0.95$		50/550	1500

Note: Simulated category of operations is same as ILS facility category unless otherwise noted.

*Simulated Category II-III operations with automatic landing.

†Simulated Category II operations with manual landing.

*NA = Not applicable

No. 4	CV-880	LSI
No. 7	CV-880	LSI
No. 10	CV-880	IS*
No. 12	CV-880	LSI

The standard deviation of the sink rate at touchdown arising because of random atmospheric disturbance effects is small (approximately 0.340 ft/sec) for the 8 runs wherein that statistic is computed.

The longitudinal dimension of the $\pm 2\sigma$ touchdown footprint is well within the permissible range for all runs. It is interesting to notice, however, that the longitudinal dispersion arising from atmospheric disturbances alone is much smaller than that arising from the combined effects of atmospheric disturbances and ILS Glide Slope beam alignment error and structure. (This may be seen by comparing entries in Table 3 with comparable entries in Table 3 of Ref. 1.) In fact, the longitudinal dispersion for the combination of inputs is much larger than the root-sum-squared values for the separate inputs acting alone. The mechanism of this effect can be appreciated by considering the approximate equation for the $\pm 2\sigma$ touchdown footprint dimension (Eq. C-14 from Ref. 1):

$$X_{TD_2} - X_{TI_1} \doteq 4 \left[\sigma_X \sqrt{1 - \rho^2_{XH}} \right]_{\bar{H}=0}$$

If the expression in the brackets is squared and the quantities are considered to consist of two (or more) uncorrelated components, then

$$\sigma^2_X(1 - \rho^2_{XH}) = \sigma^2_{X1} + \sigma^2_{X2} + \ldots - \frac{(C_{XH1} + C_{XH2} + \ldots)^2}{\sigma^2_{H1} + \sigma^2_{H2} + \ldots}$$

where C_{XH} is the covariance of X and H. It is clear that if all σ^2_{Xi} are of comparable size, all σ^2_{Hi} are of comparable size, and the magnitude of C_{XH1} is very large in comparison to the other C_{XHi} then

$$\sigma_X^2(1 - \rho_{XH}^2) \geq \left(\sigma_{X1}^2 - \frac{C_{XH1}^2}{\sigma_{H1}^2}\right) + \left(\sigma_{X2}^2 - \frac{C_{XH2}^2}{\sigma_{H2}^2}\right) + \ldots$$

$$\geq \left(\sigma_{X1}^2 - \frac{C_{XH1}^2}{\sigma_{H1}^2}\right) + \sigma_{X2}^2 + \ldots$$

where the righthand side is sum-square of the components.

All pilot acceptance related factors in Table 3, the standard deviations of pitch attitude and normal acceleration, are well within the permissible ranges for all runs for which these quantities were computed. Notice that the values computed are mainly specific to the aircraft and are to a small extent specific to the control system.

The missed approach rate predicted for the 8 runs wherein atmospheric disturbance inputs are included is acceptable. However, the missed approach rate for the Piper PA-30 is 8 percent higher than the target missed approach rate of 0.05. In attempting to complete the runs for the Piper PA-30, the autothrottle law described in Ref. 2 was found to be ineffective. (No autothrottle at all would result in better performance.) The autothrottle law of Ref. 2 was used for the simulation work reported in Ref. 1 without modification, and appears to be almost entirely responsible for the poor landing performance reported in Ref. 1 for the Piper PA-30 and the invented control system. The autothrottle gains are modified to the values listed in Table 4 for the simulation runs reported herein. These gain values were derived by reference to the longitudinal acceleration equation for the Piper PA-30. The root-mean-square throttle activity for the modified and unmodified autothrottle control law gains is comparable. However, dynamic performance for the modified autothrottle is superior.

The data for Glide Slope identification numbers 10, 16, and 24 permit some tentative assessment of the benefits of inertial augmentation in the Glide Slope coupler law. In every case, the addition of inertial augmentation reduced the longitudinal dimension of the $\pm 2\sigma$ touchdown footprint by the modest amount of 15 percent, and, in two out of three cases, the mean touchdown point is closer to that for the ideal Glide Slope, 500 ft (from Table 3, Ref. 1).

TABLE 4

GAIN VALUES FOR MODIFIED PA-30 AUTOTHROTTLE

$1/\tau_u$ = 0.5 rad/sec

K_u = 25.4 lb-thrust/(ft/sec)

K_{I_u} = 1.25 (lb-thrust/sec)/(ft/sec)

$1/\tau_\theta$ = 0.5 rad/sec

$K_{\theta'}$ = 1800. lb-thrust/rad

APPLICATION OF FLIGHT INSPECTION TOLERANCES

The purpose of this subsection is to demonstrate the effectiveness of the proposed flight inspection filter concept in discriminating against those ILS Glide Slope data records for which out-of-specification approach and landing performance is indicated by simulation results. This demonstration proceeds by comparison of hypothetical facility rejections based upon simulated system performance evaluation with facility rejections based upon simulated flight inspections using the filter system concept.

The tests applied to the simulation data are as follows. The responses in actual glide path deviation (ETAP), indicated glide path deviation (ETAE) and actual glide path deviation rate (ETAPD) of Filter System No. 2 to the differential trace (ETACB) of the flight inspection data for each of the 12 different ILS Glide Slope facilities* are compared with the 2σ tolerance levels corresponding to each response variable and the differential trace itself. The test fails for a given facility if any one response variable exceeds the corresponding 2σ tolerance level given in Fig. 3 for more than 5 percent of the record length†. (For more details concerning application

*Figures B-1a through B-12a of Appendix B.

†The record lengths from simulation are somewhat shorter than those which would result in flight inspection since only the last 750 ft of descent is simulated. The last 750 ft does cover the most crucial phase of the approach and landing however.

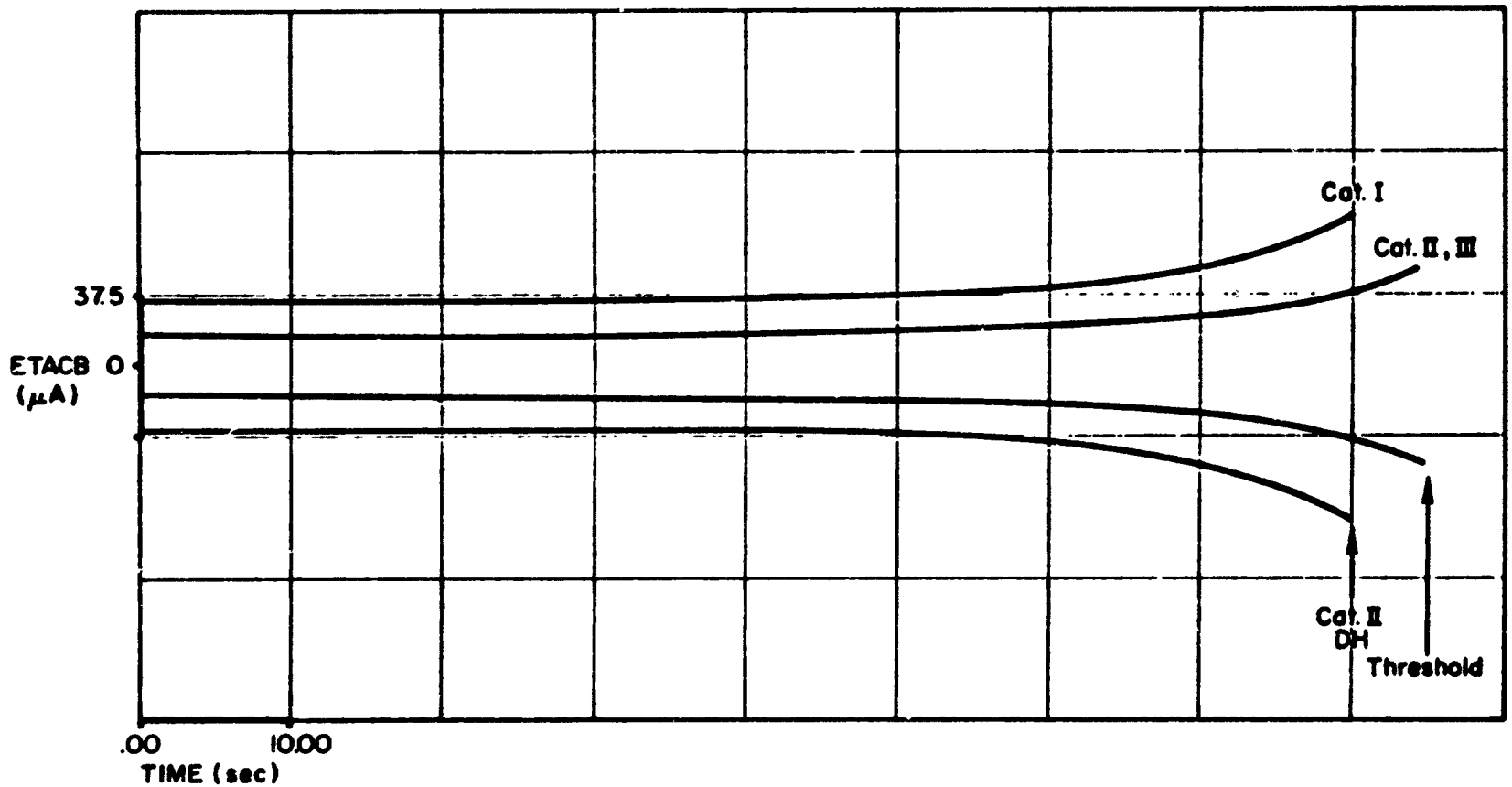

a) ETACB

Figure 3. 2σ Tolerance Levels for Application to Filter System No. 2 Responses in Appendix B

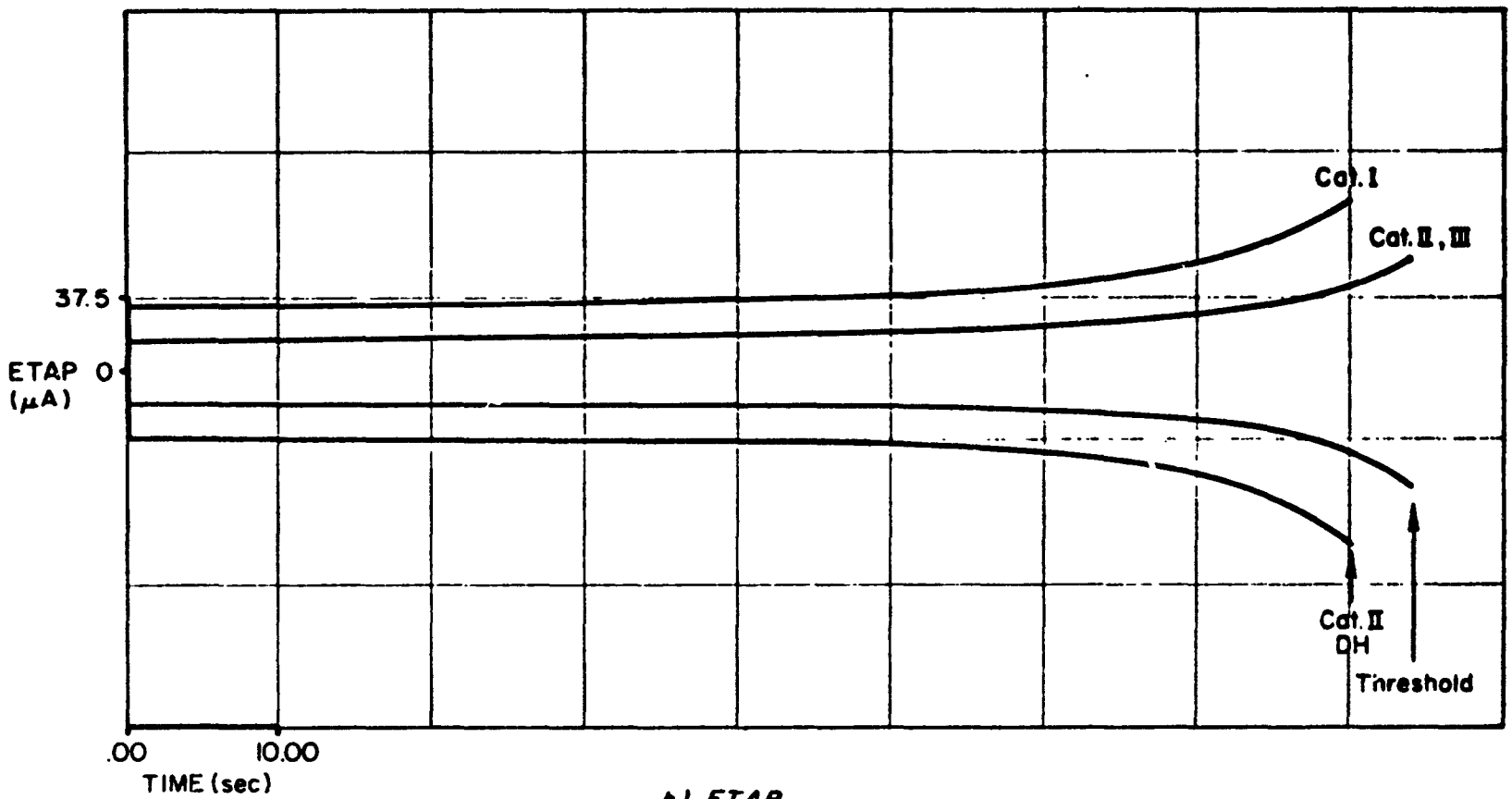

b) ETAP

Figure 3. (Continued)

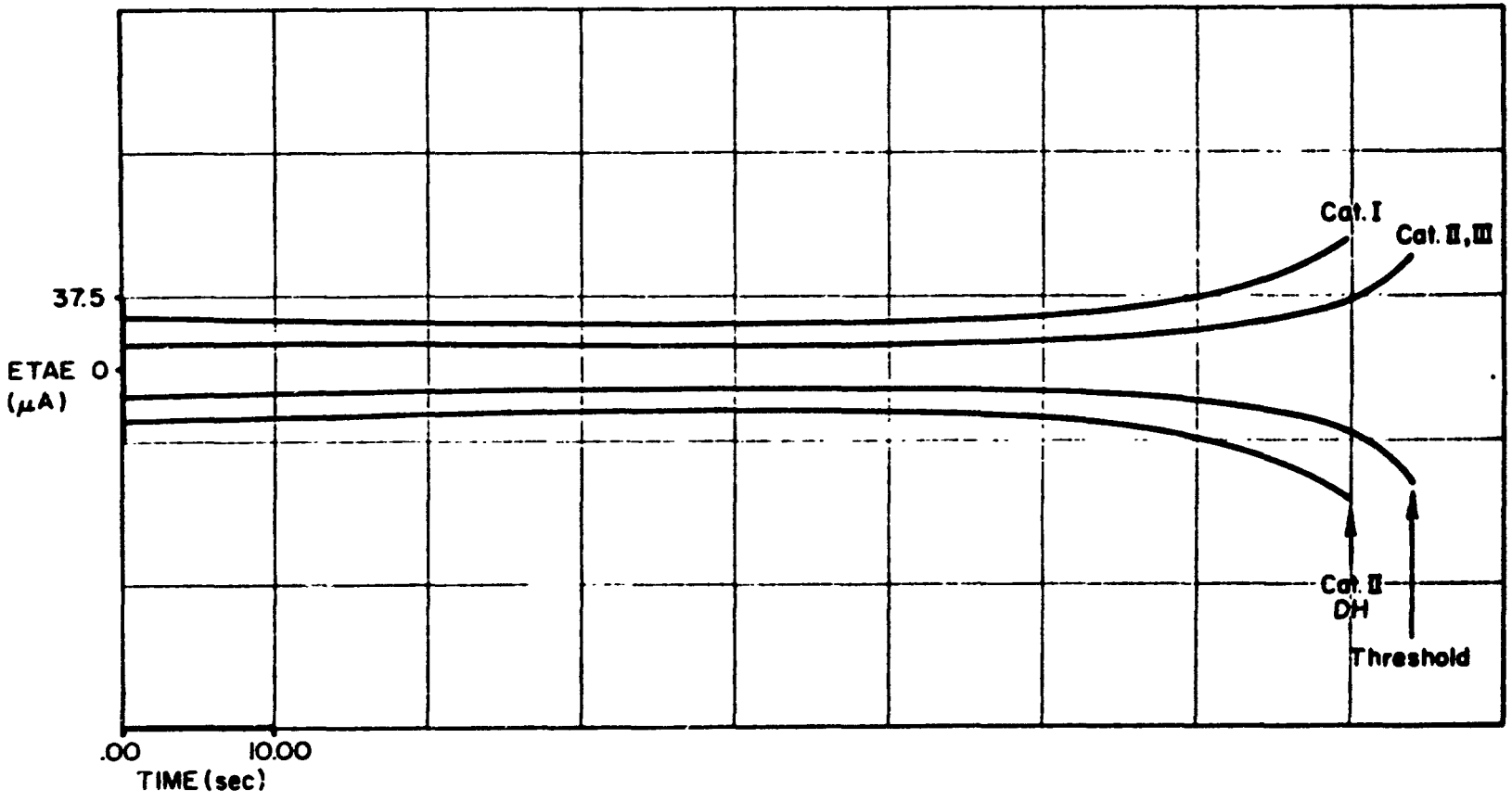

c) ETAE

Figure 3. (Continued)

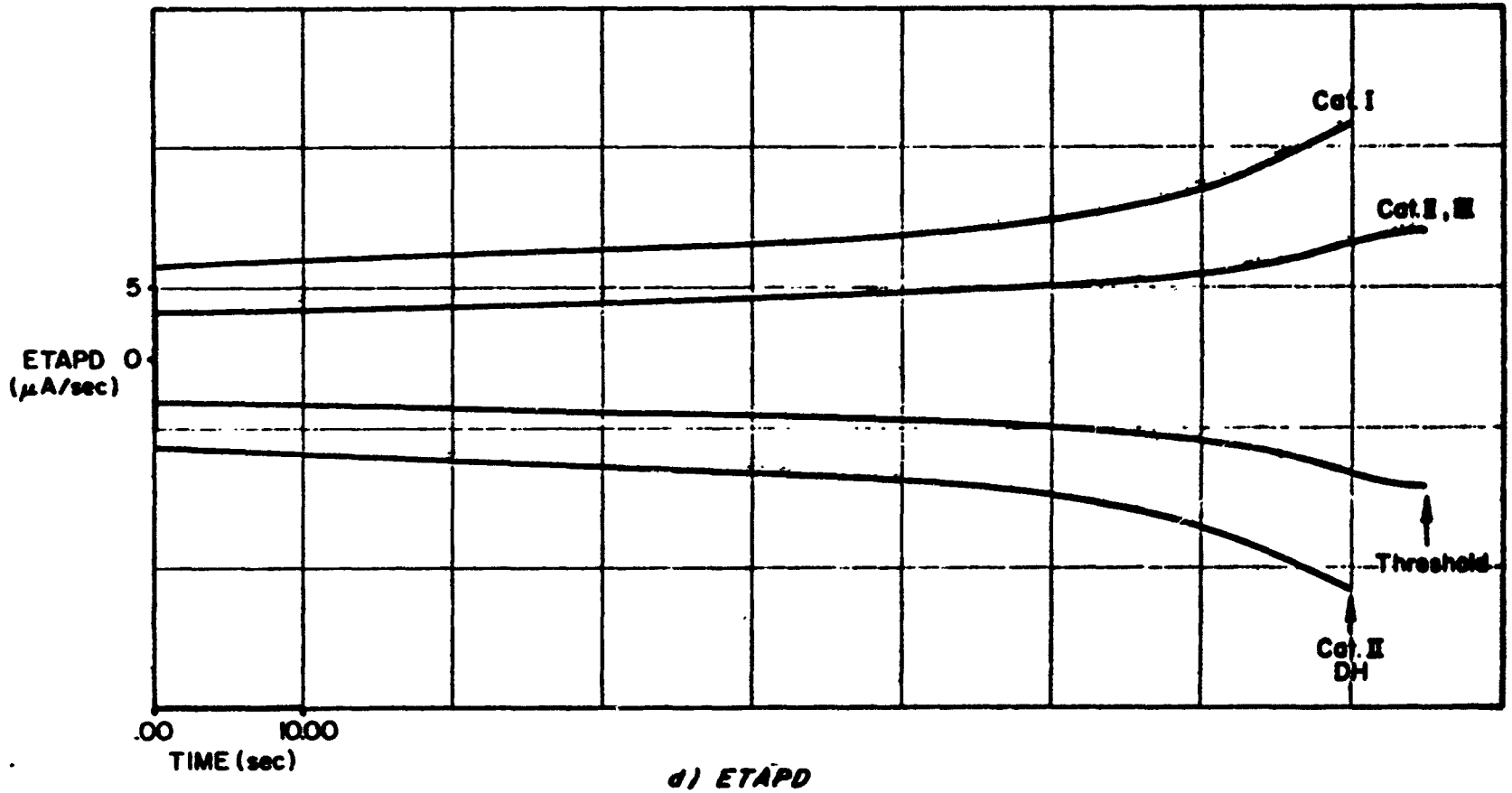

d) ETAPD

Figure 3. (Concluded)

of these tolerances, refer to the "Data Analysis" subsection in Section III of Ref. 1.) This test is applied for two levels of the tolerances. One level is appropriate for Category I facility performance; the second level is appropriate for Category II or III facility performance. The results of this test (blank or P = pass, F = fail) are indicated by the above-the-line entries in Table 5 for each variable and category of performance.

Table 5 also contains the results of comparing the simulated responses of the CV-880/LSI aircraft/control system combination in actual glide path deviation, indicated glide path deviation and actual glide path deviation rate to the differential trace of the flight inspection data for the same 12 ILS Glide Slope facilities* with critical 2σ levels (given in Fig. 4) which just permit acceptable approach and landing performance. (These levels are developed in Ref. 1.). The test fails for a given facility if any one response variable exceeds the corresponding 2σ level for more than 5 percent of the record length. This test is applied for levels appropriate for Category I operational performance and for Category II or III operational performance. The results of this test (blank or P = pass, F = fail) are indicated by the below-the-line entries in Table 5 for each variable and category of performance.

Comparison results summarized in Table 5 show that all facilities rejected on the basis of simulated system performance at a given operational category level are also rejected on the basis of simulated flight inspection for that category level. Furthermore, only two facilities rejected by the simulated flight inspection are found to be marginally acceptable by the simulated system performance evaluation out of the twelve facilities tested at each of two operational category levels. These findings tend to indicate that flight inspections using the filter concept tend to be slightly conservative.

*Figure B-13a, B-14a, B-16a through B-23a, B-25a, and B-26a of Appendix B.

TABLE 5

COMPARISON OF TEST RESULTS FOR TOLERANCES UPON FILTER SYSTEM NO. 2 OUTPUTS AND UPON AIRCRAFT/CONTROL SYSTEM OUTPUTS

GLIDE SLOPE ID. NO.	ACTUAL ILS FACILITY CATEGORY	VARIABLE UNDER TEST AND TEST CATEGORY								FACILITY TEST RESULTS	
		ETACB		ETAP		ETAE		ETAPD			
		I	II-III	I	II-III	I	II-III	I	II-III	I	II-III
1	III				F/P						F/P
3	III										
4	II										
5	II										
6	II										
7	II										
9	I		F/F		F/F		F/F		F/F		F/F
11	I								F/F		F/F
12	I						F/P		F/P		F/P
13	I						F/F		F/F		F/F
14	I		F/P[1]		F/P		F/F		F/F		F/F
15	I		F/F	F/P	F/F	F/F	F/F	F/P	F/F	F/F	F/F

Legend

F/ = Test fails for Filter System No. 2 output

/F = Test fails for CV-880/LSI simulation output

/P = Test passes for CV-880/LSI simulation output

No entry indicates test passes for Filter System No. 2 output and for CV-880/LSI simulation output.

Note:

1. The "Pass" is an artifact of the ETACB trace presentation in Fig. B-25.

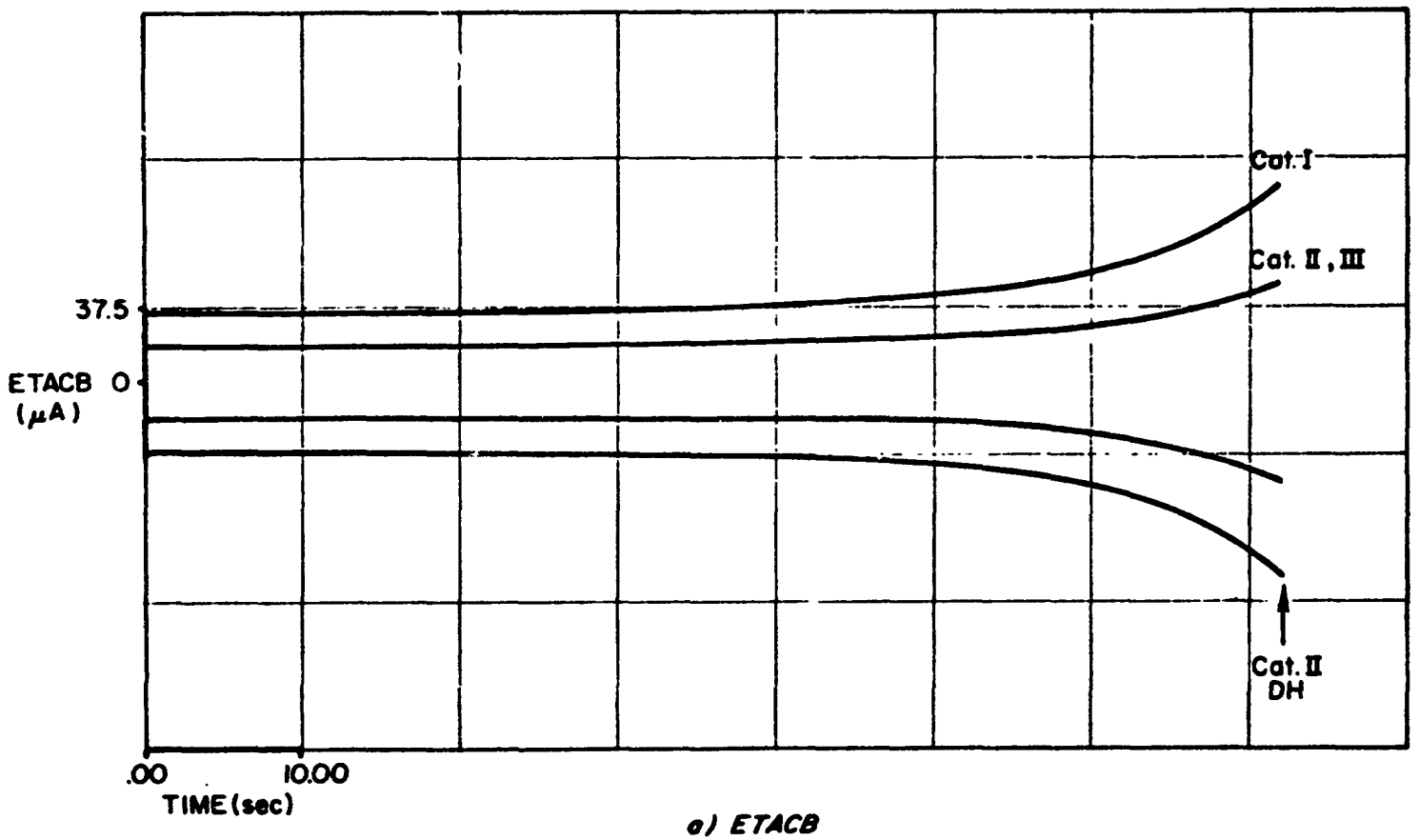

Figure 4. Critical 2σ Levels Corresponding to Key CV-880 Simulation Response Variables in Appendix B

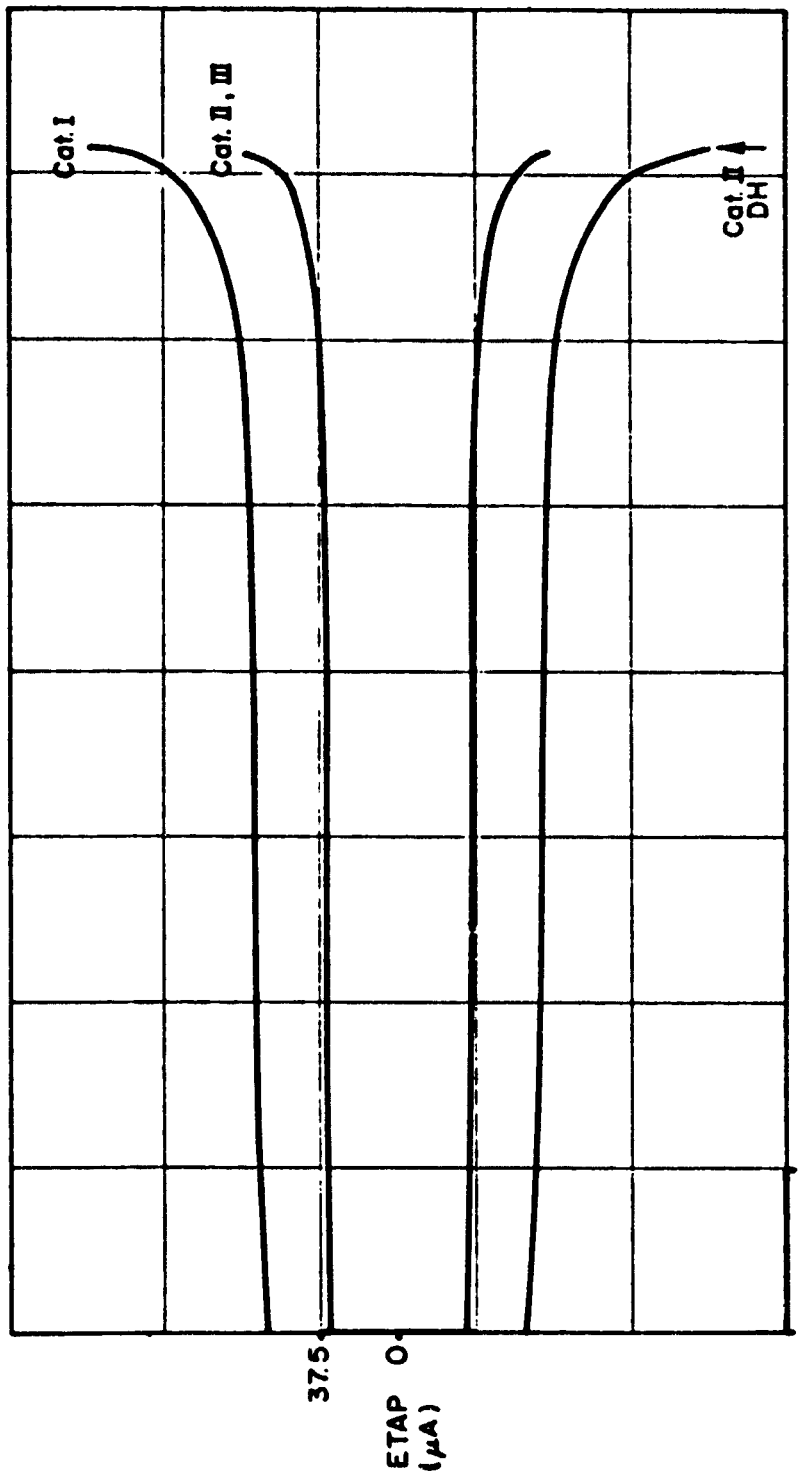

Figure 4. (Continued)

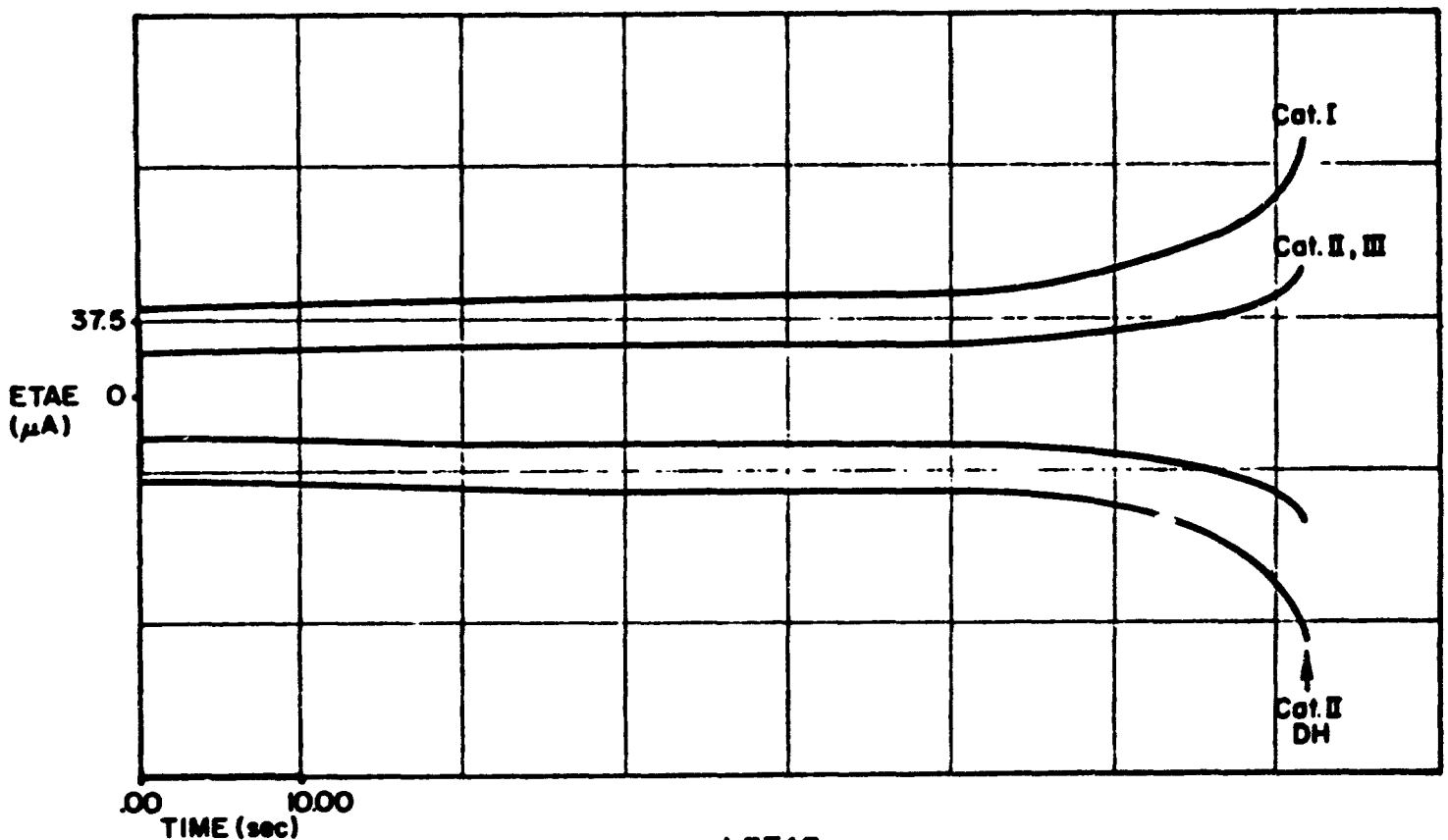

c) ETAE

Figure 4. (Continued)

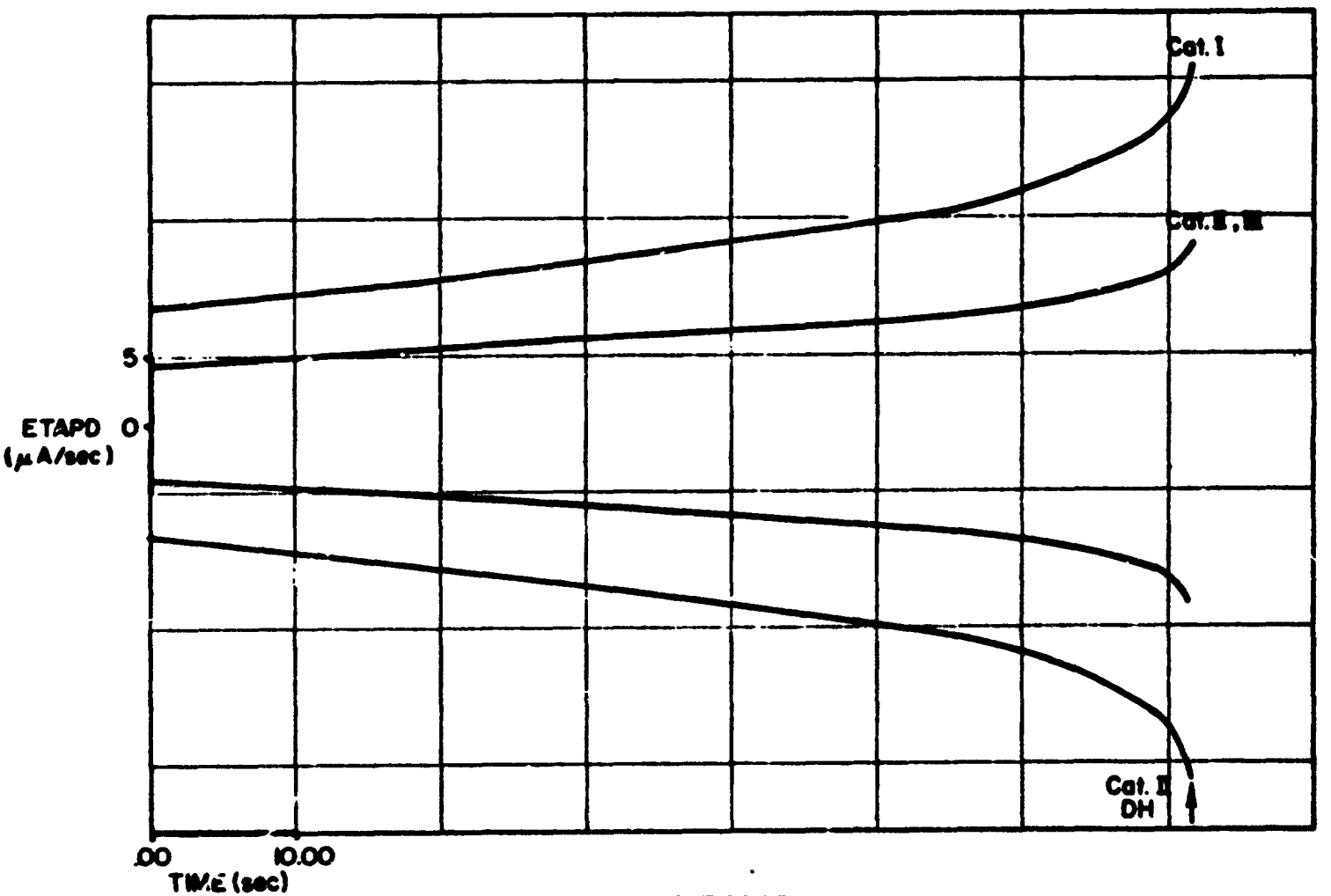

d) ETAPD

Figure 4. (Concluded)

Other observations of interest from Table 5 are as follows.

- Two Category I ILS Glide Slope facilities (Nos. 11 and 13) are apparently acceptable for Category II-III service insofar as tolerances on the differential trace are concerned. (Recall this tolerance is comparable to the existing flight inspection standard on structure except in ILS Approach Zone 3 wherein the tolerance becomes increasingly less restrictive than the existing flight inspection standard as the runway threshold is approached.) However, tolerances applied to the indicated path deviation and/or the actual path deviation rate outputs of the flight inspection filter system result in rejection of these facilities for Category II-III service. This finding illustrates the increased discrimination provided by tolerances applied to the several filter system outputs in comparison to the level of discrimination obtained when tolerances are applied to the differential trace alone.

- Only one facility, commissioned for Category I service (No. 12), has a Category II-III level of performance. However, the conservative nature of the filter system obscures this fact in this particular instance.

- All ILS Glide Slope facility data records except two (Nos. 1 and 15) pass the tolerance tests for their actual commissioned service category. In the case of No. 1, simulated system performance shows that this facility is actually marginally acceptable for its actual commissioned service category, but the conservative nature of the filter system obscures this fact.

The above findings tend to confirm the position that flight inspections based upon the filter system concept are successful in discriminating against those ILS Glide Slope facilities for which out-of-specification approach and landing performance can be expected. Furthermore, the filter system concept does not result in the rejection of any nonmarginal ILS Glide Slope facilities. Therefore, the method is not overly conservative.

Finally, it is interesting to note that the data in Table 3 indicate that the Category II-III level of landing performance is achievable with inertially augmented Glide Slope coupling for Category I facilities No. 10 and No. 16.

SECTION IV

CONCLUSIONS

This section provides a summary of the major conclusions reached as a result of the system simulation studies reported herein.

- More accurate estimates of indicated and actual glide path deviation and glide path deviation rate are provided by Filter System No. 2 (aircraft with perfect rate-of-climb and airspeed control and proportional-plus-integral coupler model) than by Filter System No. 1.

- There is substantial similarity in the gross nature of the responses for all aircraft and Glide Slope coupling techniques among themselves and with respect to the responses estimated using Filter Systems No. 1 and 2.

- The inertially augmented coupler has substantially attenuated responses to "high" frequency ILS Glide Slope structure for all variables except indicated glide path deviation (as one would expect). This is the principal feature differentiating the aircraft/control system combinations simulated. The inertially augmented coupler also results in a modest reduction in longitudinal touchdown dispersion.

- The simulation techniques reported in Ref. 1 can be used to predict a typical mean longitudinal touchdown point using flight inspection data for a specific ILS Glide Slope facility and can predict the typical longitudinal dimension of the $\pm 2\sigma$ touchdown dispersion footprint arising from winds, wind shear and turbulence.

- Disturbances arising from facility-to-facility variability in ILS Glide Slope structure, and winds, wind shear and turbulence combine in a synergistic way which causes longitudinal touchdown dispersion for the combination of all disturbances to greatly exceed the root-sum-square dispersions for each disturbance acting separately.

- The 2σ tolerances (developed in Ref. 1) applied to the corresponding responses of Filter System No. 2 are successful in discriminating against those ILS Glide Slope facilities which produce out-of-specification approaches and landings.

REFERENCES

1. Hofmann, Lee Gregor, et al., ILS Glide Slope Standards. Part I: A Review of Flight Inspection Standards Affecting Landing Performance and Comparison with Limits Evolved from a Systems Analysis, FAA-RD-74-119, I, June 1975.

2. Koziol, J. S., Jr., Simulation Model for the Piper PA-30 Light Maneuverable Aircraft in the Final Approach, DOT-TSC-FAA-71-11, July 1971.

APPENDIX A

FILTER SYSTEM AND AIRCRAFT/CONTROL SYSTEM SIMULATION RESPONSE PLOTS FOR PROTOTYPE GLIDE SLOPE FAULT INPUTS

The data in this appendix are arranged in the manner summarized in Tables A-1 and A-2. Table A-1 provides a cross reference of identification numbers (in first column) assigned to the prototype Glide Slope faults described verbally in the second column. Graphical presentations of these faults are available in the figures whose numbers are listed in the third and fourth columns. The graphical presentations are given both in linear units (feet) in the DCL ($\bar{d}_c$) trace of these figures, and in angular units (μA) in the ETACB ($\bar{\eta}_c$) trace. Filter system responses to the various prototype Glide Slope fault inputs are given in the figures designated in the

TABLE A-1

SUMMARY OF FILTER SYSTEM RESPONSE DATA TO PROTOTYPE GLIDE SLOPE FAULT INPUTS

NO.	PROTOTYPE GLIDE SLOPE FAULT DESCRIPTION	FIGURE NO. FOR RESPONSE OF FILTER NO. 1	FIGURE NO. FOR RESPONSE OF FILTER NO. 2
1	20 ft step at 10K ft range		A-1
2	20 ft step at 4K ft range	A-2	A-3
3	10 ft cosine 3K ft wavelength	A-4	A-5
4	10 ft cosine 1K ft wavelength		A-6
5	3 ft cosine 1K ft wavelength		A-7
6	Large amplitude arbitrary function		A-8
7	Large amplitude arbitrary function		A-9
8	Moderate amplitude arbitrary function		A-10
9	Moderate amplitude arbitrary function	A-11	A-12

TABLE A-2

SUMMARY OF AIRCRAFT/CONTROL SYSTEM COMBINATION RESPONSE DATA TO PROTOTYPE GLIDE SLOPE FAULT INPUTS

PROTOTYPE GLIDE SLOPE FAULT NUMBER	AIRCRAFT/CONTROL SYSTEM COMBINATION RESPONSE FIGURE NUMBER			
	CV-880 LSI	CV-880 INERTIALLY AUGMENTED	CV-880 FLIGHT DIRECTOR	PA-30 INVENTED
1	A-13			
2	A-14	A-15	A-16	A-17
3	A-18	A-19		
4	A-20			
5	A-21			
6	A-22			
7	A-23			
8	A-24			
9	A-25	A-26	A-27	A-28

third and fourth columns of Table A-1. Table A-2 provides a cross reference of the aircraft/control system responses to the various prototype Glide Slope fault inputs by input number, aircraft/control system configuration, and figure number. The details of the filter systems are given in Figs. 1 and 2 in the main text and in Ref. 1. Details of the aircraft/control system combinations simulated are given in Appendix B of Ref. 1. Definitions of the symbols used appear in the front matter.

REMARKS ON SIMULATION DATA

Filter system response data appearing in Figs. A-1 through A-12 closely simulate results which would be obtained in a hypothetical field test of the filter system. The only assumption made is that the inspecting aircraft is approaching at constant ground speed and rate of descent. This assumption

is close to the facts of actual operation. The filter system responses extend down to the point where the ideal path asymptote has an altitude of 50 ft. This point nominally corresponds to the point of runway threshold crossing.

The aircraft/control system combination response data appearing in Figs. A-13 through A-28 have the following characteristics requiring further explanation. The DCB ($\bar{d}_c$) trace represents the Glide Slope forcing function. The ETACB ($\bar{\eta}_c$) trace is derived from the DCB data. The DCB trace is active until the Category II decision height is reached on a manually completed landing (flight director and Piper PA-30 cases). Below the decision height the DCB trace is set to zero. On automatically completed landings, the DCB trace is active until the flare initiation altitude is reached. Below that altitude, the DCB trace is held constant at the value prevailing at flare initiation. All flight director and Piper PA-30 cases utilize the Glide Slope forcing function in simulated Category II approaches with manually completed landings (designated II M). The other two cases, the CV-880 with the LSI automatic landing system (LSI) or with an inertially augmented version of the LSI automatic landing system (IS), utilize the Glide Slope forcing function in simulated Category II or III approaches with automatic landing.

Finally, the magnitude of most, if not all, of the prototype Glide Slope faults is much larger than could be tolerated in actual operation. For example, all prototype Glide Slope faults except No. 5 fail to meet the Category I flight inspection standard for structure (±30 μA on a 3σ basis). Furthermore, Glide Slope faults No. 1, 3, 4, 6, 7, 8, and 9 were not tracked within the required tolerance for continuing a Category II approach (±37.5 μA or ±12 ft whichever is larger, from an altitude of 700 ft down to the decision altitude) by the systems simulated, even in the complete absence of atmospheric disturbance effects. The prototype Glide Slope faults nevertheless have been used as supplied.

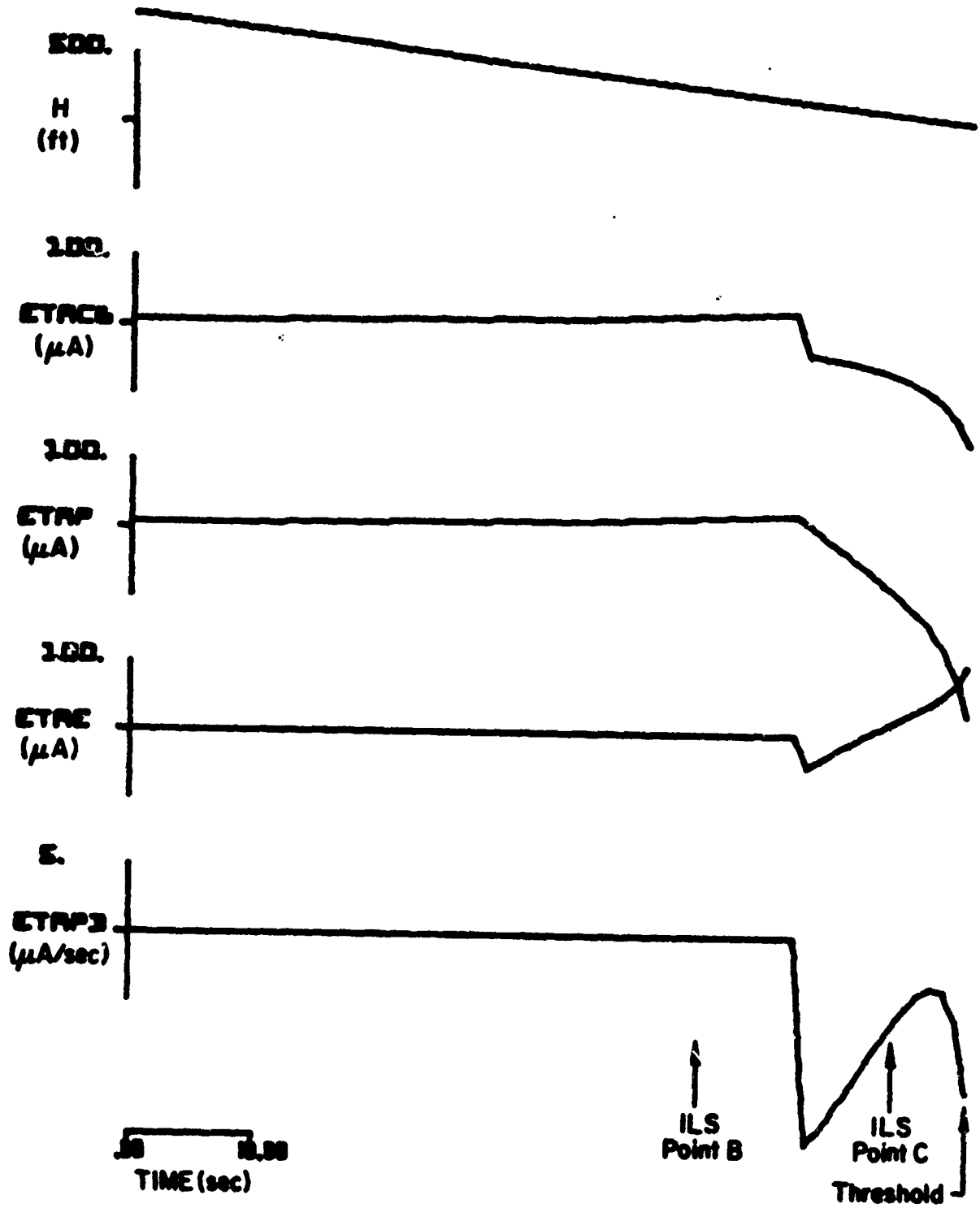

(a)

Figure A-1. Responses of Filter System No. 2 to Prototype Glide Slope Fault No. 1

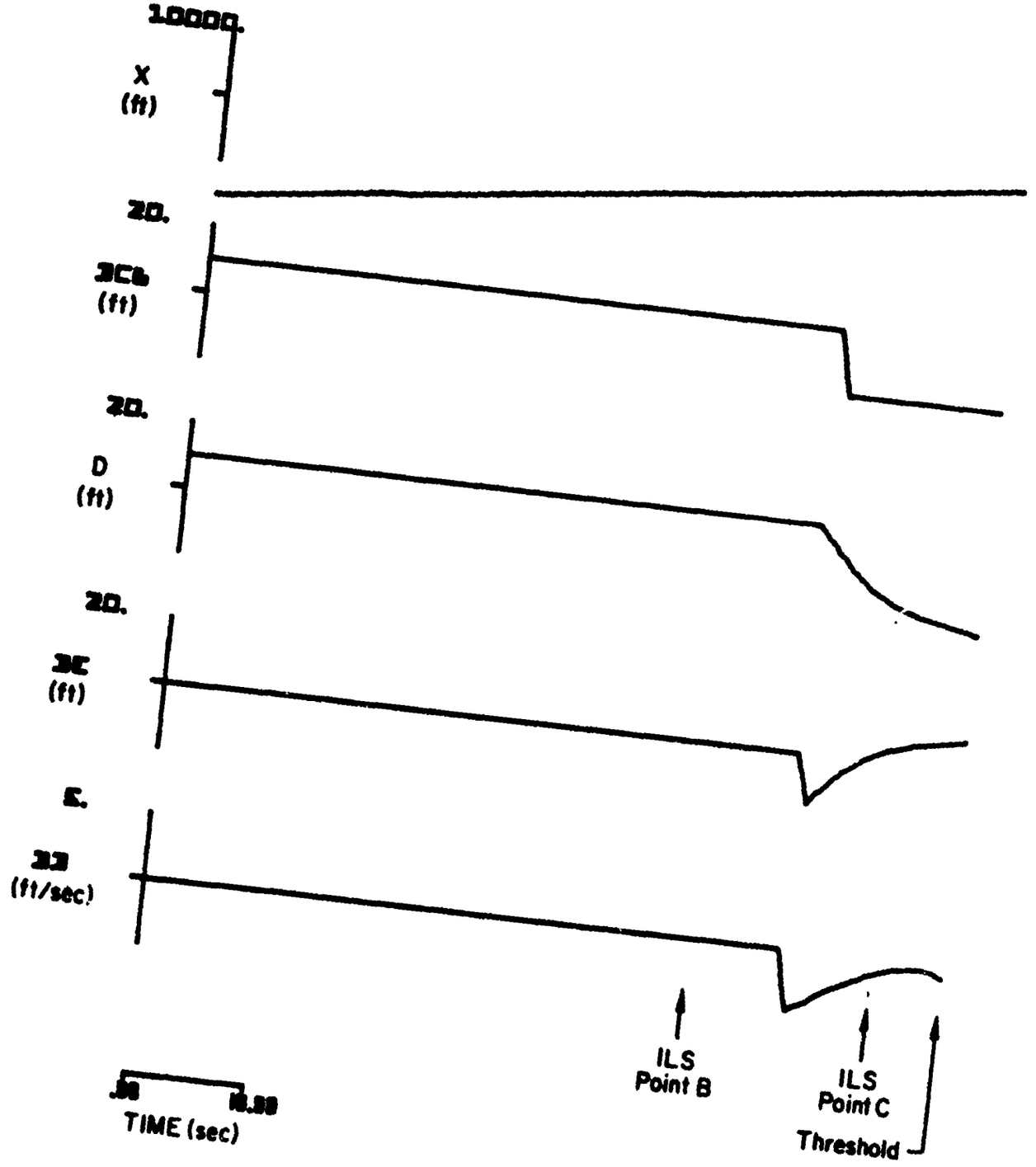

(b)

Figure A-1. (Concluded)

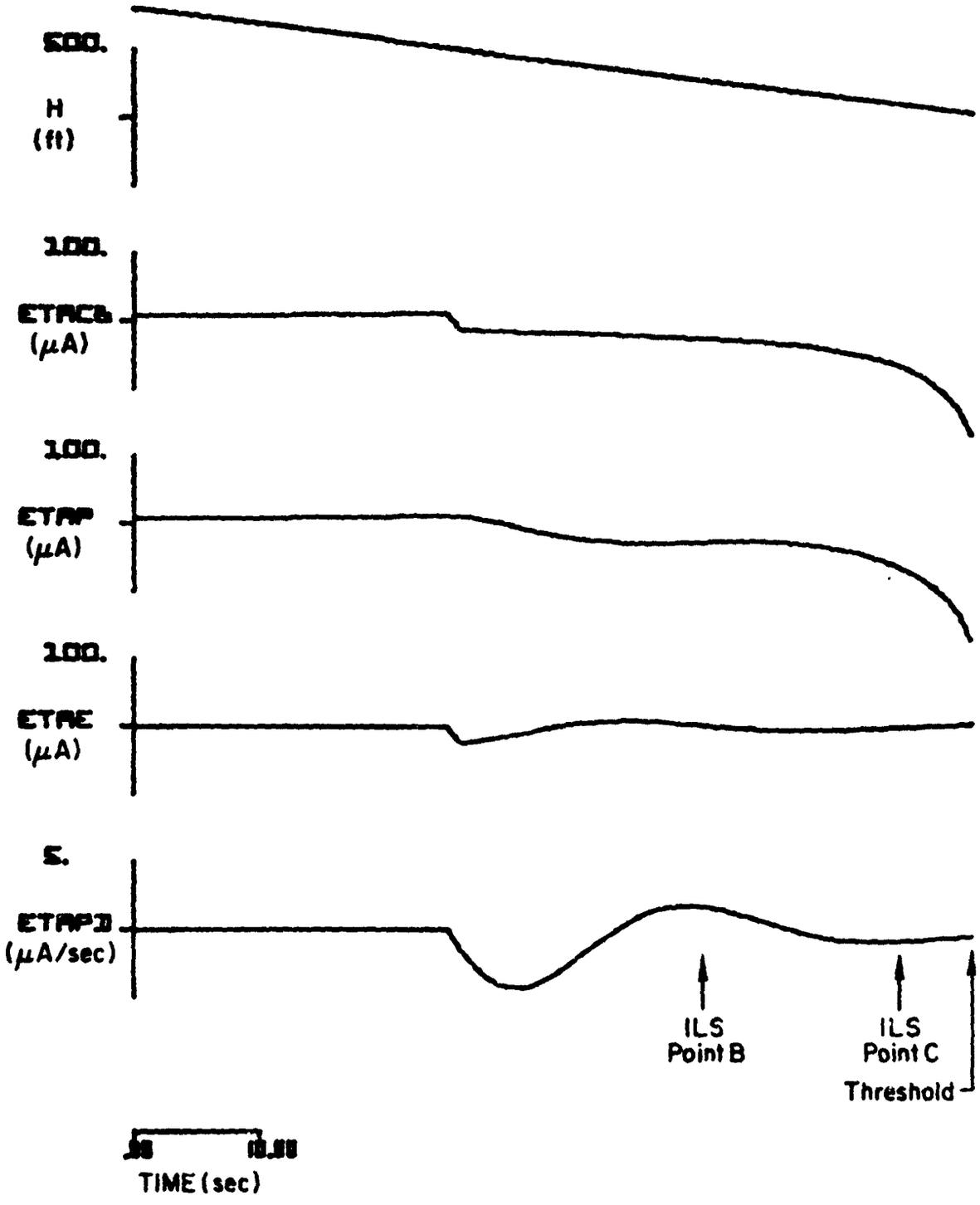

(a)

Figure A-2. Responses of Filter System No. 1 to Prototype Glide Slope Fault No. 2

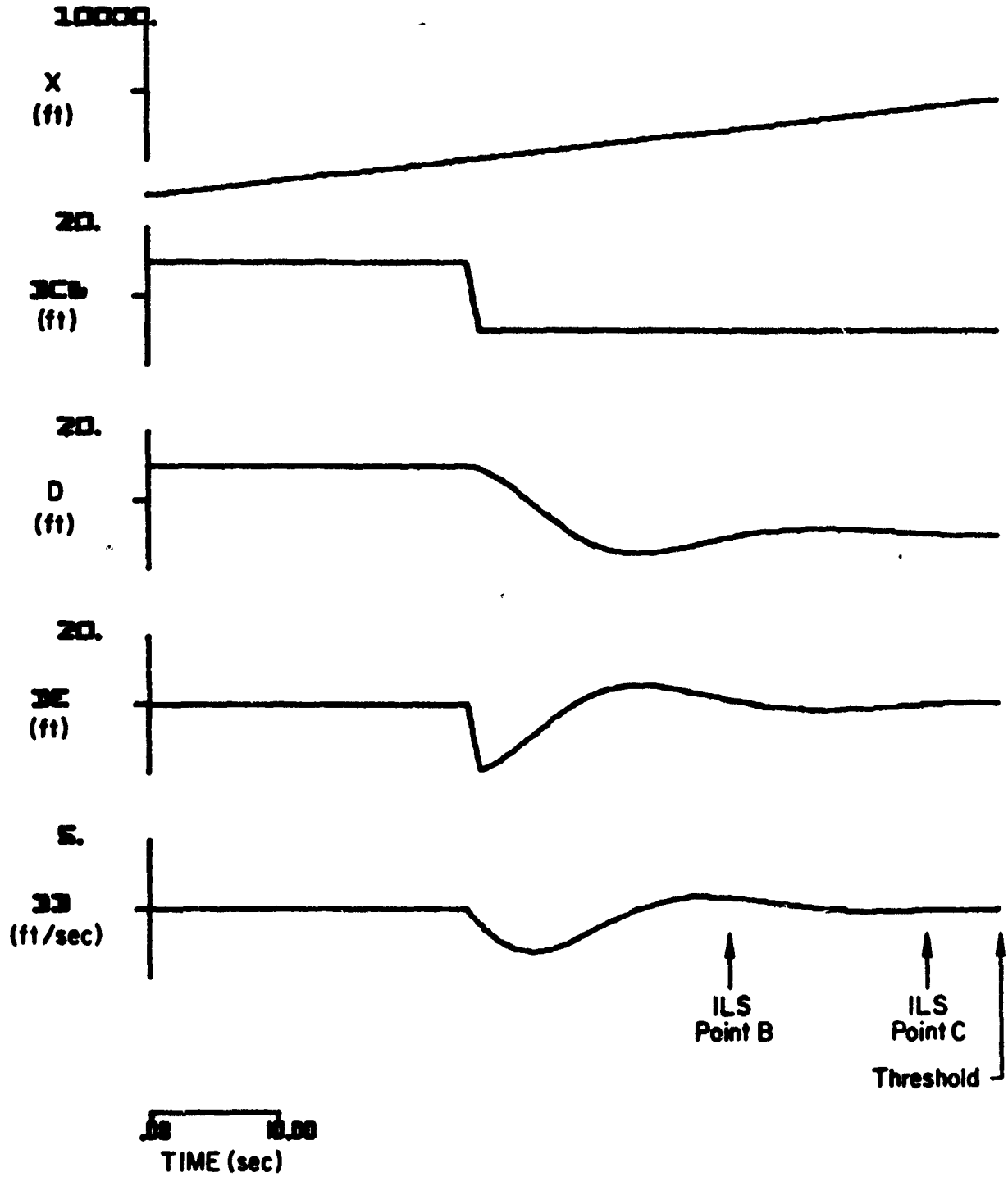

(b)

Figure A-2. (Concluded)

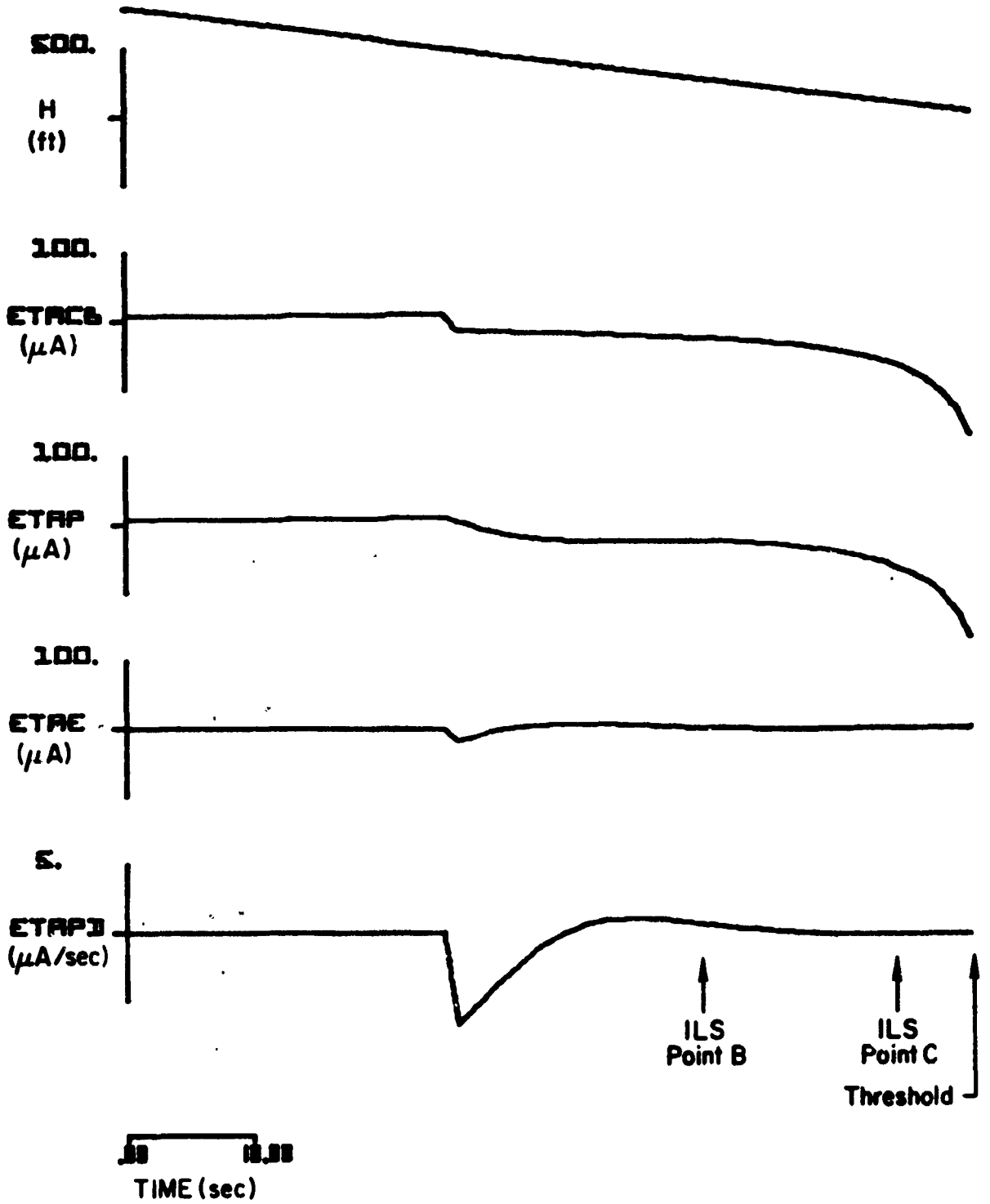

(a)

Figure A-3. Responses of Filter System No. 2 to Prototype Glide Slope Fault No. 2

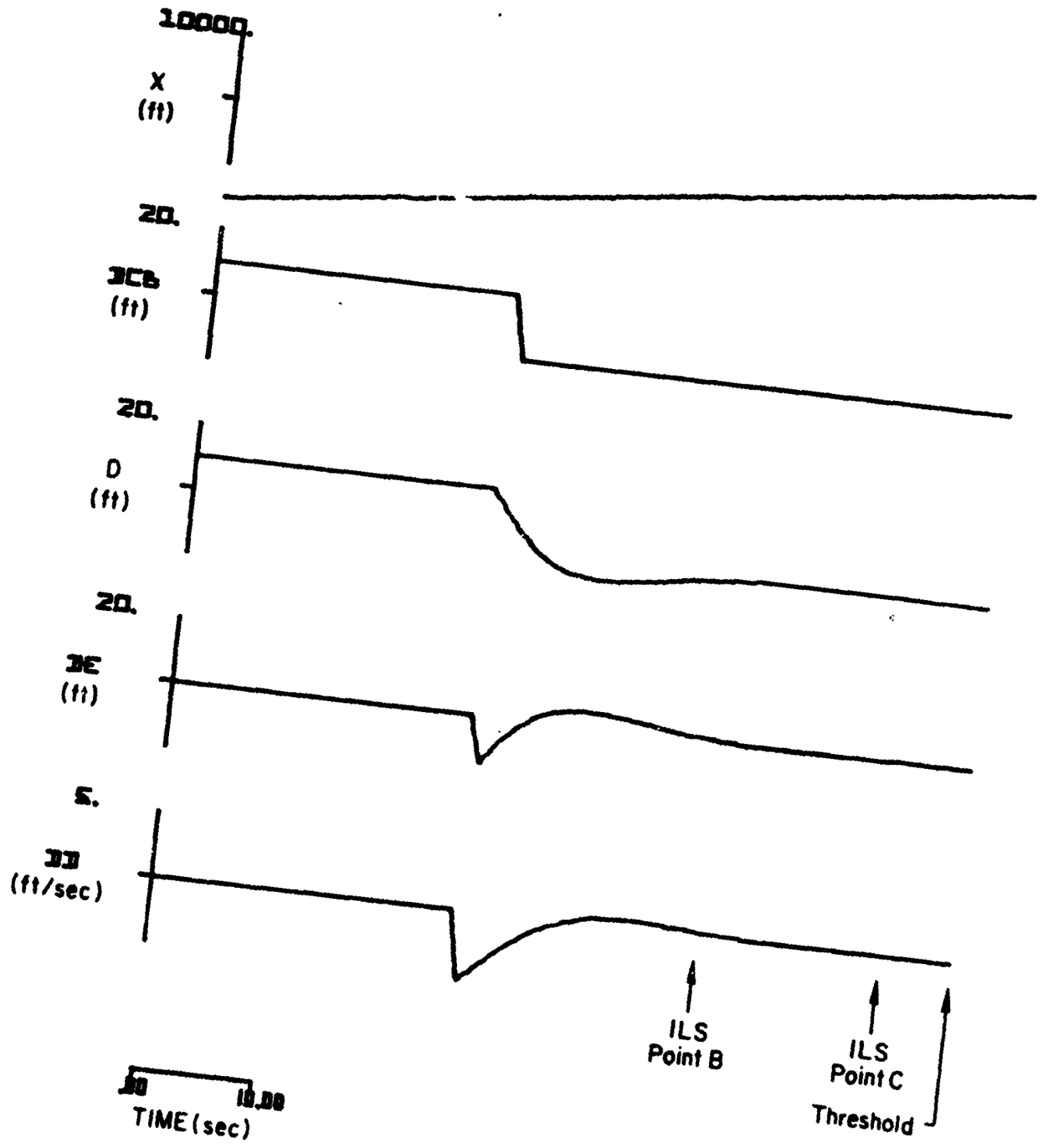

(b)

Figure 4-3. (Concluded)

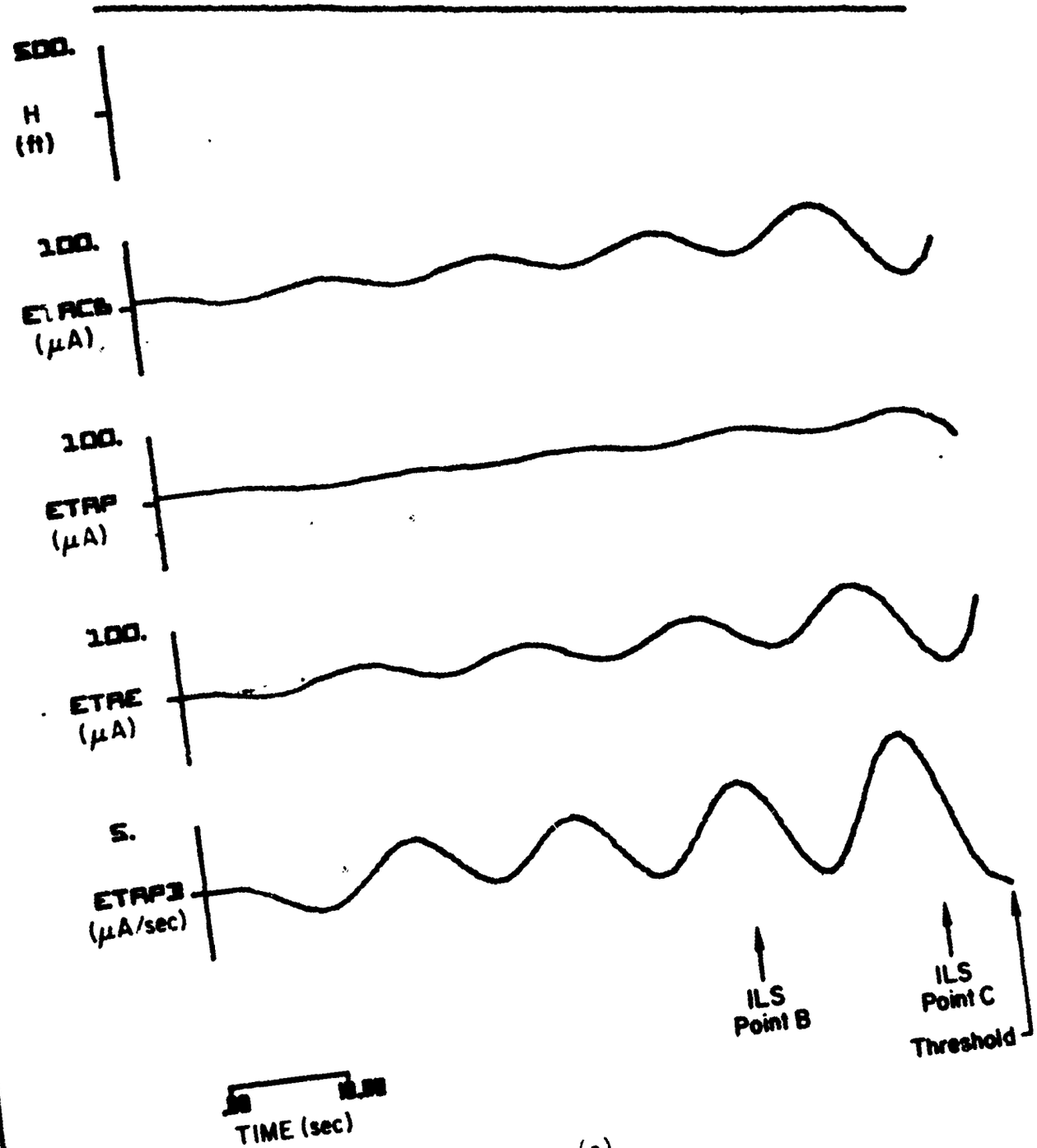

(a)

Figure A-4. Responses of Filter System No. 1 to Prototype Glide Slope Fault No. 3

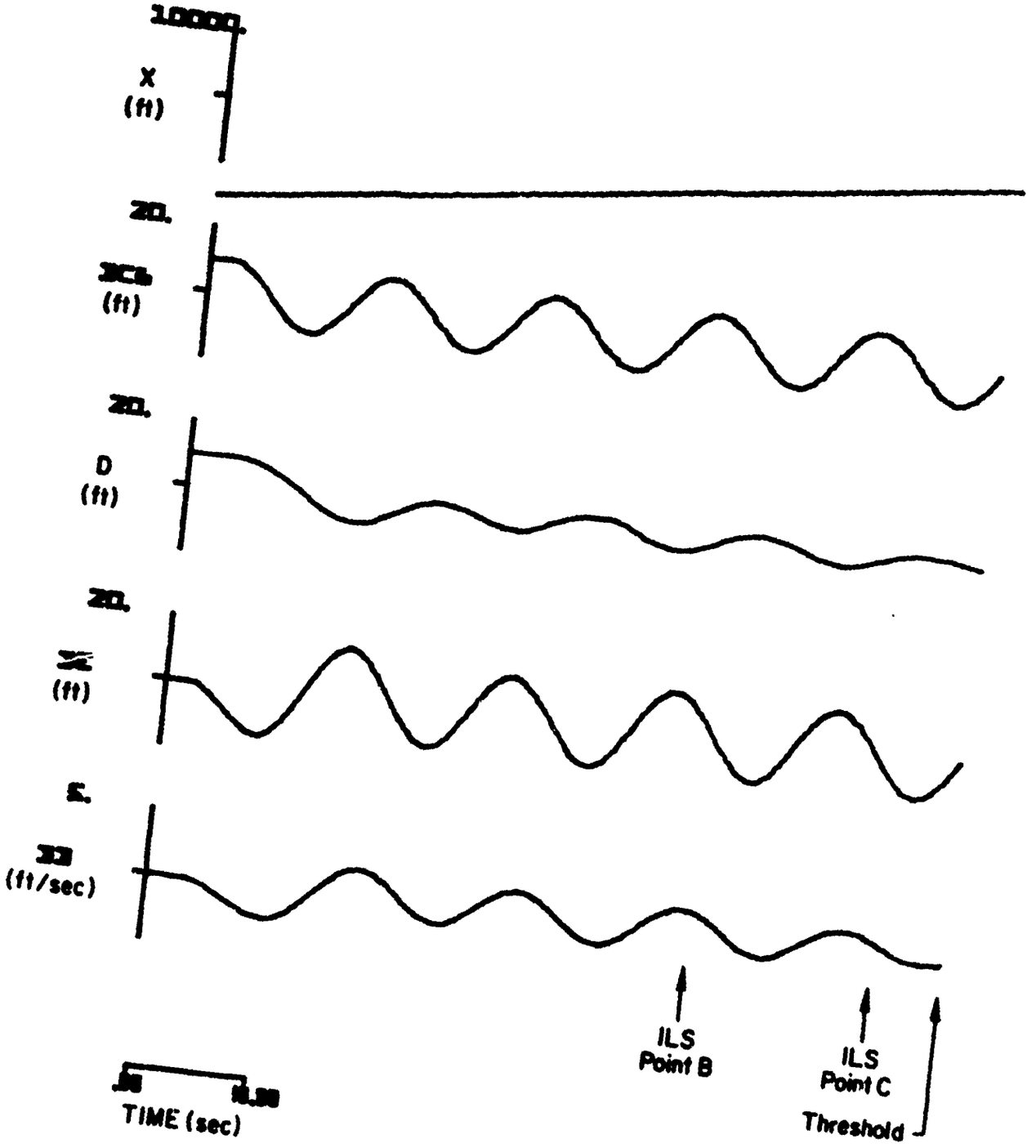

(b)

Figure A-4. (Concluded)

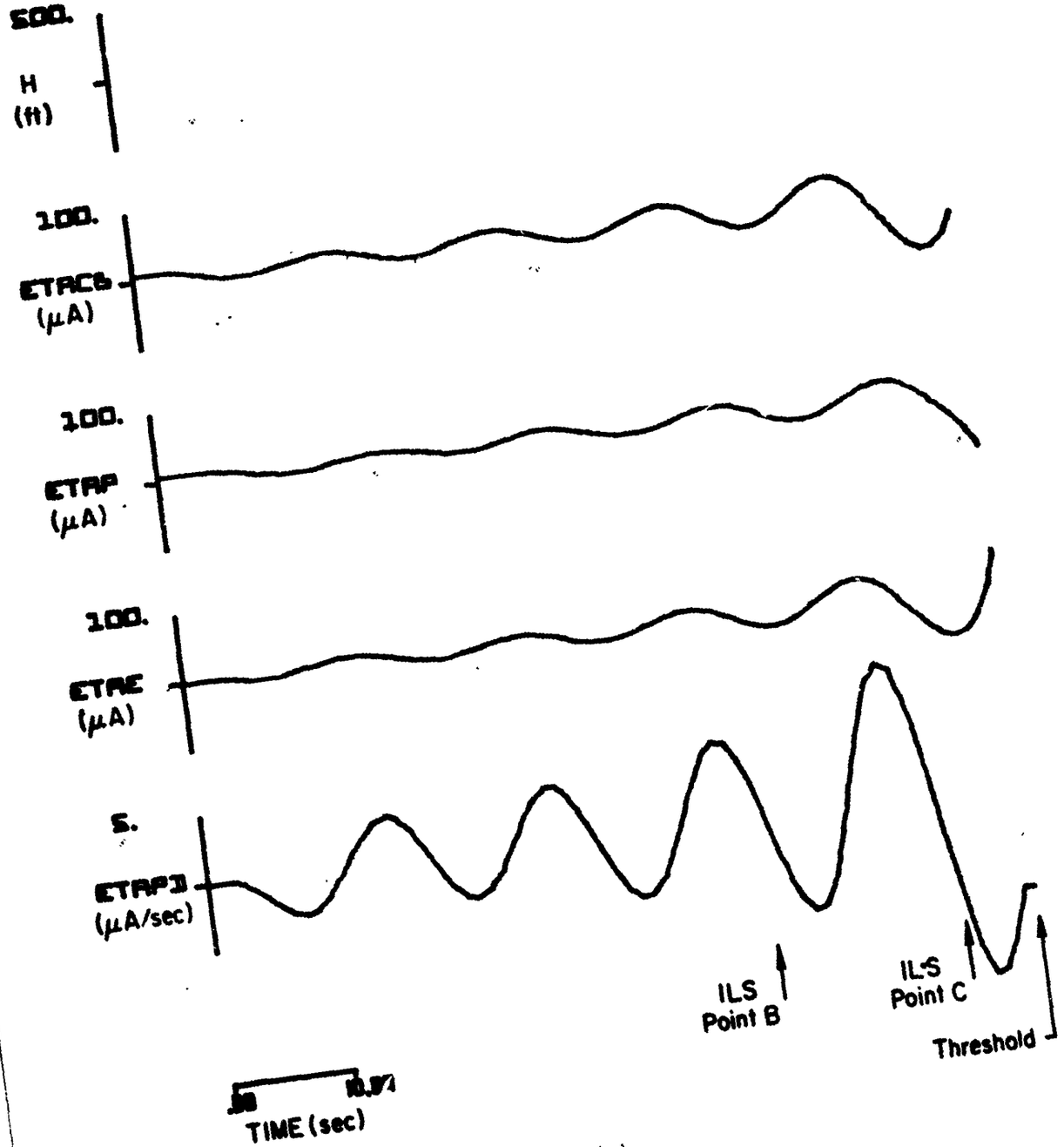

(a)

Figure A-5. Responses of Filter System No. 2 to Prototype Glide Slope Fault No. 7

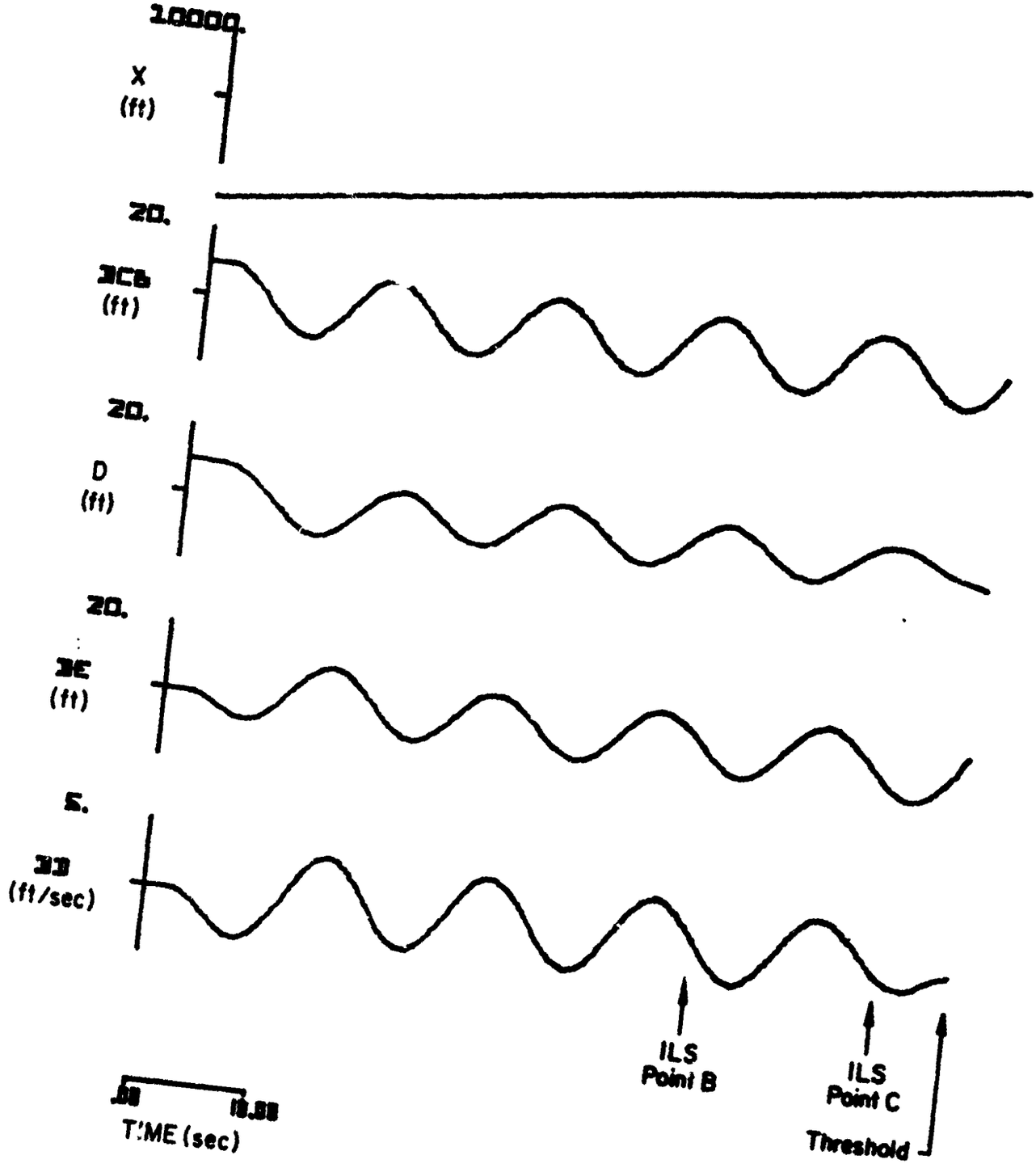

(b)

Figure A-5. (Concluded)

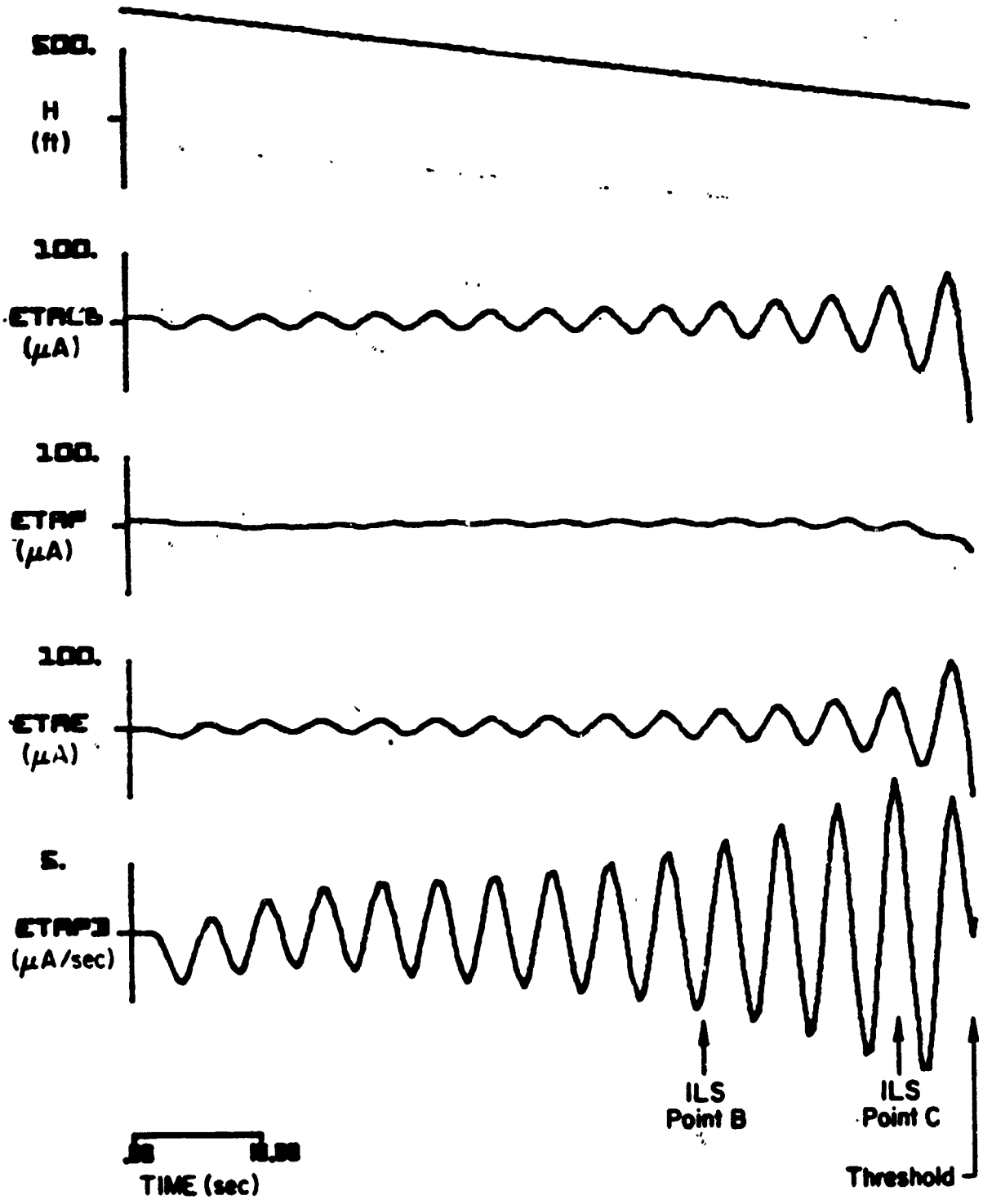

(a)

Figure A-3. Responses of Filter System No. 2 to Prototype Glide Slope Fault No. 4

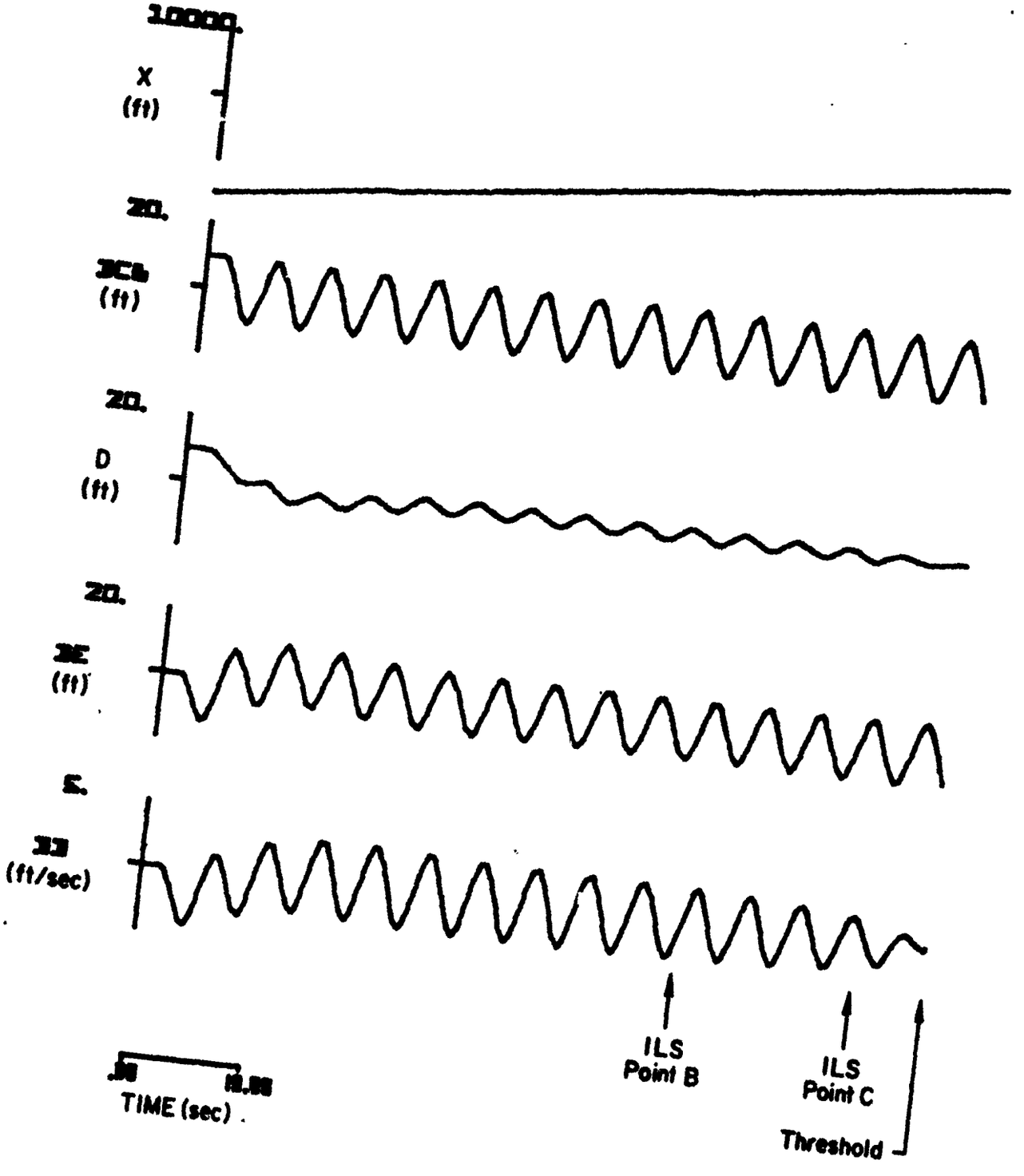

(b)

Figure A-6. (Concluded)

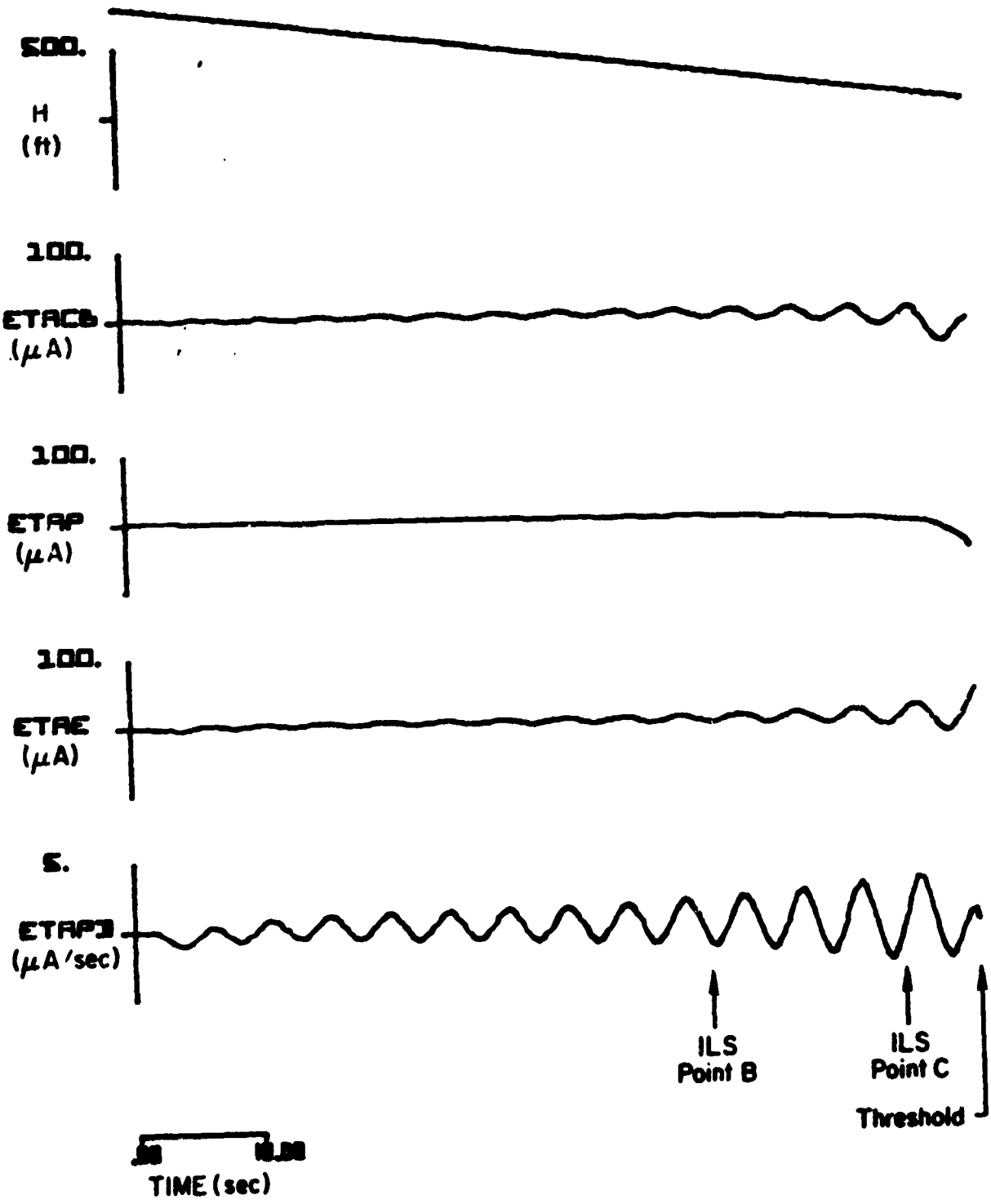

(a)

Figure A-7. Responses of Filter System No. 2 to Prototype Glide Slope Fault No. 5

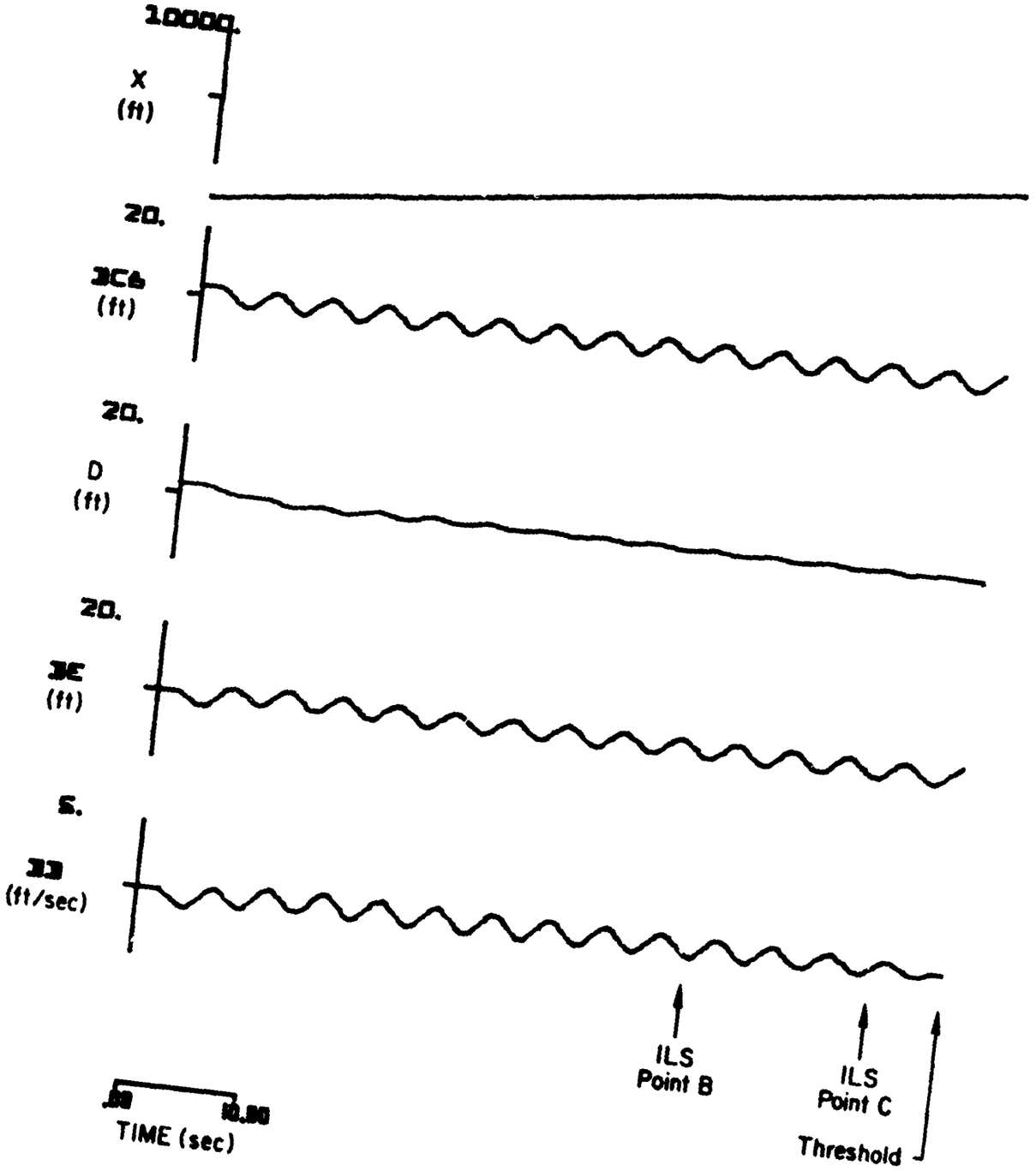

(b)

Figure A-7. (Concluded)

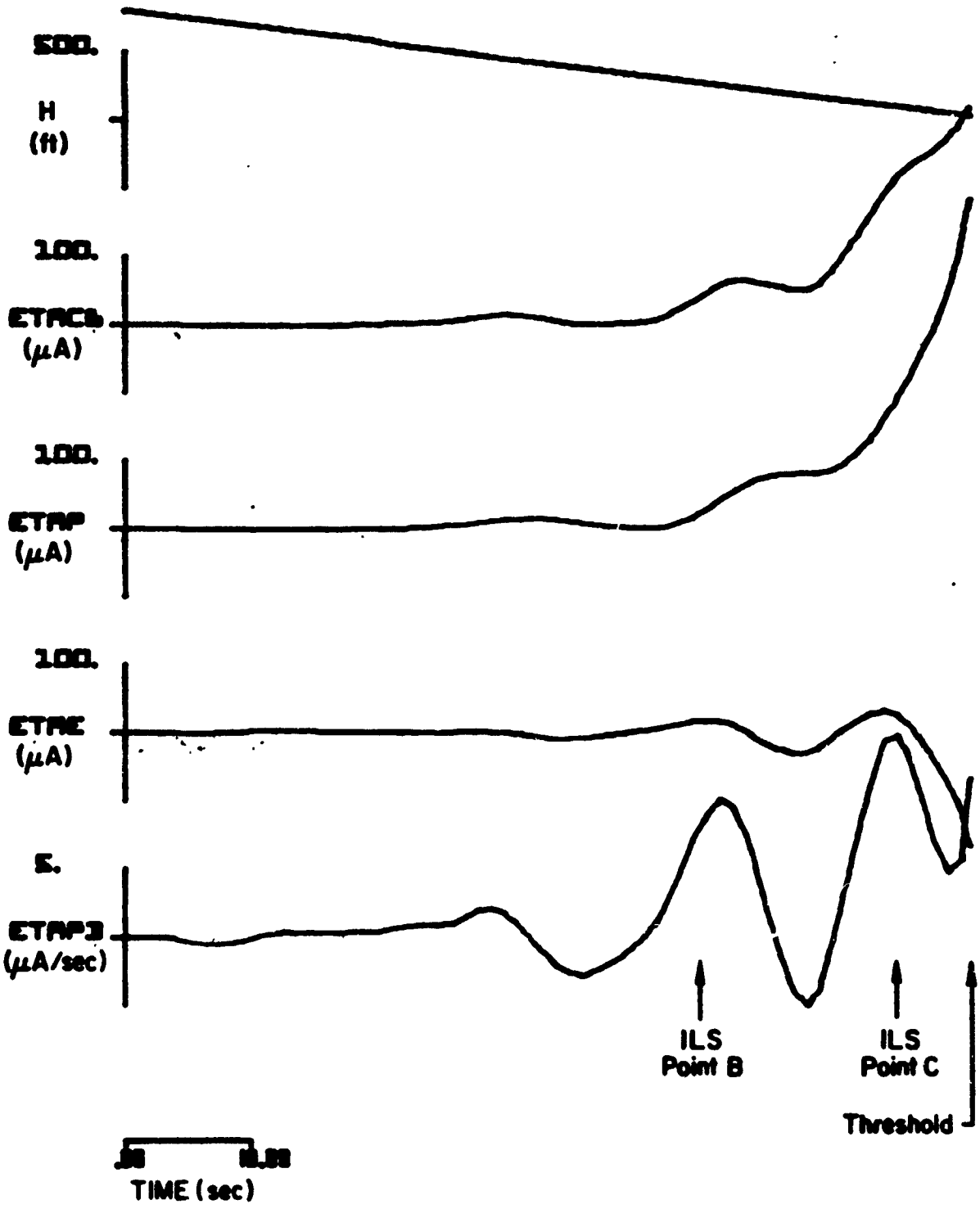

(a)

Figure A-8. Responses of Filter System No. 2 to Prototype Glide Slope Fault No. 6

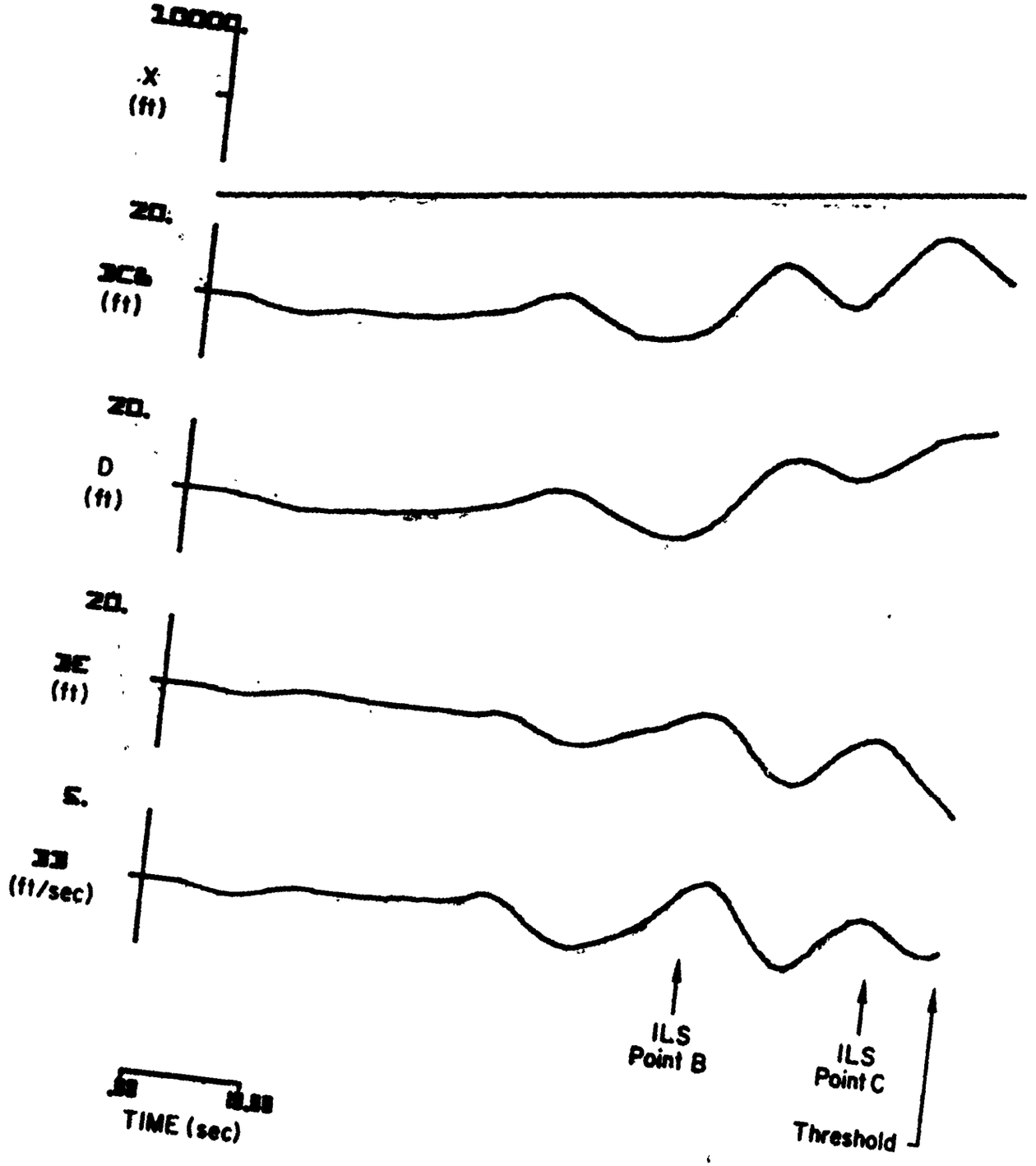

(b)

Figure A-8. (Concluded)

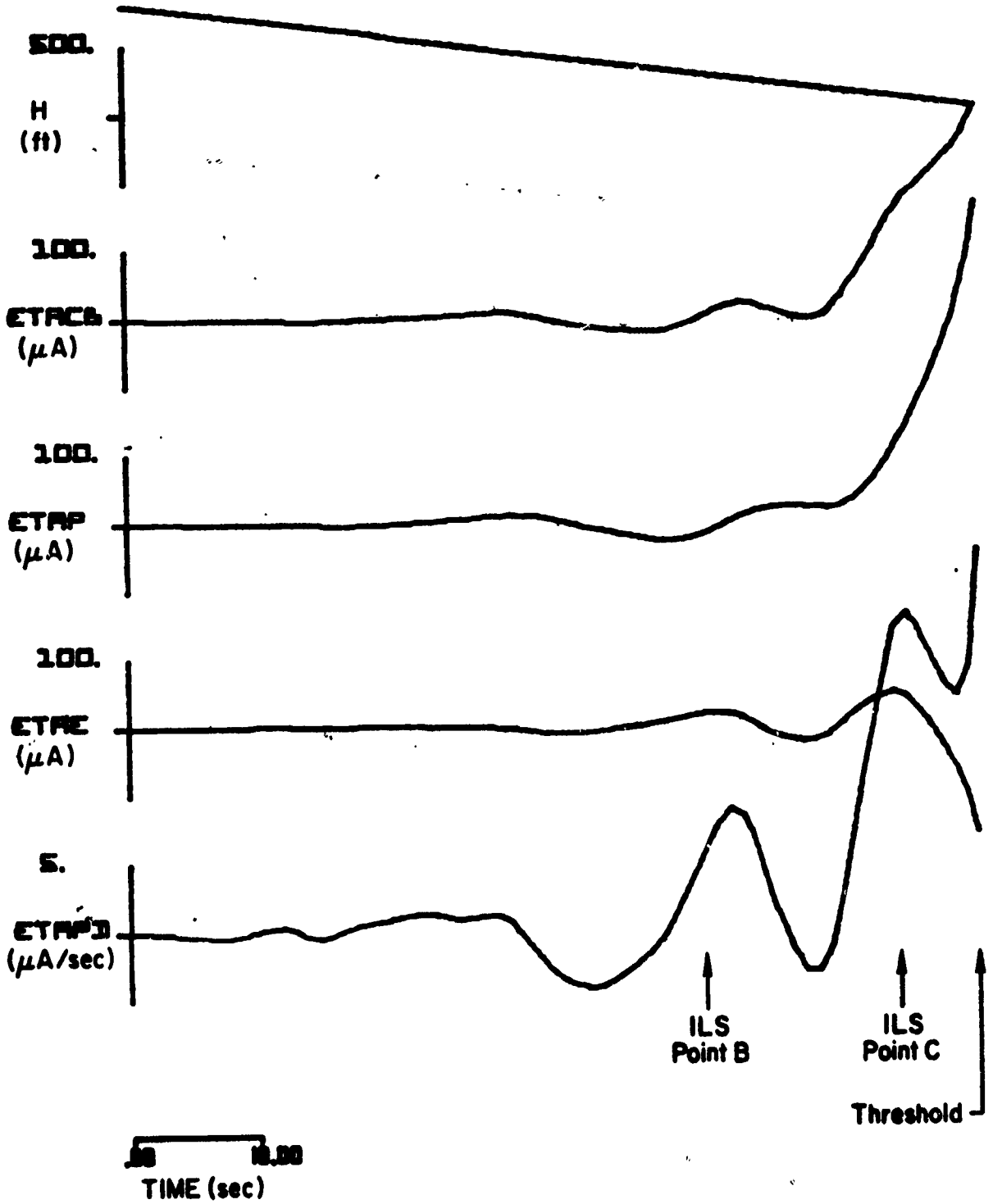

(a)

Figure A-9. Responses of Filter System No. 2 to Prototype Glide Slope Fault No. 7

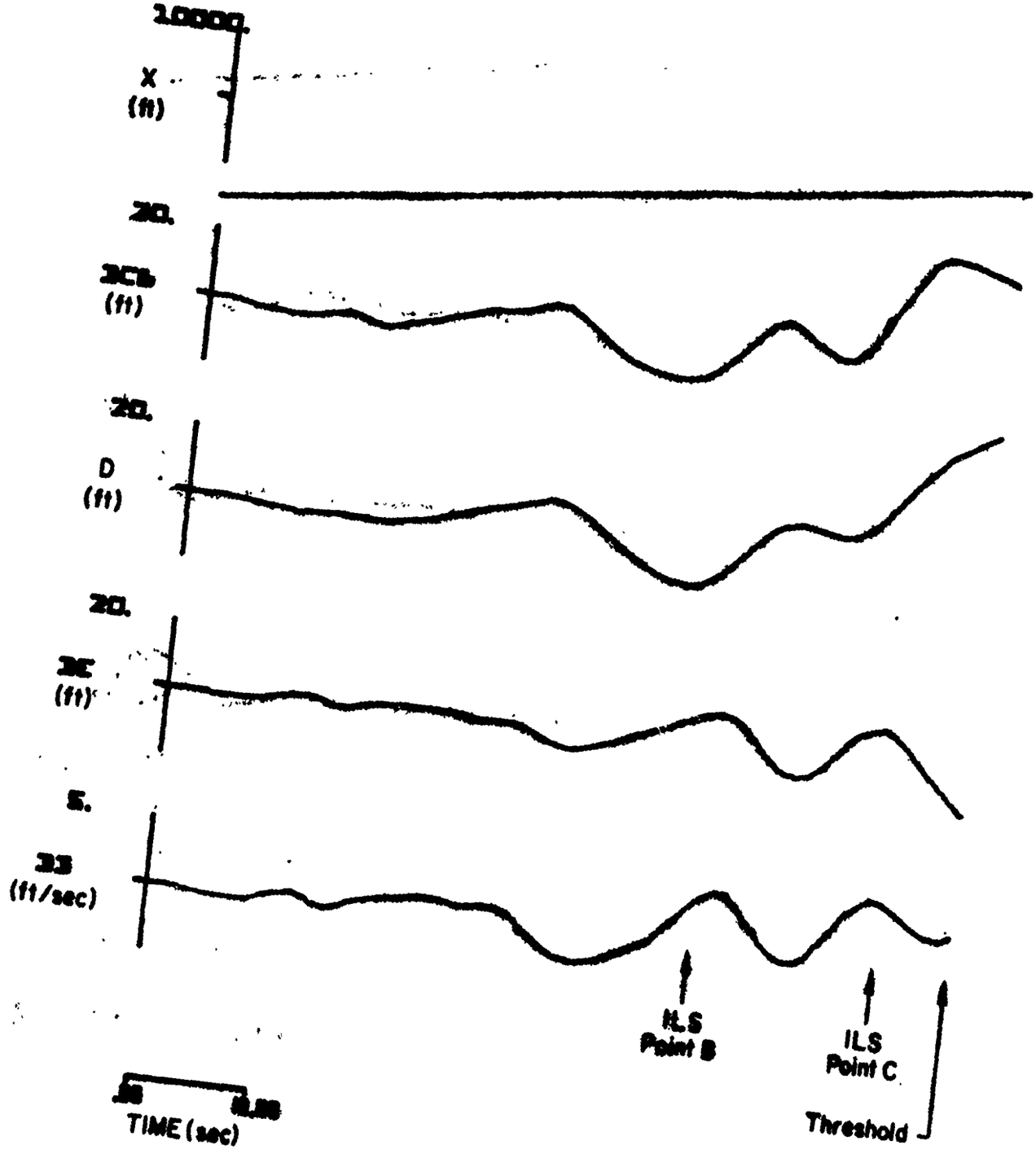

(b)

Figure A-9. (Concluded)

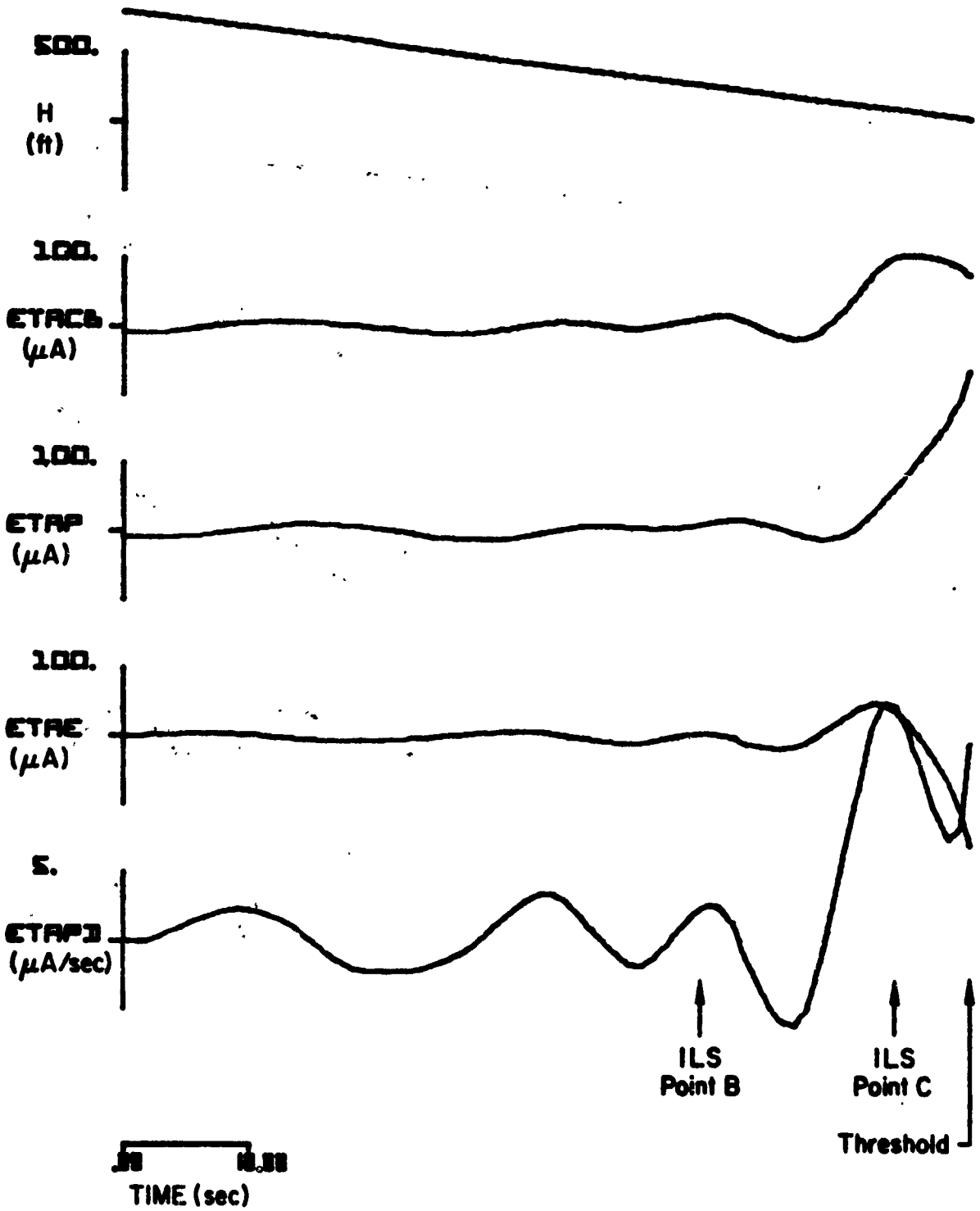

(a)

Figure A-10. Responses of Filter System No. 2 to Prototype Glide Slope Fault No. 8

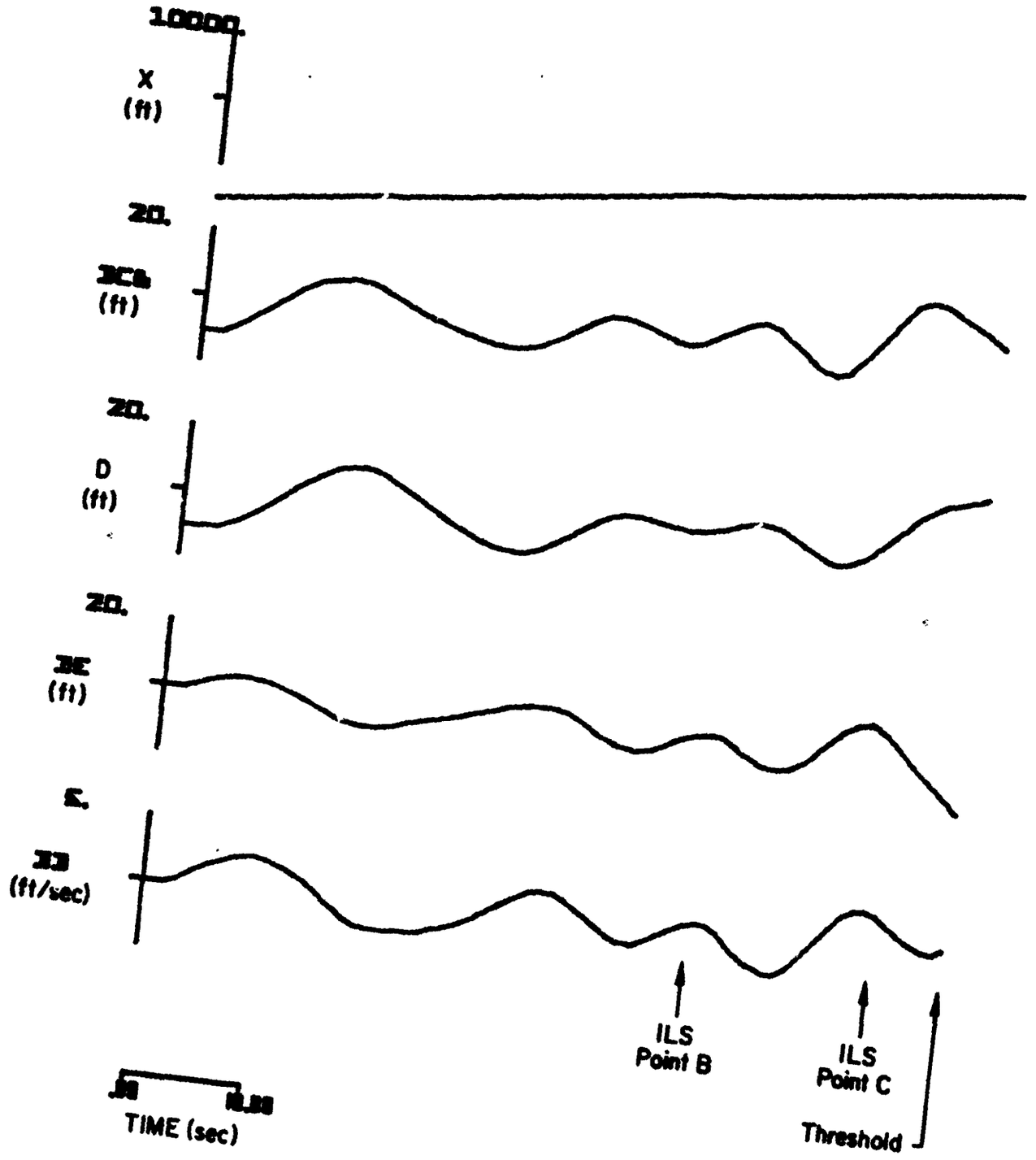

(b)

Figure A-10. (Concluded)

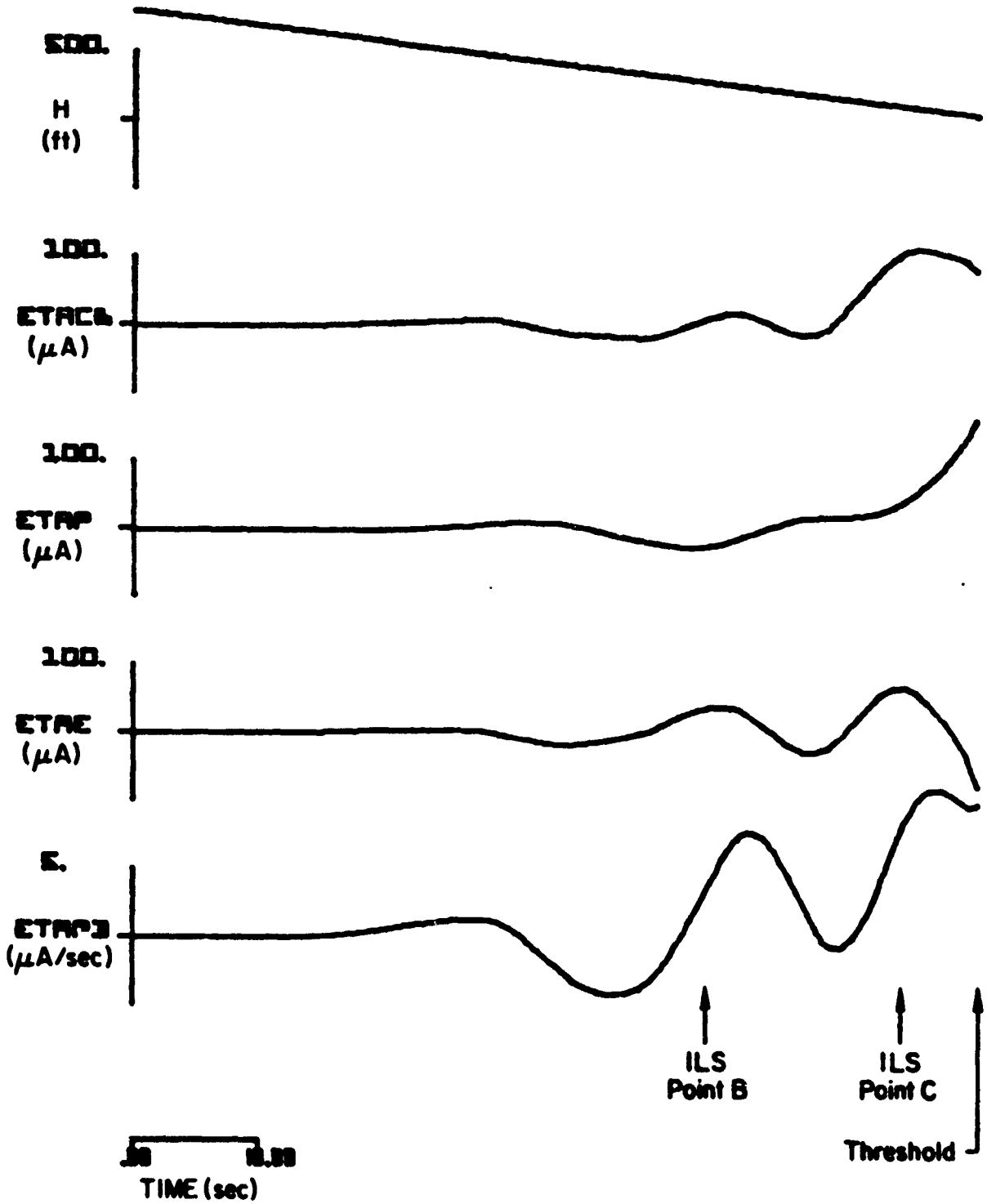

(a)

Figure A-11. Responses of Filter System No. 1 to Prototype Glide Slope Fault No. 9

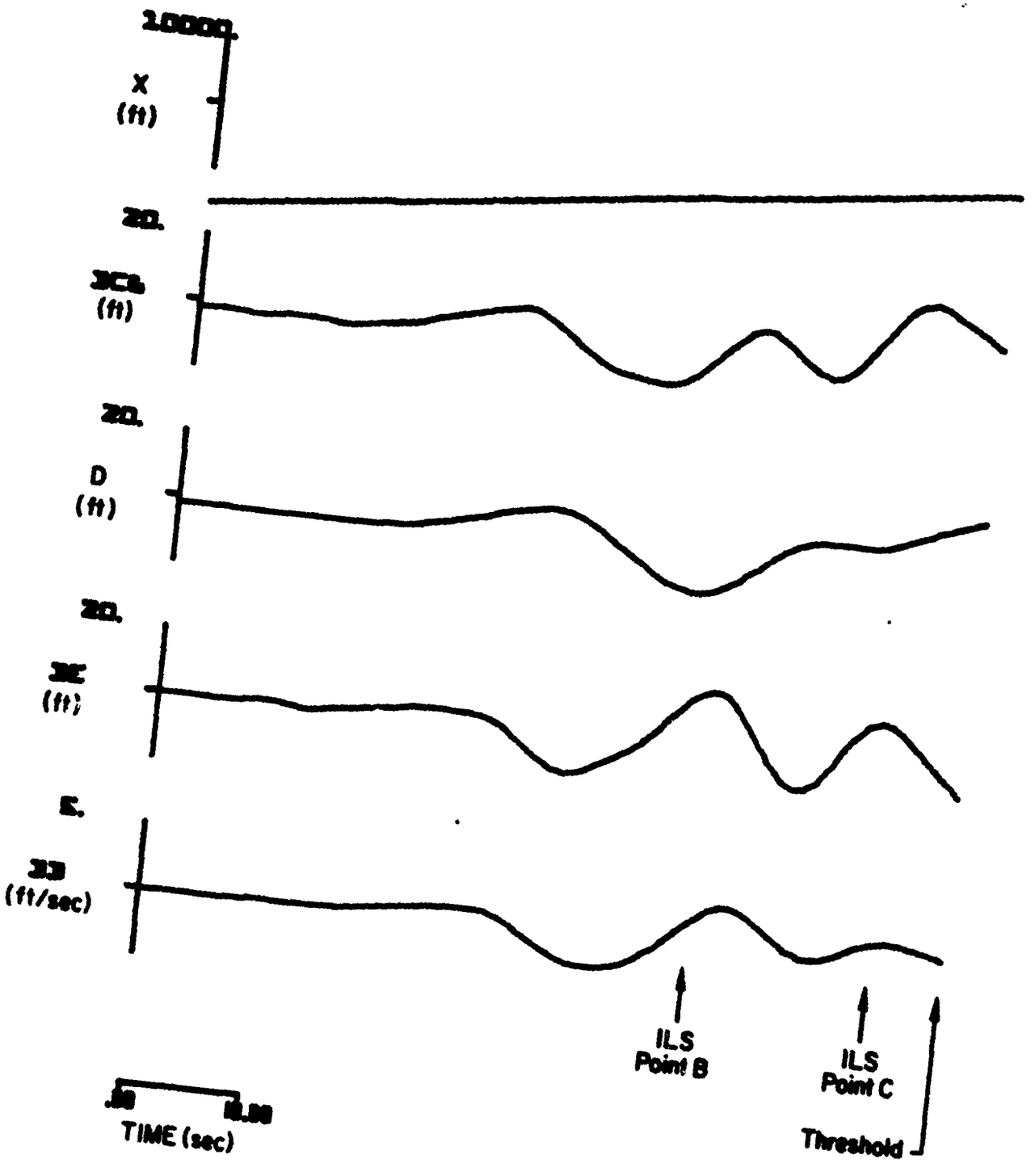

(b)

Figure A-11. (Concluded)

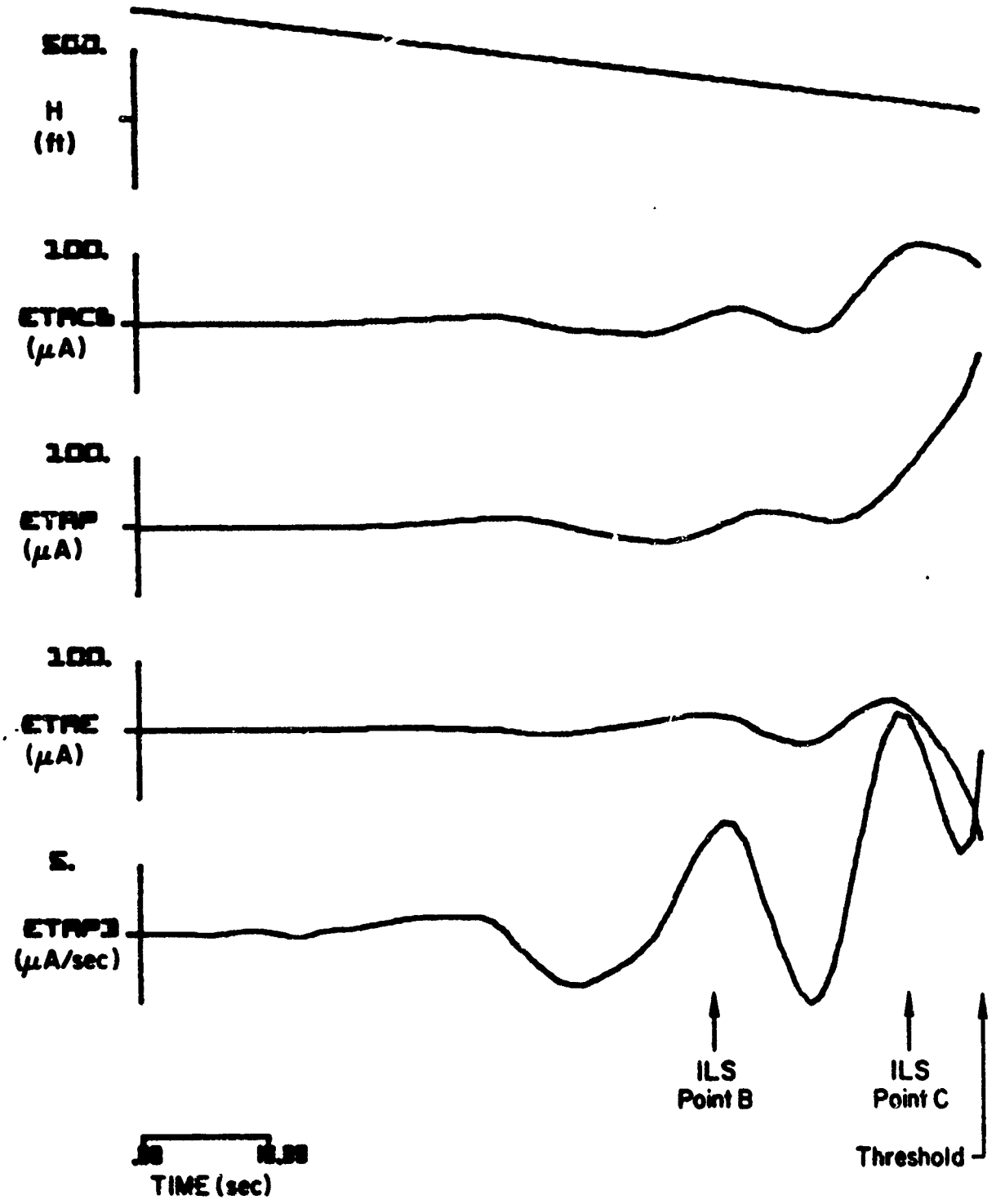

(a)

Figure A-12. Responses of Filter System No. 2 to Prototype Glide Slope Fault No. 9

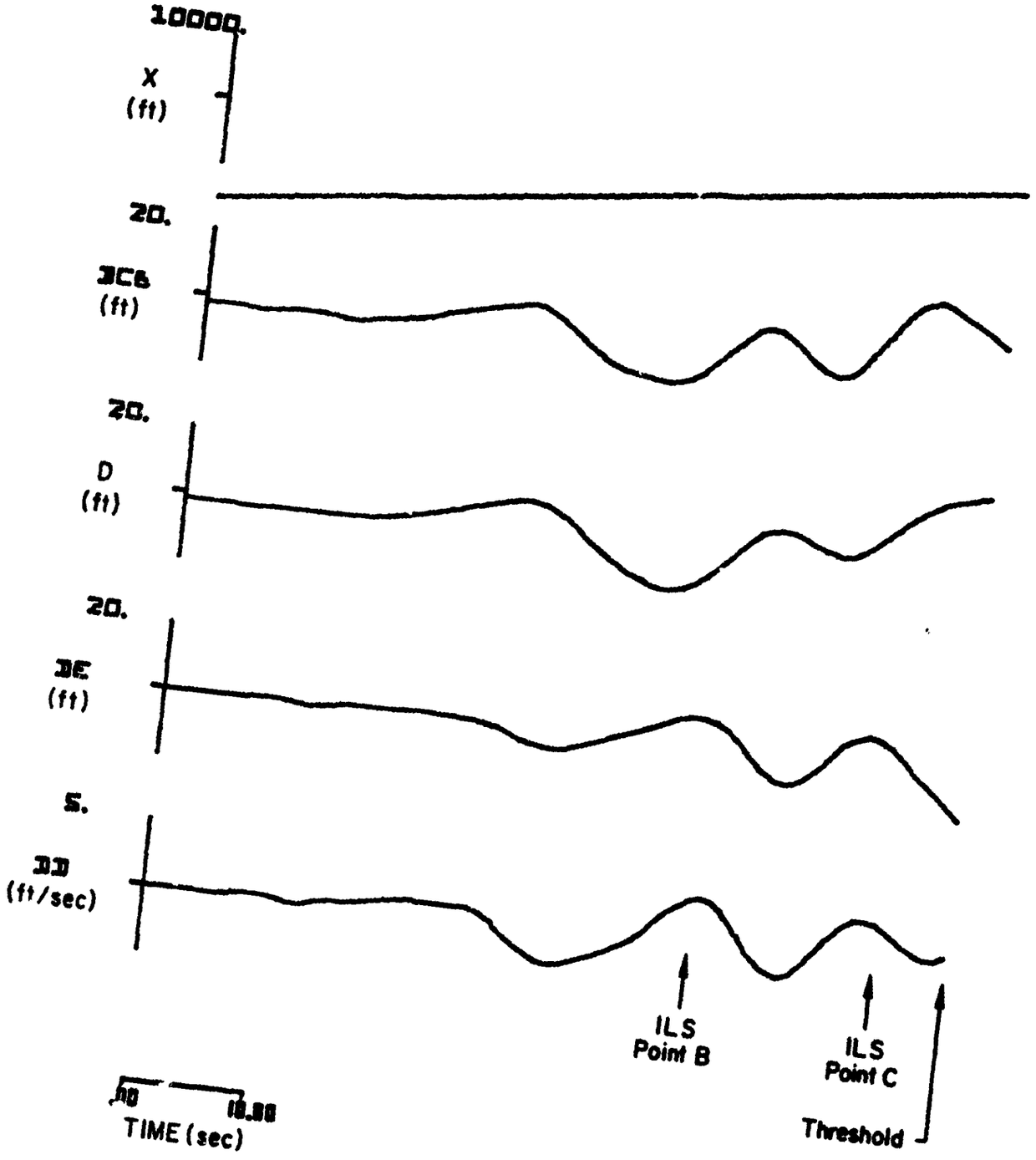

(b)

Figure A-12. (Concluded)

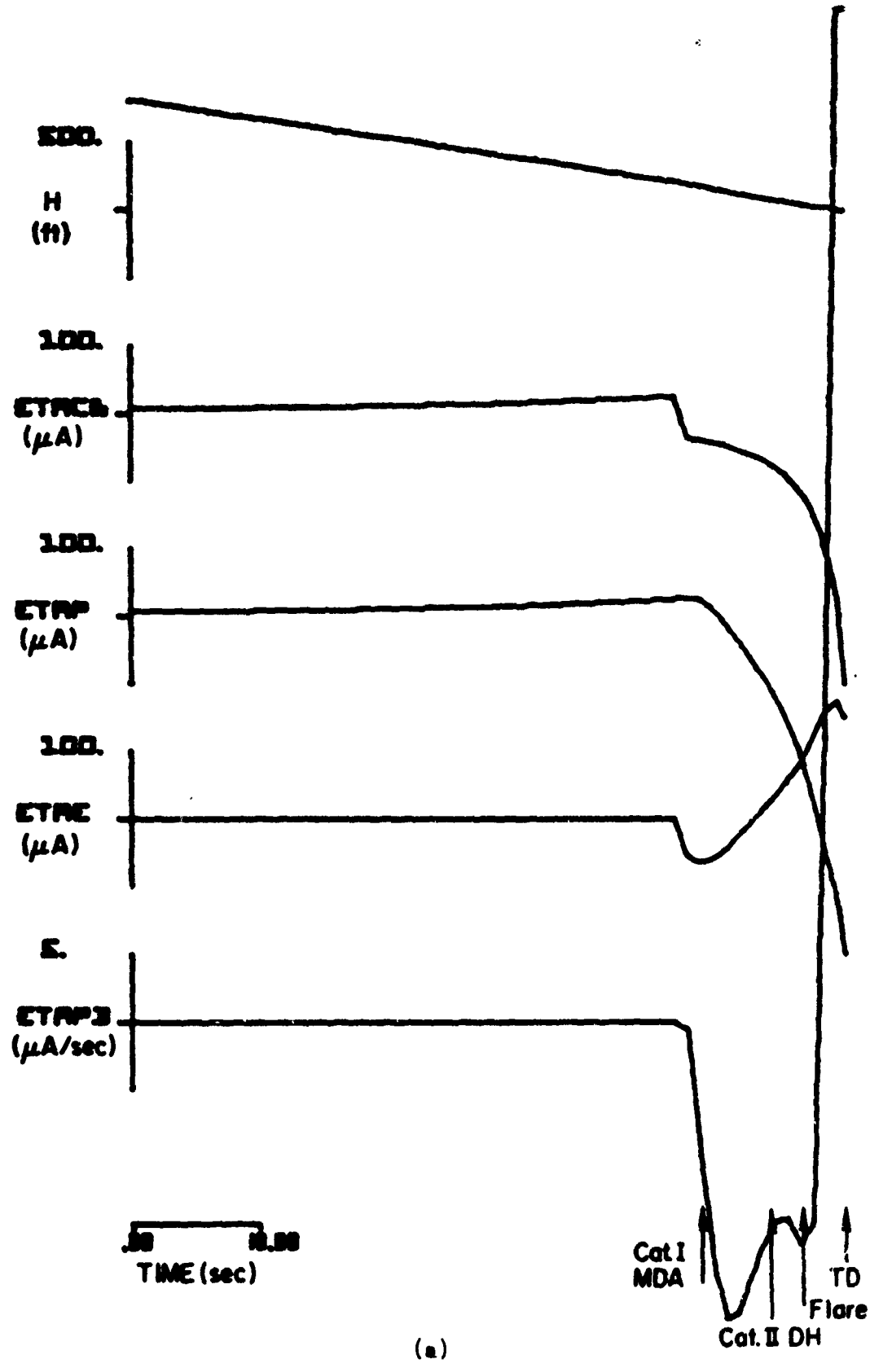

(a)

Figure A-13. Responses of the CV-880 Aircraft with LSI Automatic Landing System and Conventional Glide Slope Coupling to Prototype Glide Slope Fault No. 1

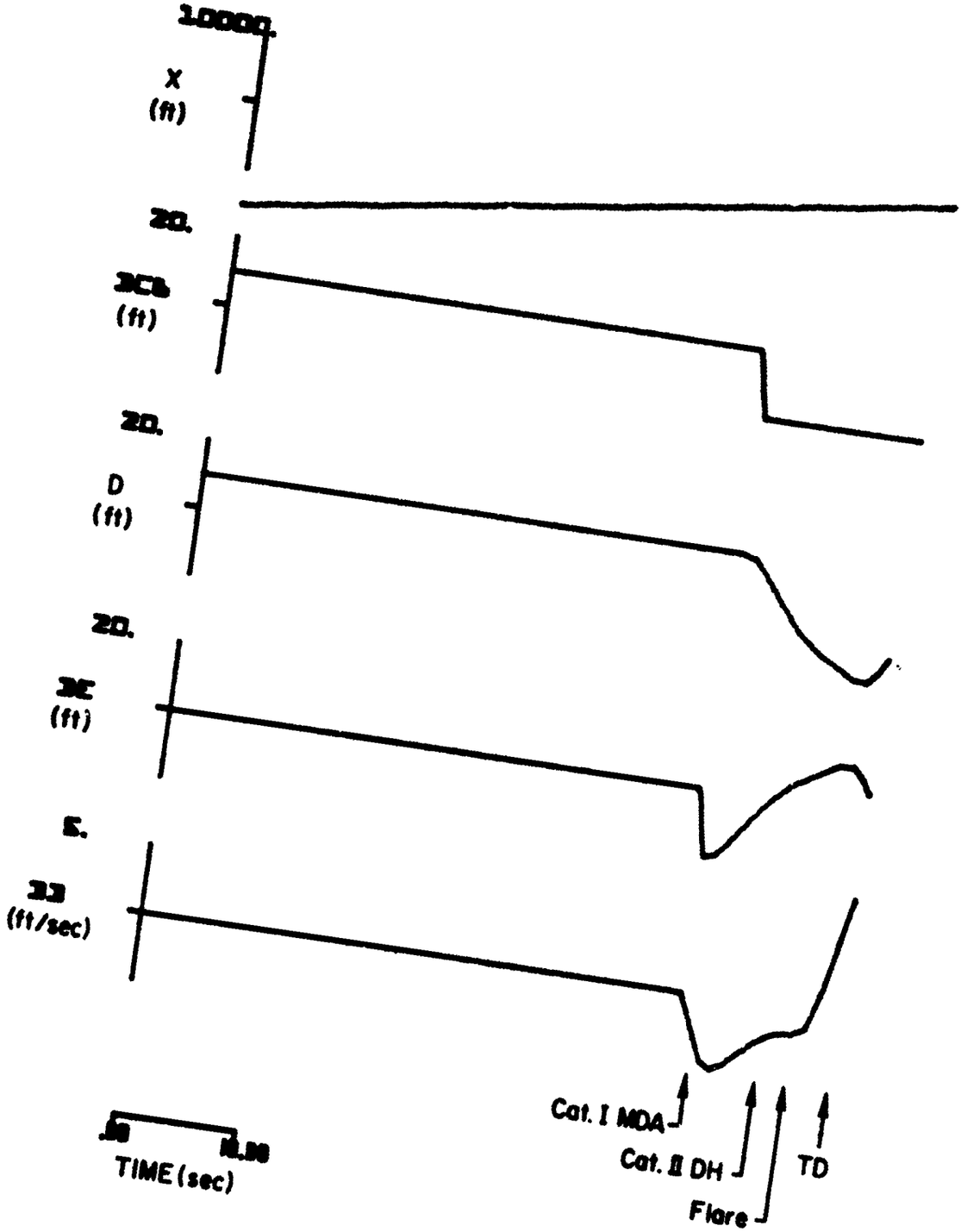

(b)

Figure A-13. (Continued)

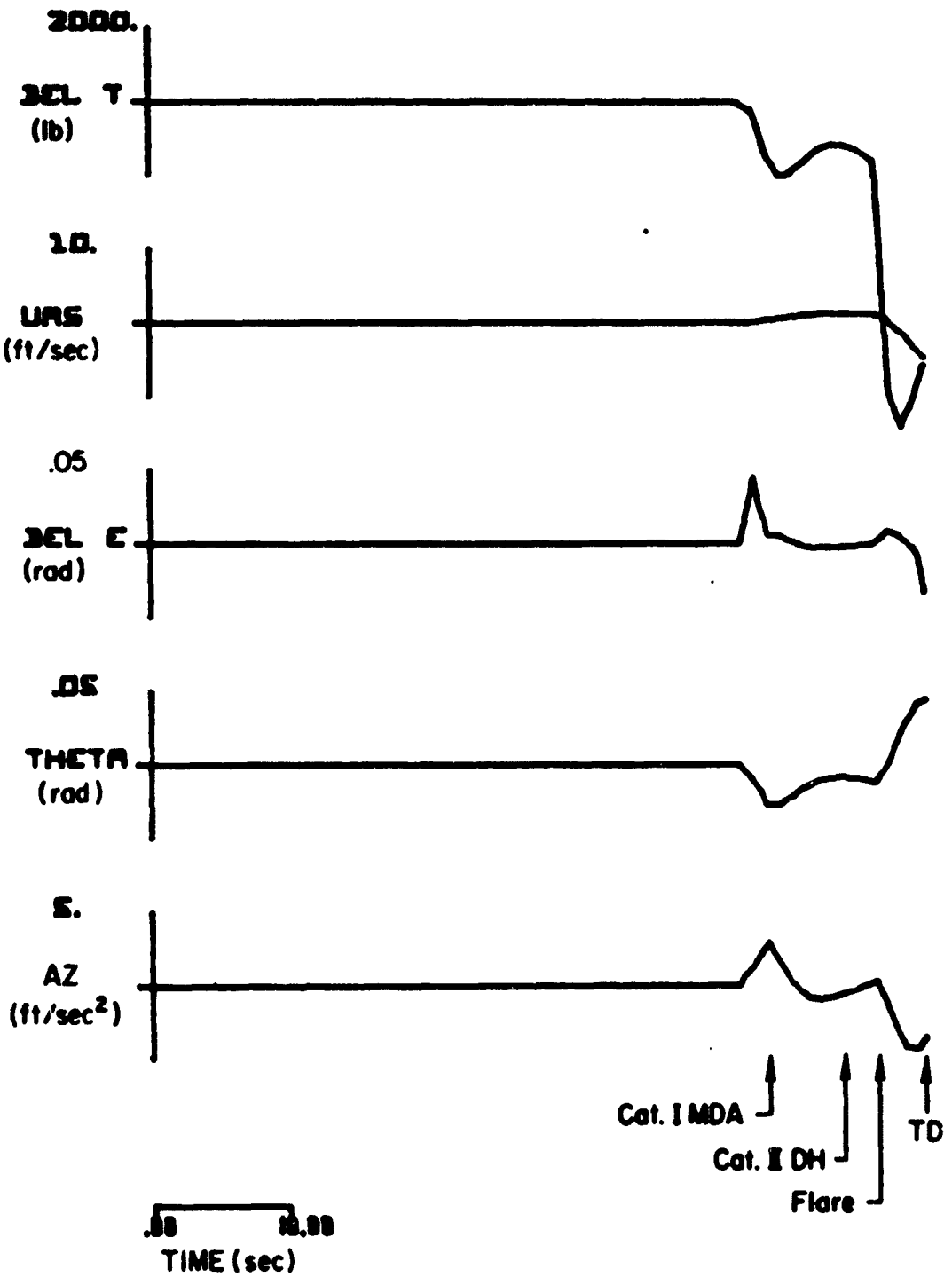

(c)

Figure A-13. (Concluded)

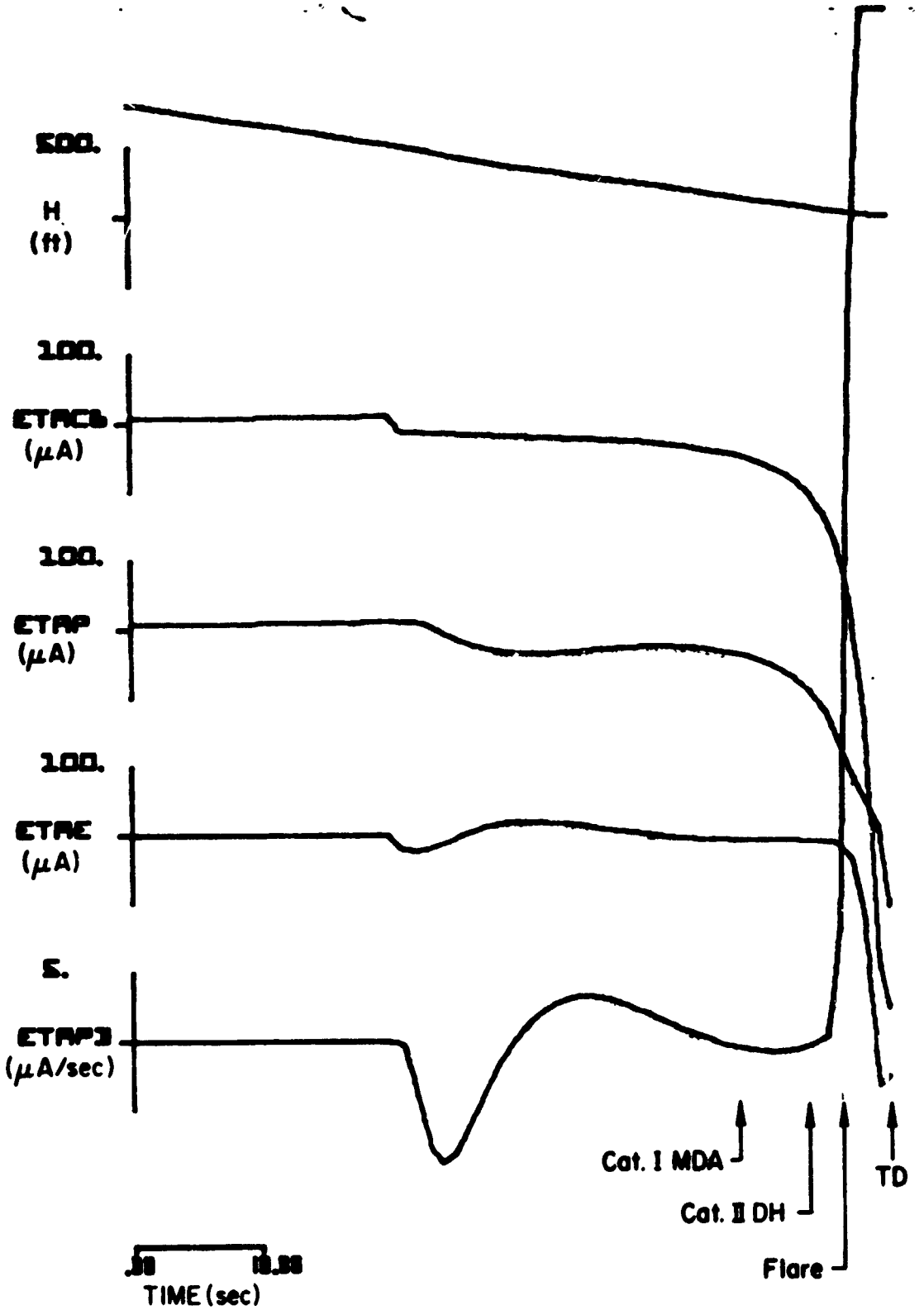

(a)

Figure A-14. Responses of the CV-880 Aircraft with LSI Automatic Landing System and Conventional Glide Slope Coupling to Prototype Glide Slope Fault No. 2

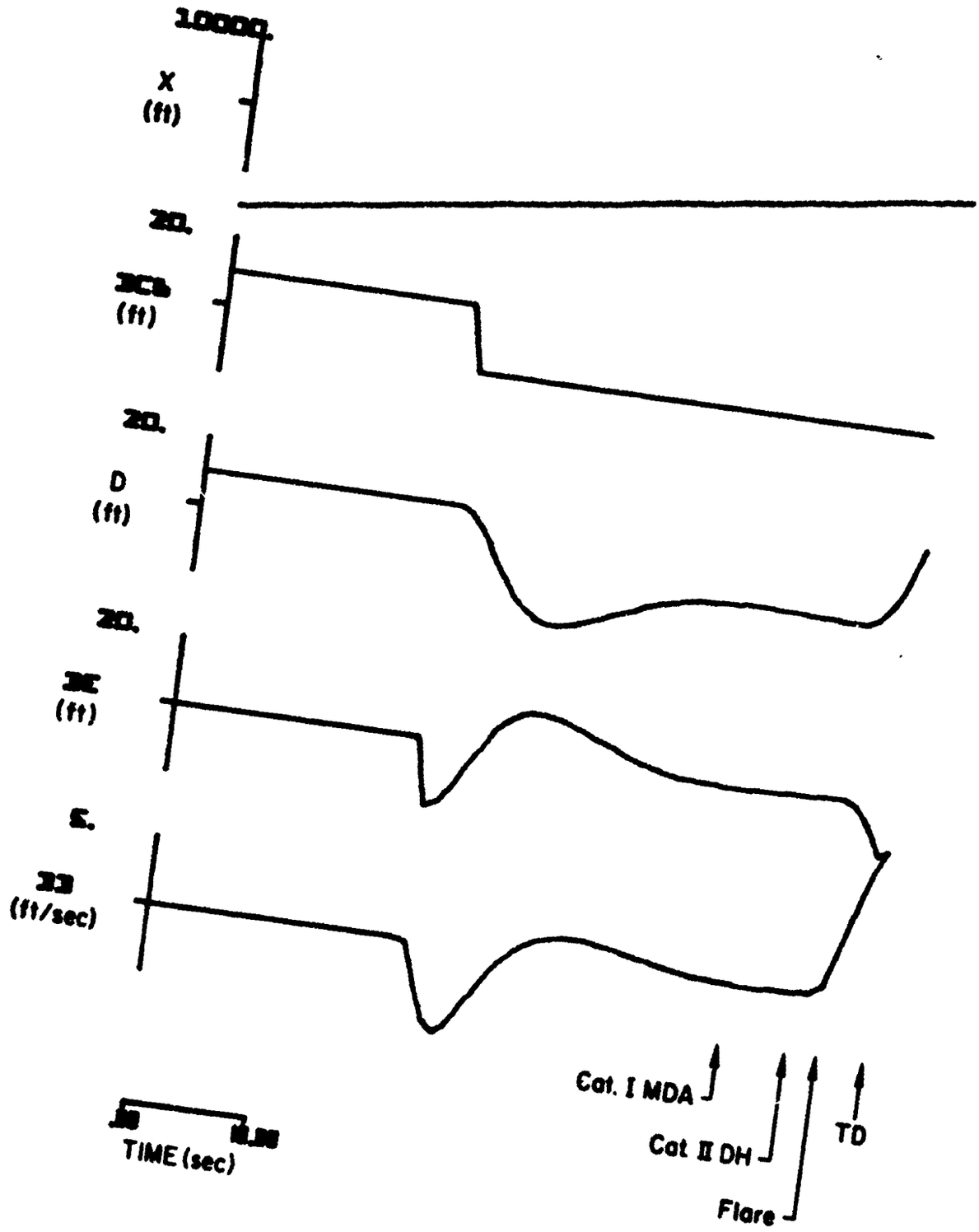

(b)

Figure A-14. (Continued)

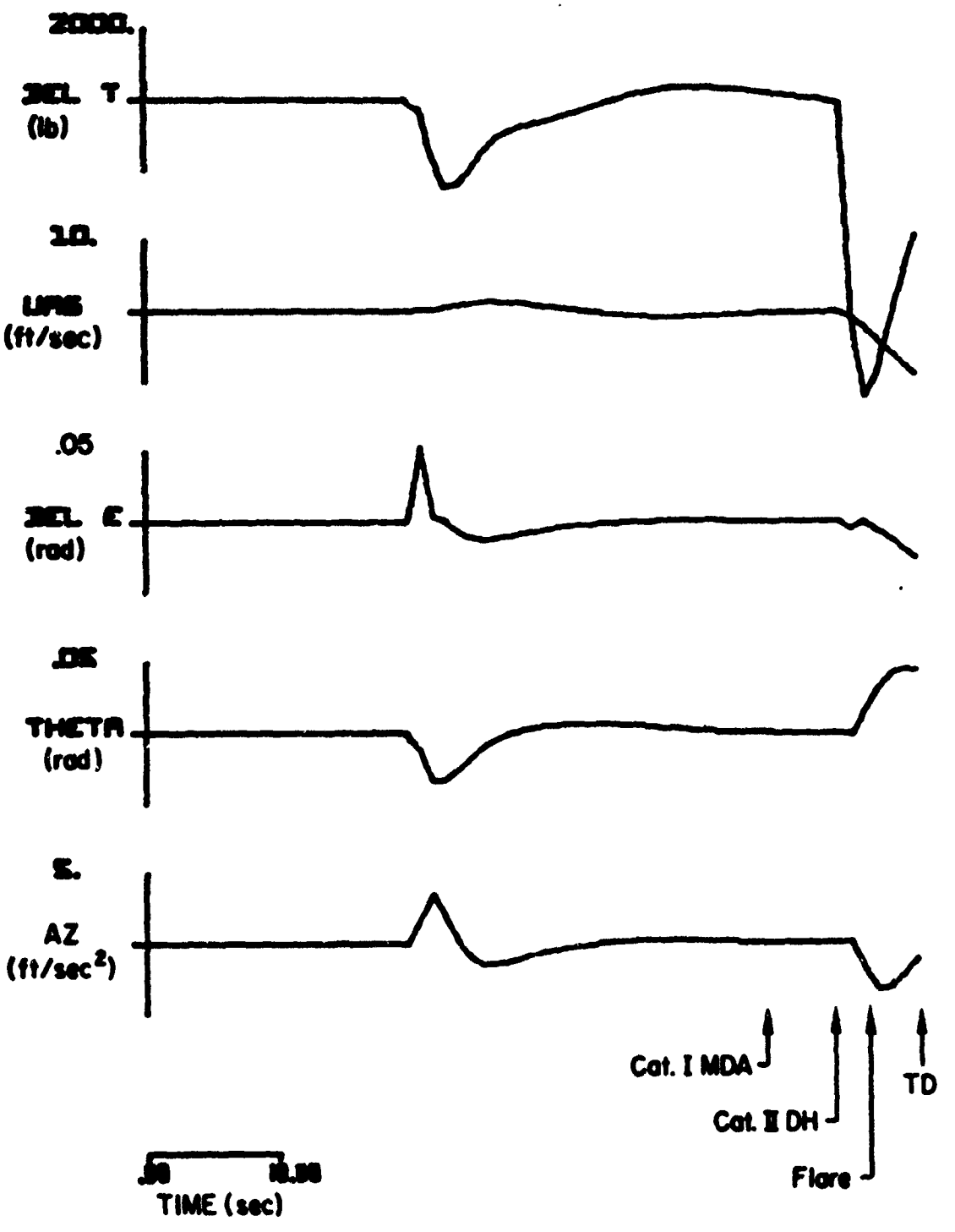

(c)

Figure A-14. (Concluded)

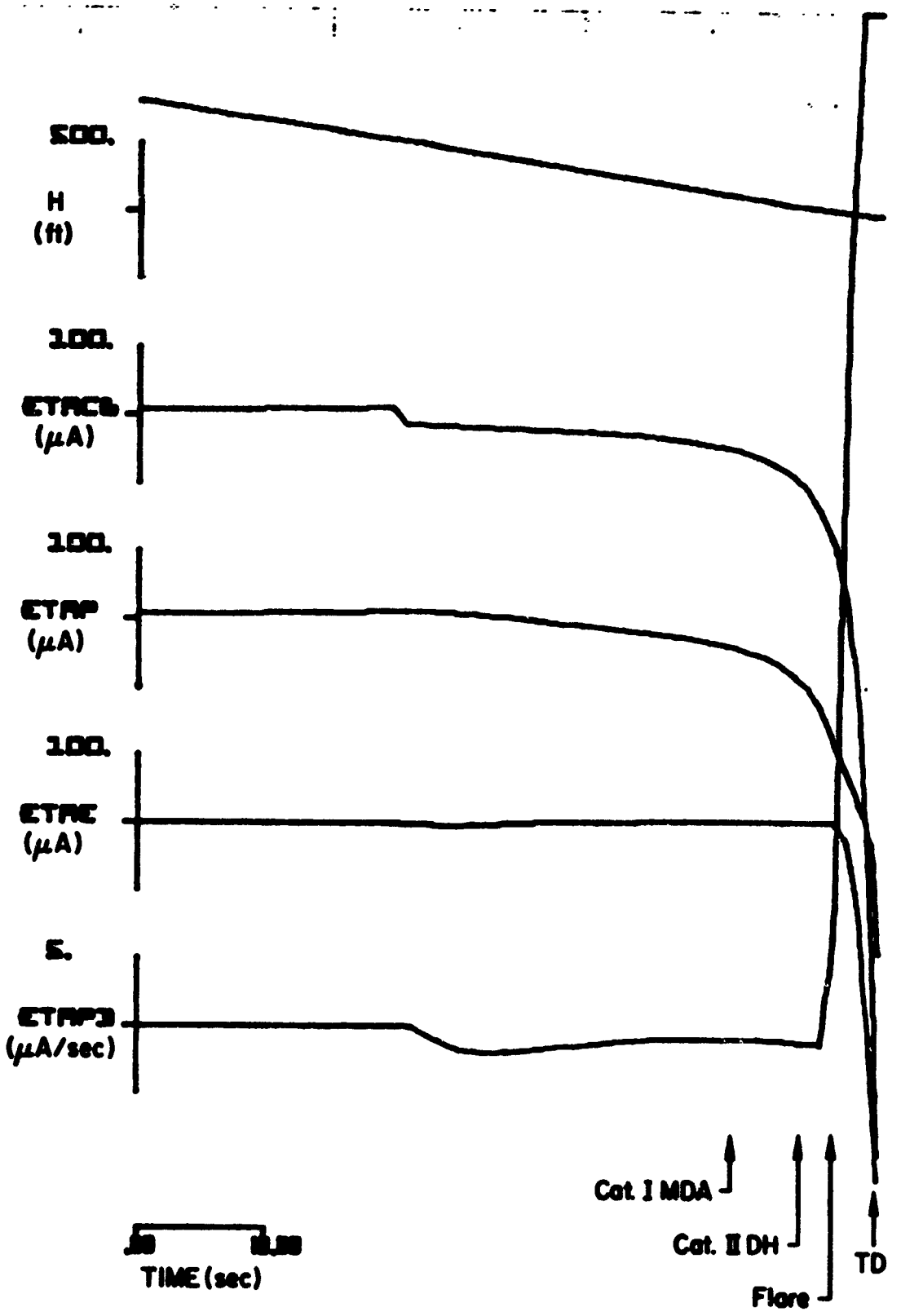

(a)

Figure A-15. Responses of the CV-880 Aircraft with LSI Automatic Landing System and Inertially Augmented Glide Slope Coupling to Prototype Glide Slope Fault No. 2

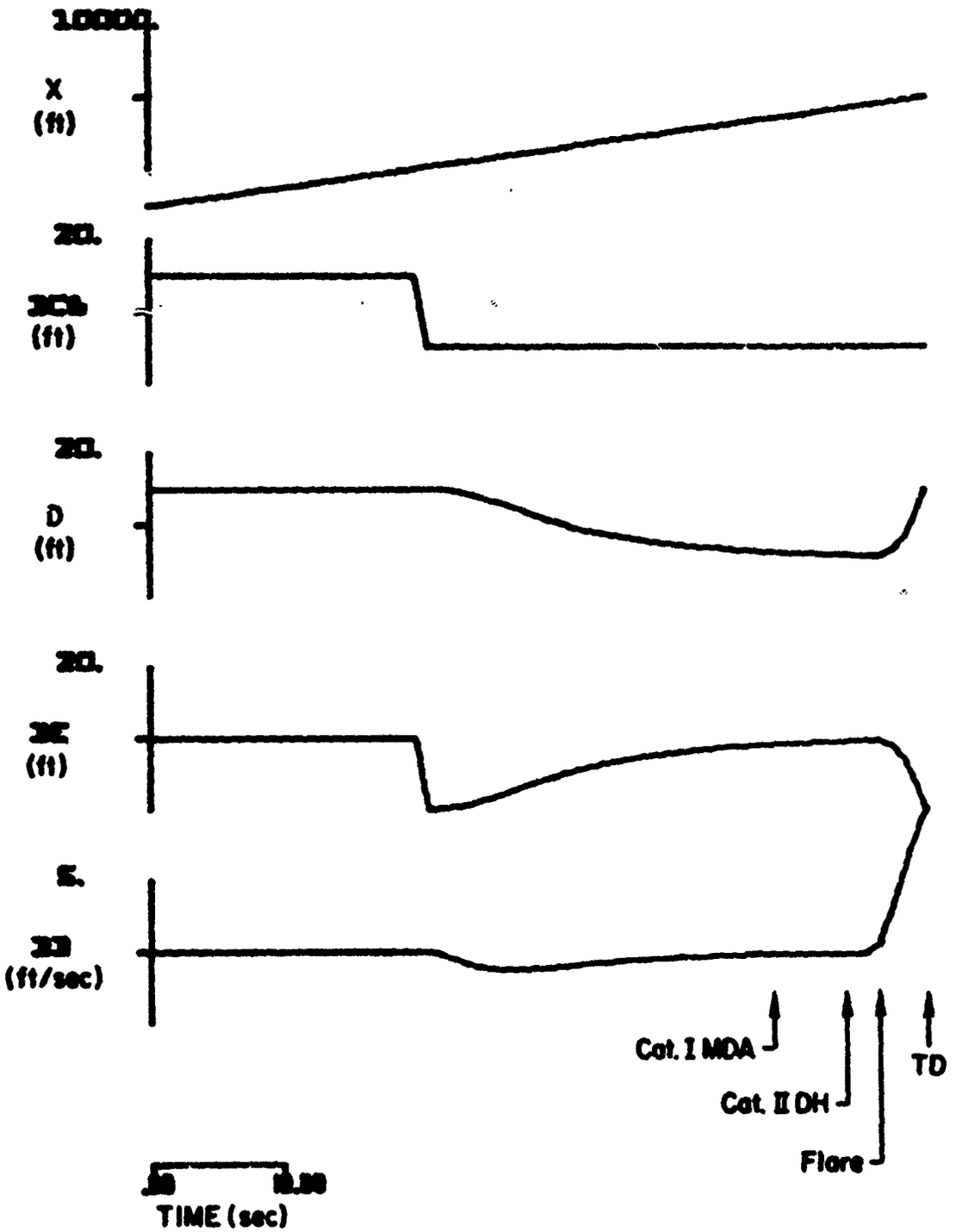

(b)

Figure A-15. (Continued)

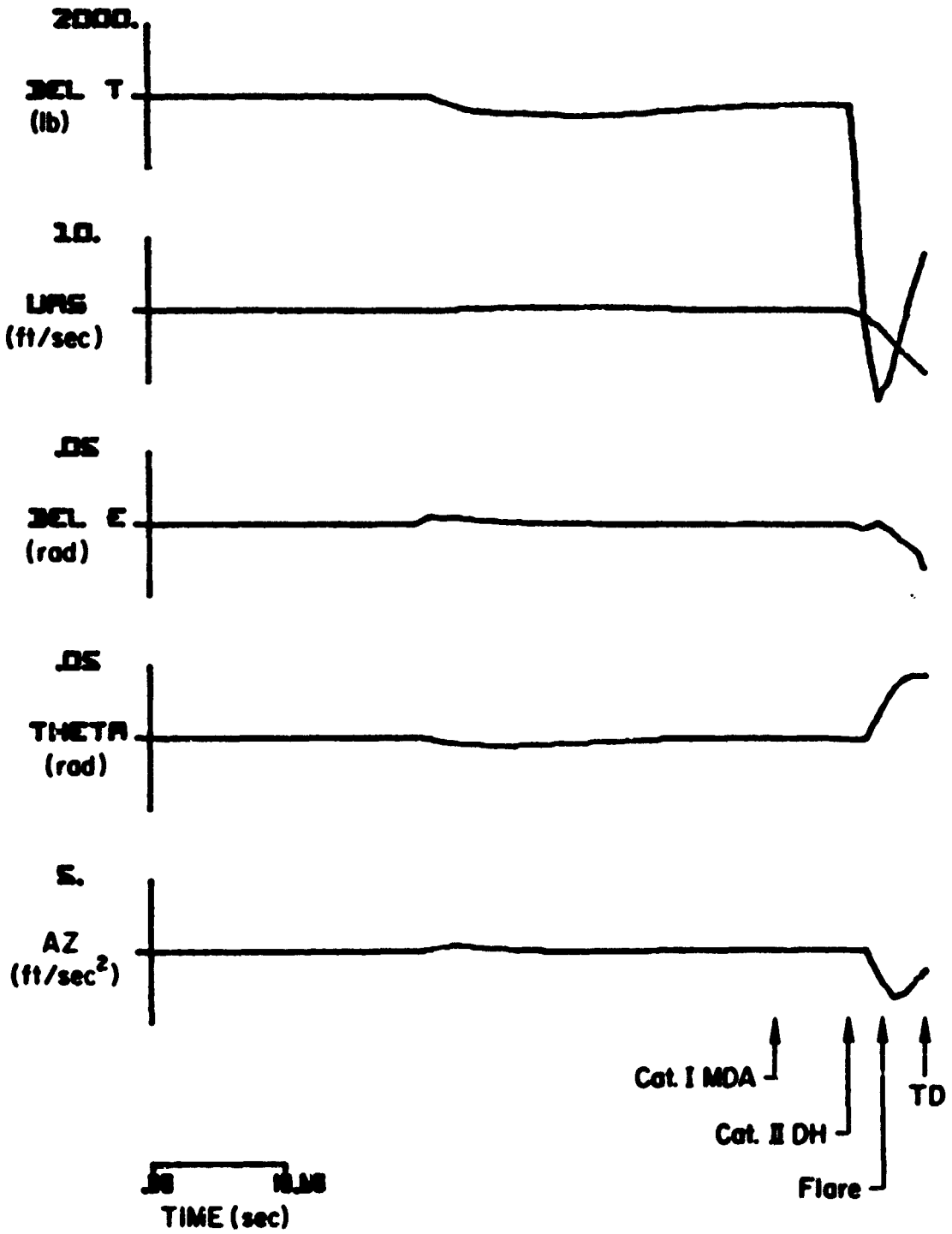

(c)

Figure A-15. (Concluded)

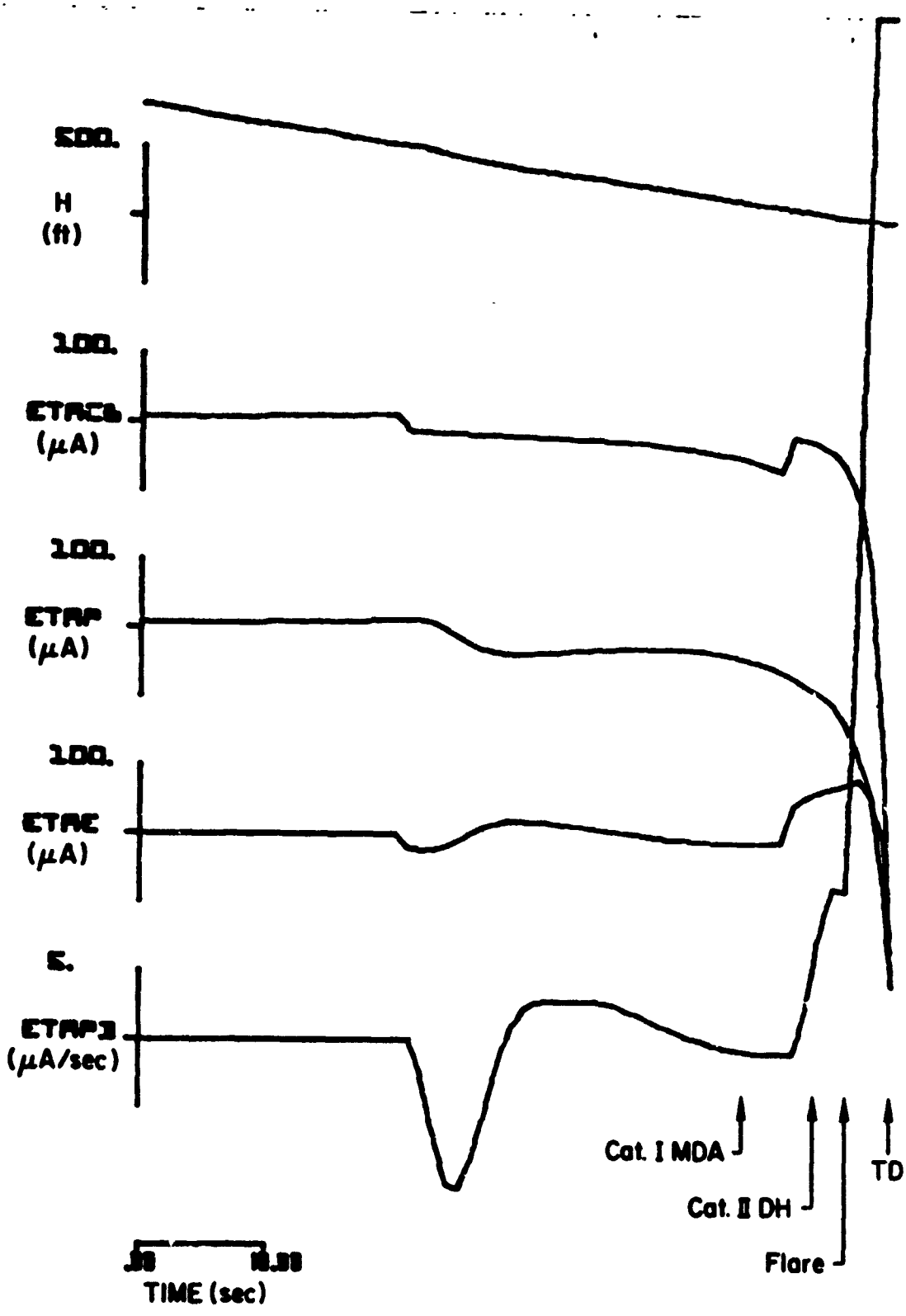

(a)

Figure A-16. Responses of the CV-880 Aircraft with Manually Controlled Flight Director System and Conventional Glide Slope Coupling to Prototype Glide Slope Fault No. 2

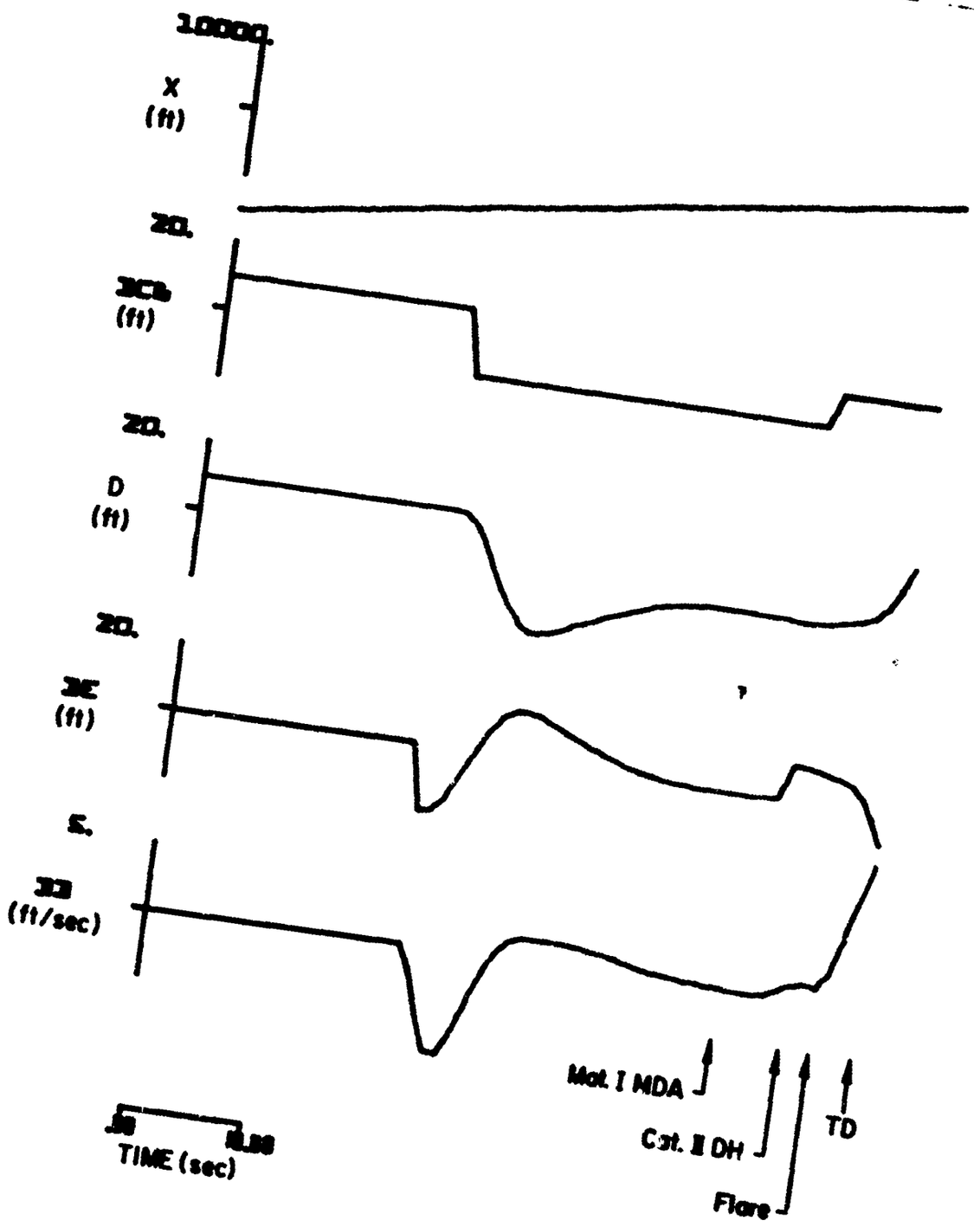

(b)

Figure A-16. (Continued)

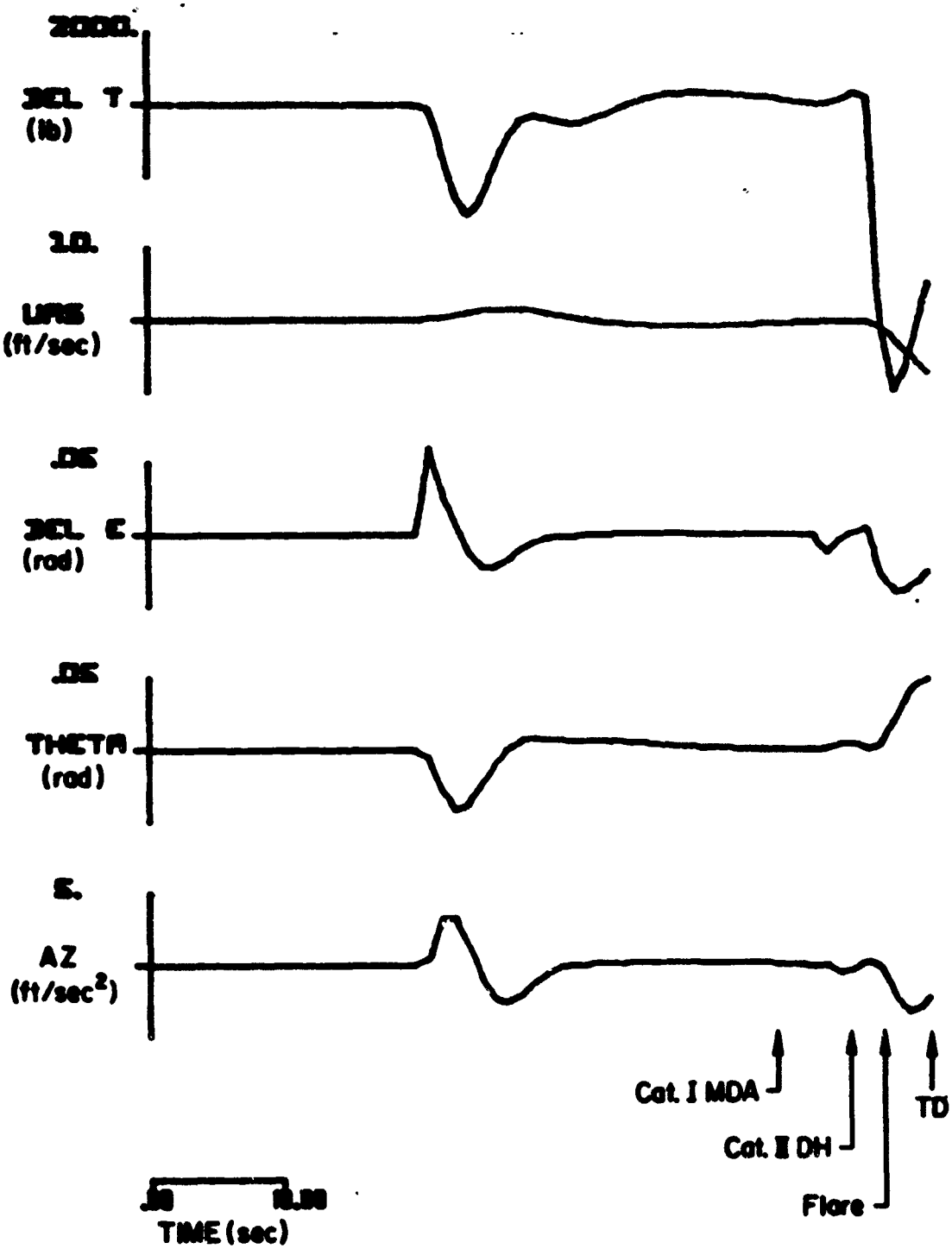

(c)

Figure A-16. (Concluded)

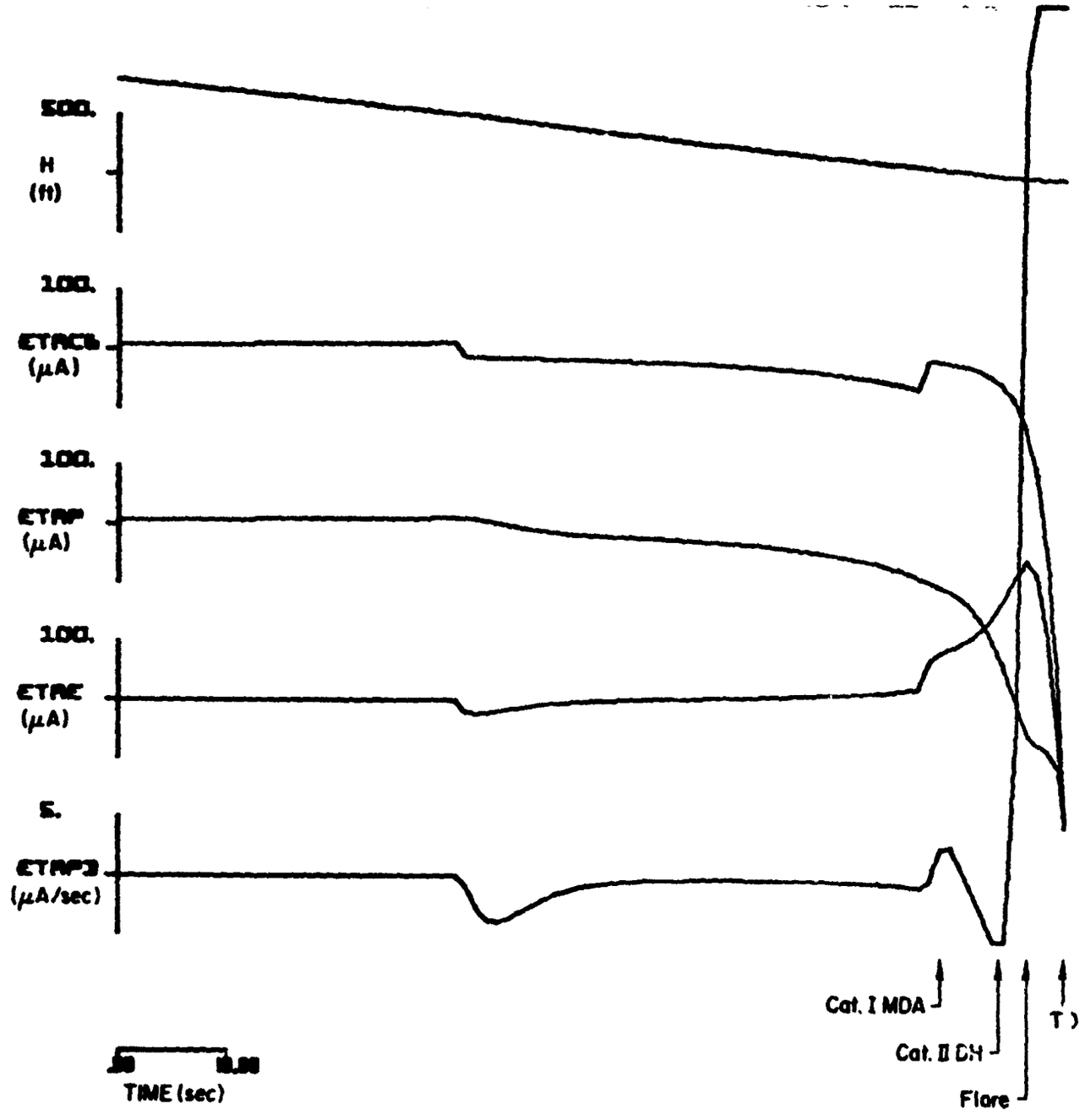

(a)

Figure A-17. Responses of the Piper PA-30 Aircraft with Invented Flight Control System and Conventional Glide Slope Coupling to Prototype Glide Slope Fault No. 2

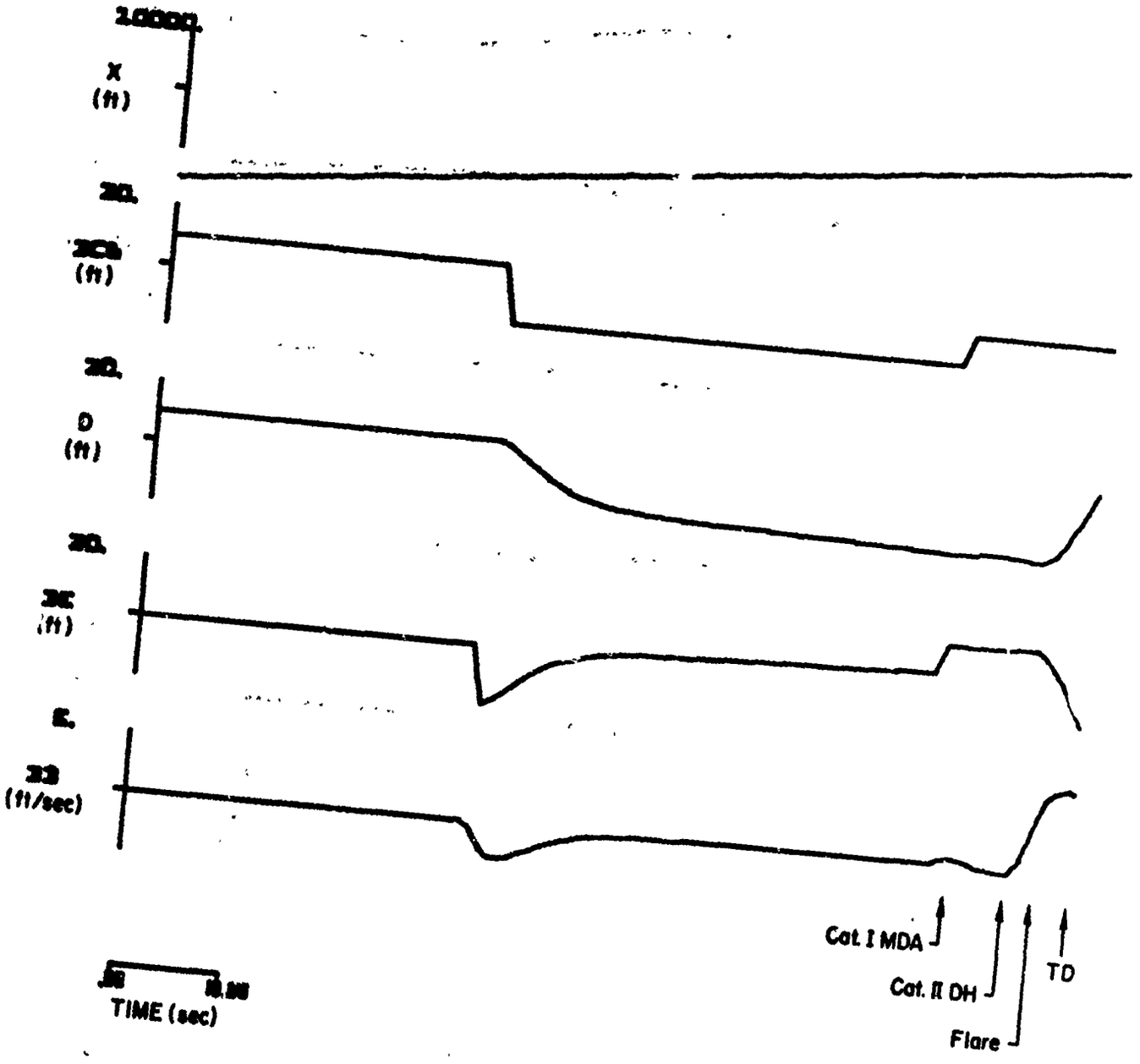

(b)

Figure A-17. (Continued)

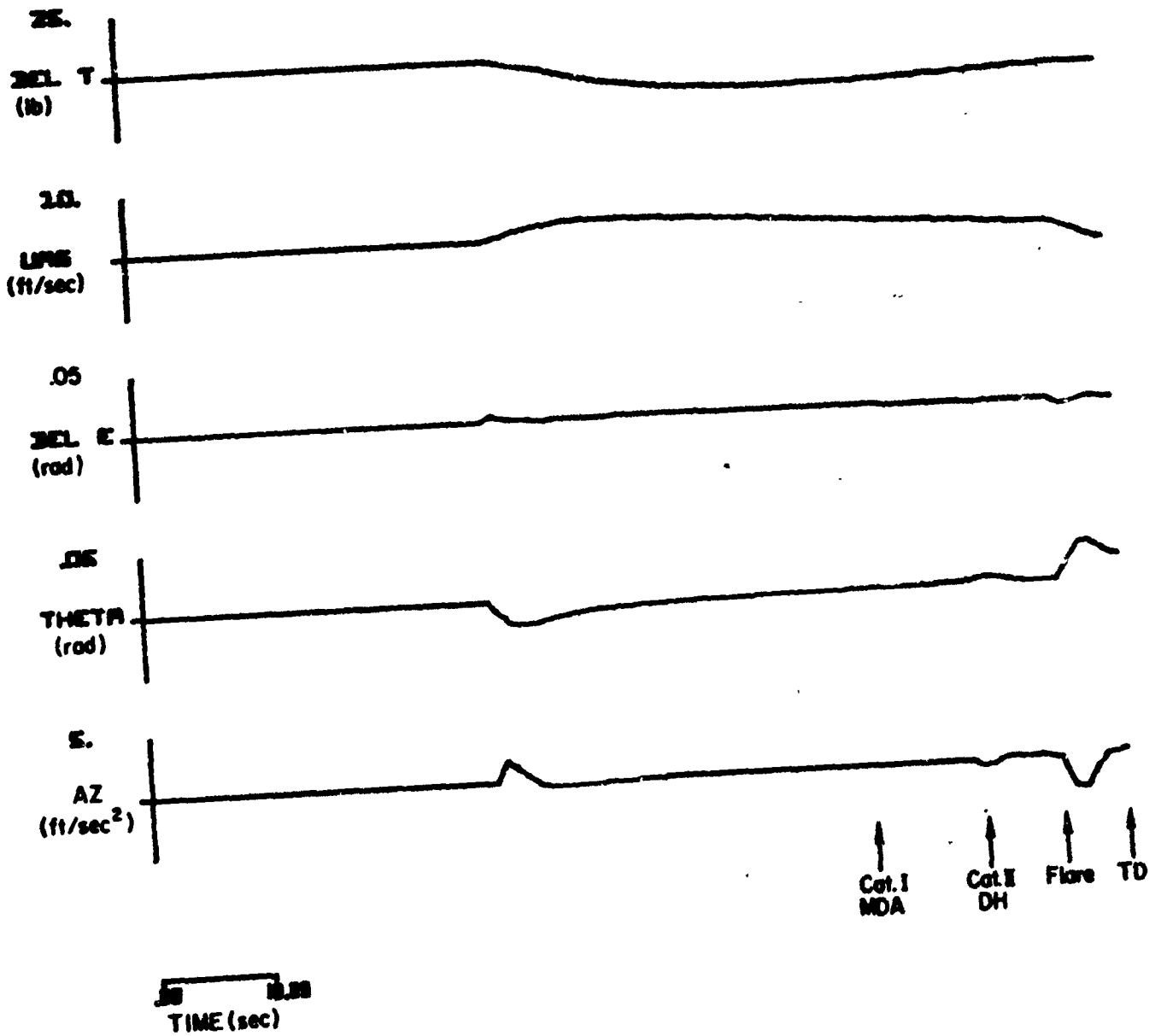

(c)

Figure A-17. (Concluded)

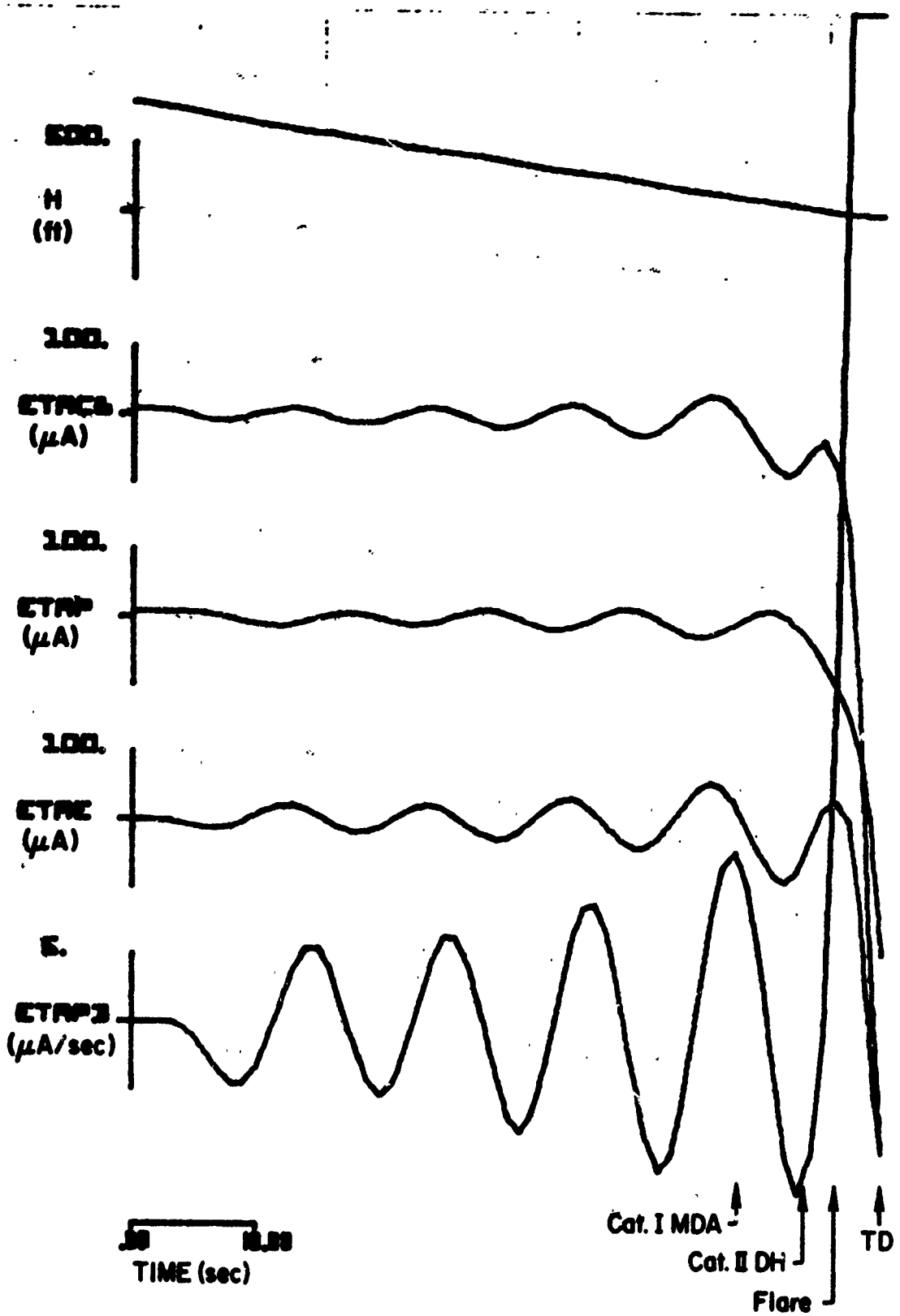

(a)

Figure A-18. Responses of the CV-880 Aircraft with LSI Automatic Landing System and Conventional Glide Slope Coupling to Prototype Glide Slope Fault No. 3

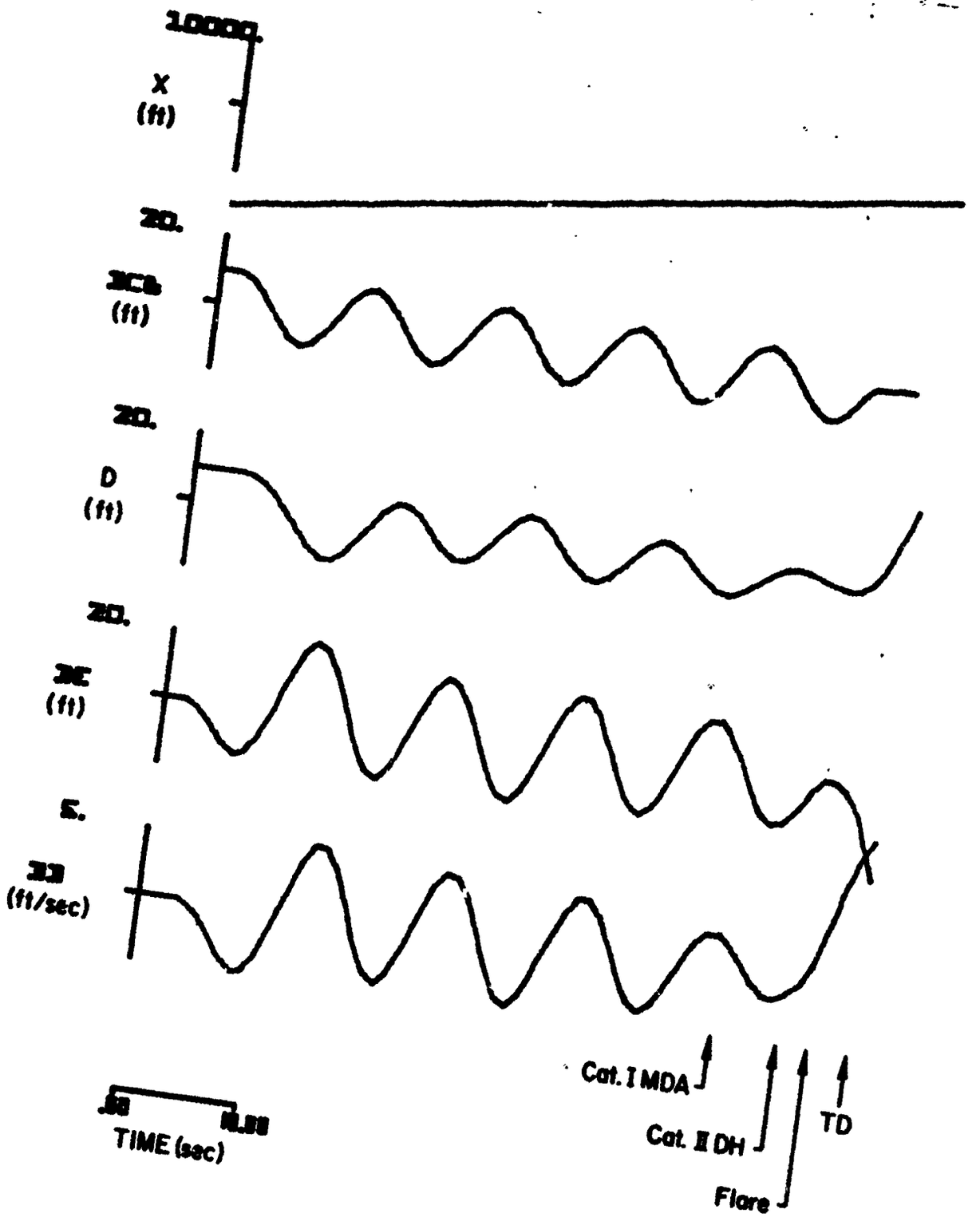

(b)

Figure A-18. (Continued)

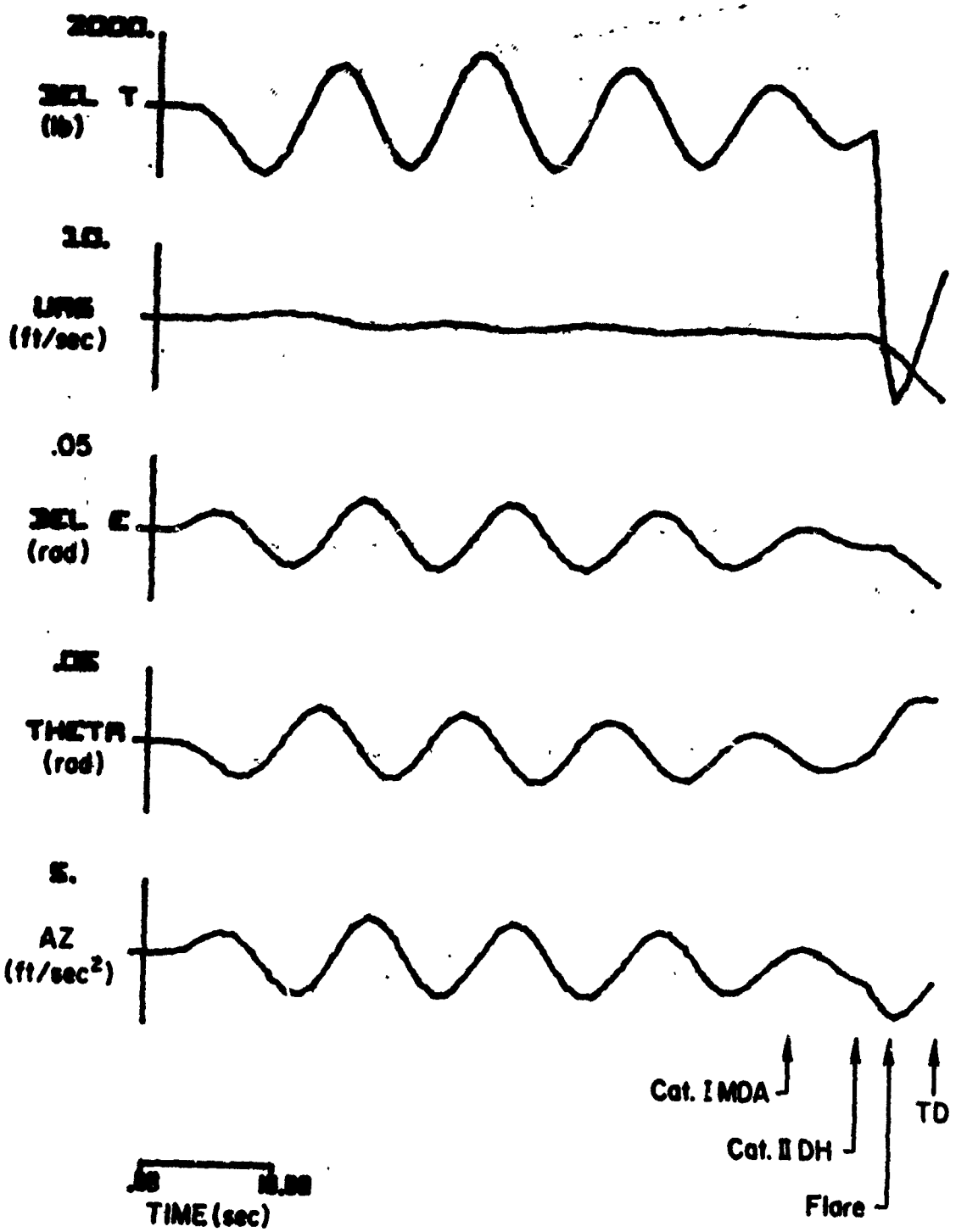

(c)

Figure A-18. (Concluded)

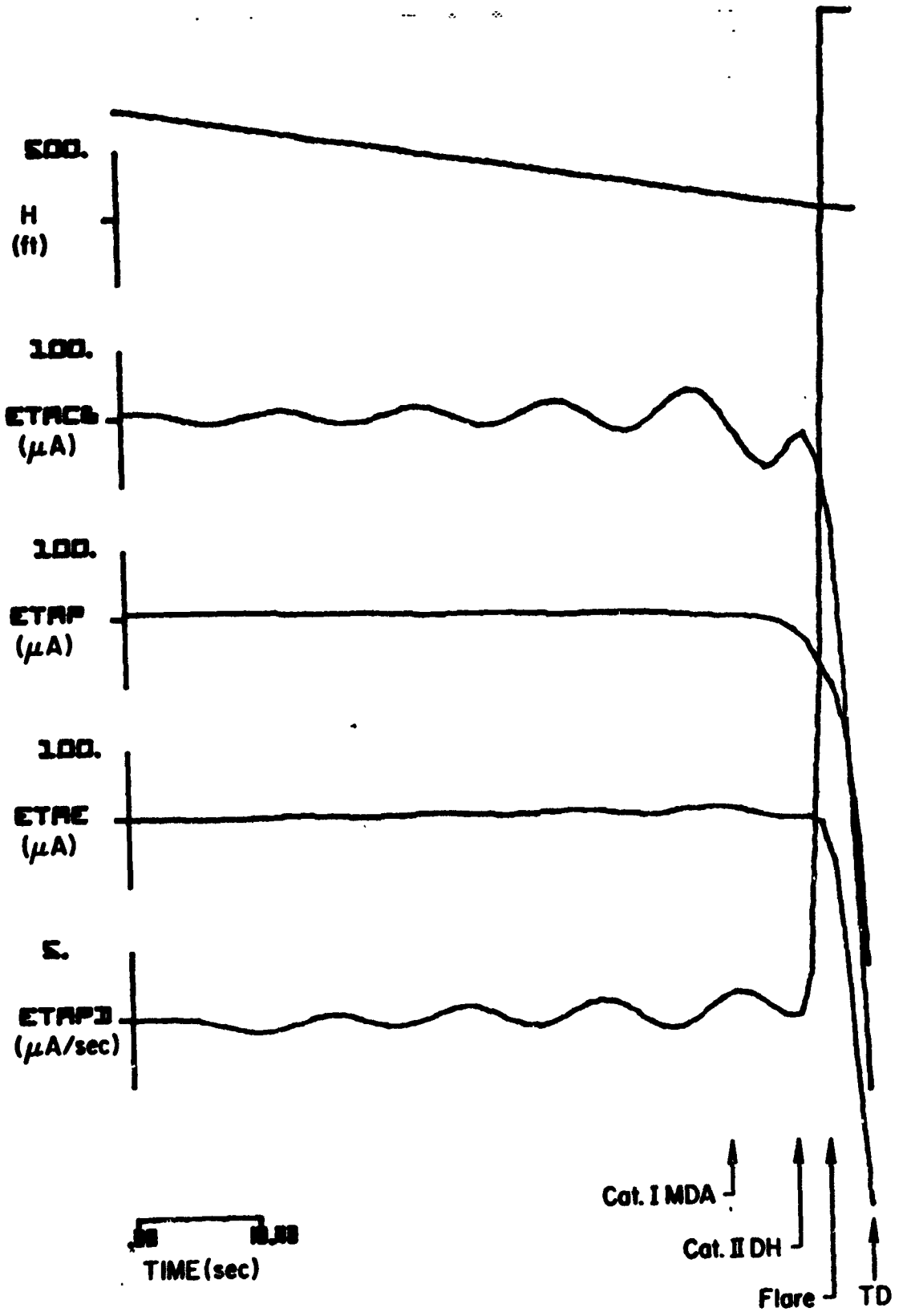

(a)

Figure A-19. Responses of the CV-880 Aircraft with LSI Automatic Landing System and Inertially Augmented Glide Slope Coupling to Prototype Glide Slope Fault No. 3

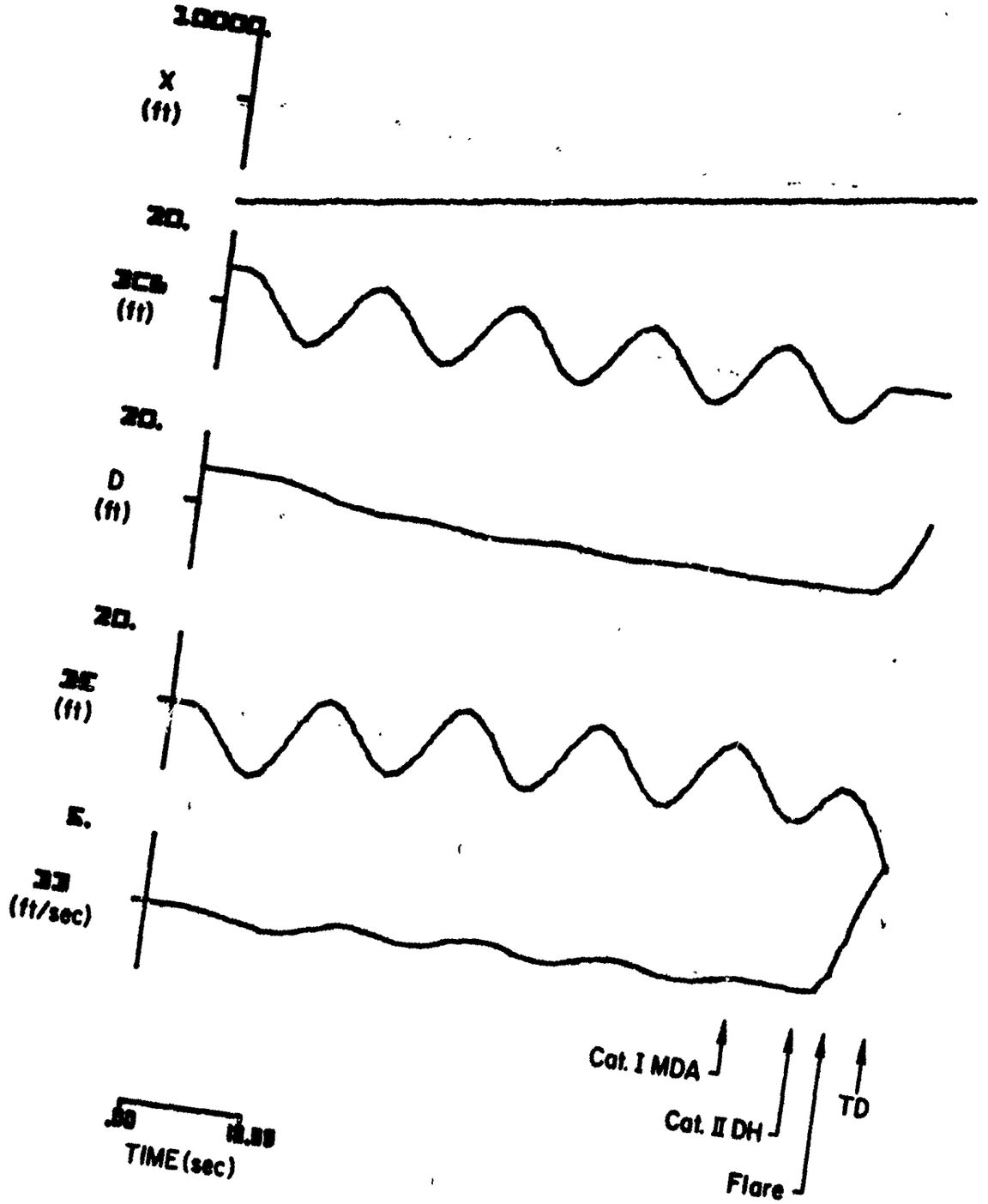

(b)

Figure A-19. (Continued)

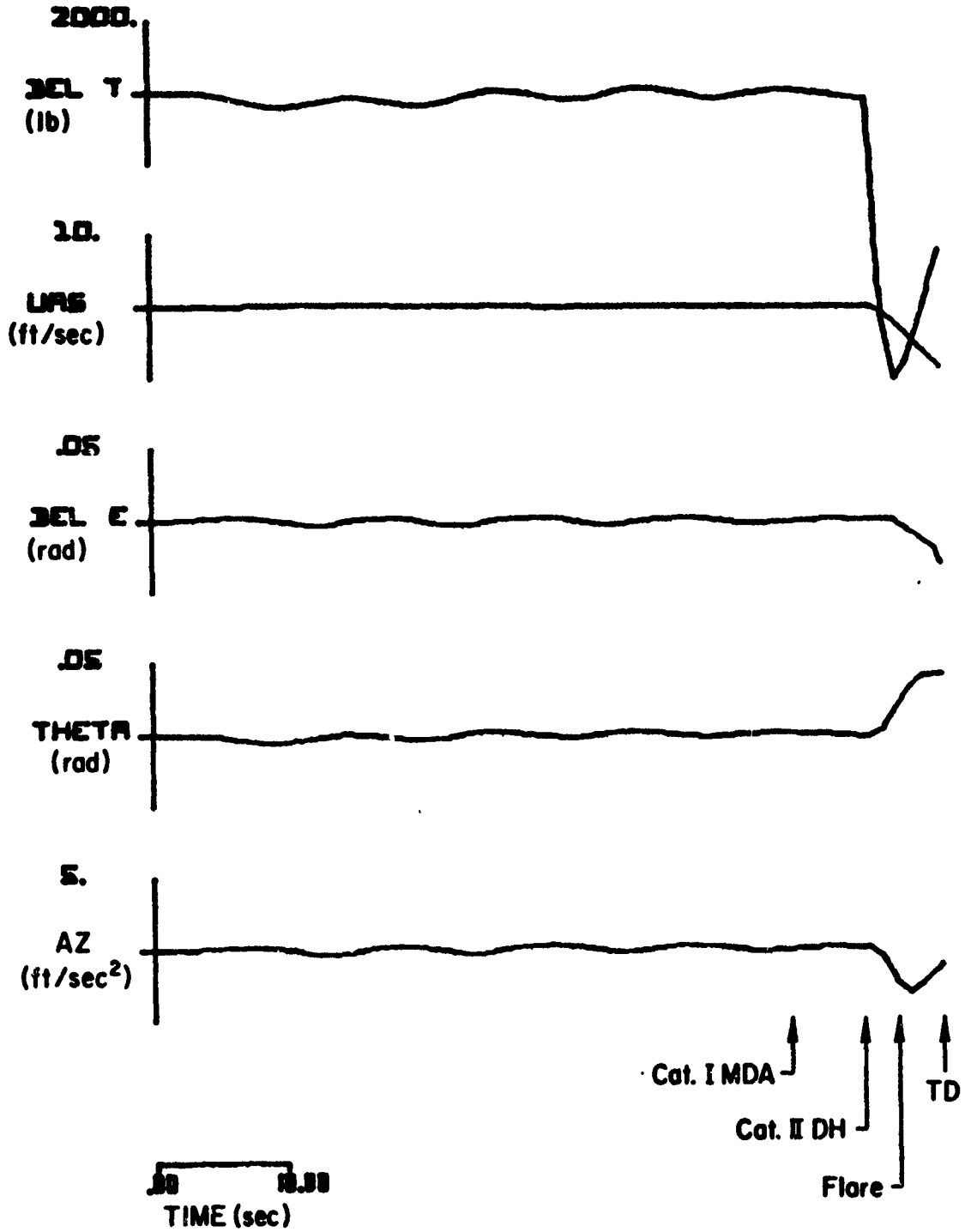

(c)

Figure A-19. (Concluded)

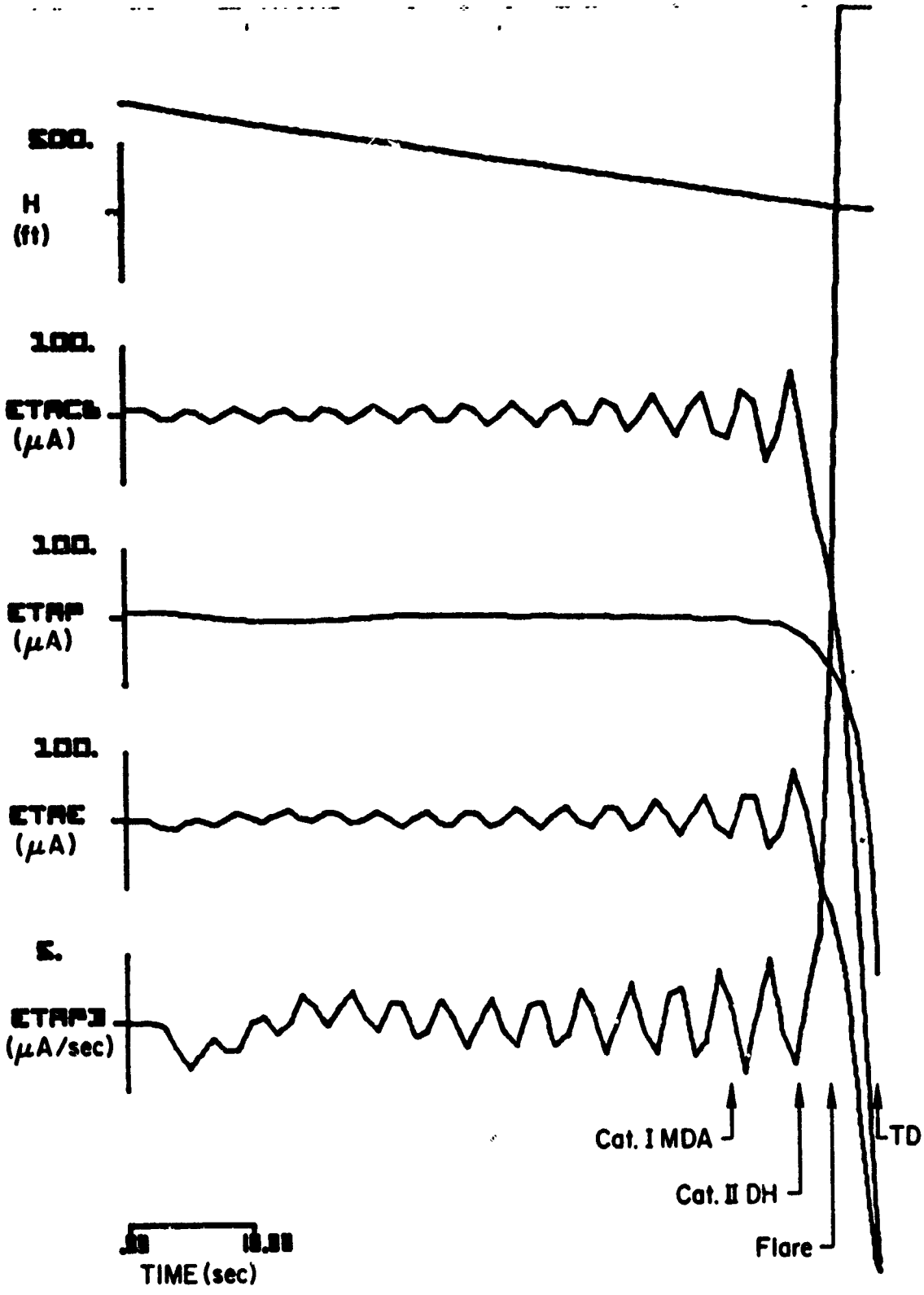

(a)

Figure A-20. Responses of the CV-880 Aircraft with LSI Automatic Landing System and Conventional Glide Slope Coupling to Prototype Glide Slope Fault No. 4

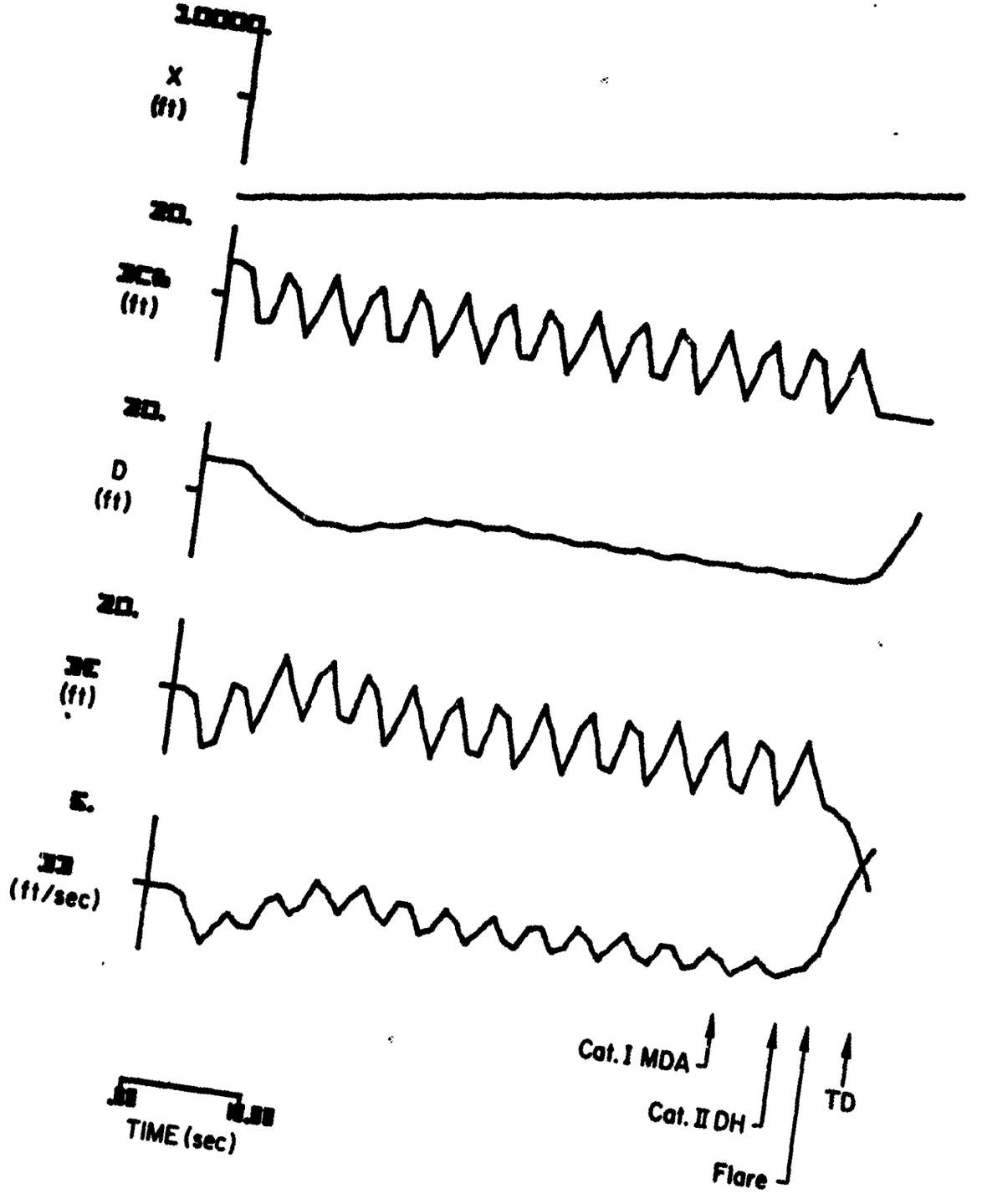

(b)

Figure A-20. (Continued)

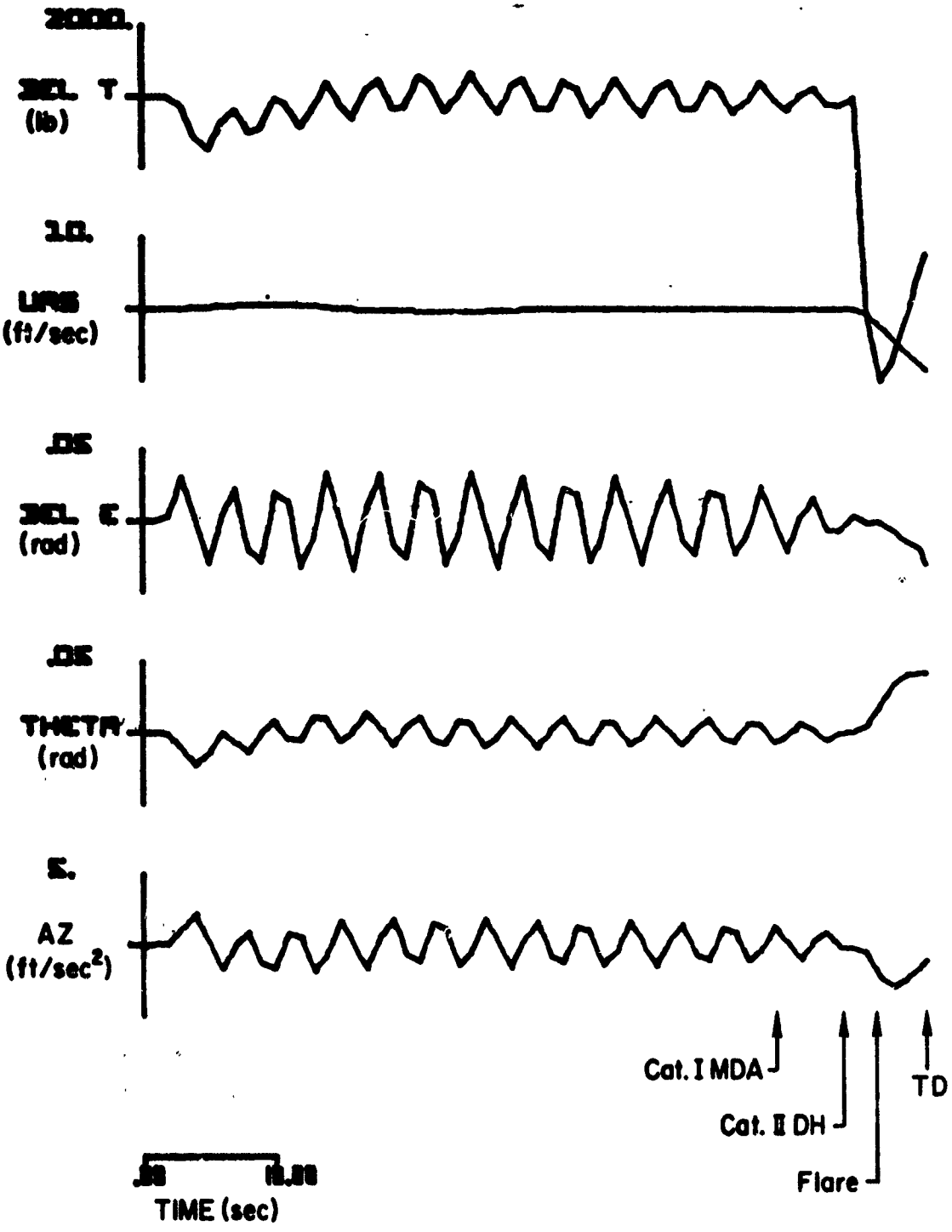

(c)

Figure A-20. (Concluded)

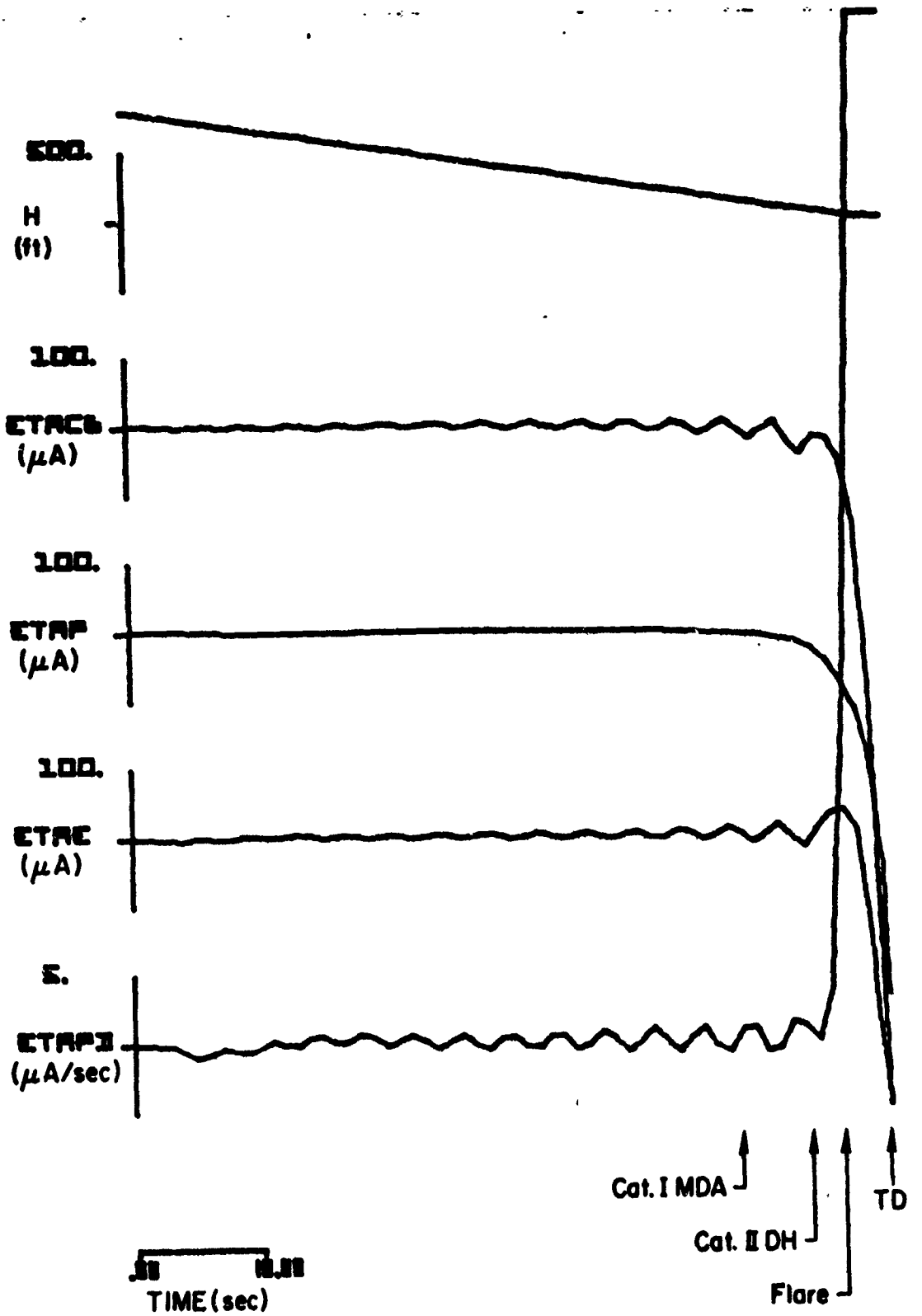

(a)

Figure A-21. Responses of the CV-880 Aircraft with LSI Automatic Landing System and Conventional Glide Slope Coupling to Prototype Glide Slope Fault No. 5

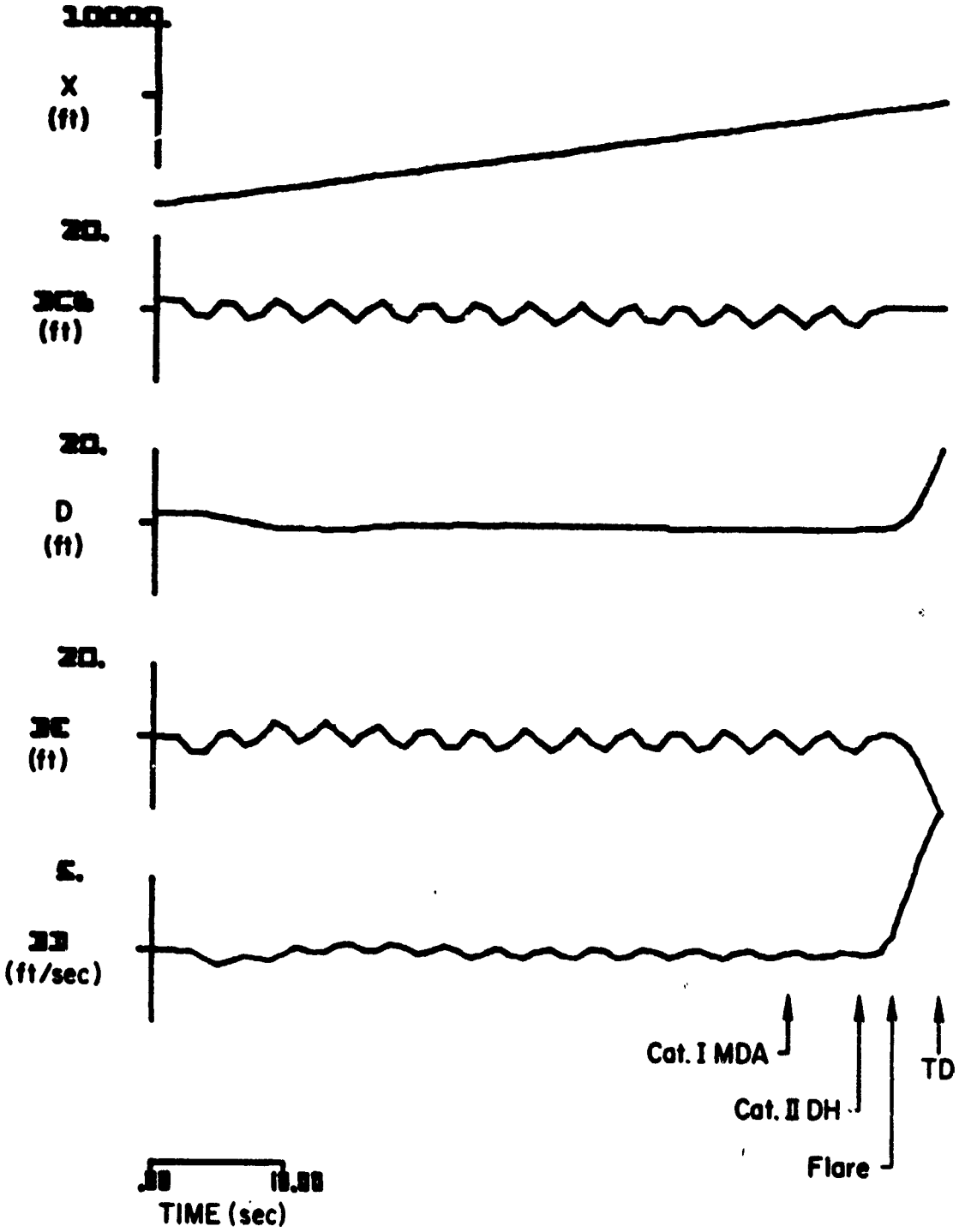

(b)

Figure A-21. (Continued)

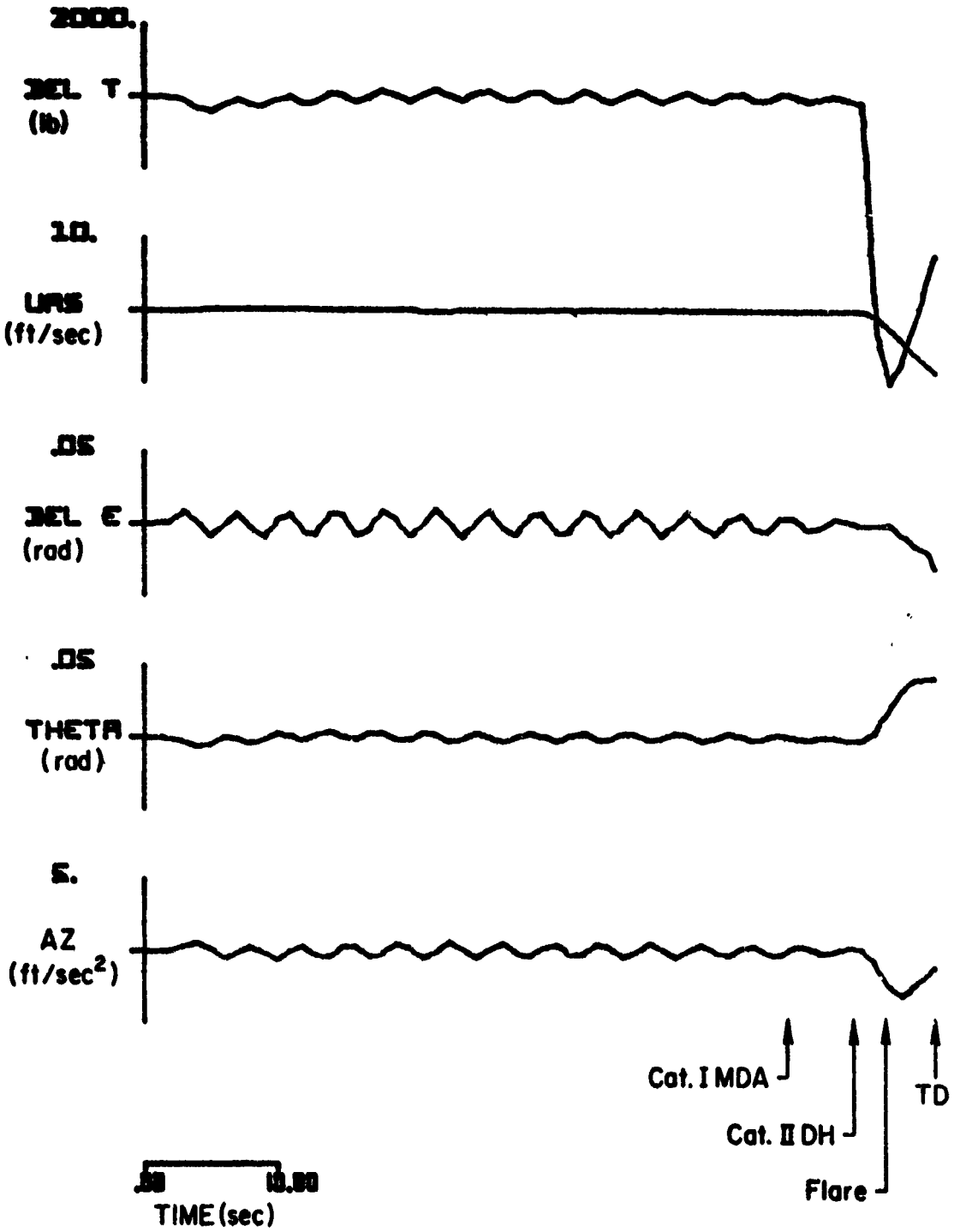

(c)

Figure A-21. (Concluded)

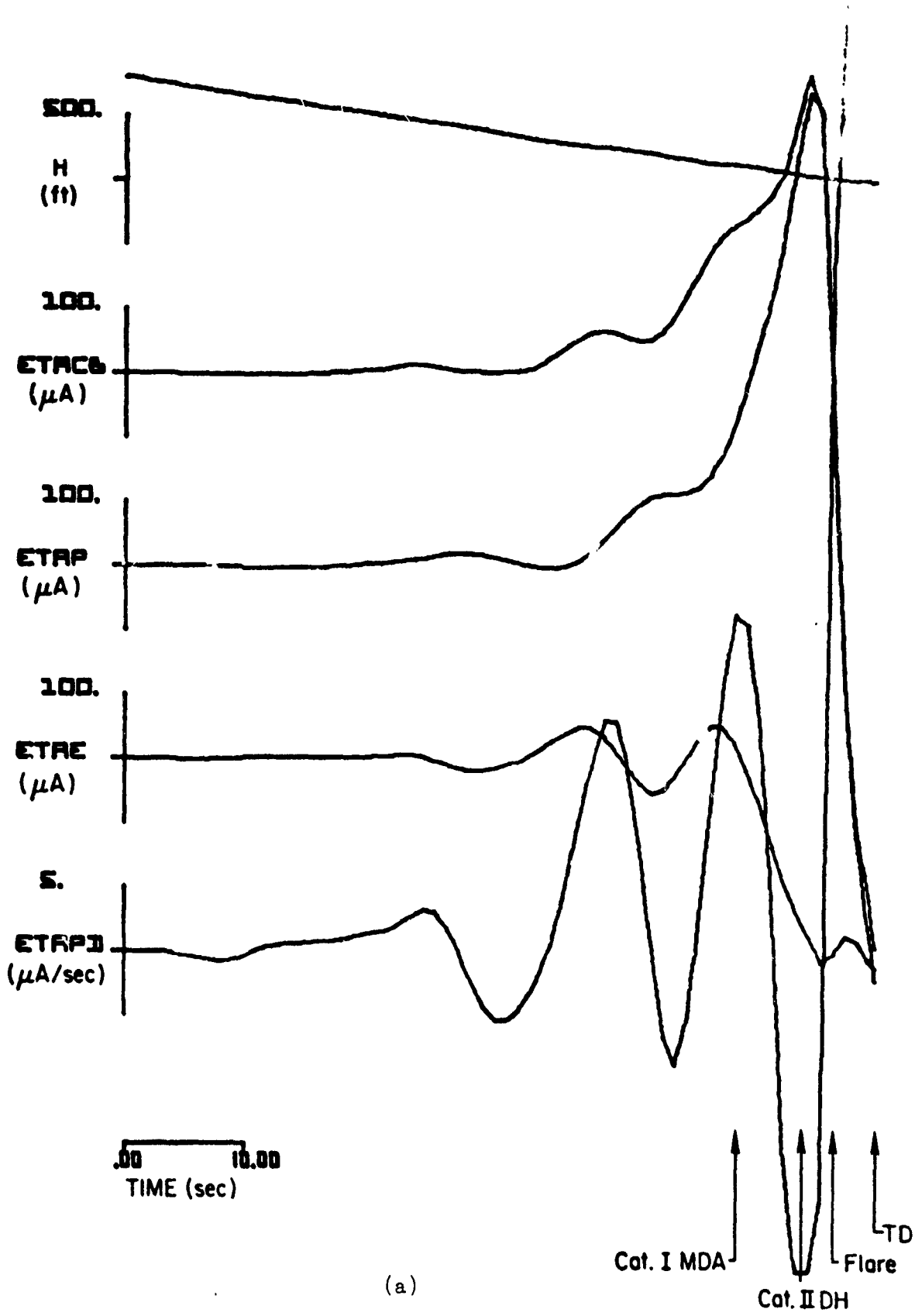

(a)

Figure A-22. Responses of the CV-880 Aircraft with LSI Automatic Landing System and Conventional Glide Slope Coupling to Prototype Glide Slope Fault No. 6

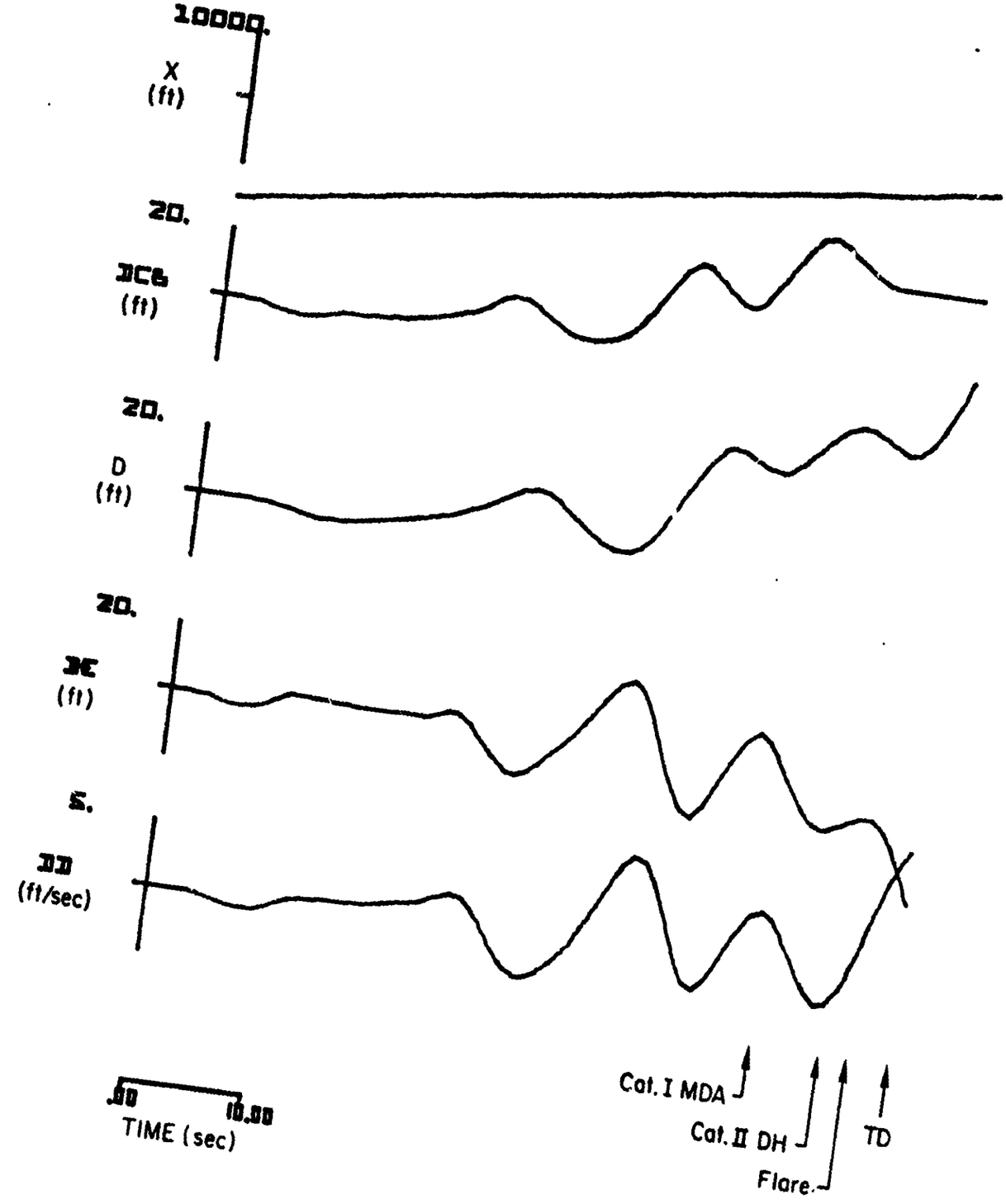

(b)

Figure A-22. (Continued)

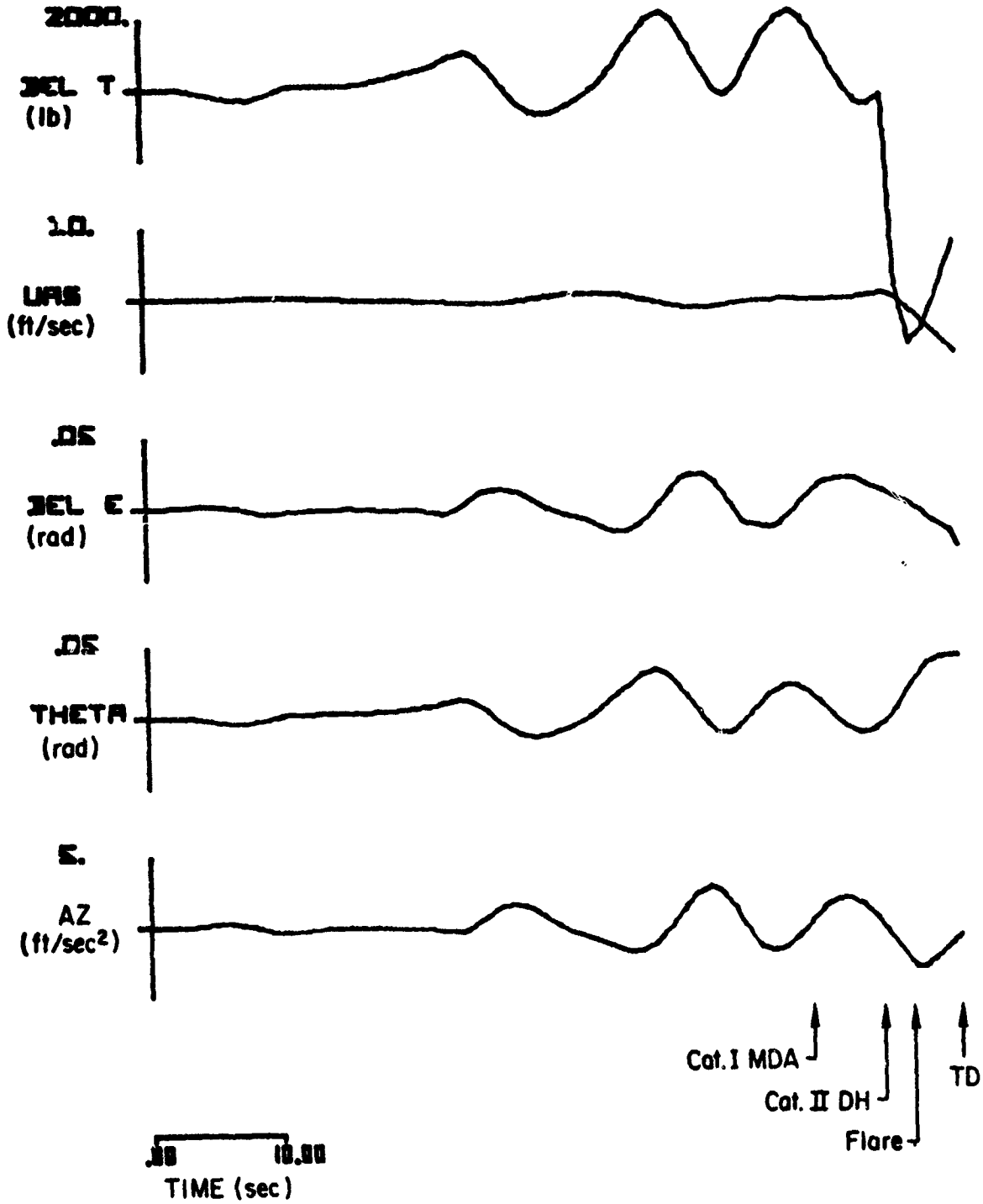

(c)

Figure A-22. (Concluded)

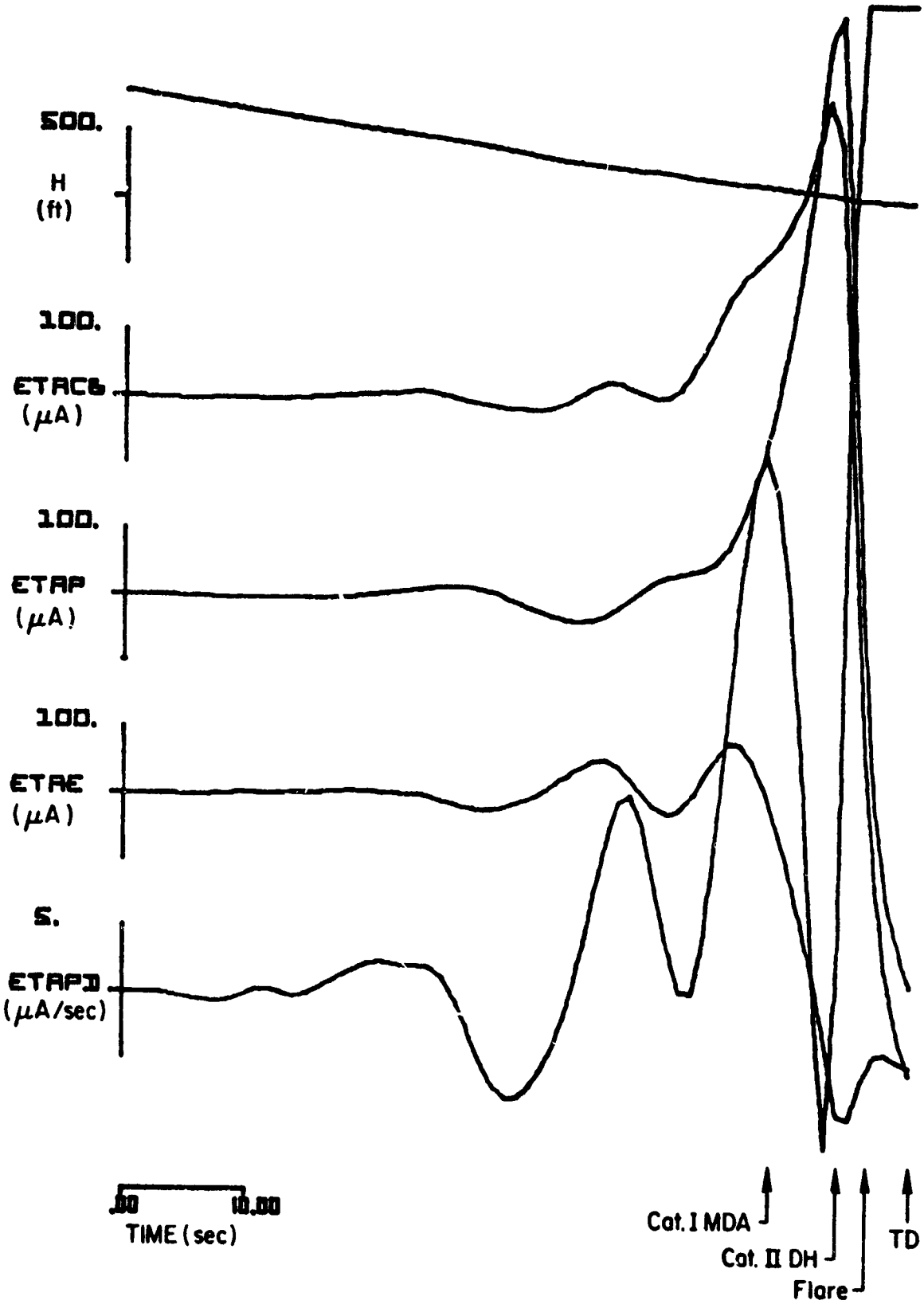

(a)

Figure A-23. Responses of the CV-880 Aircraft with LSI Automatic Landing System and Conventional Glide Slope Coupling to Prototype Glide Slope Fault No. 7

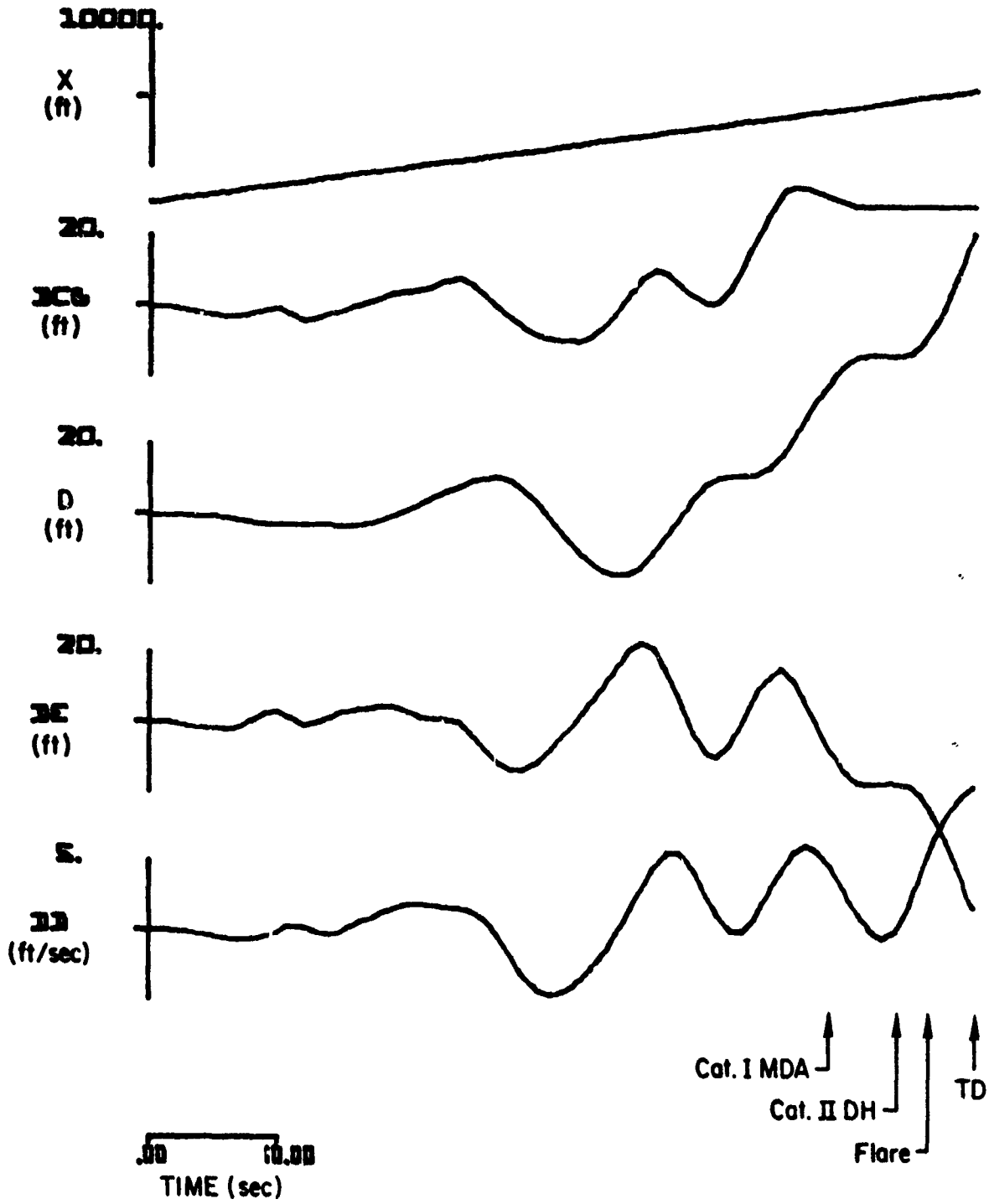

(b)

Figure A-23. (Continued)

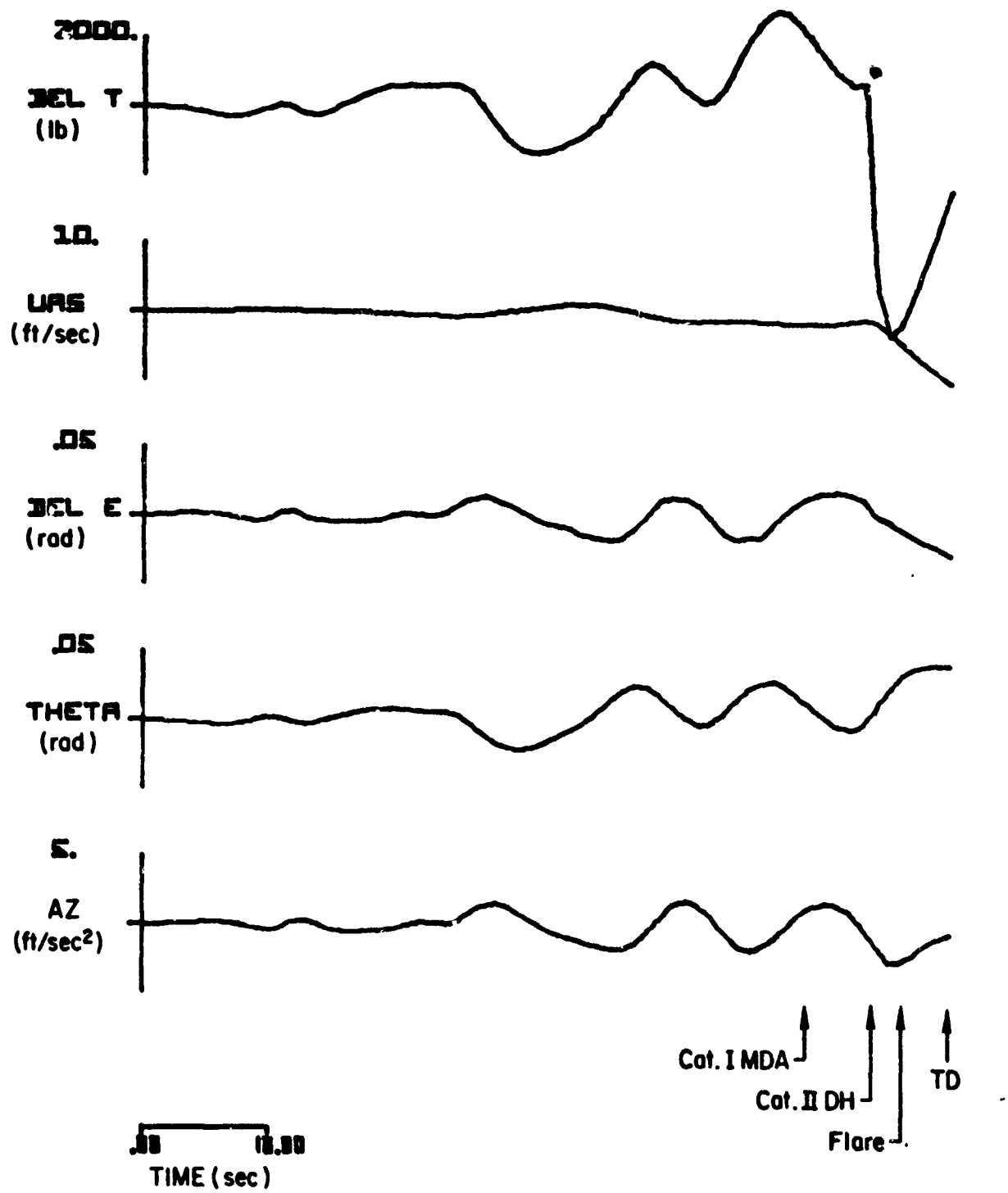

(b)

Figure A-23. (Concluded)

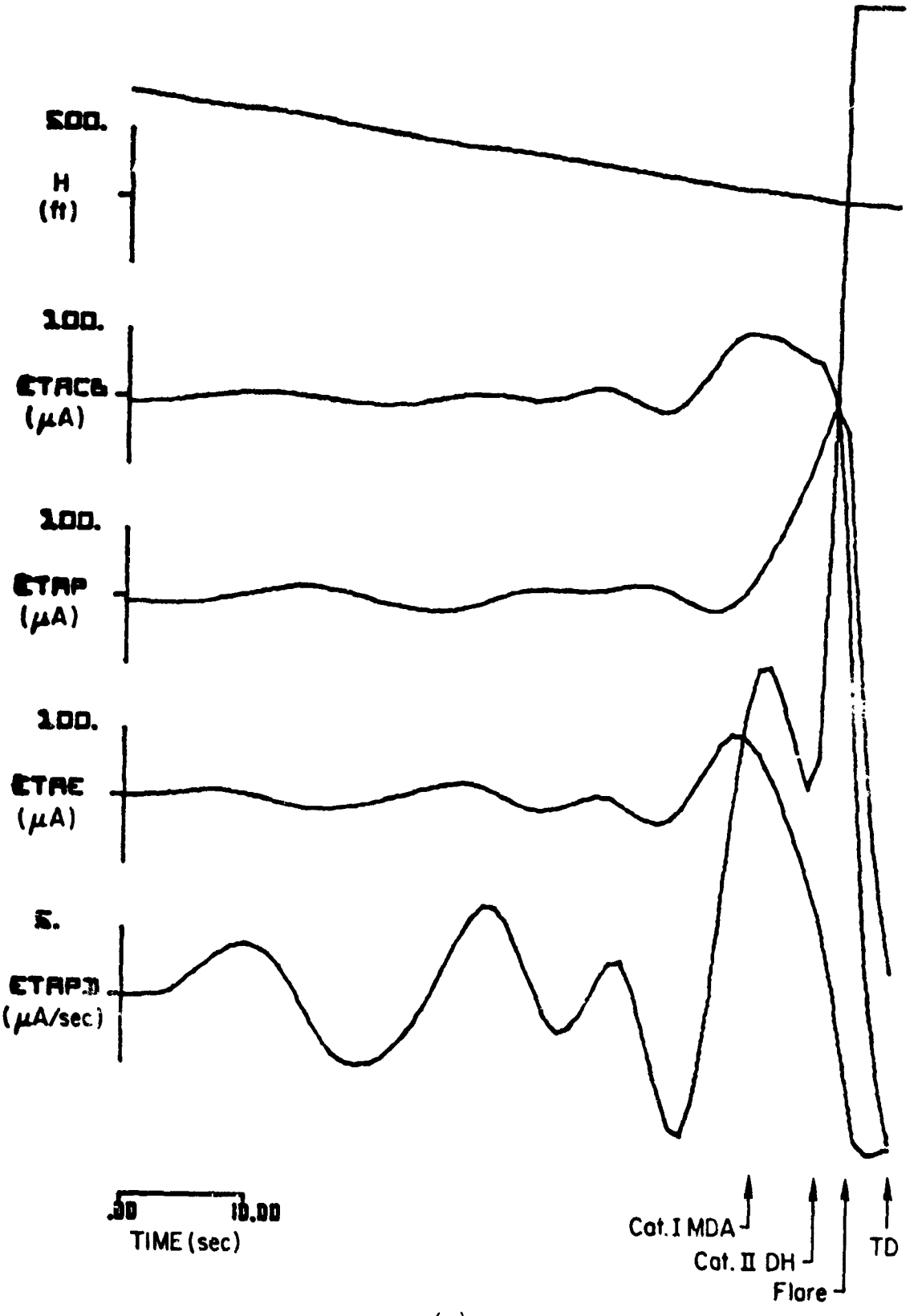

(a)

Figure A-24. Responses of the CV-880 Aircraft with LSI Automatic Landing System and Conventional Glide Slope Coupling to Prototype Glide Slope Fault No. 8

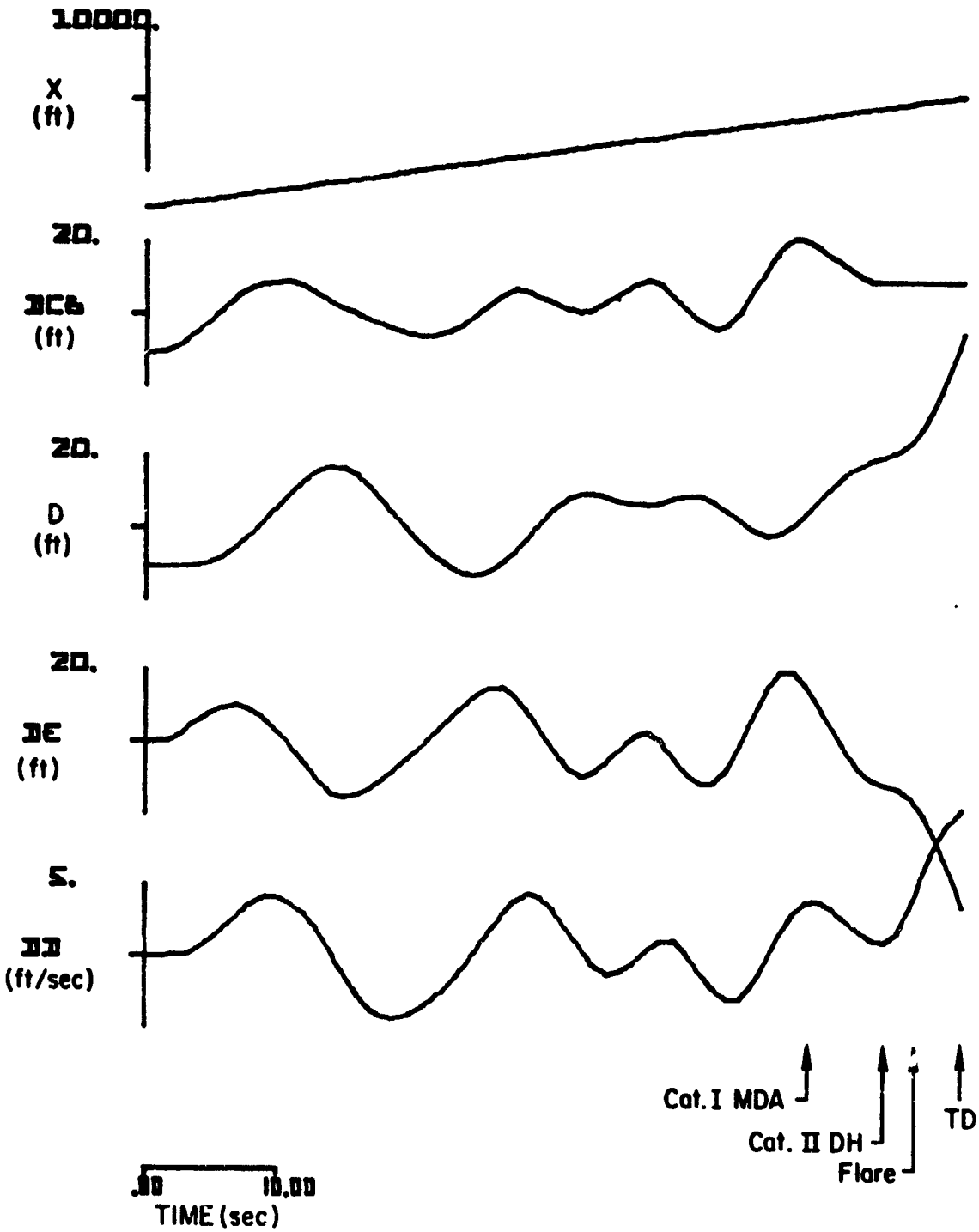

(b)

Figure A-24. (Continued)

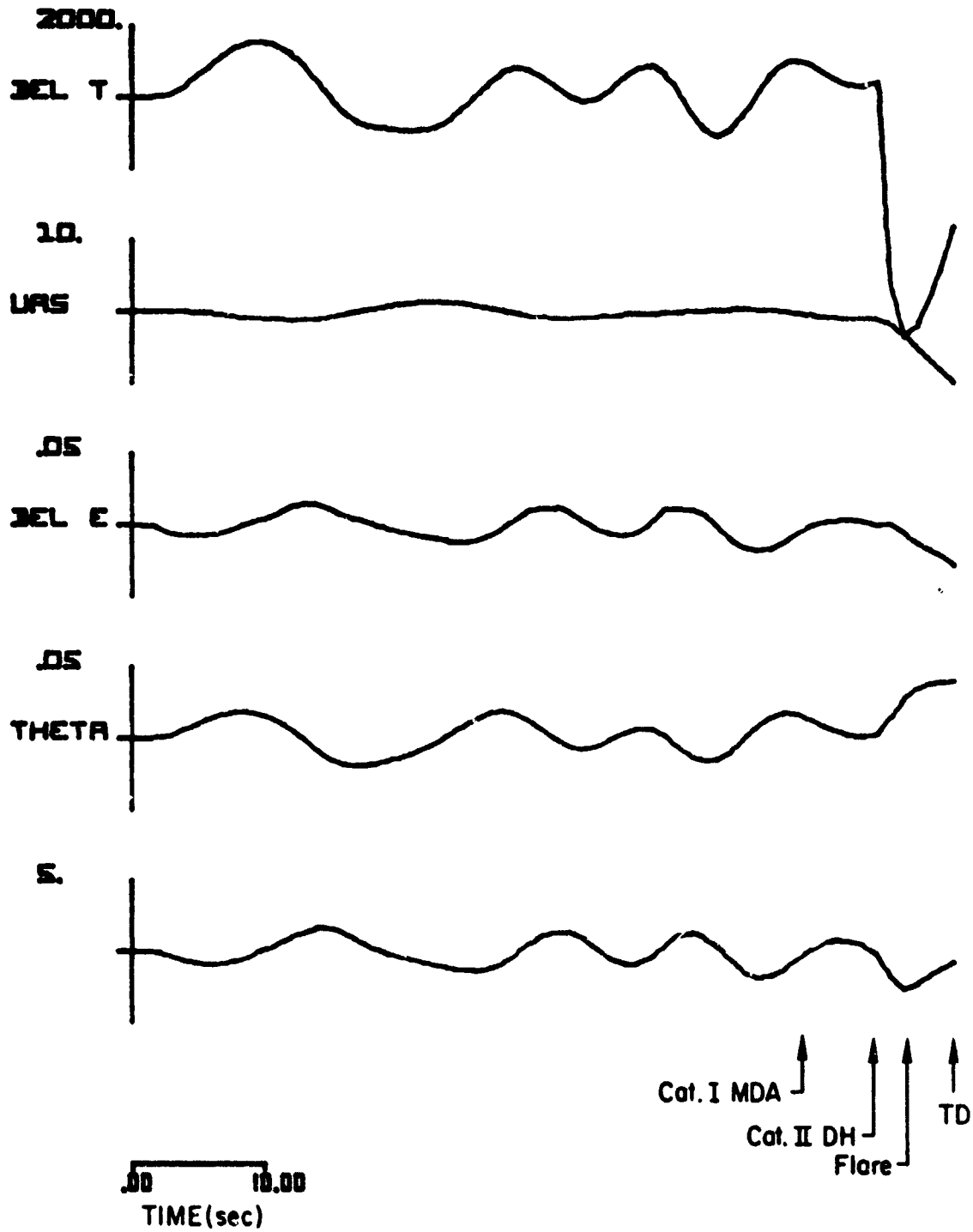

(c)

Figure A-24. (Concluded)

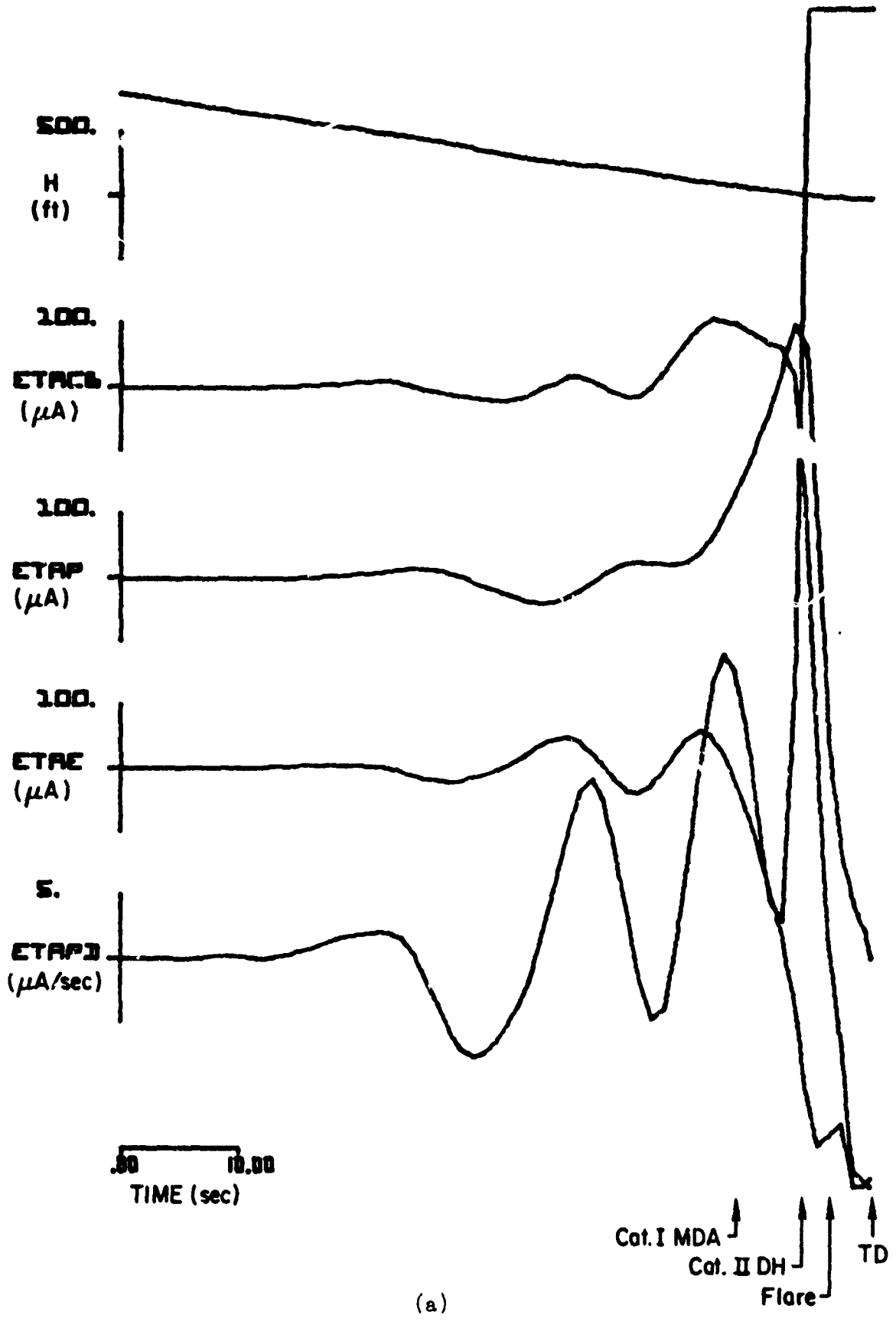

(a)

Figure A-25. Responses of the CV-880 Aircraft with LSI Automatic Landing System and Conventional Glide Slope Coupling to Prototype Glide Slope Fault No. 9

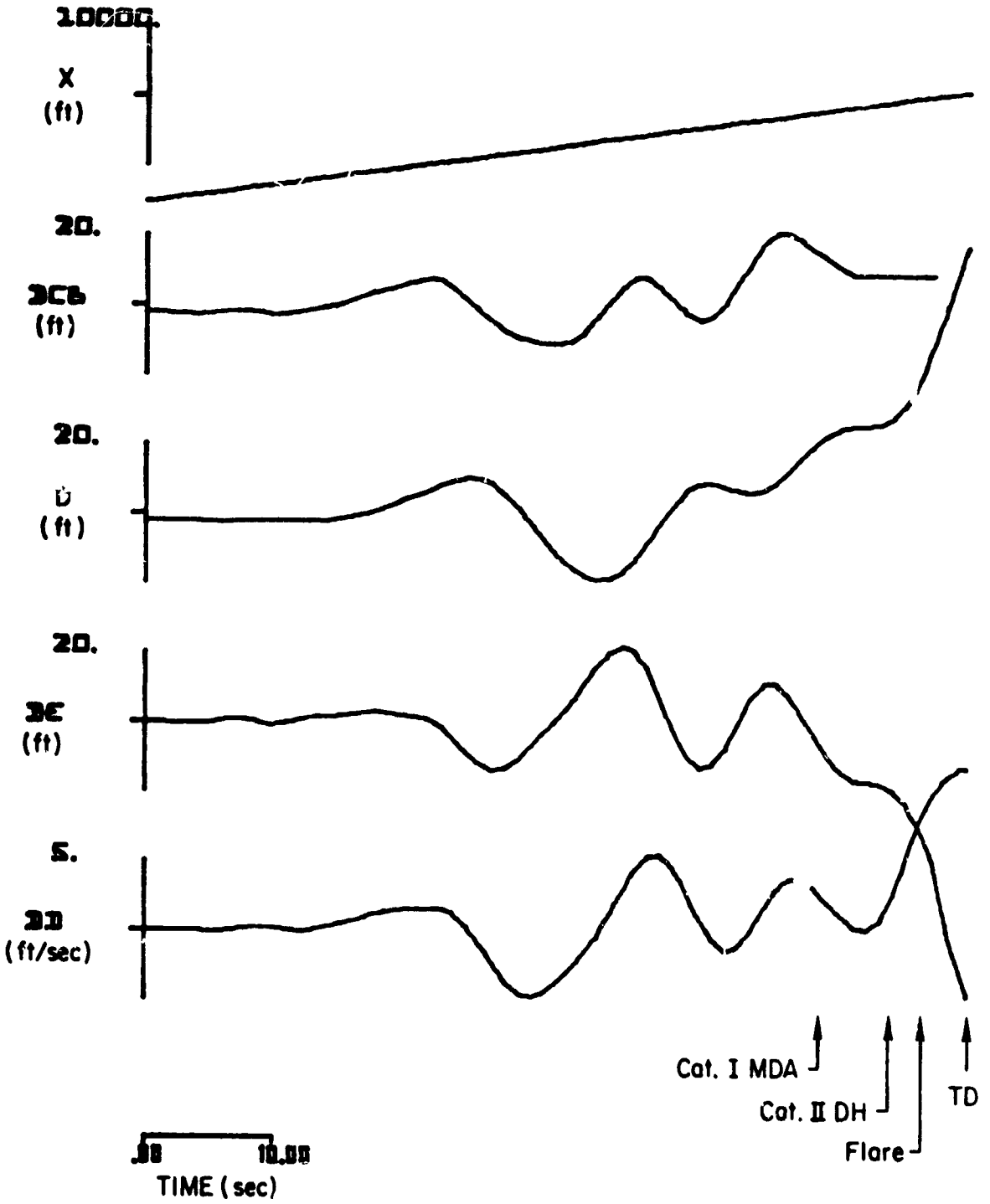

(b)

Figure A-25. (Continued)

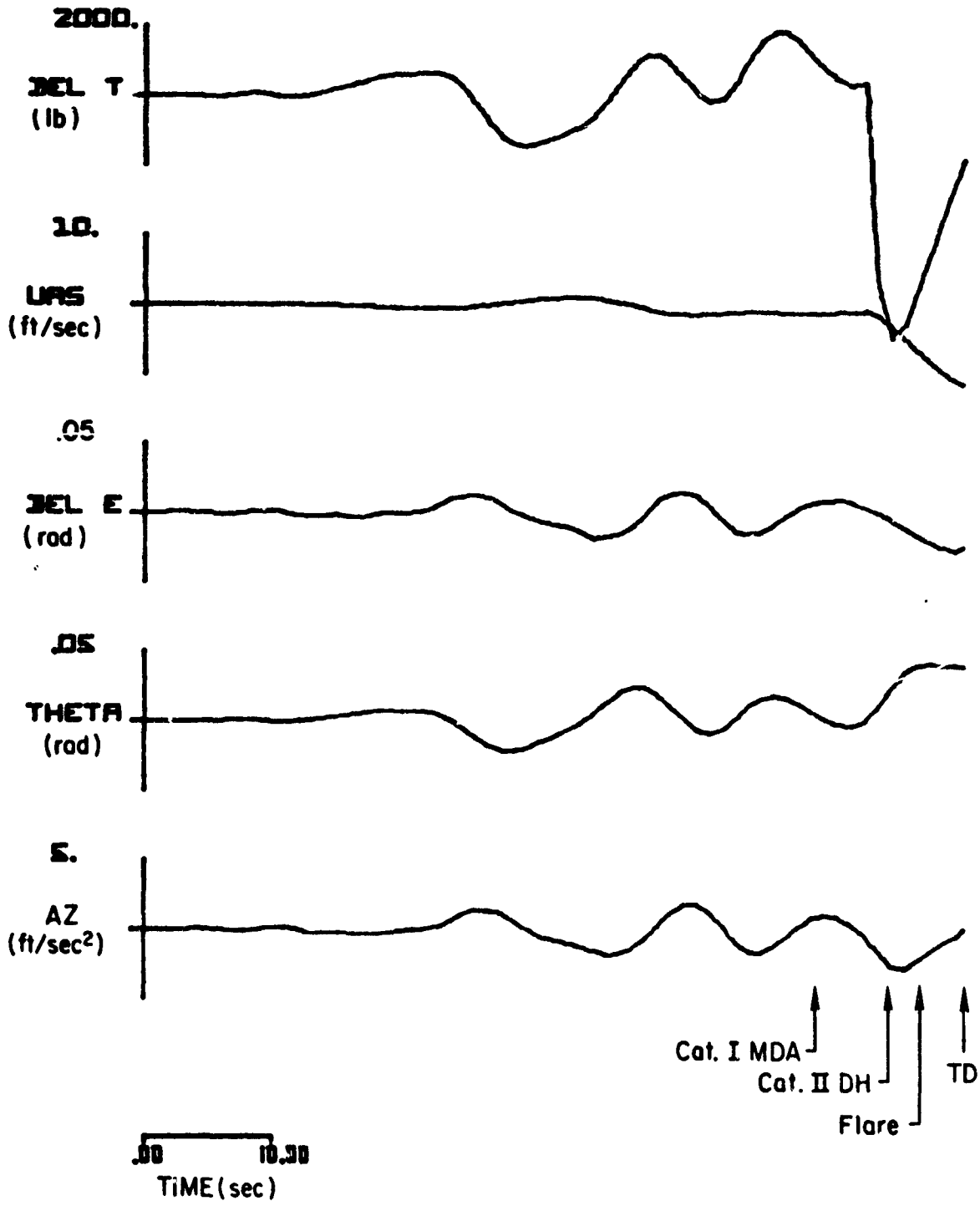

(c)

Figure A-25. (Concluded)

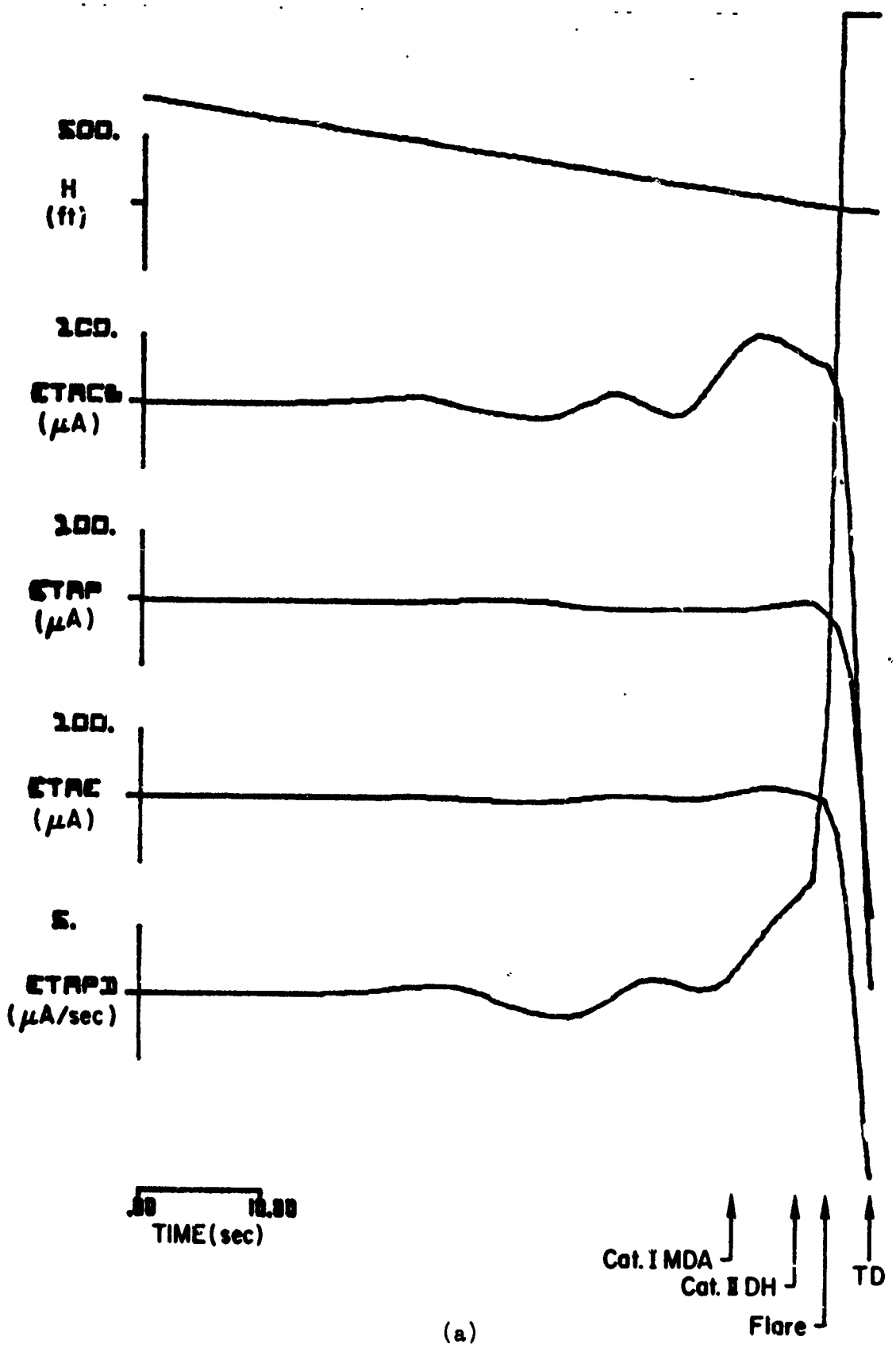

Figure A-26. Responses of the CV-880 Aircraft with LSI Automatic Landing System and Inertially Augmented Glide Slope Coupling to Prototype Glide Slope Fault No. 9

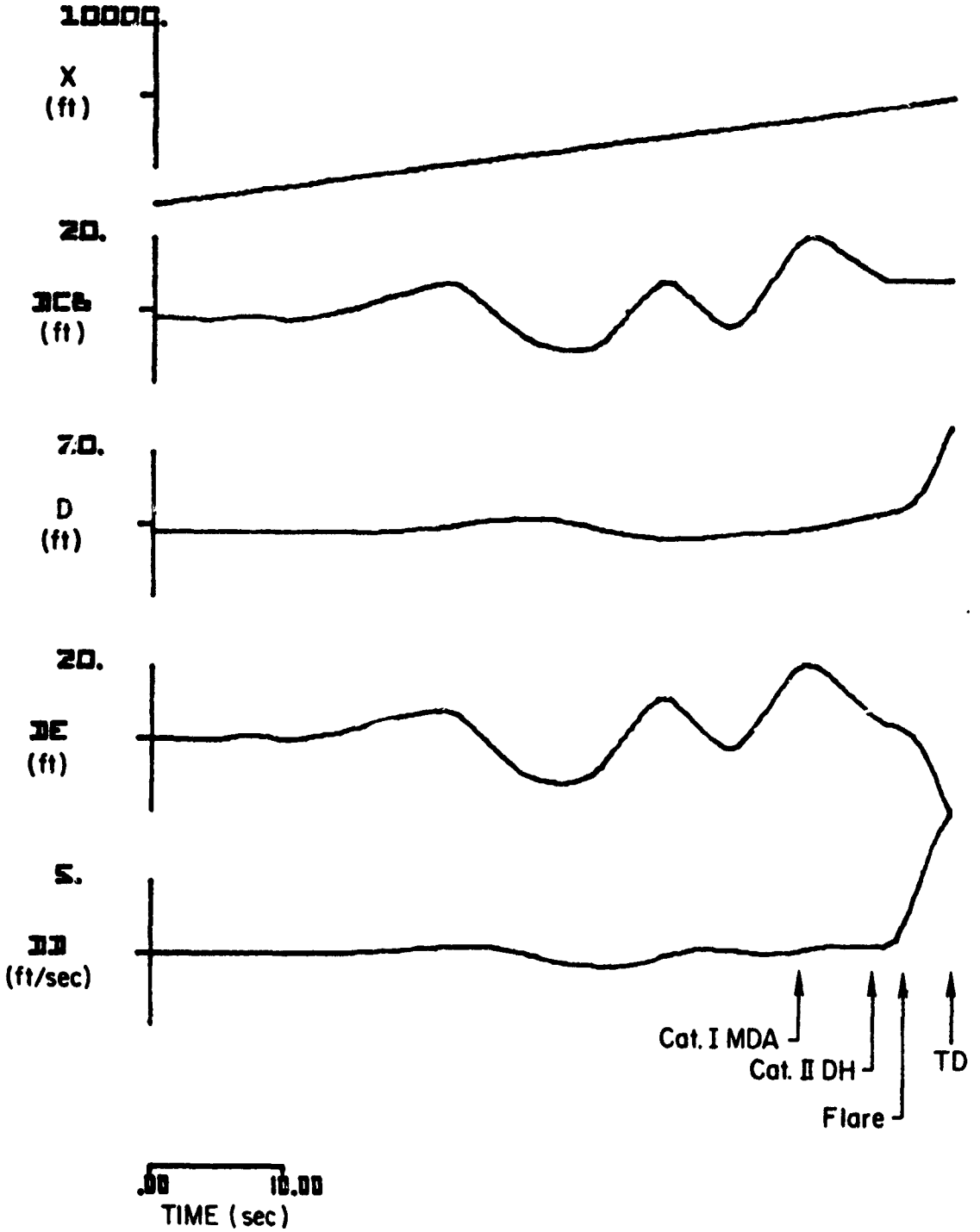

(b)

Figure A-26. (Continued)

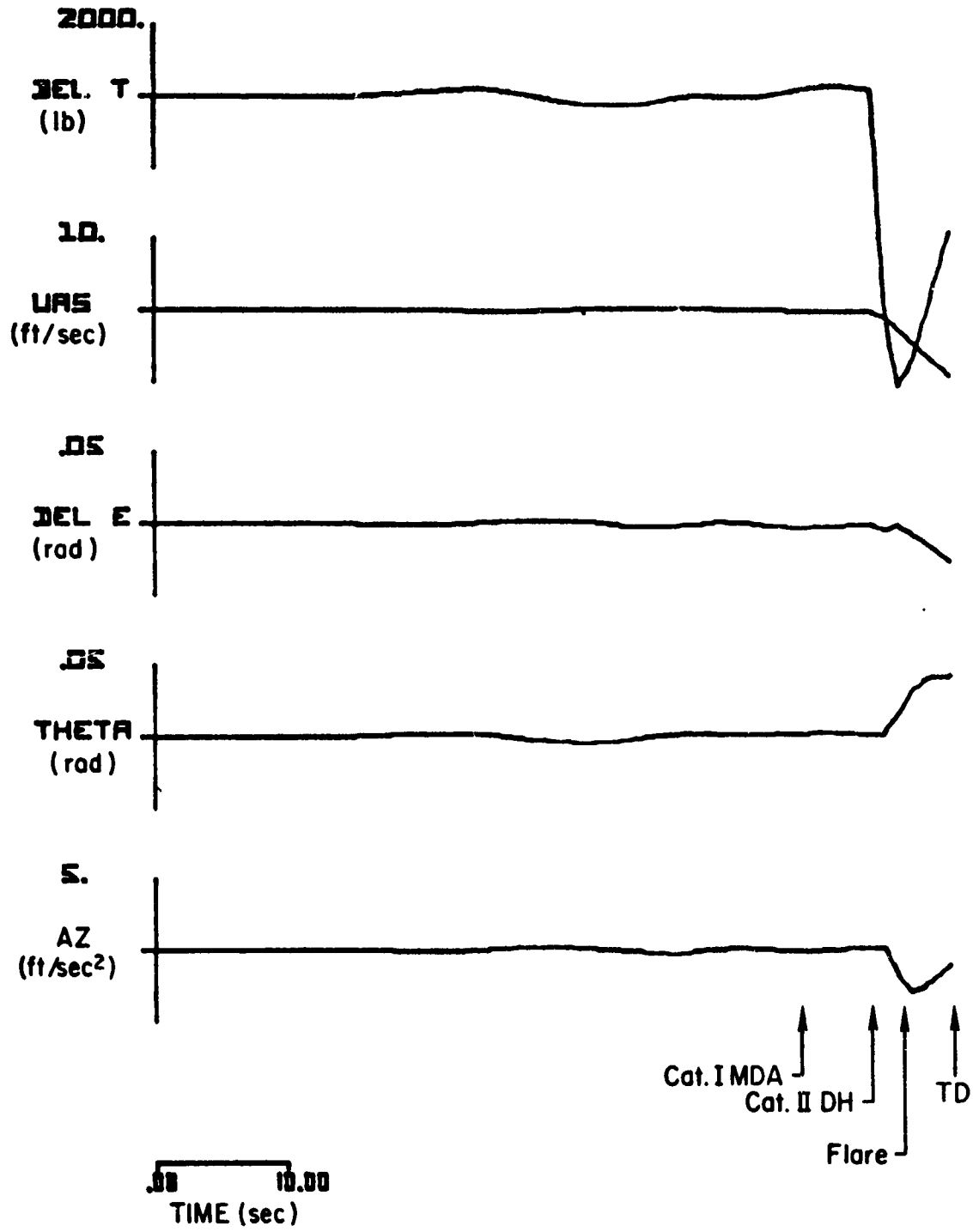

(c)

Figure A-26. (Concluded)

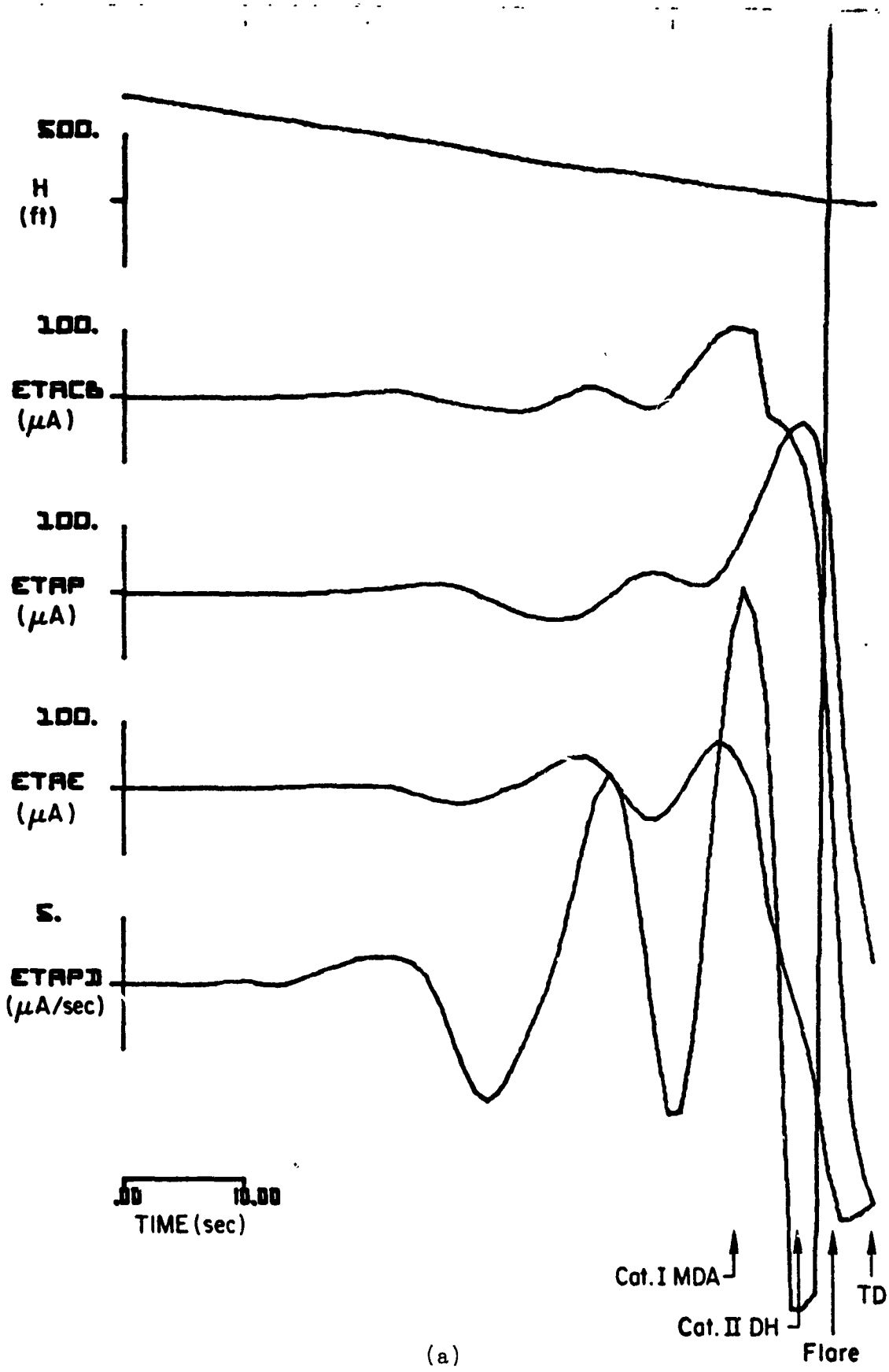

(a)

Figure A-27. Responses of the CV-880 Aircraft with Manually Controlled Flight Director System and Conventional Glide Slope Coupling to Prototype Glide Slope Fault No. 9

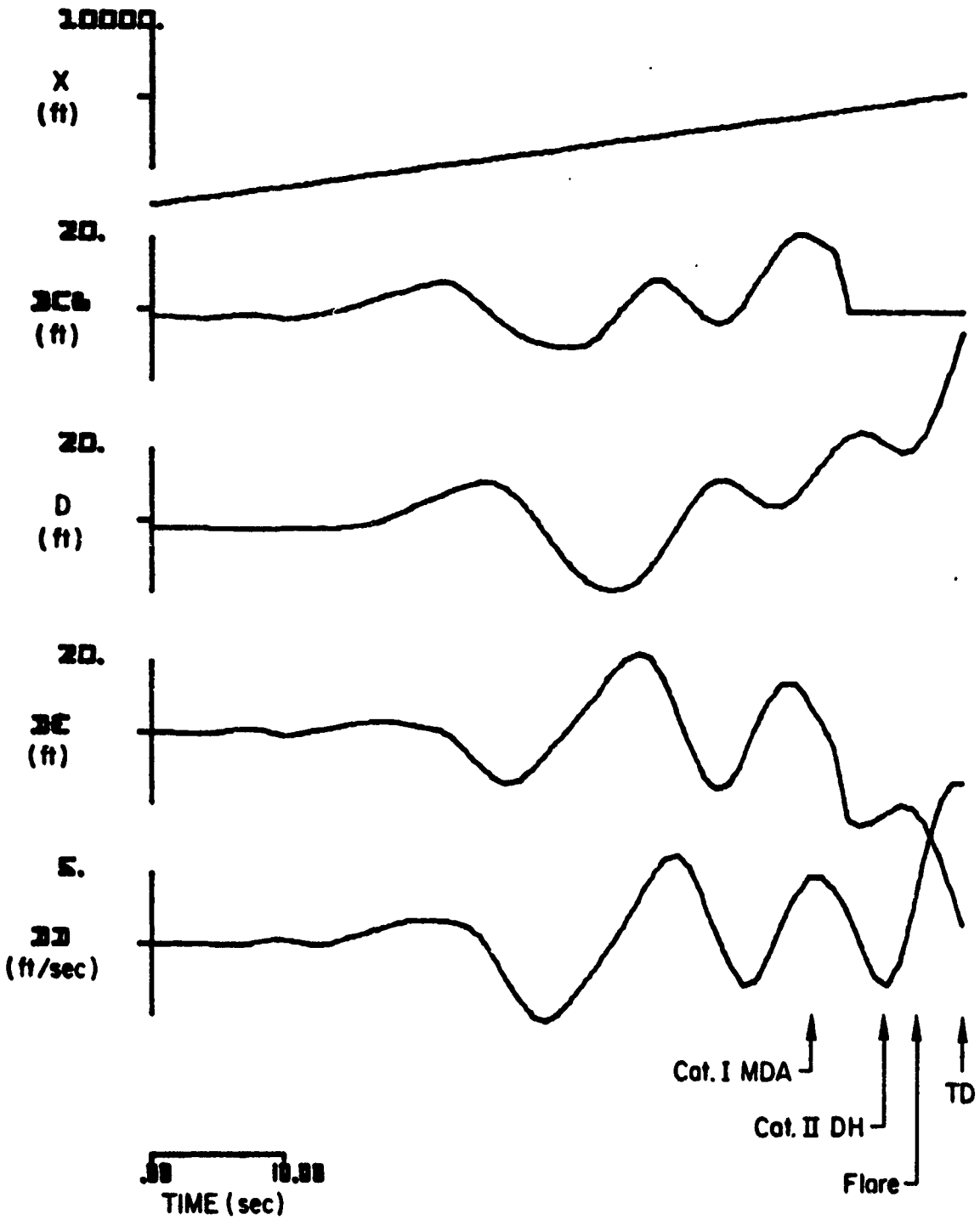

(b)

Figure A-27. (Continued)

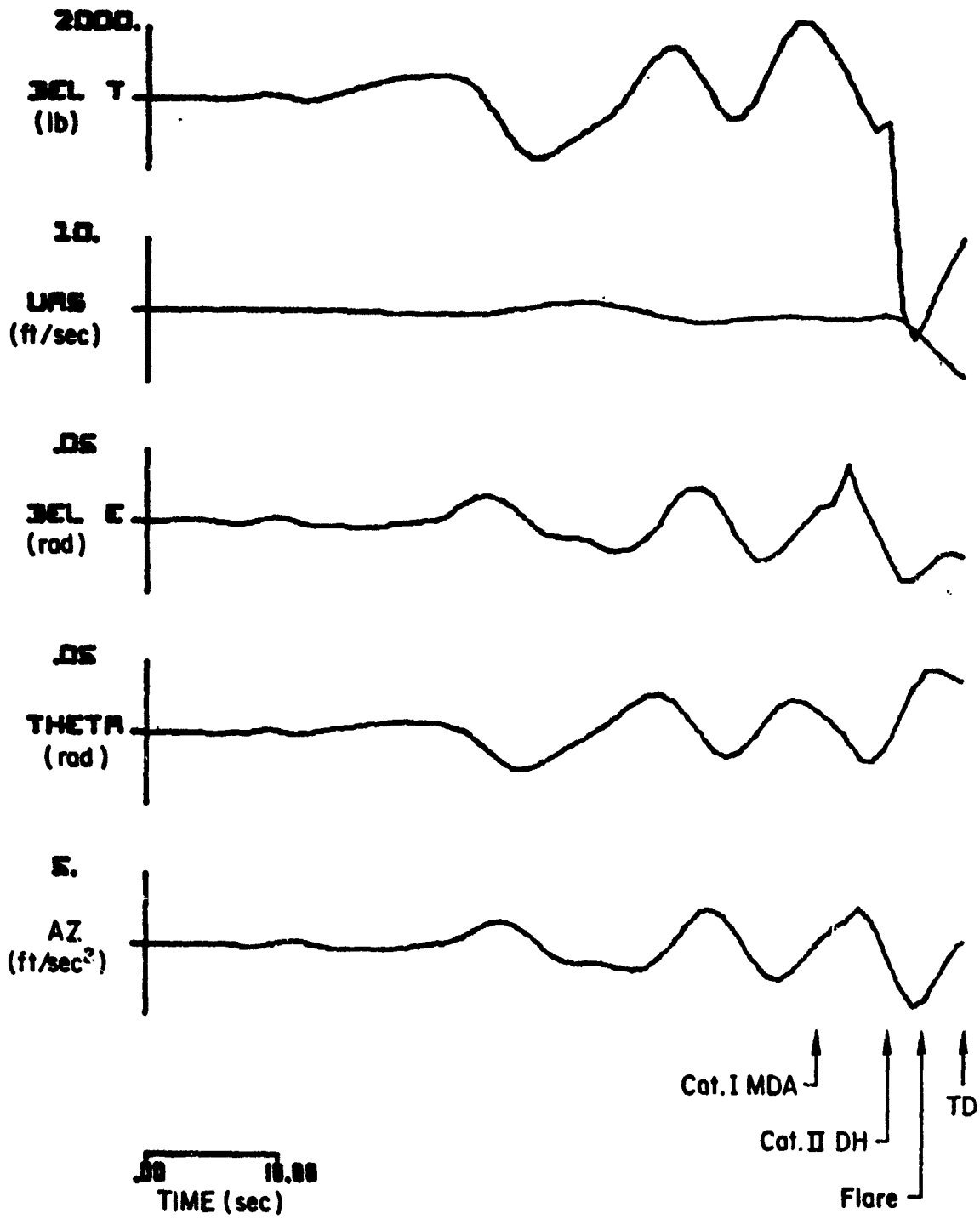

(c)

Figure A-27. (Concluded)

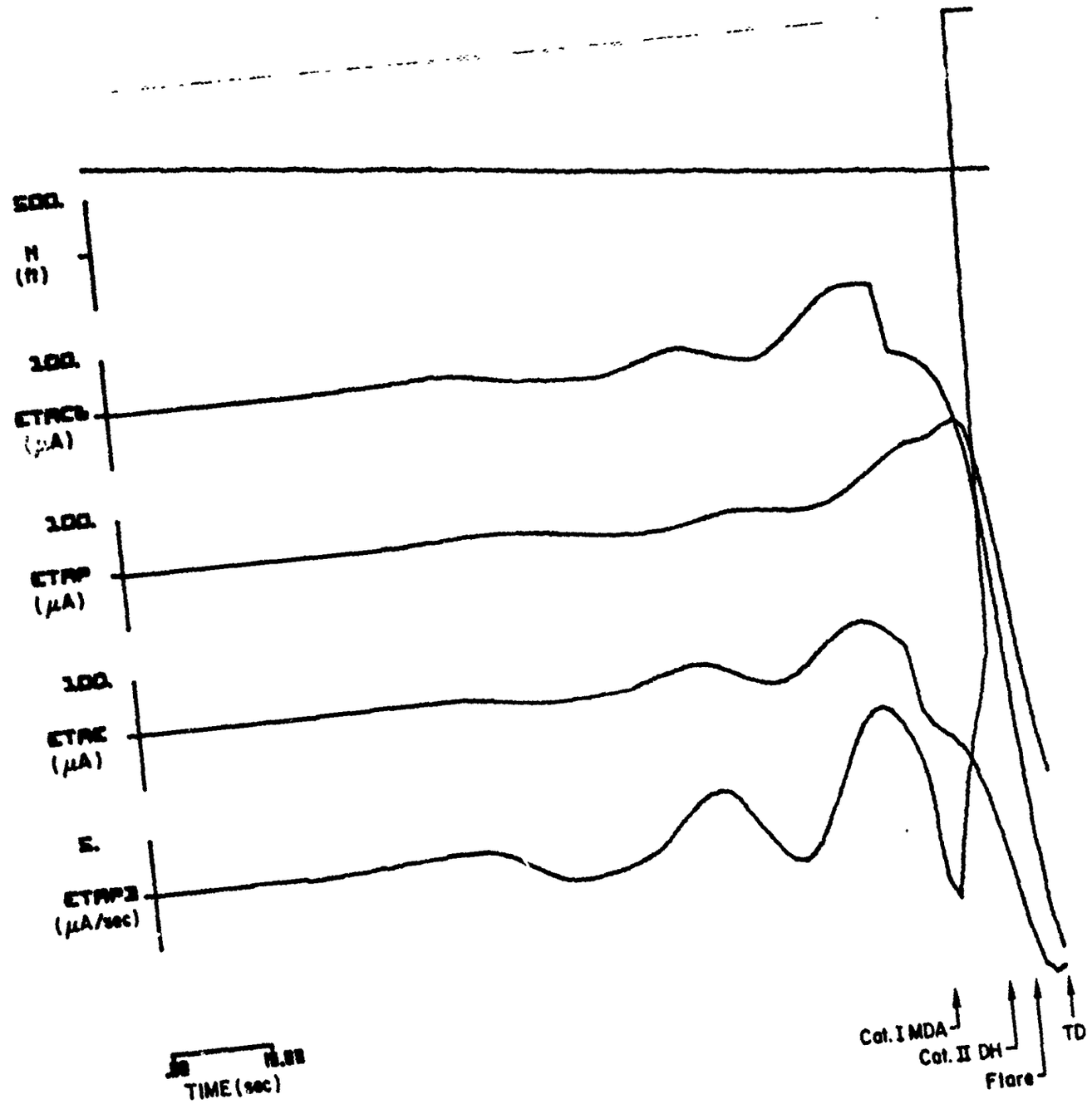

(a)

Figure A-28. Responses of the Piper PA-30 Aircraft with Invented Flight Control System and Conventional Glide Slope Coupling to Prototype Glide Slope Fault No. 9

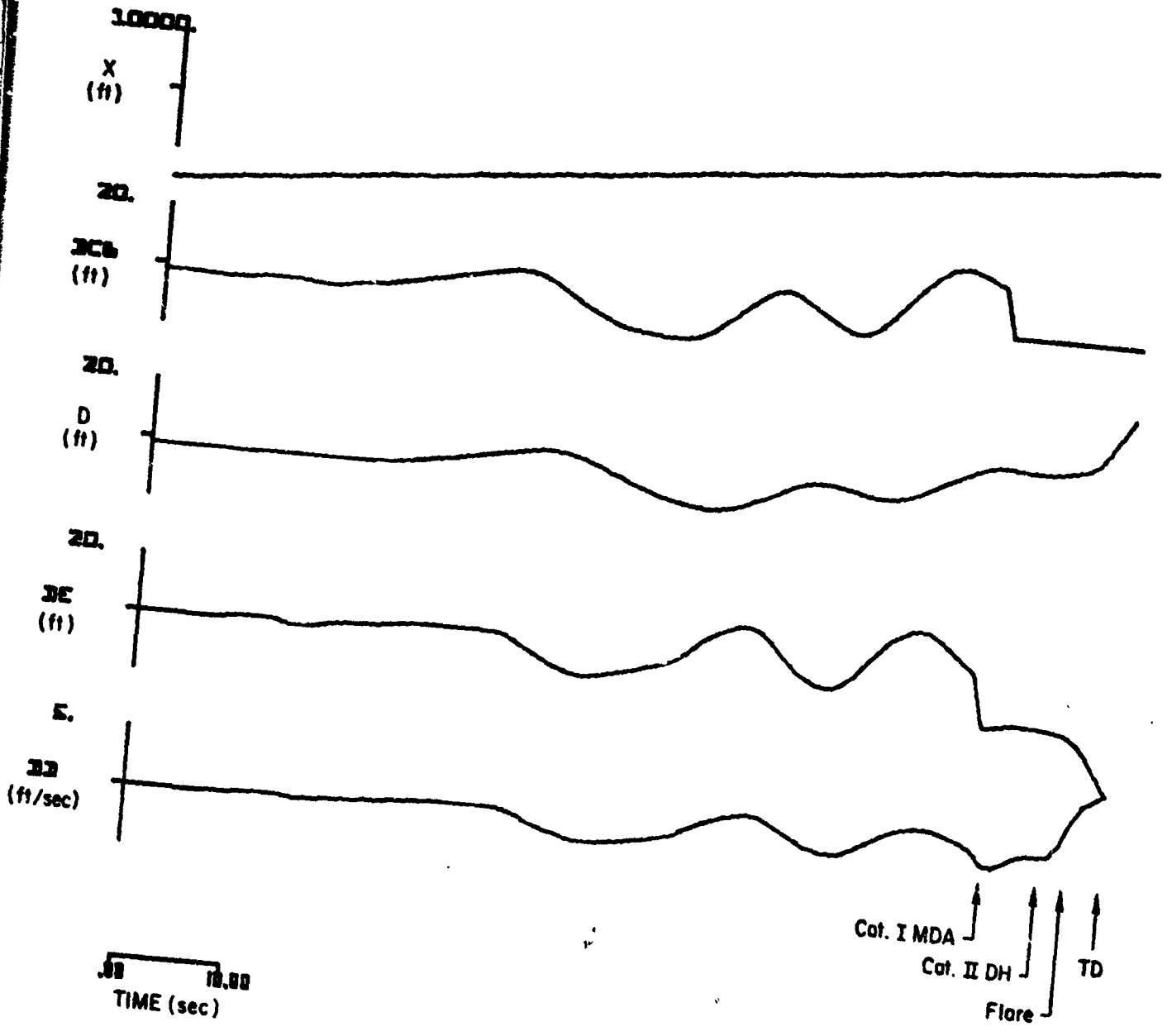

(b)

Figure A-28. (Continued)

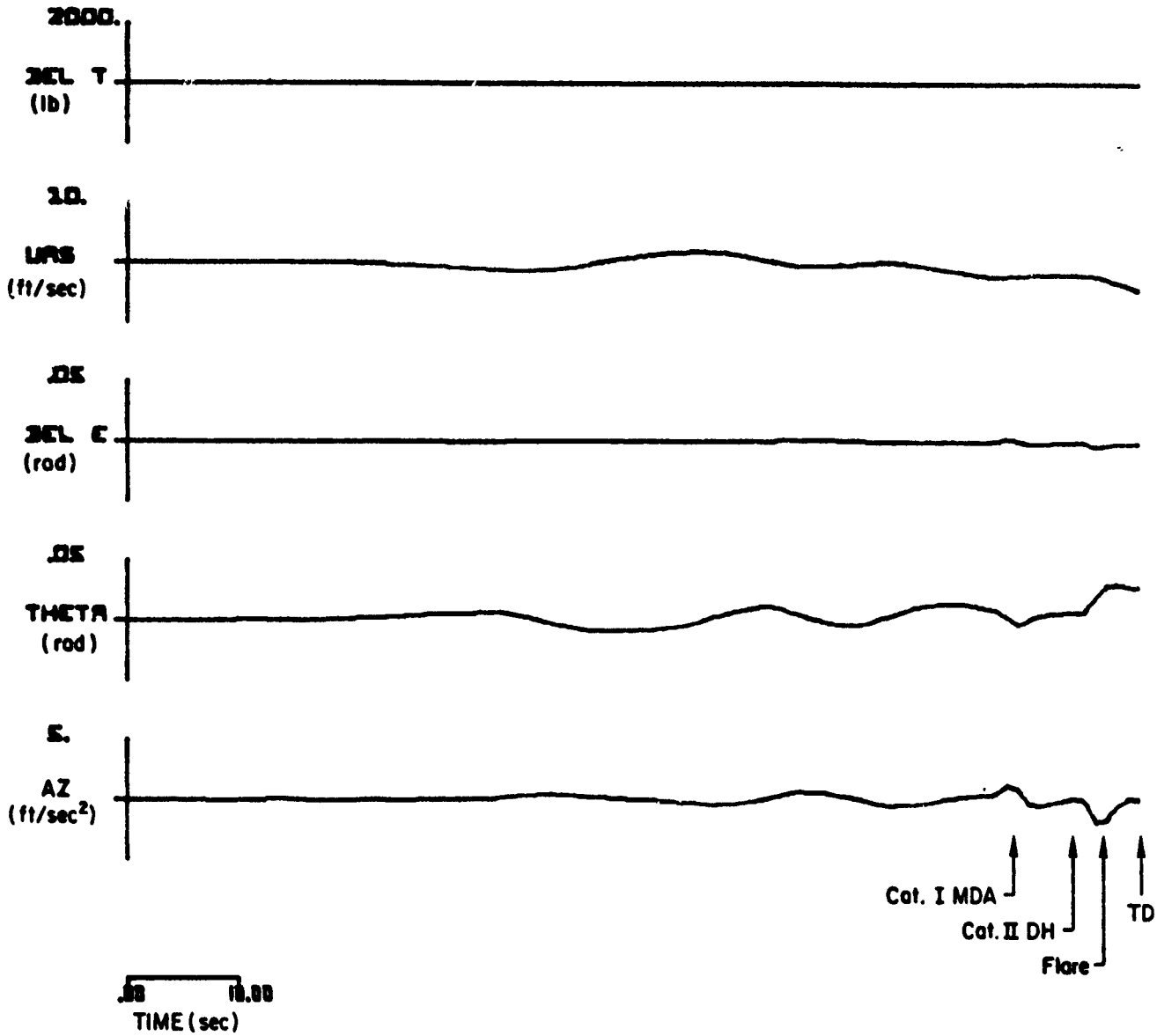

(c)

Figure A-28. (Concluded)

APPENDIX B

FILTER SYSTEM AND AIRCRAFT/CONTROL SYSTEM SIMULATION RESPONSE PLOTS FOR ACTUAL ILS GLIDE SLOPE FLIGHT INSPECTION DATA INPUT

Table B-1 provides background information for the 16 actual ILS Glide Slope flight inspection records used as inputs to the filter system and aircraft/control system simulations. This table also provides a working identification number (first column) for each record. Graphical presentations of the differential trace from these records are available (Figs. B-1 through B-12 and Figs. B-27, 31, 35, and 39). The graphical presentations are given in both linear units (feet) as measured with respect to a straight line at the commissioned angle for the particular Glide Slope facility, and in angular units (μA) as would be measured with respect to the ideal 0 DDM path by a radio telemetering theodolite set to the commissioned angle for the particular Glide Slope facility. The linear unit measurement is the DCB ($\overline{d}_c$) trace, and the angular measurement is the ETACB ($\overline{\eta}_c$) trace in the series of figures which follow.

The data in this appendix are arranged in the manner summarized in Tables B-2 and B-3. The second column of Table B-2 lists figure numbers for the responses of Filter System No. 2 to the various ILS Glide Slope flight inspection data inputs. The third through sixth columns of Table B-2 list figure numbers for the responses of the various aircraft/control system combinations to the various ILS Glide Slope flight inspection data inputs. The odd numbered figures listed in Table B-3 contain similar response data for 4 additional ILS Glide Slope flight inspection data inputs. The even numbered figures listed in Table B-3 present the standard deviations in the response variables arising from random levels of wind and wind shear from one approach to the next, and from stochastic turbulence. Defintions of the symbols used appear in the front matter.

TABLE B-1

SUMMARY OF ACTUAL GLIDE SLOPE FLIGHT INSPECTION DATA RECORDS

WORKING IDENTIFICATION NUMBER	FACILITY	TYPE	CATEGORY	DATE
1	Atlanta, GA 9R	Null Ref.	III	2/13/73
2	Atlanta, GA	Capture Effect	III	3/19/73
3	Atlanta, GA	Capture Effect	III	3/23/73
4	Pittsburgh, PA 10L	Capture Effect	II	8/5/70 ?
5	San Francisco, CA	Null Ref.	II	5/6/69
6	Oakland, CA	Null Ref.	II	5/2/69
7	JFK, NY 4R	Null Ref.	II	1/28/69
9	Staunton, VA	SB Ref.	I	?
10	Staunton, VA	End Fire	I	?
11	Staunton, VA	End Fire	I	McF. Rept.
12	Bradford, PA	Null Ref.	I	10/3/70
13	Bradford, PA	Null Ref.	I	7/22/74
14	Columbus, GA 5	Redlich Array	I	9/23/70
15	Columbus, GA 5	Null Ref.	I	?
16	Columbus, GA 5	Capture Effect	I	9/28/71
24	La Guardia, NY 22	Wave Guide (Before Modification)	II	10/6/73

TABLE B-2

SUMMARY OF FIGURE NUMBERS FOR FILTER SYSTEM AND AIRCRAFT/CONTROL SYSTEM RESPONSE DATA TO ACTUAL GLIDE SLOPE DATA

GLIDE SLOPE RECORD ID NO.	FILTER SYSTEM NO. 2	AIRCRAFT/CONTROL SYSTEM COMBINATION			
		CV-880 LSI	CV-880 INERTIALLY AUGMENTED	CV-880 FLIGHT DIRECTOR	PA-30 INVENTED
1	B-1	B-13			
3	B-2	B-14			B-15
4	B-3	B-16			
5	B-4	B-17			
6	B-5	B-18			
7	B-6	B-19			
9	B-7	B-20			
11	B-8	B-21			
12	B-9	B-22			
13	B-10	B-23			B-24
14	B-11	B-25			
15	B-12	B-26			

TABLE B-3

SUMMARY OF FIGURE NUMBERS FOR AIRCRAFT/CONTROL SYSTEM RESPONSES TO ACTUAL GLIDE SLOPE DATA, WIND, WIND SHEAR AND TURBULENCE

GLIDE SLOPE RECORD ID NO.	AIRCRAFT/CONTROL SYSTEM COMBINATION			
	CV-880 LSI	CV-880 INERTIALLY AUGMENTED	CV-880 FLIGHT DIRECTOR	PA-30 INVENTED
2	B-27, 28			B-29, 30
10	B-31, 32	B-33, 34		
16	B-35, 36	B-37, 38		
24	B-39, 40	B-41, 42		

REMARKS ON SIMULATION DATA

Filter system response data appearing in Figs. B-1 through B-12 closely simulate results which would be obtained in a field test of the filter system at the given ILS Glide Slope facility. The only assumption made is that the inspecting aircraft is approaching at constant ground speed and rate of descent. This assumption is close to the facts of actual operation. The filter system responses extend down to the point where the ideal path asymptote has an altitude of 50 ft. This point nominally corresponds to the point of runway threshold crossing.

The aircraft/control system combination response data appearing in Figs. B-13 through B-26 and odd numbered figures B-27 through B-41 have the following characteristics requiring further explanation. The DCB ($\bar{d}_c$) trace represents the Glide Slope forcing function. The DCB trace is derived from the ETACB ($\bar{\eta}_c$) data. The ETACB trace is active until the Category I minimum descent altitude or Category II decision height is reached on a manually completed landing (CV-880 Category I and Piper PA-30 cases). Below the minimum descent altitude or decision height the ETACB trace is set to zero. On automatically completed landings, the ETACB trace is active until the flare initiation altitude is reached. Below that altitude the ETACB trace is held constant at the value prevailing at flare initiation. These cases include Category II or III approaches and automatic landings with the CV-880 and the LSI automatic landing system (LSI) or an inertially augmented version of the LSI automatic landing system (IS).

The standard deviation plots (even numbered figures, Figs. B-28 through B-42) require further information for correct interpretation. The first point is that the altitude, H (h), and ground range, X, traces in all figures are the mean (or expected) values of those variables. These provide the capability to read the standard deviation traces as functions of altitude, distance or time, as desired. The next feature is that the standard deviation data for each variable is presented in two components for simulated Category I approaches and manually completed landings. One component, the trace designated W in the figures, is that arising from random wind and wind shear effects. The other component, the trace designated T in the figures, is that

arising from turbulence. The total standard deviation, which is not plotted, is given by the root-sum-squared value of the two components. The standard deviation data for simulated Category II and III approaches and landings is presented in similar fashion down to the Category II decision height. However, below the decision height, the total standard deviation is plotted. This is because the standard deviation components cannot be distinguished below the decision height because the model of the missed approach decision process operates in a nonlinear manner upon the standard deviation components at the decision height. This model of the missed approach decision process is also responsible for the fact that the total standard deviation value immediately below the decision height is less than or equal to the root-sum-squared value of the standard deviation component values immediately above the decision height. This arises because the missed approach decision process is modeled in the simulation as the expected outcome of a single discrete Kalman measurement update at the decision height.

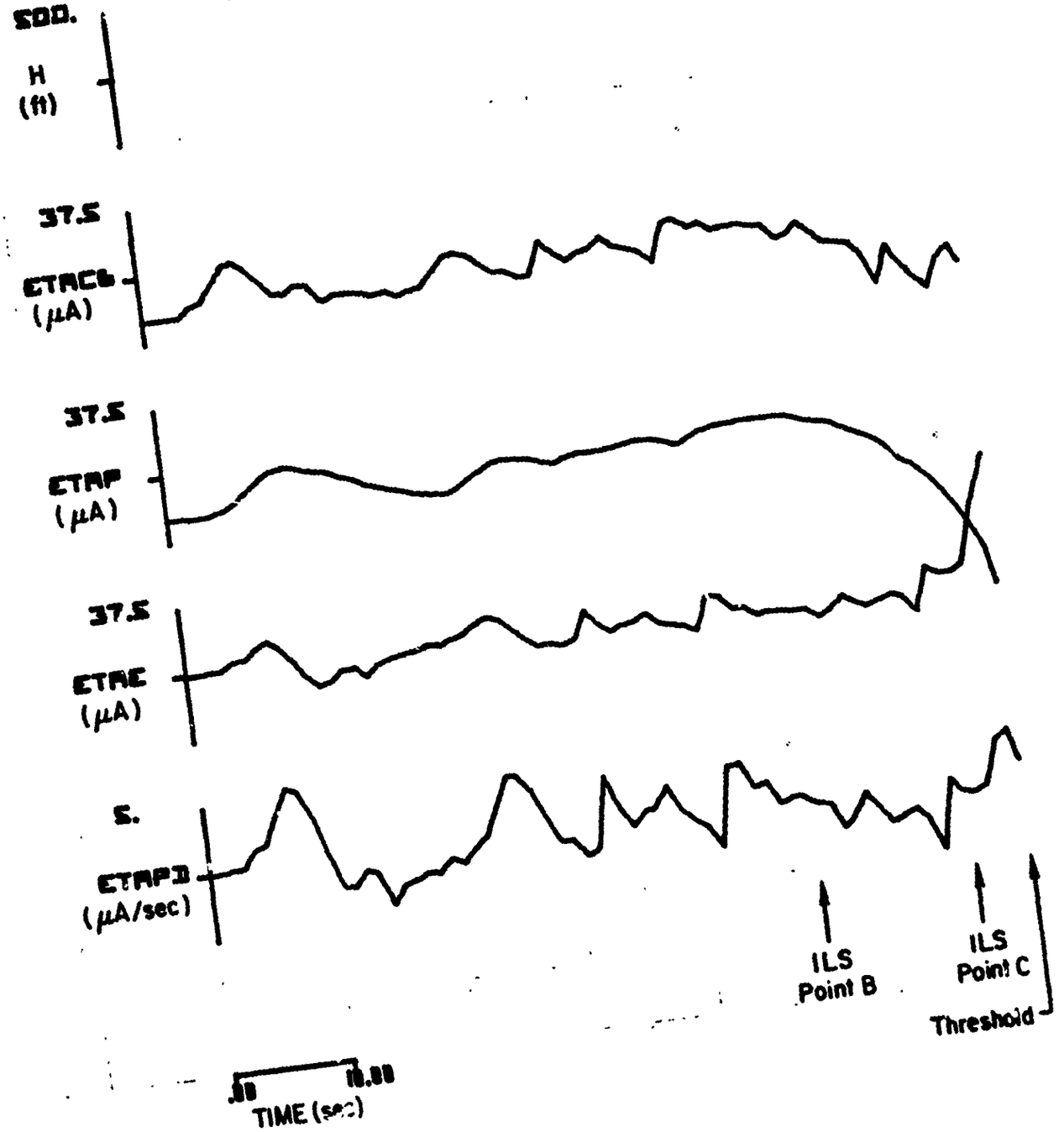

(a)

Figure B-1. Responses of Filter System No. 2 to ILS Glide Slope Input No. 1

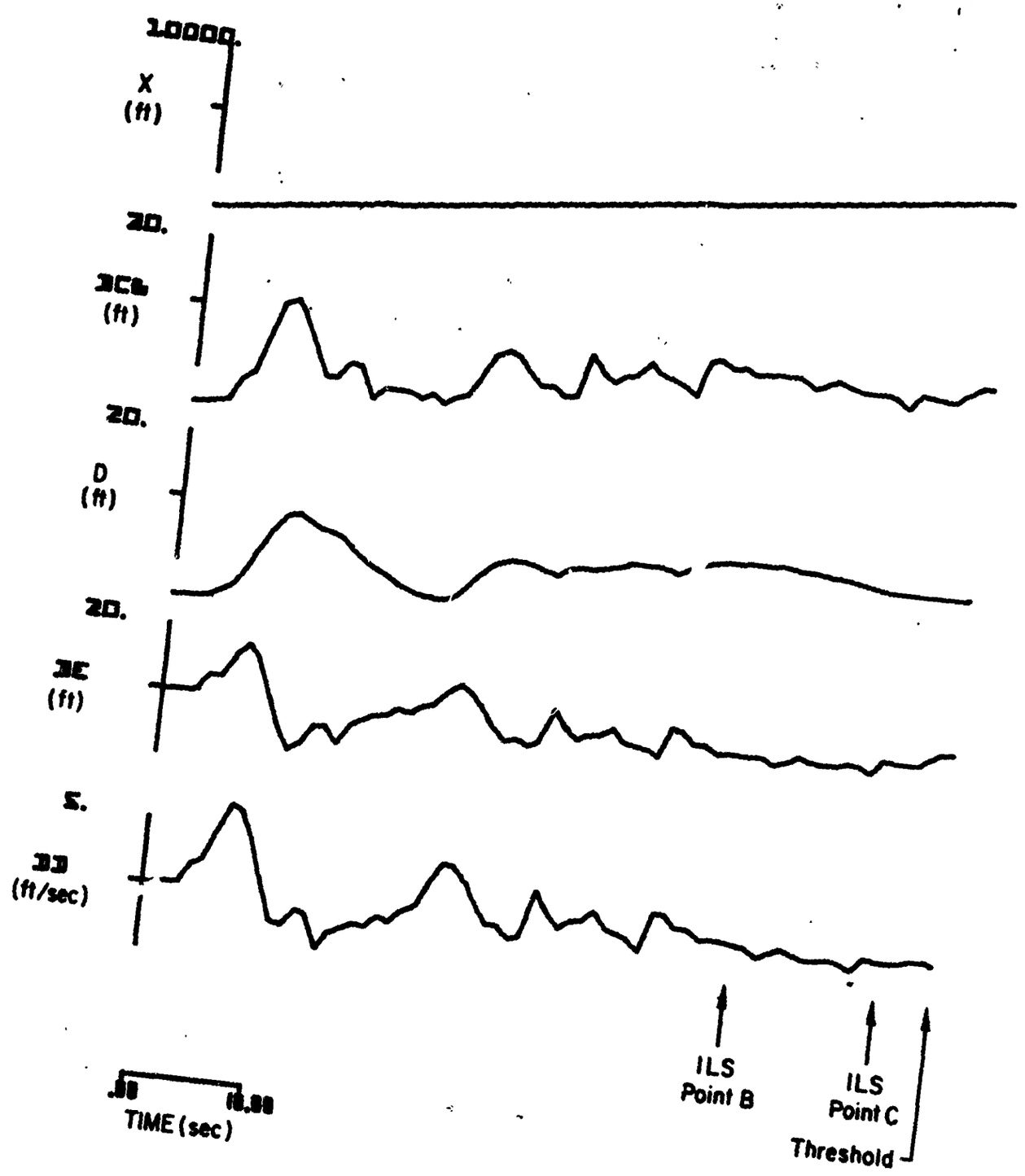

(b)

Figure B-1. (Concluded)

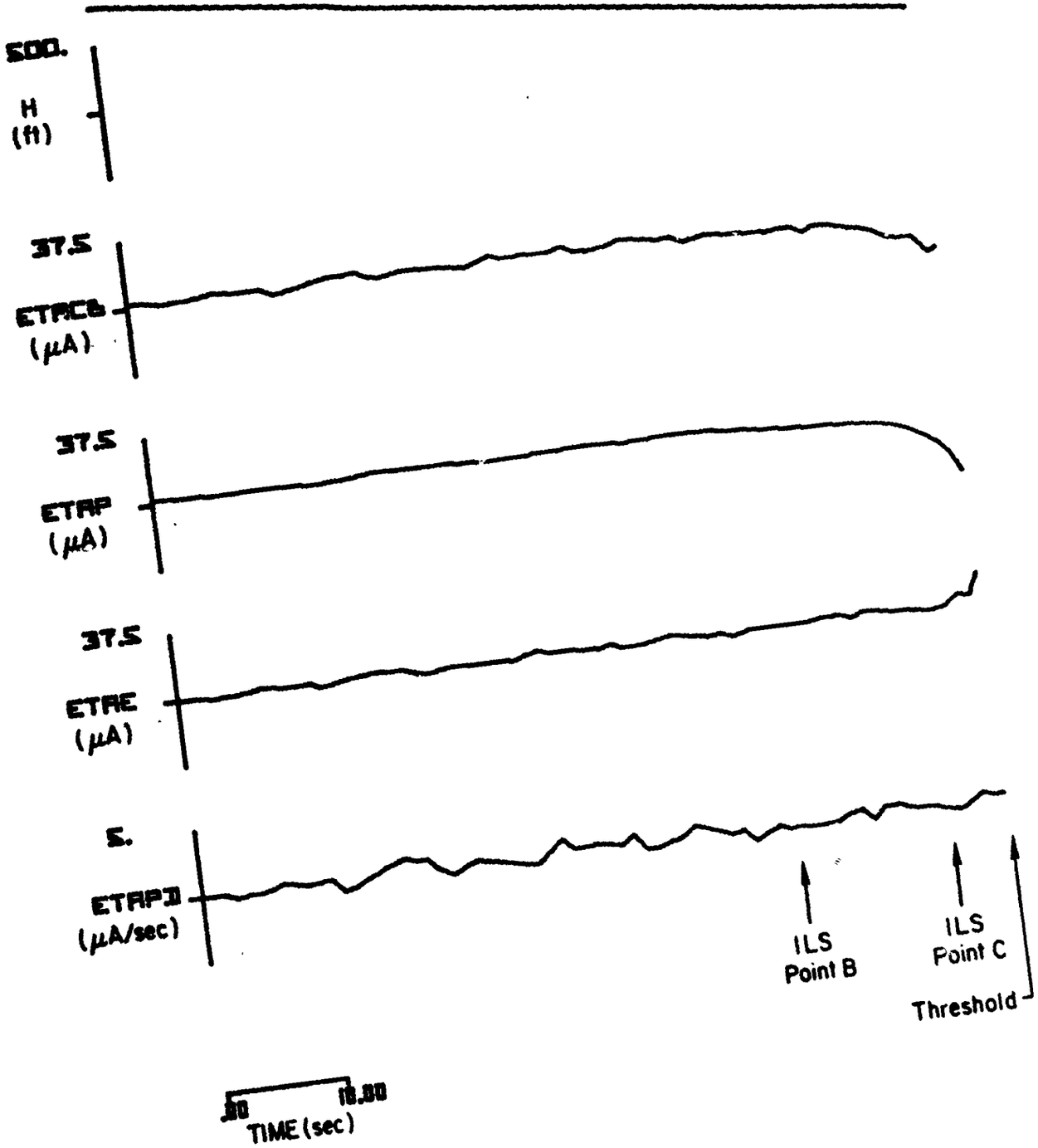

(a)

Figure B-2. Responses of Filter System No. 2 to ILS Glide Slope Input No. 3

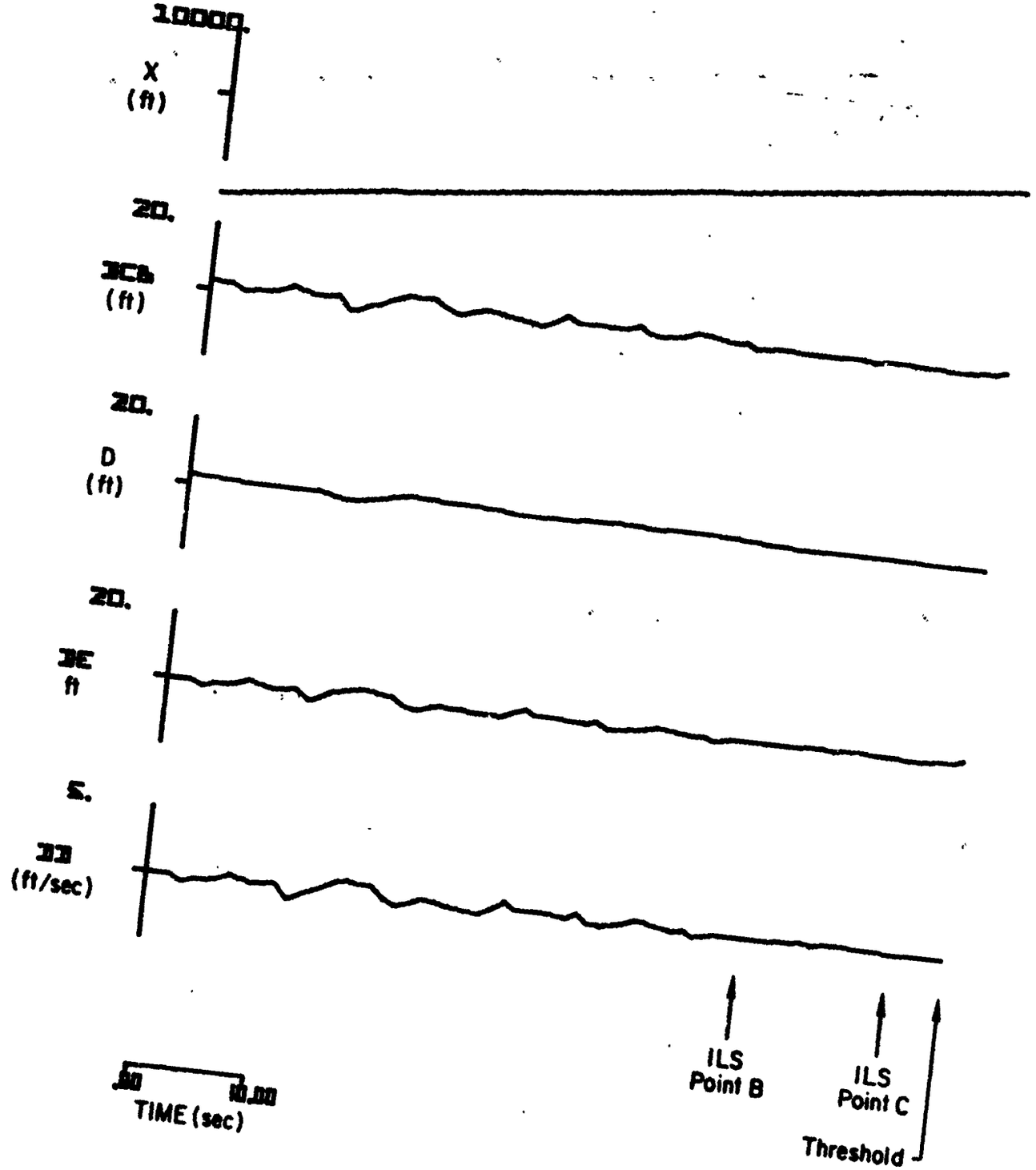

(b)

Figure B-2. (Concluded)

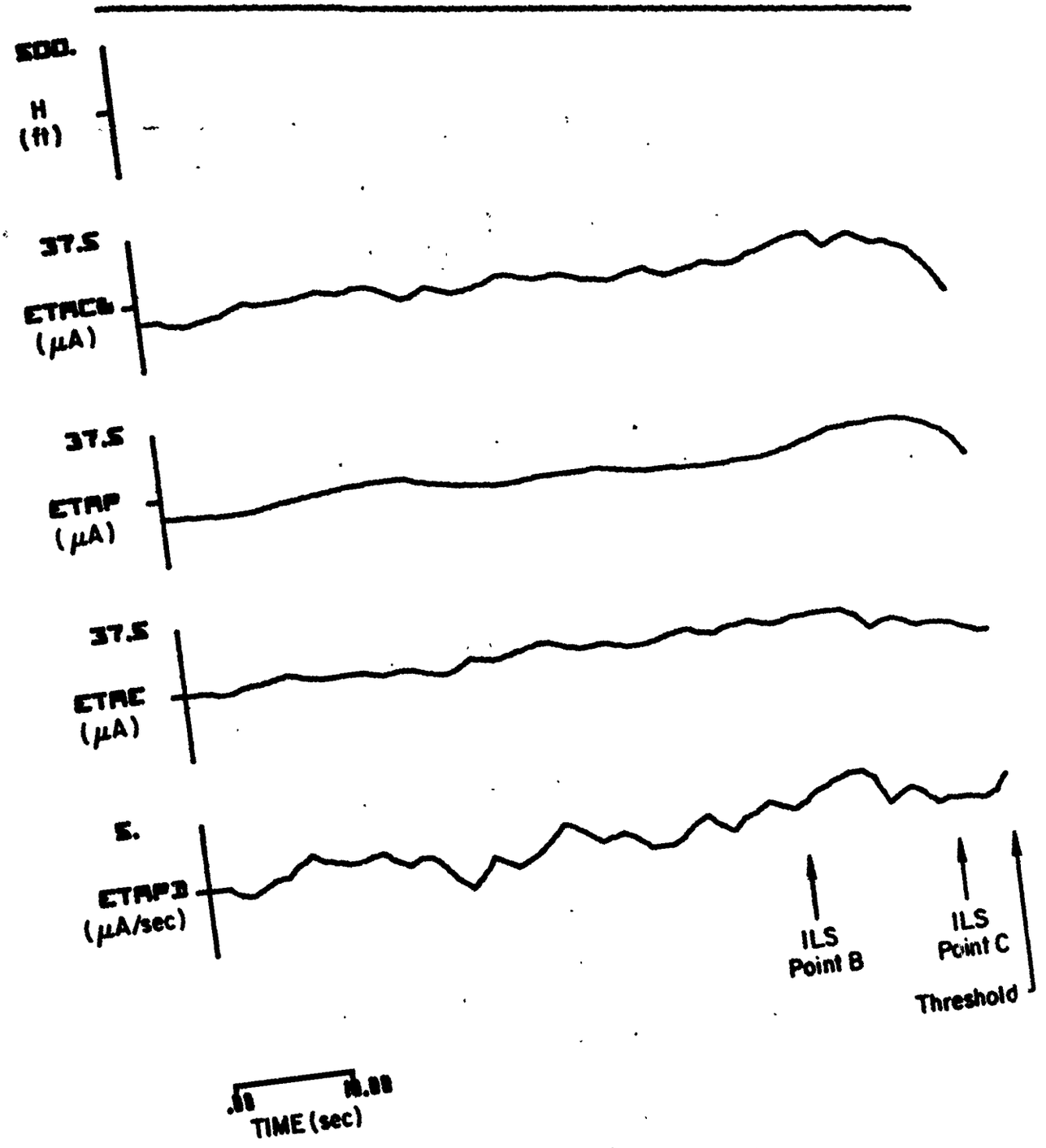

(a)

Figure B-3. Responses of Filter System No. 2 to ILS Glide Slope Input No. 4

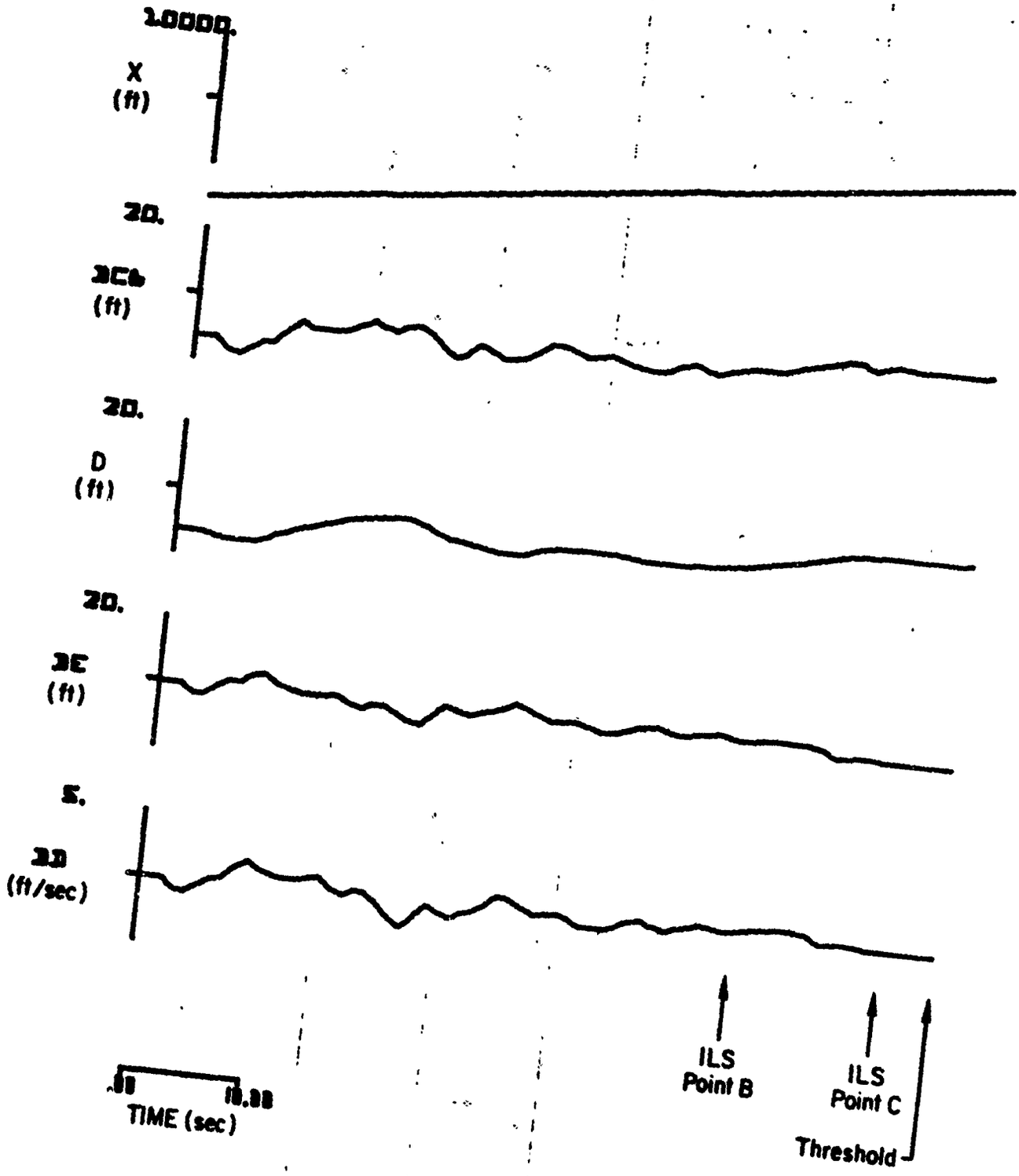

(b)

Figure B-3. (Concluded)

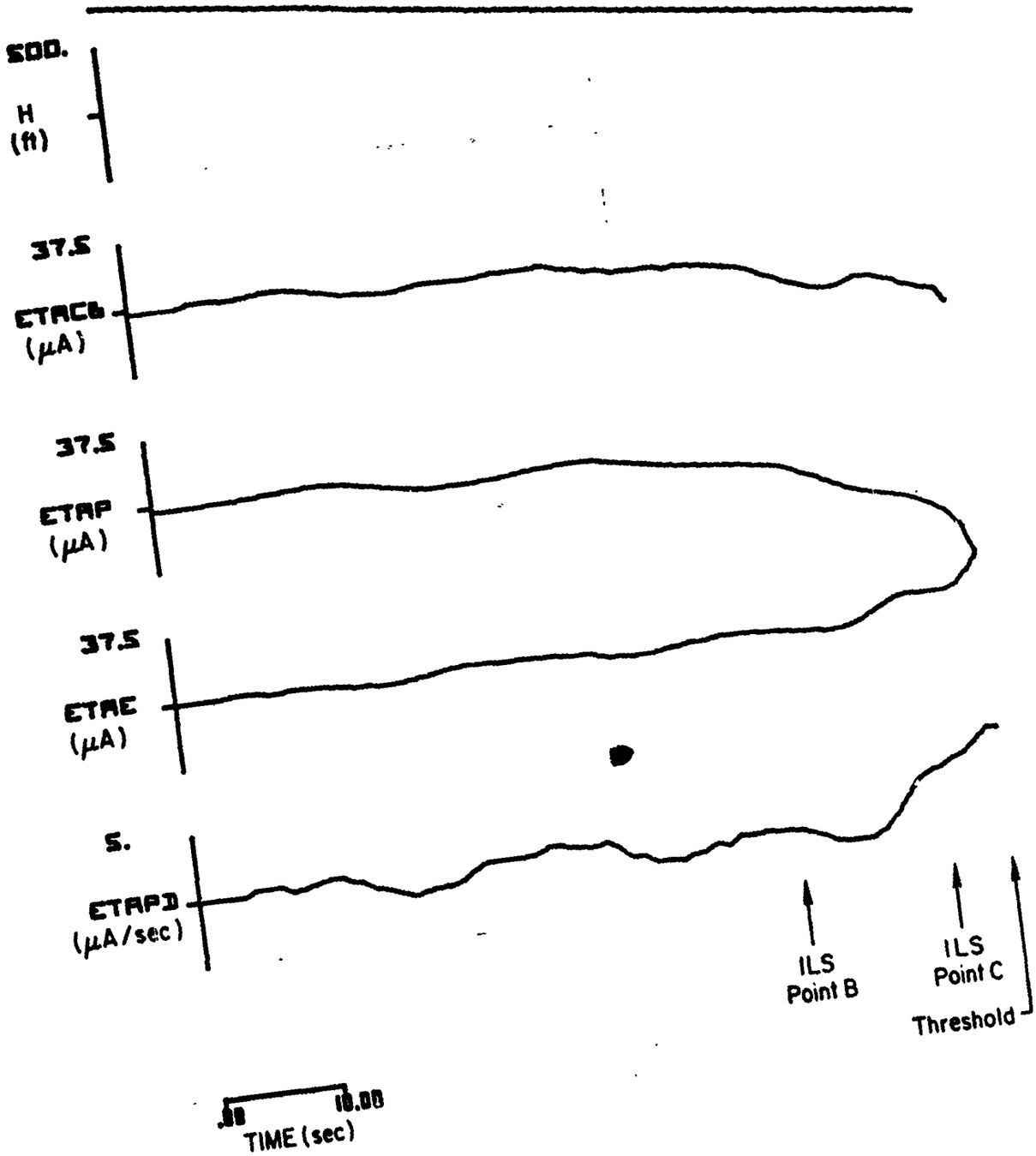

(a)

Figure B-4. Responces of Filter System No. 2 to ILS Glide Slope Input No. 5

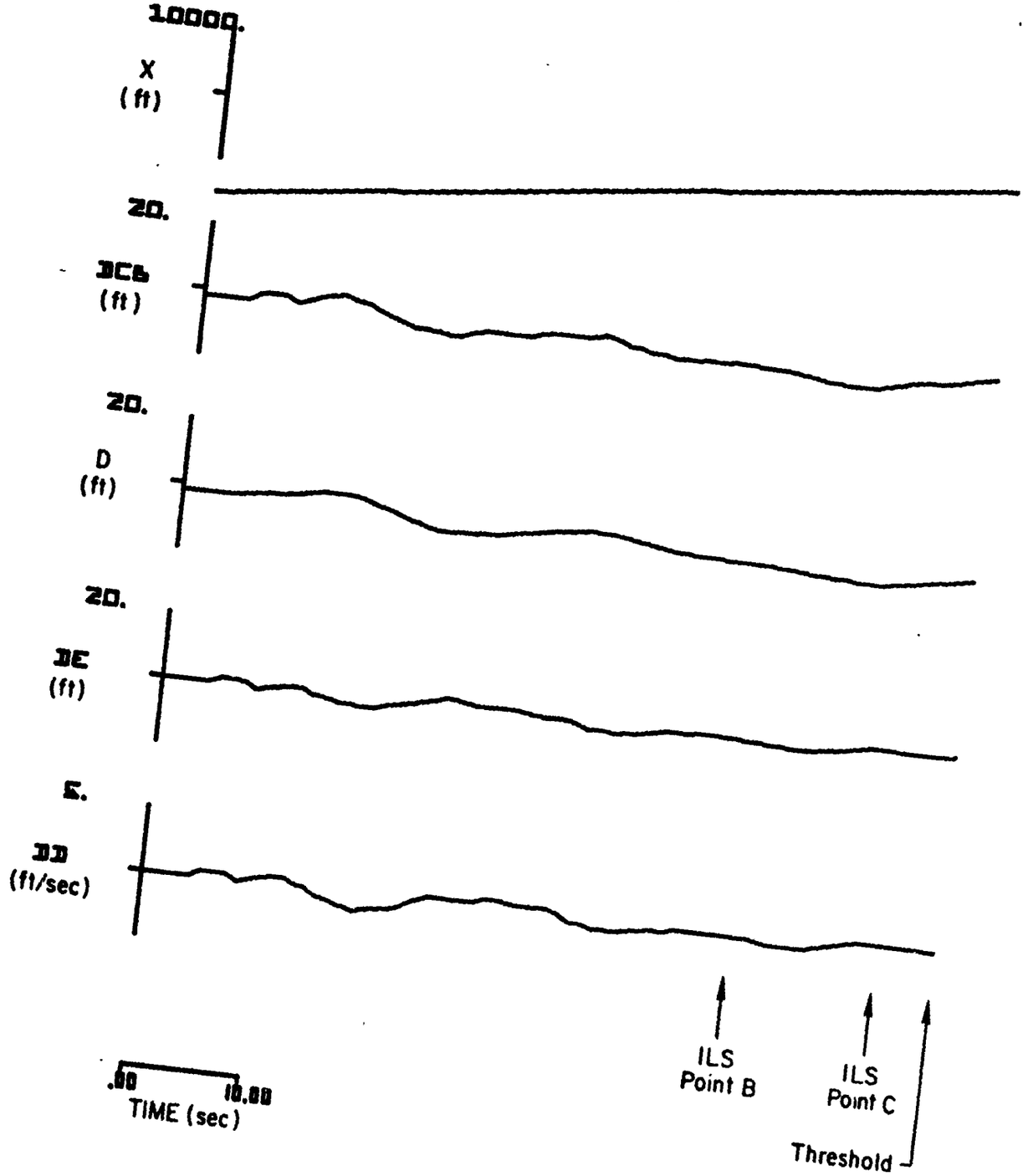

(b)

Figure B-4. (Concluded)

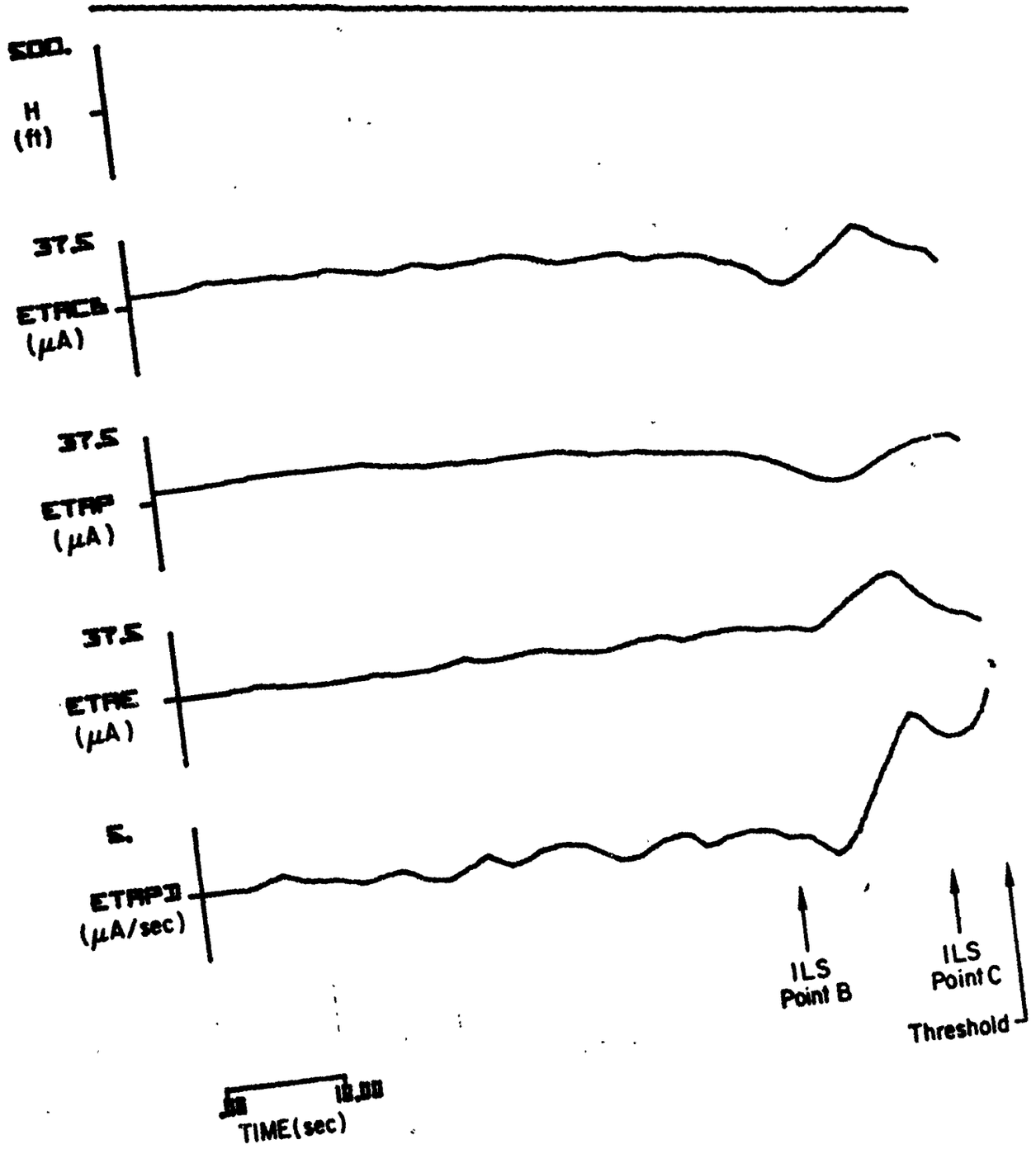

(a)

Figure B-5. Responses of Filter System No. 2 to ILS Glide Slope Input No. 6

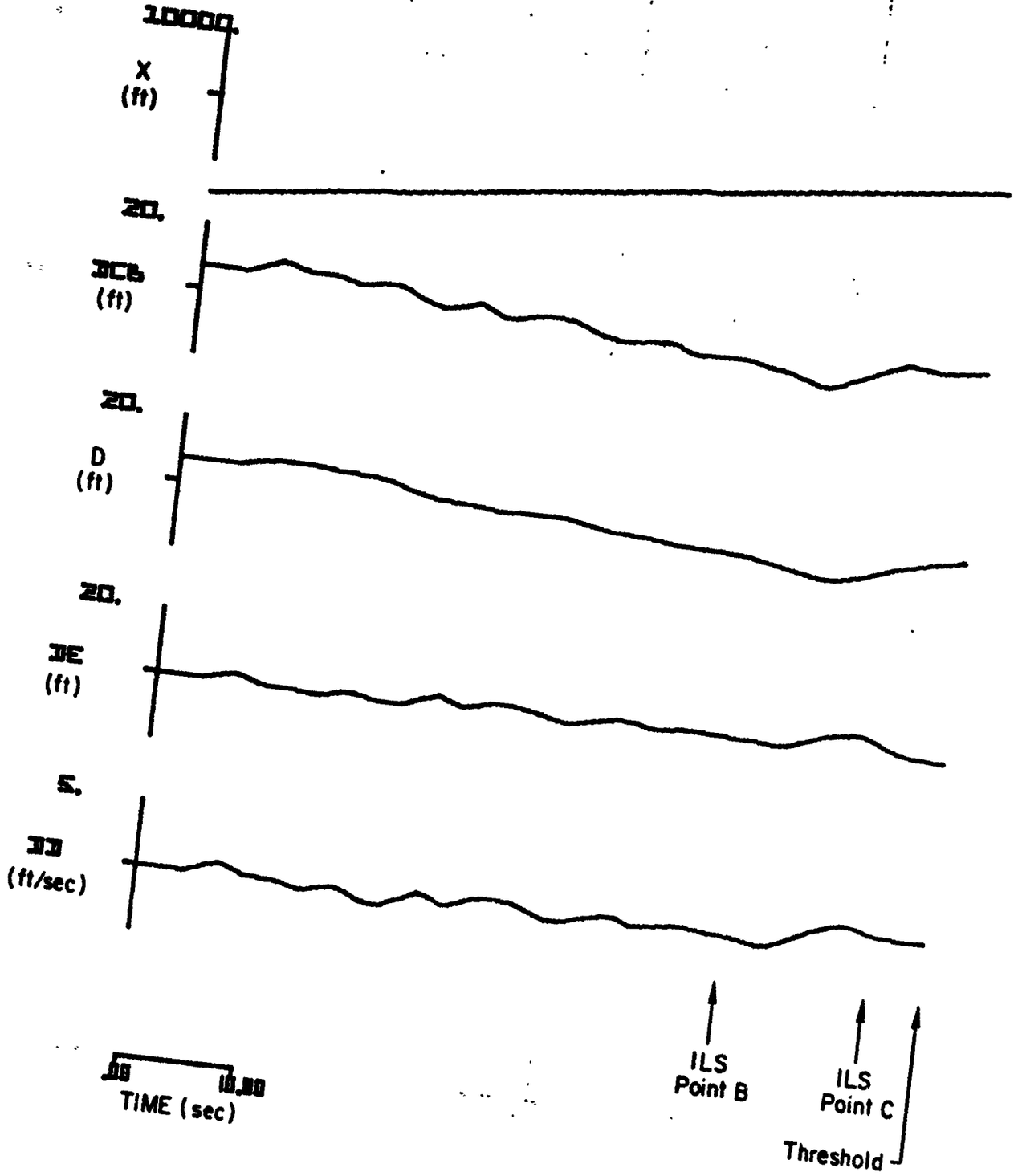

(b)

Figure B-5. (Concluded)

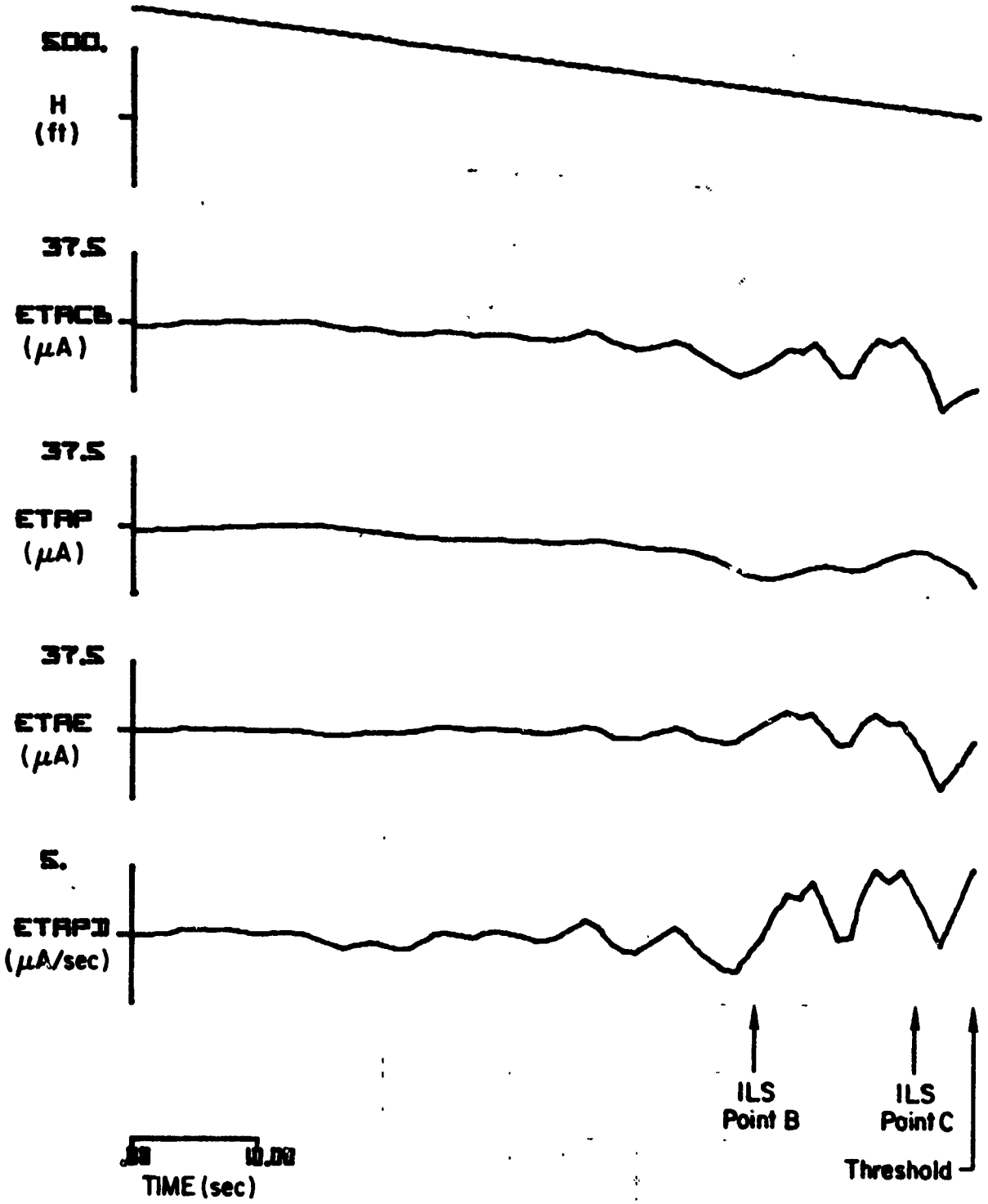

(a)

Figure B-6. Responses of Filter System No. 2 to ILS Glide Slope Input No. 7

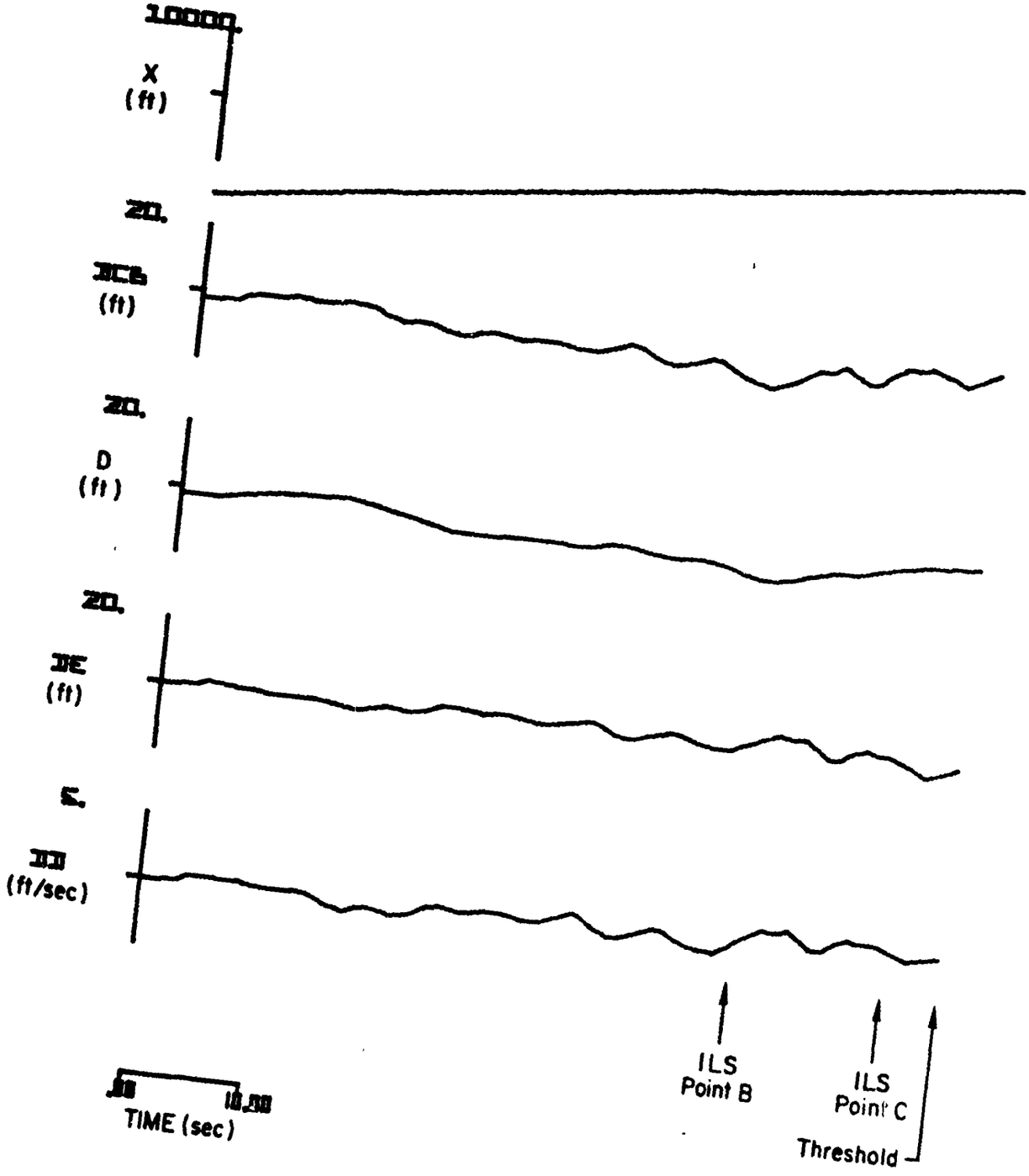

(b)

Figure B-6. (Concluded)

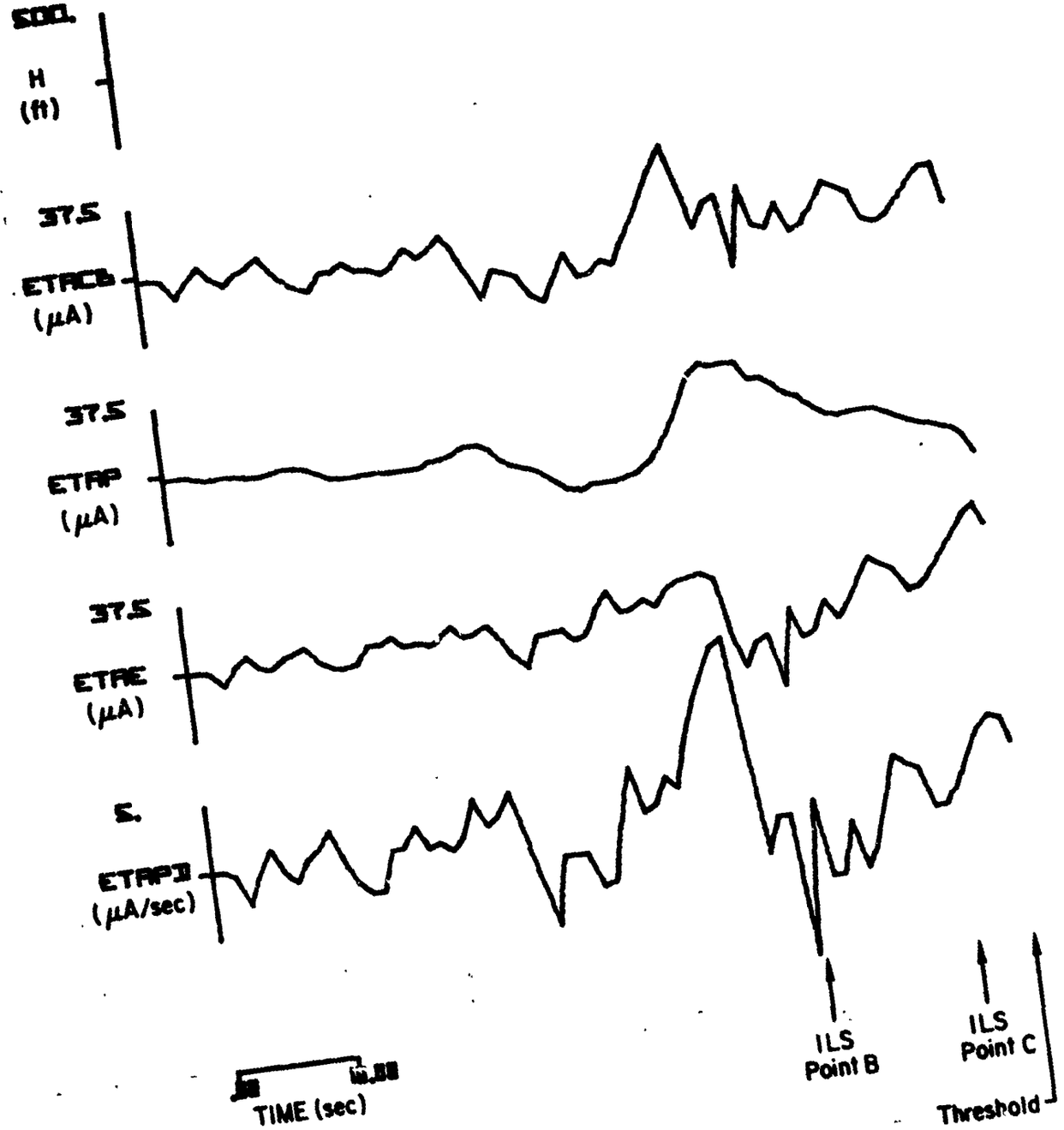

(a)

Figure B-7. Responses of Filter System No. 2 to ILS Glide Slope Input No. 9

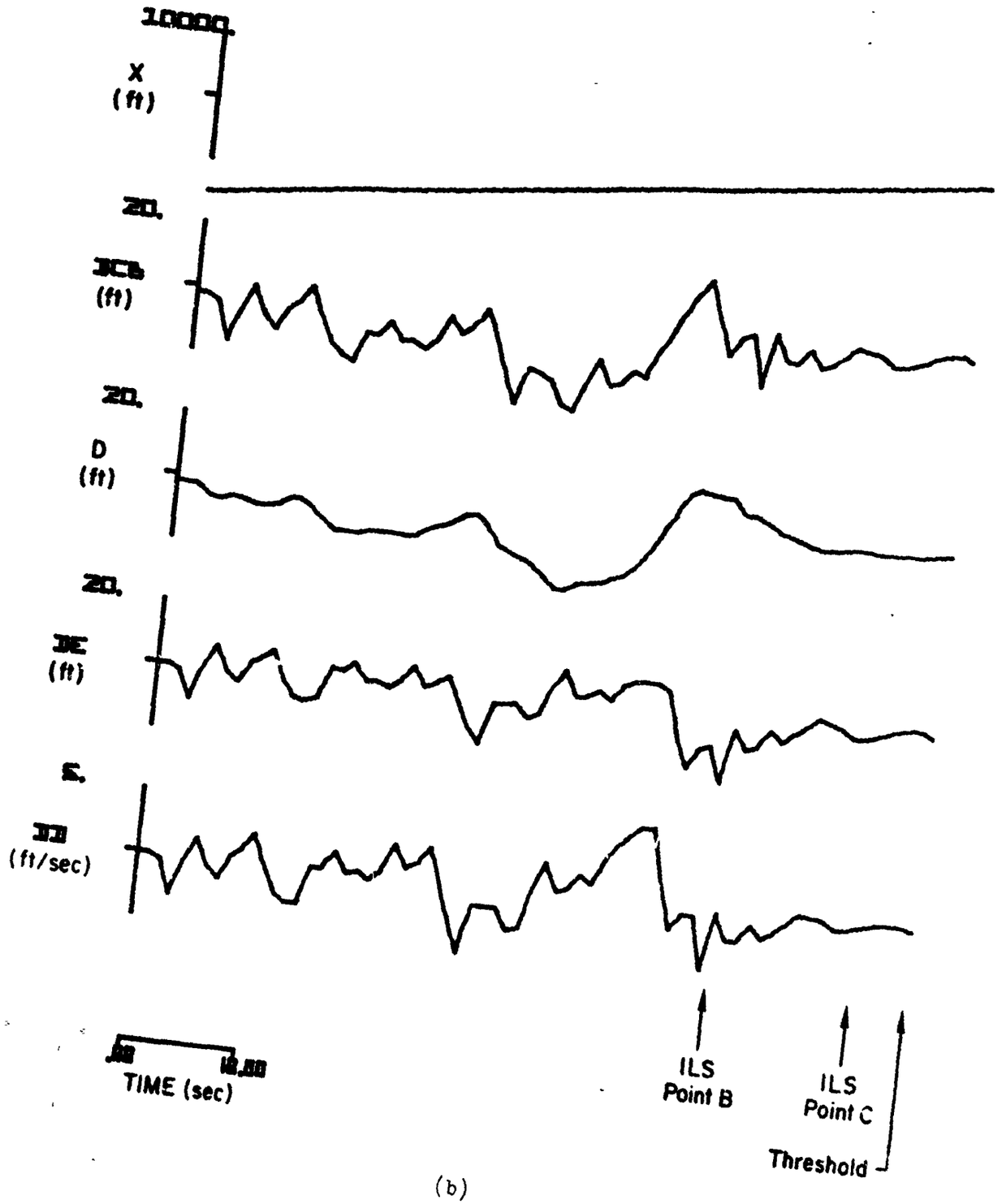

(b)

Figure B-7. (Concluded)

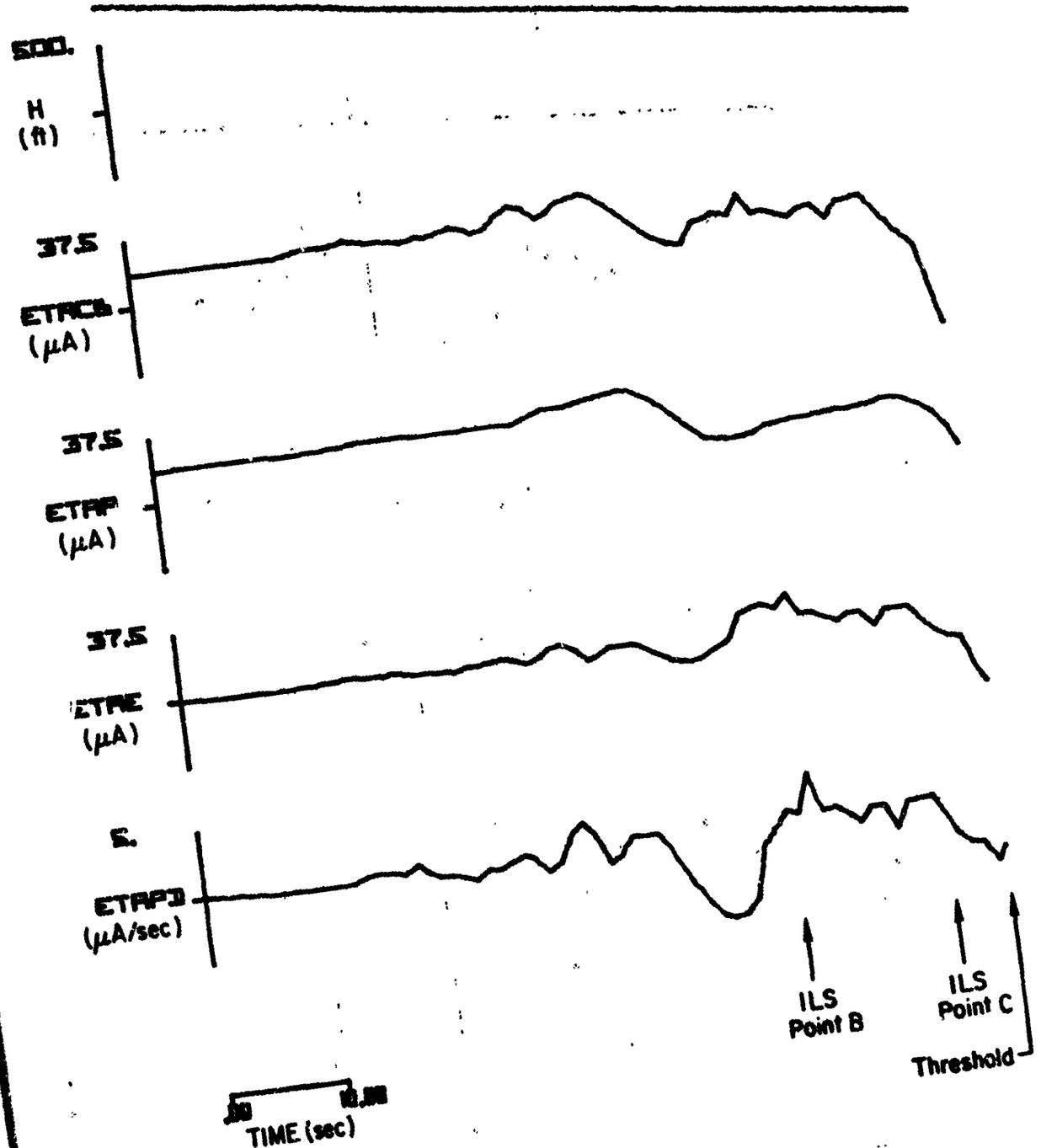

(a)

Figure B-8. Responses of Filter System No. 2 to ILS Glide Slope Input No. 11

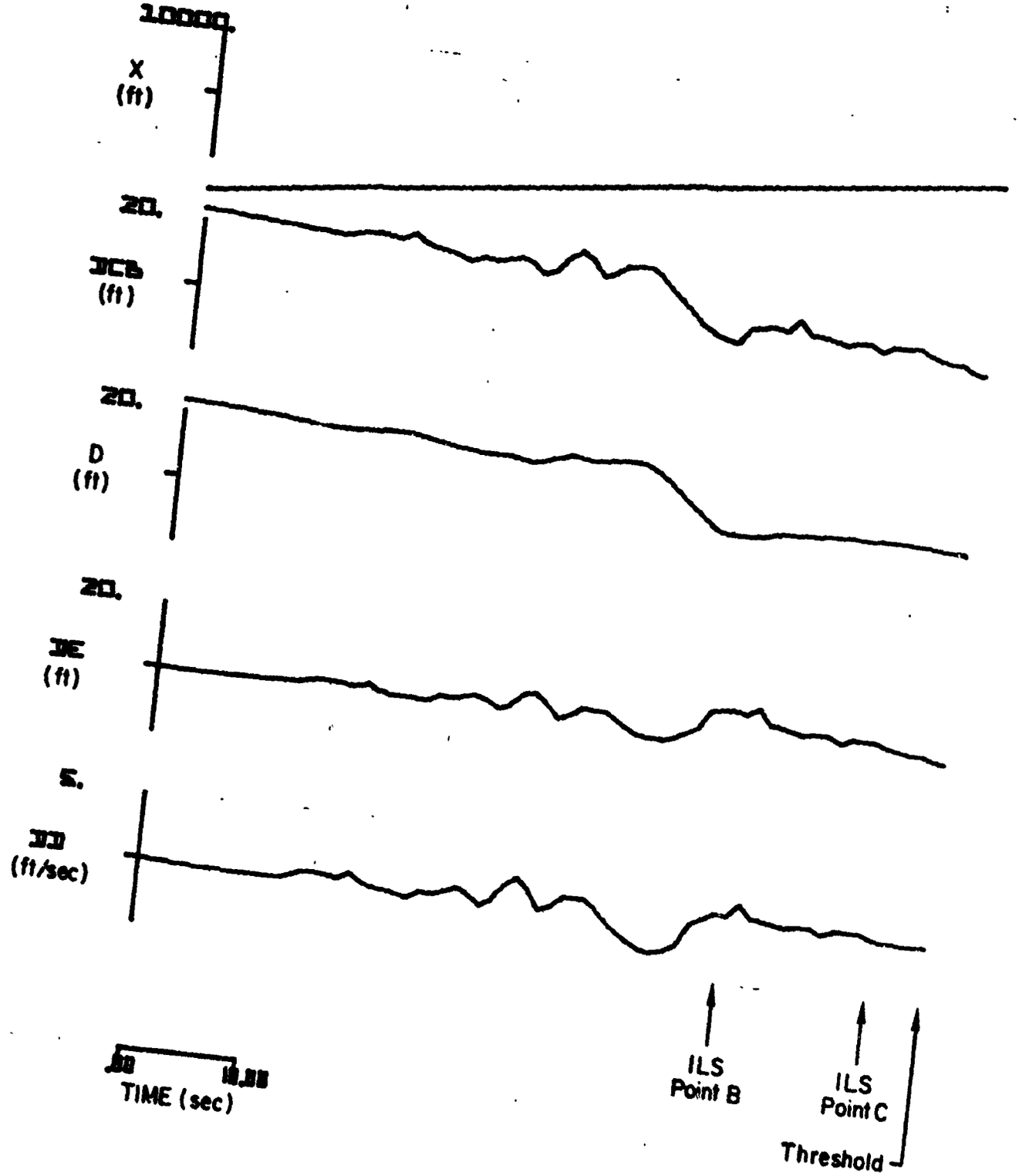

(b)

Figure B-8. (Concluded)

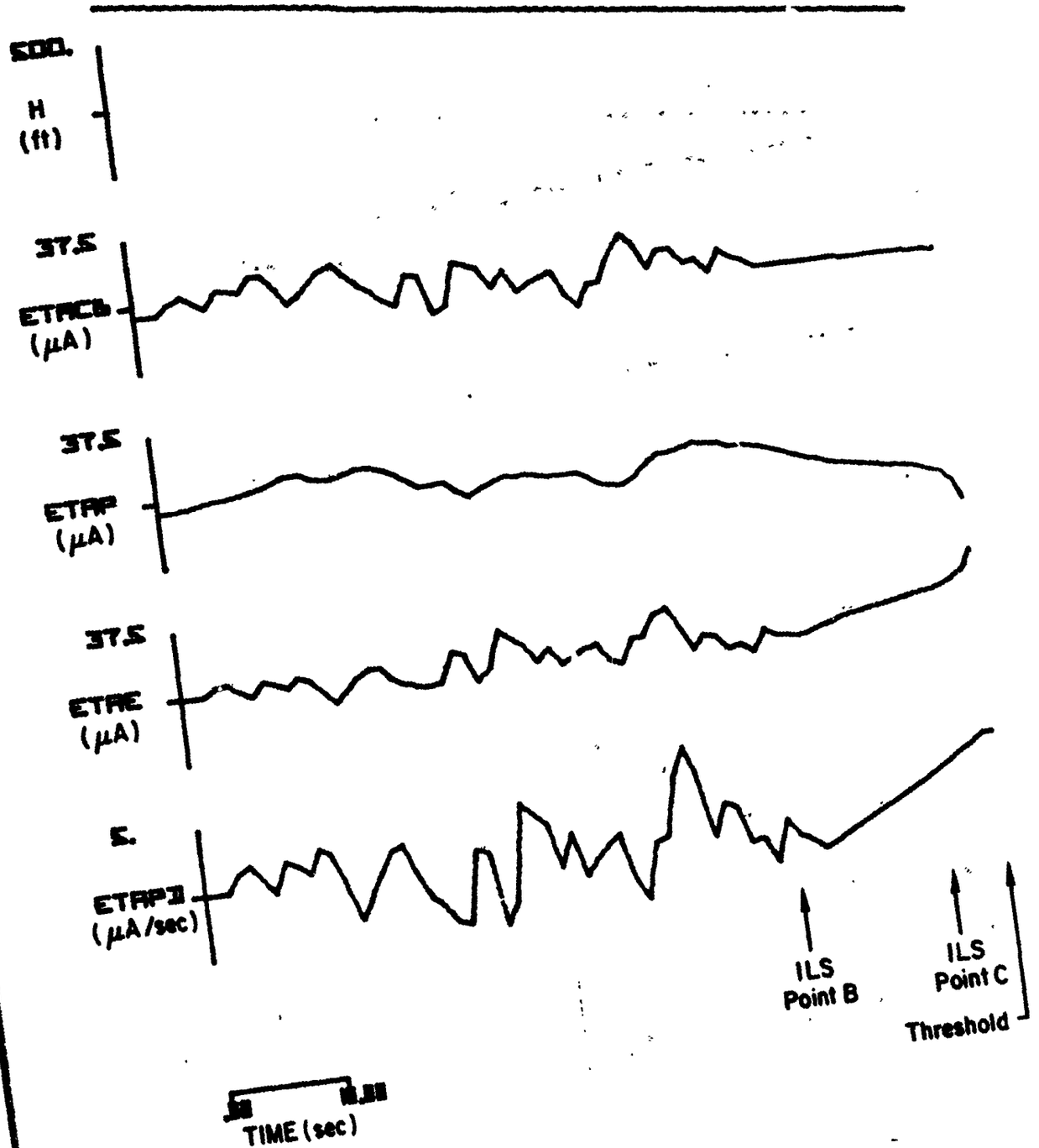

(a)

Figure B-9. Responses of Filter System No. 2 to ILS Glide Slope Input No. 12

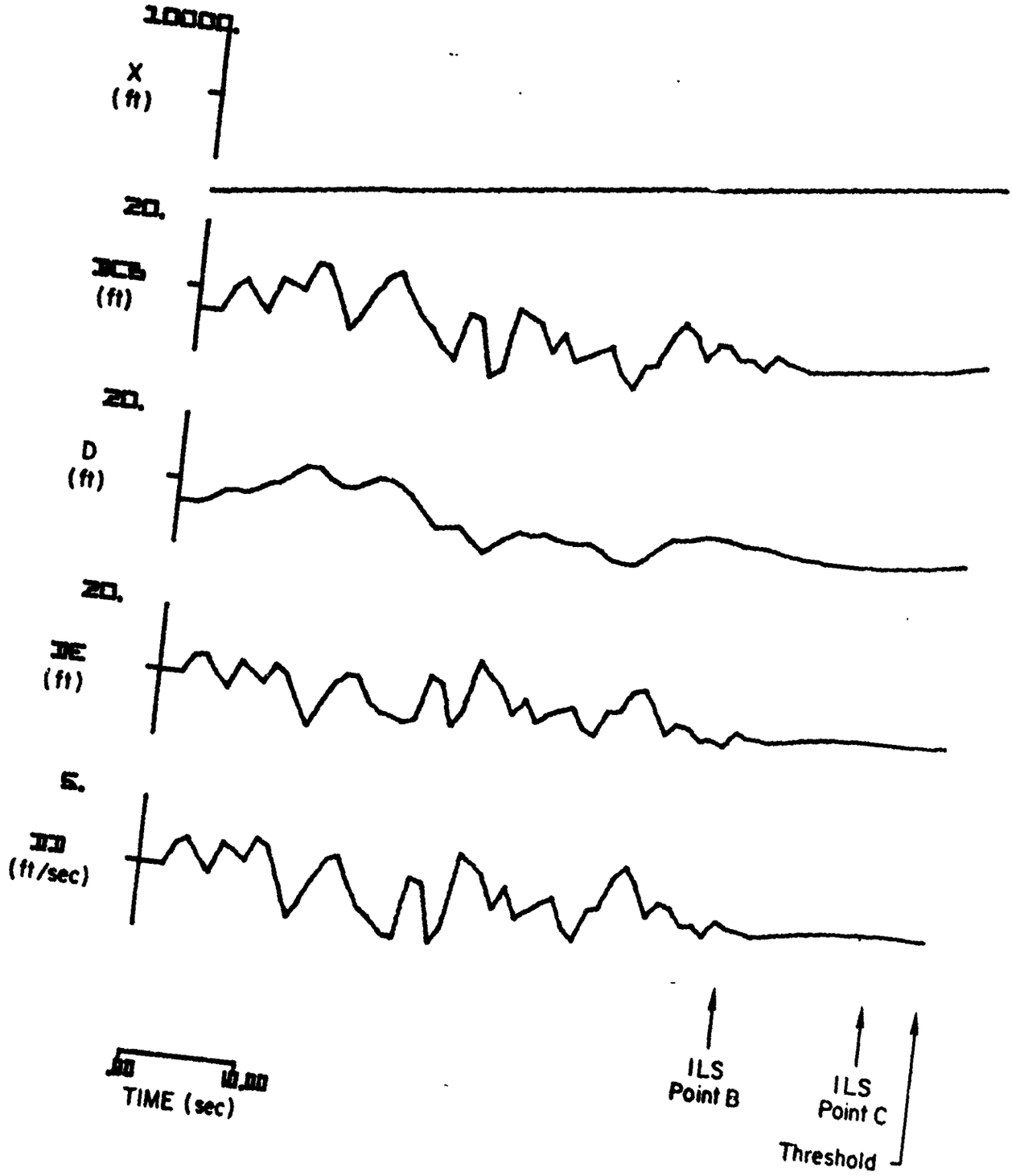

(b)

Figure B-9. (Concluded)

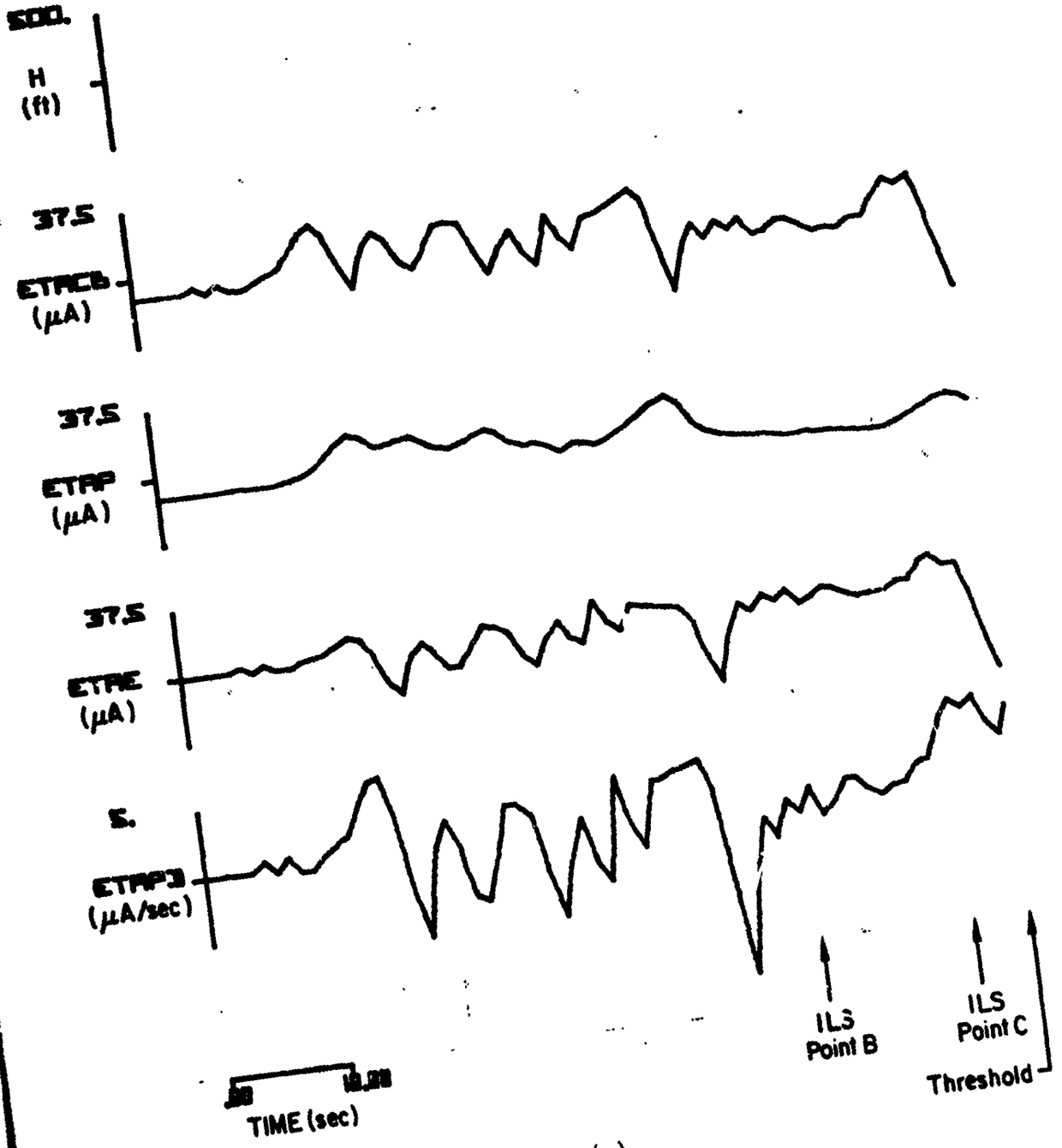

(a)

Figure B-10. Responses of Filter System No. 2 to ILS Glide Slope Input No. 13

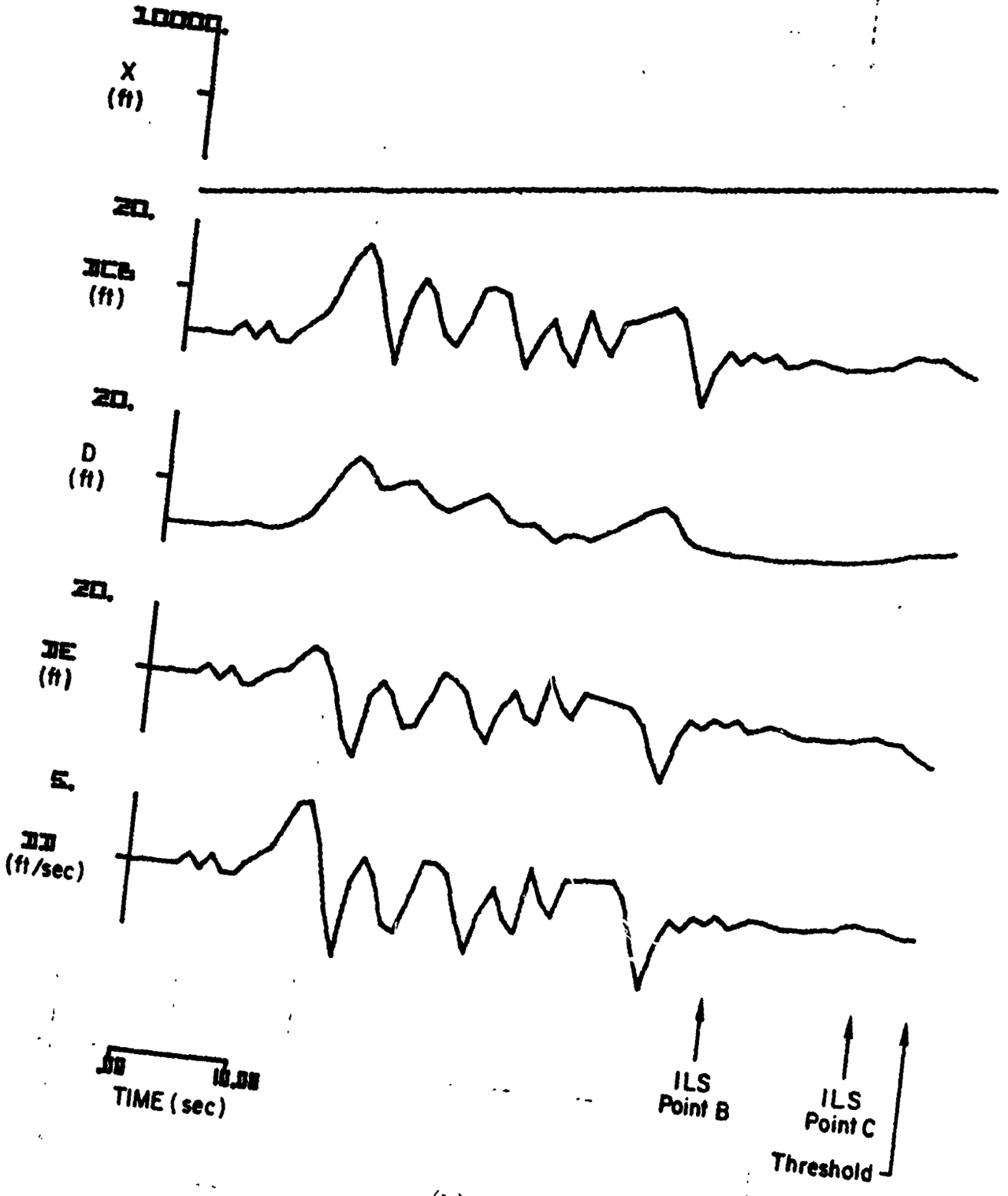

(b)

Figure B-10. (Concluded)

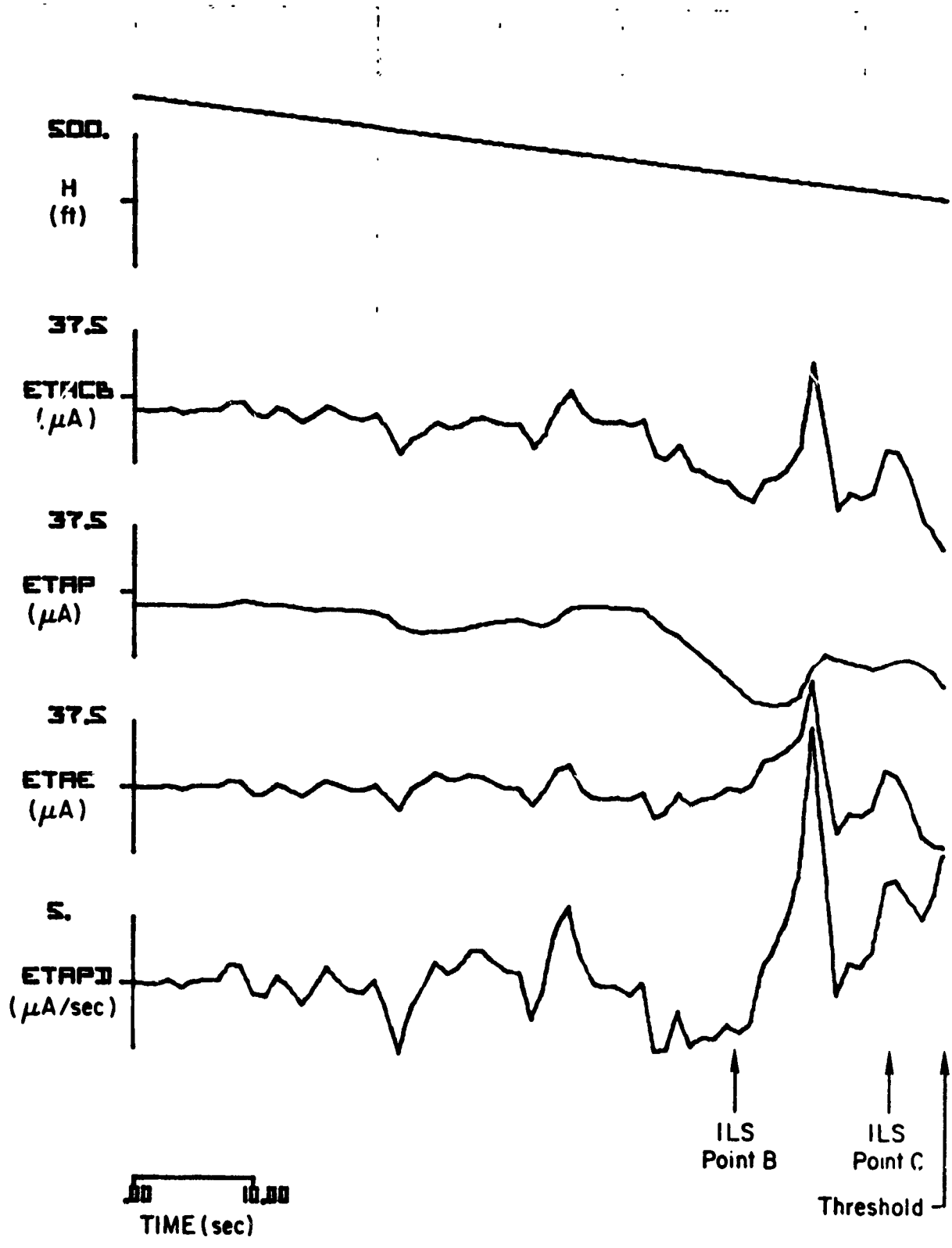

(a)

Figure B-11. Responses of Filter System No. 2 to ILS Glide Slope Input No. 14

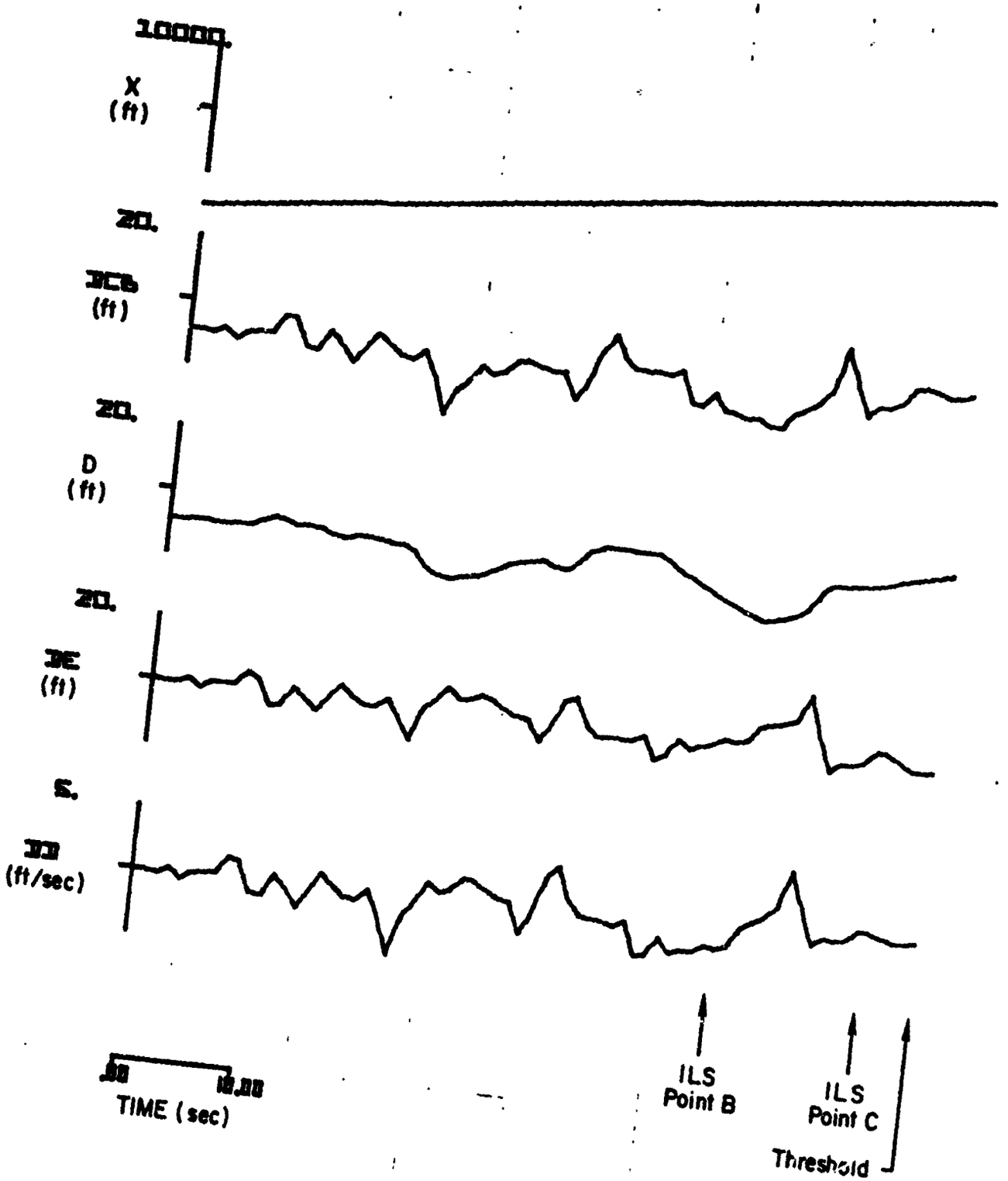

(b)

Figure B-11. (Concluded)

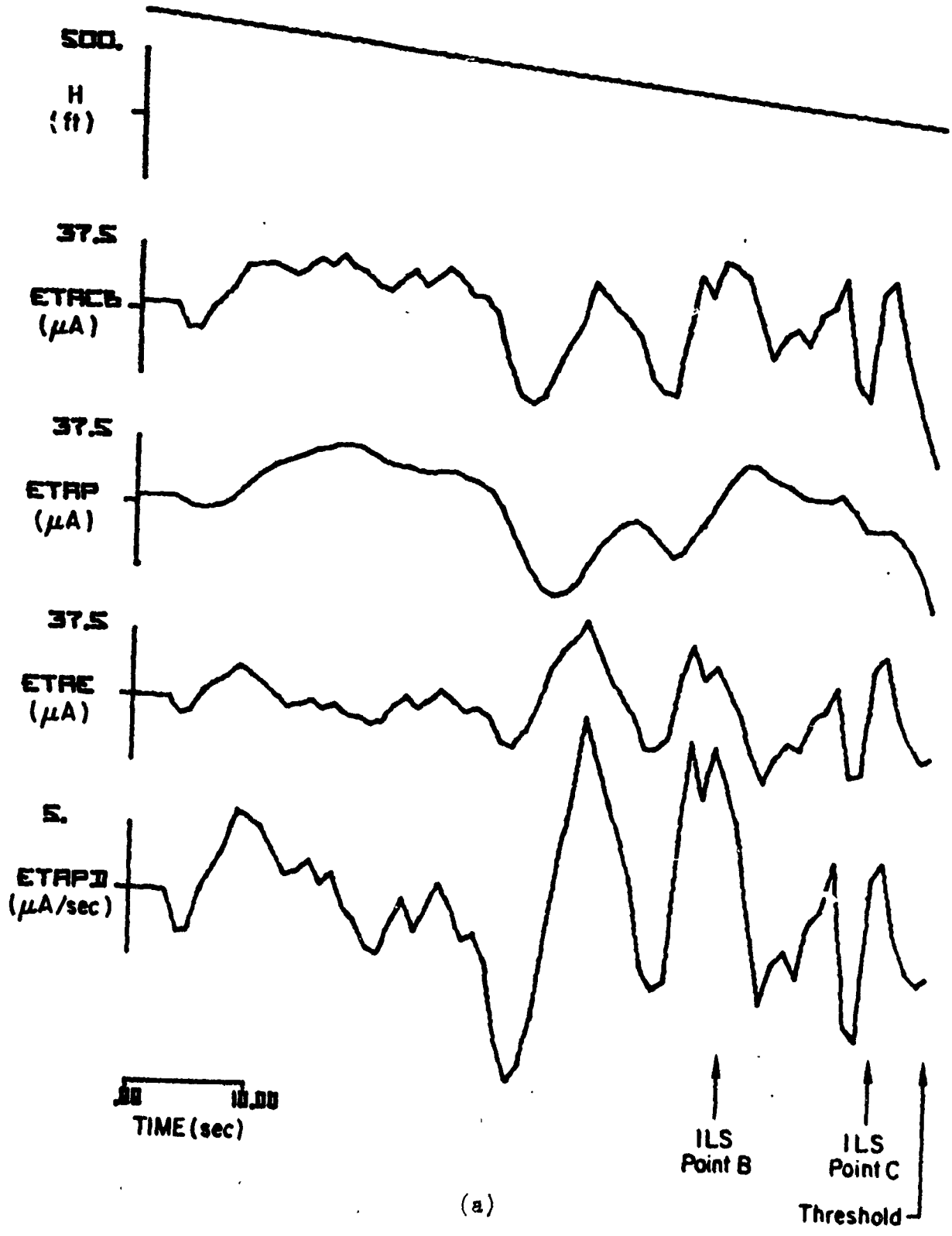

(a)

Figure B-12. Responses of Filter System No. 2 to ILS Glide Slope Input No. 15

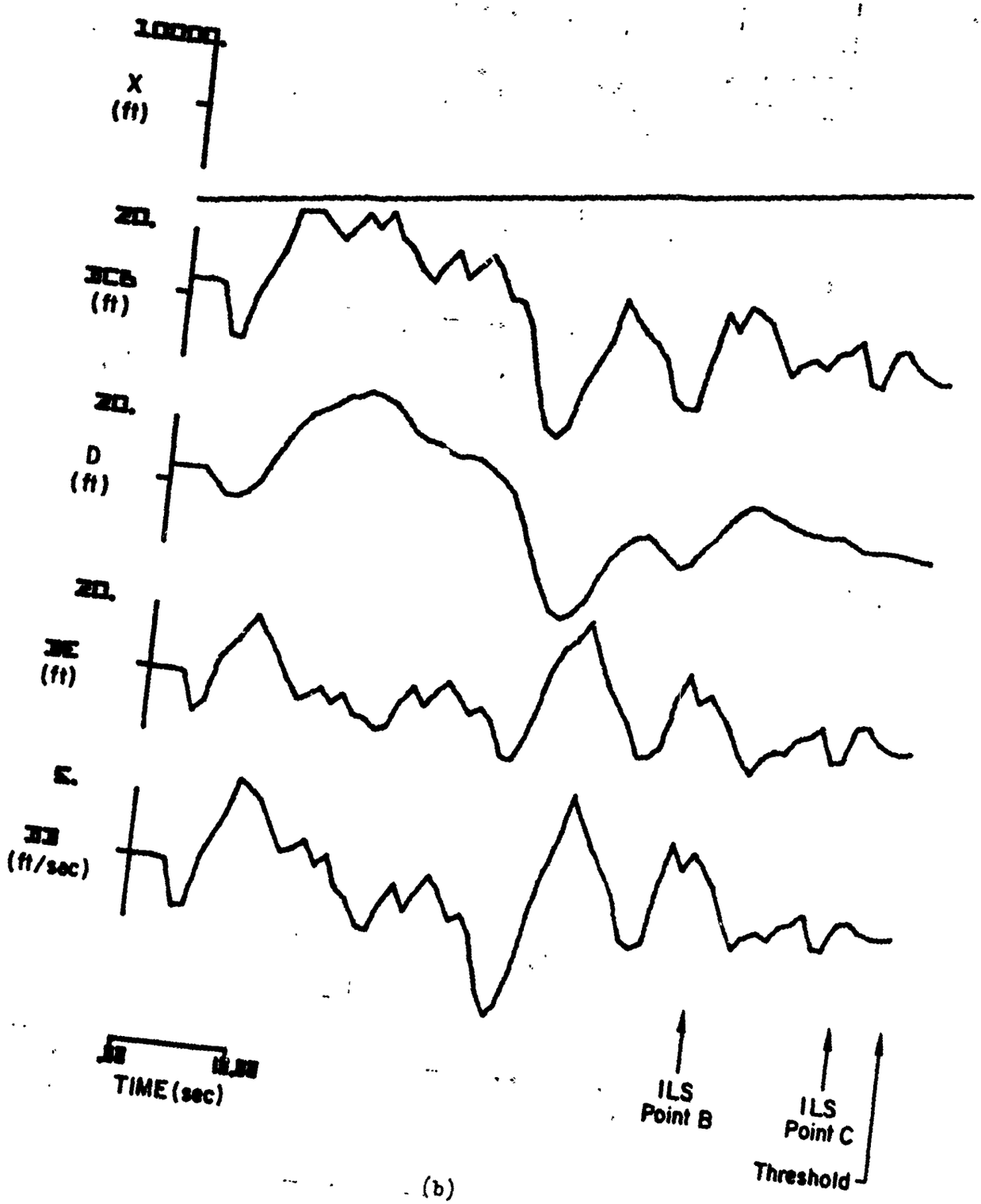

(b)

Figure B-12. (Concluded)

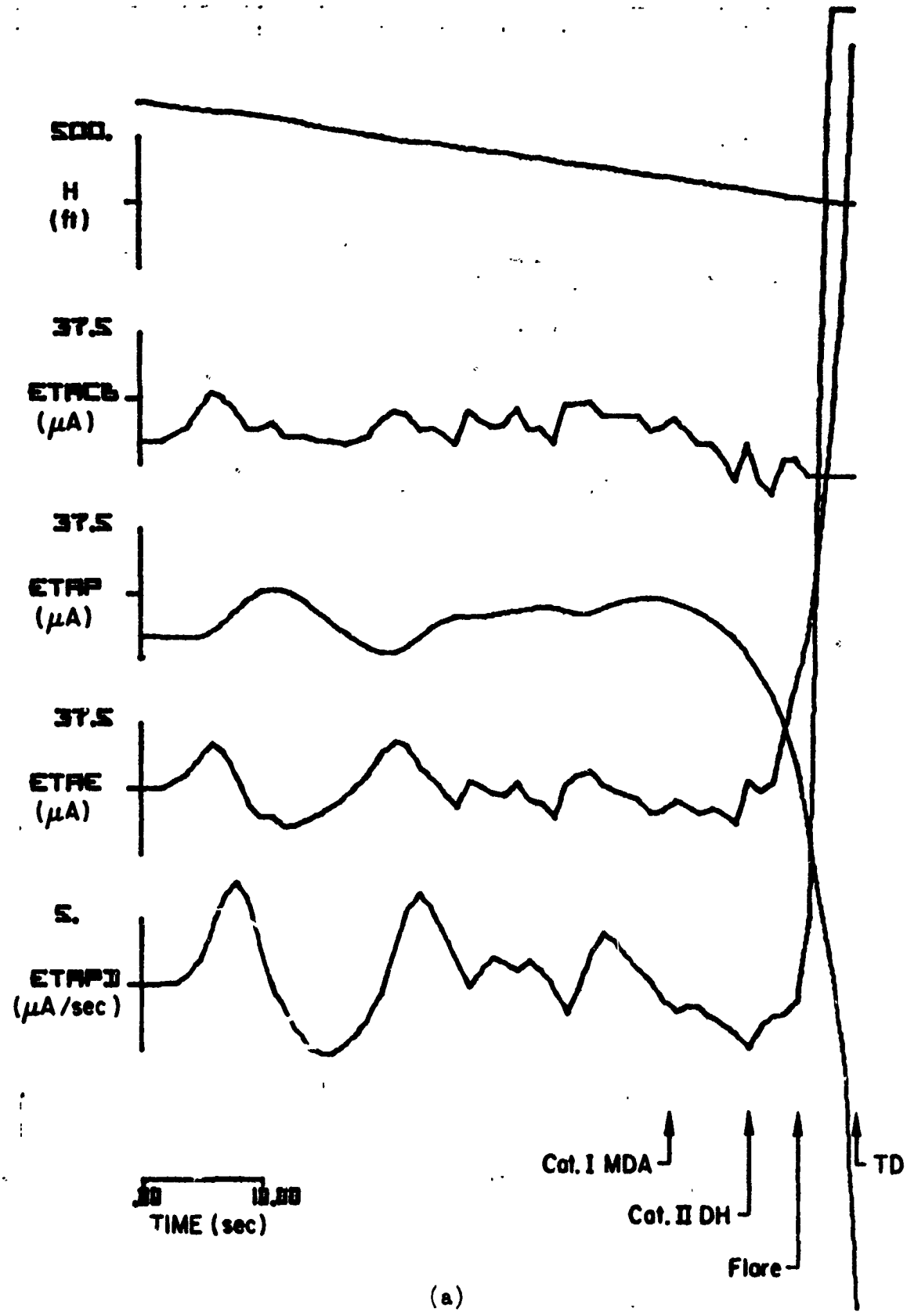

Figure B-13. Responses of the CV-880 Aircraft with LSI Automatic Landing System and Conventional Glide Slope Coupling to Glide Slope Flight Inspection Record No. 1. Category II-III Utilization Simulated

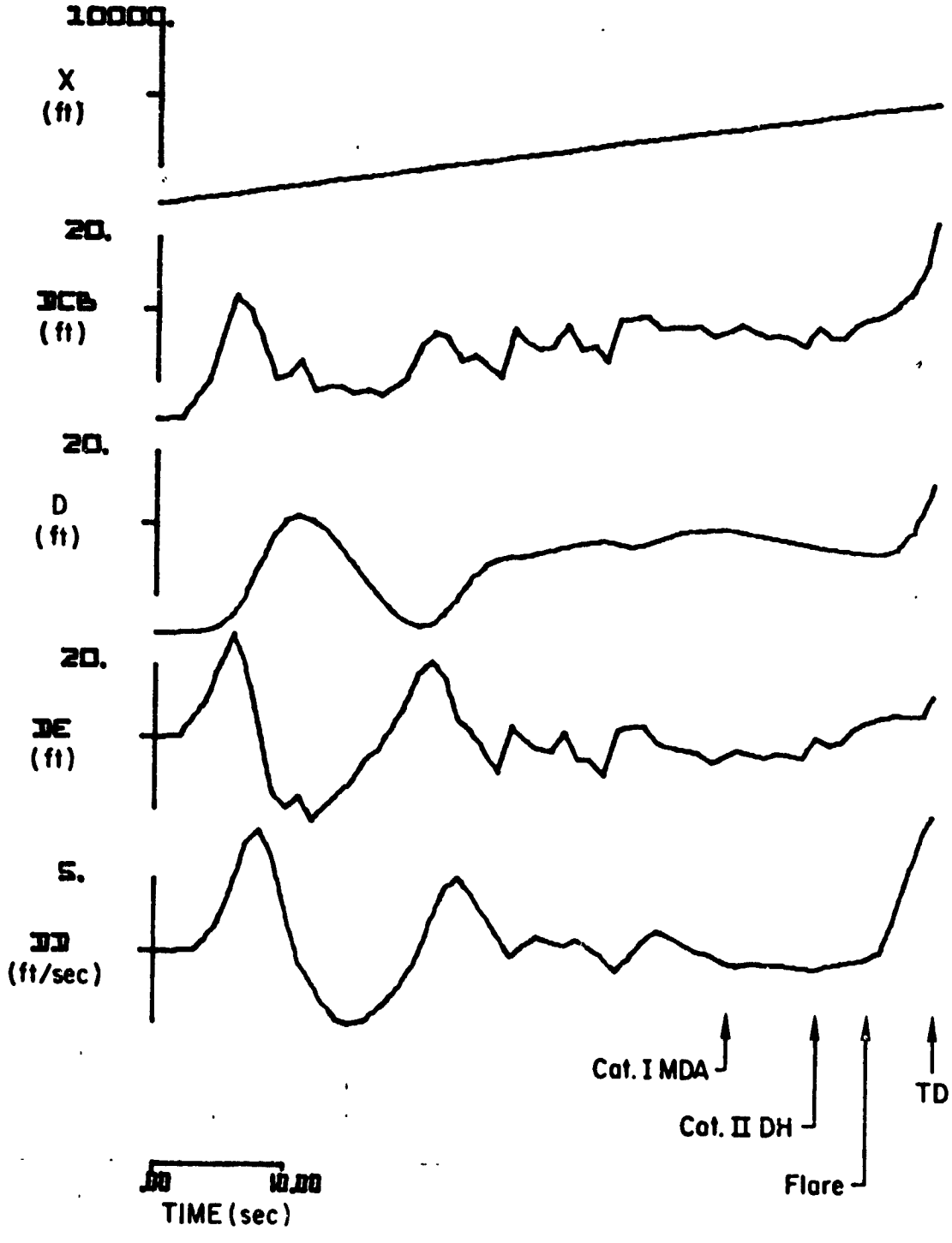

(b)

Figure B-13. (Continued)

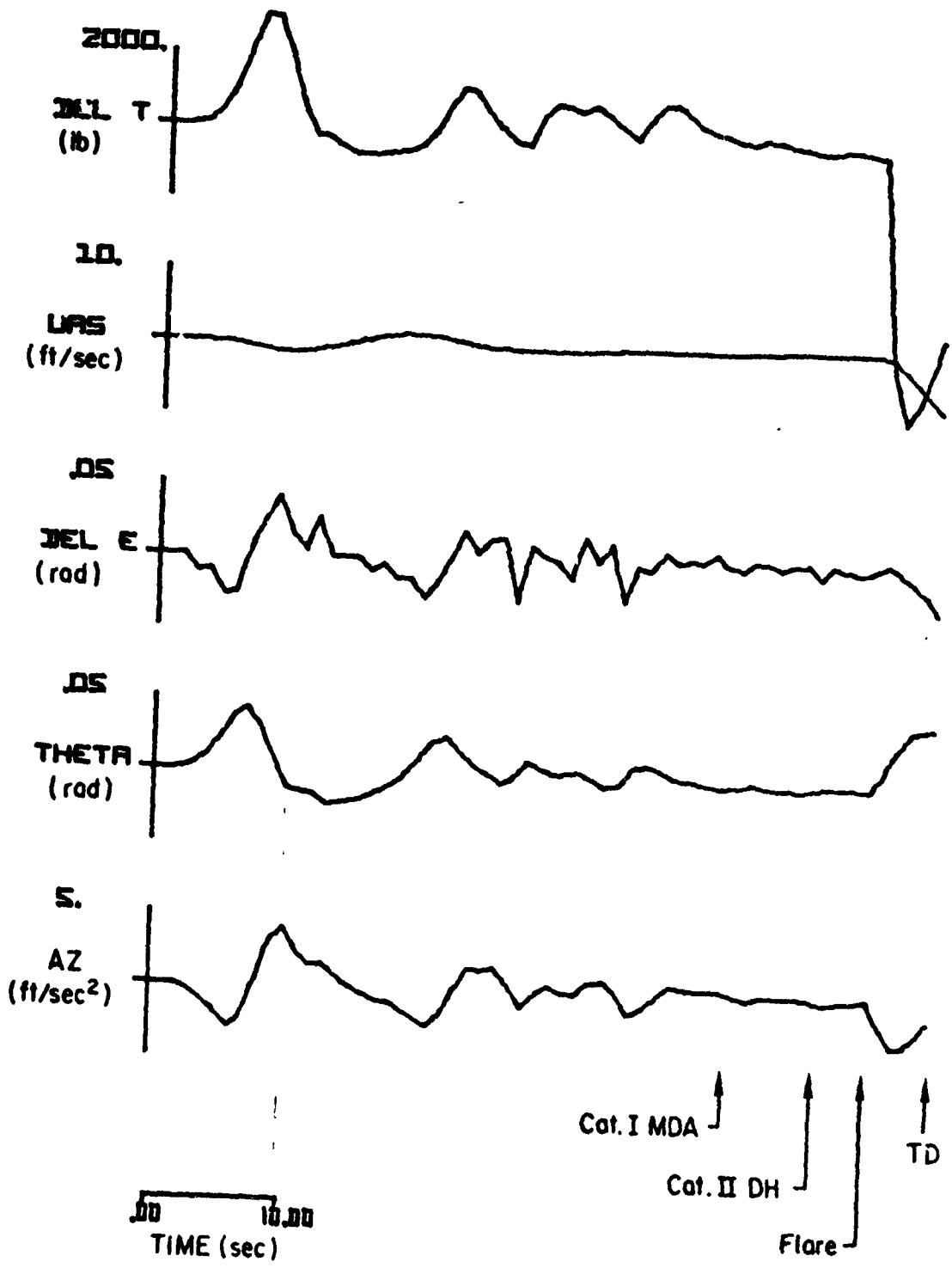

(e)

Figure B-13. (Concluded)

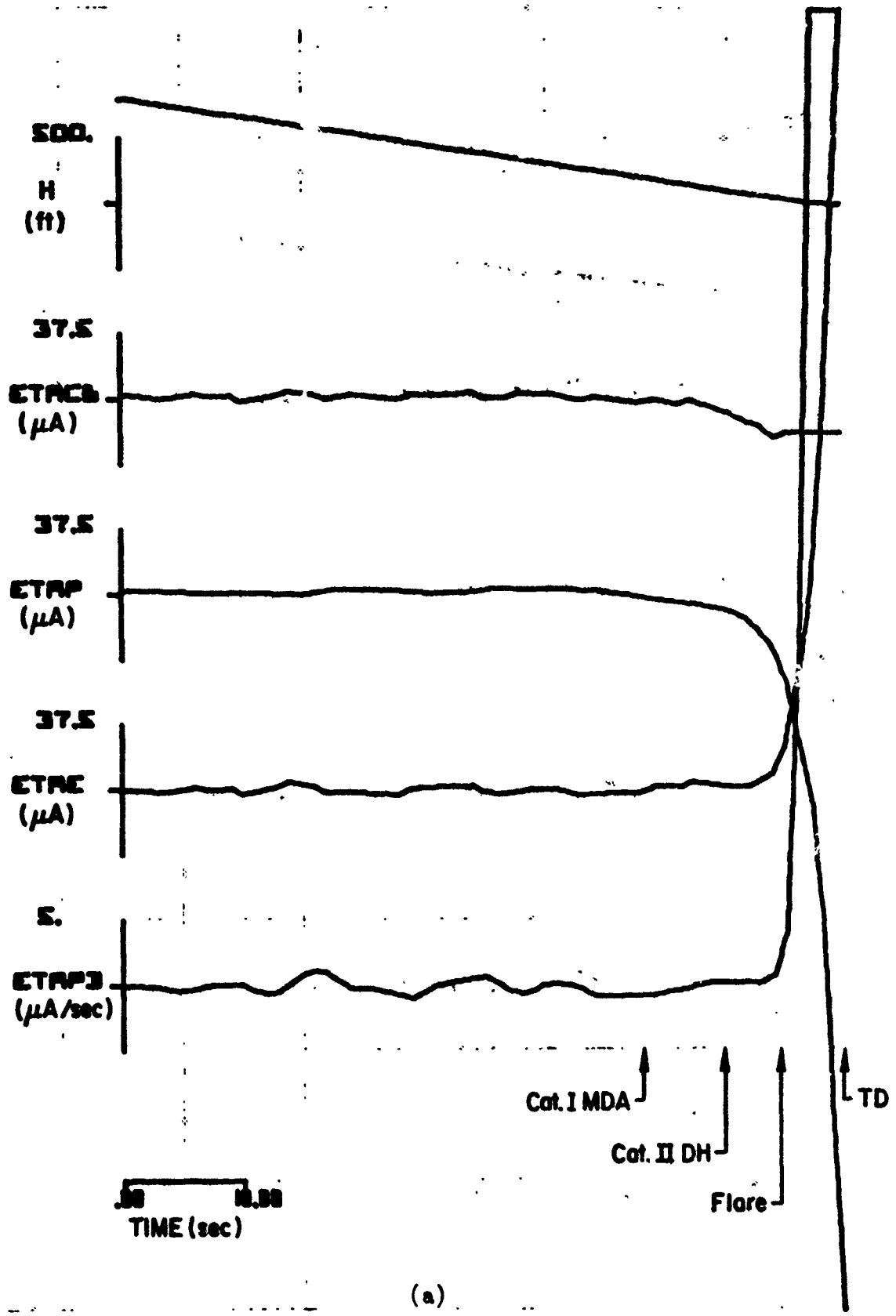

(a)

Figure B-14. Responses of the CV-880 Aircraft with LSI Automatic Landing System and Conventional Glide Slope Coupling to Glide Slope Flight Inspection Record No. 3. Category II-III Utilization Simulated

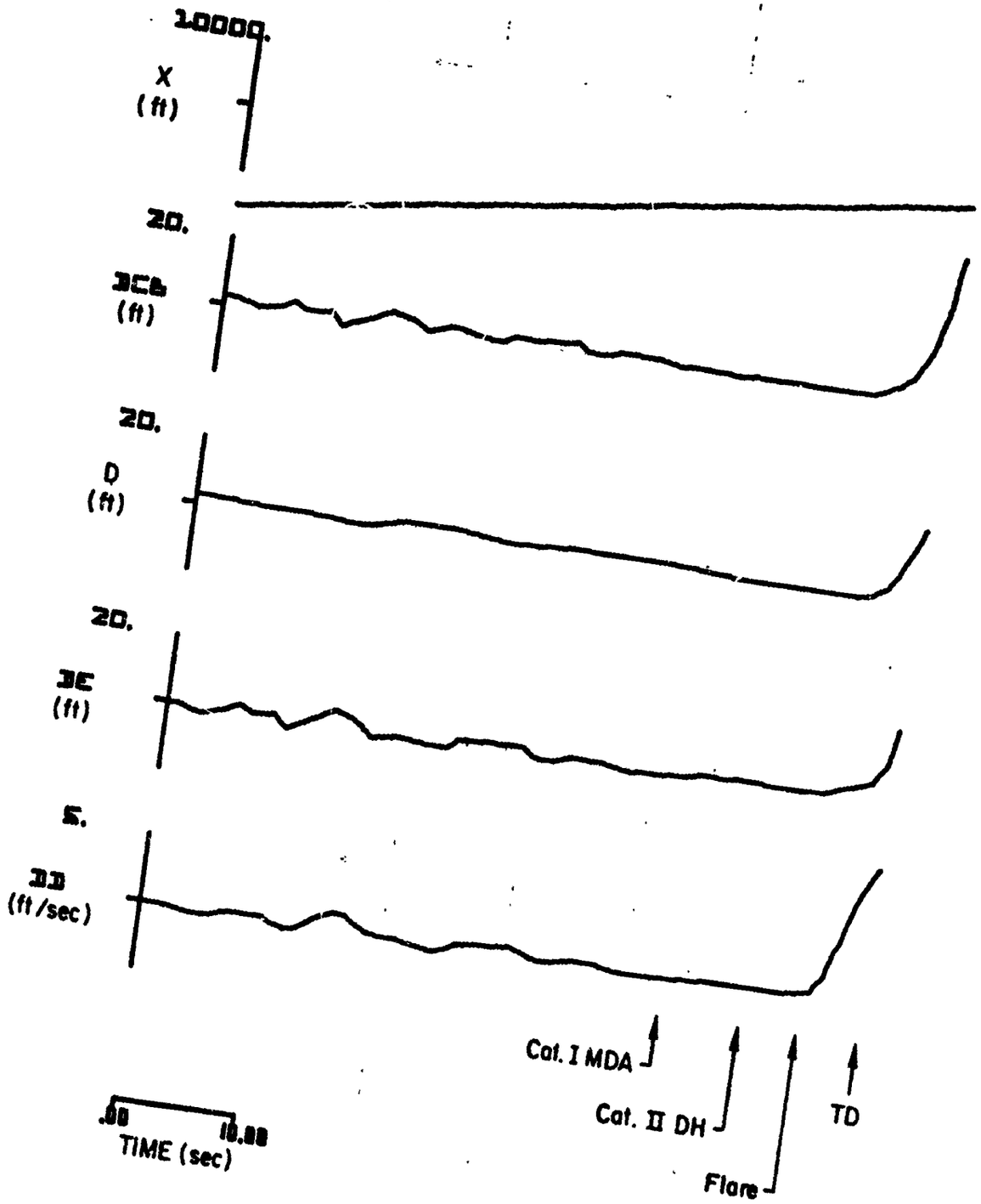

(b)

Figure B-14. (Continued)

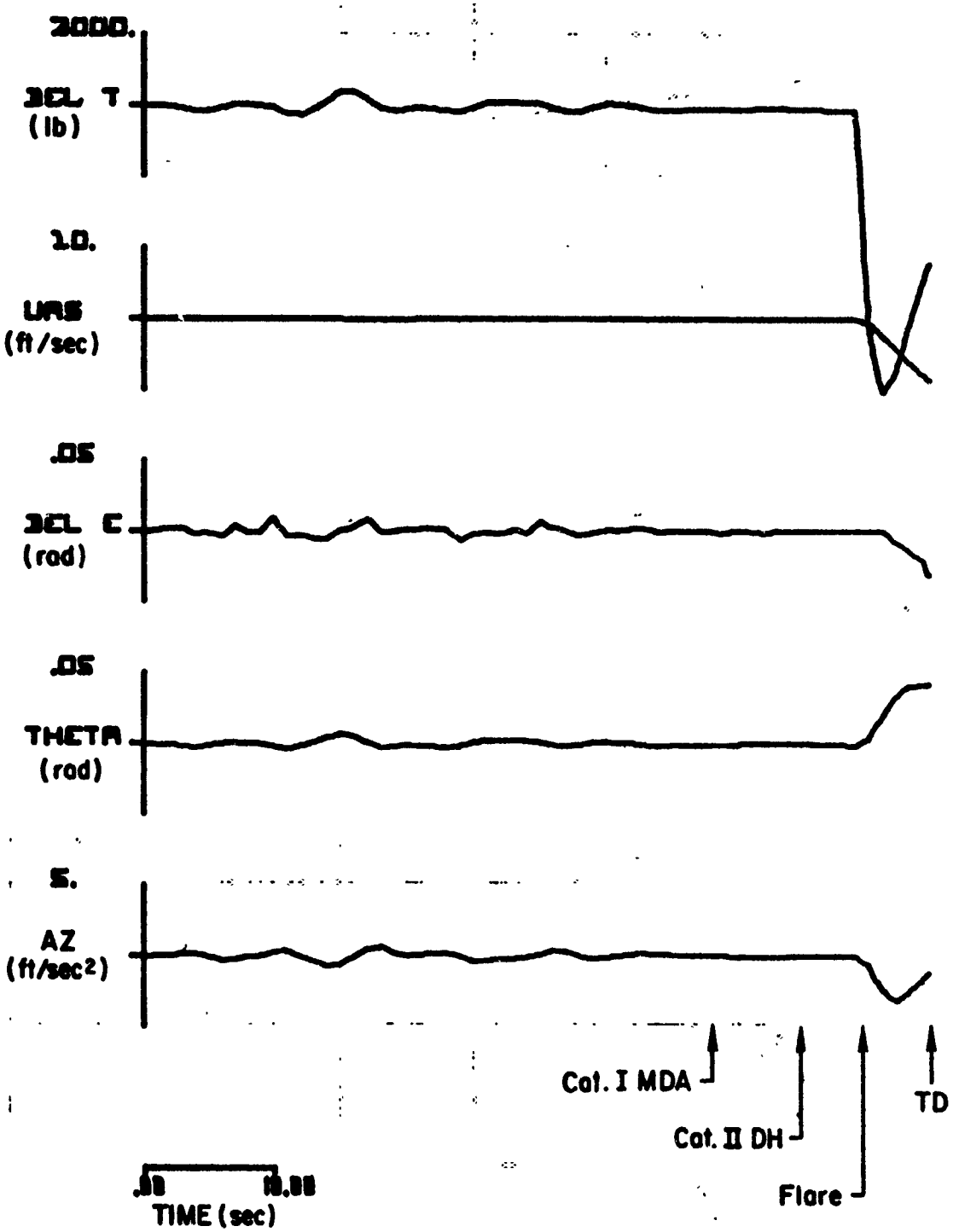

(c)

Figure B-14. (Concluded)

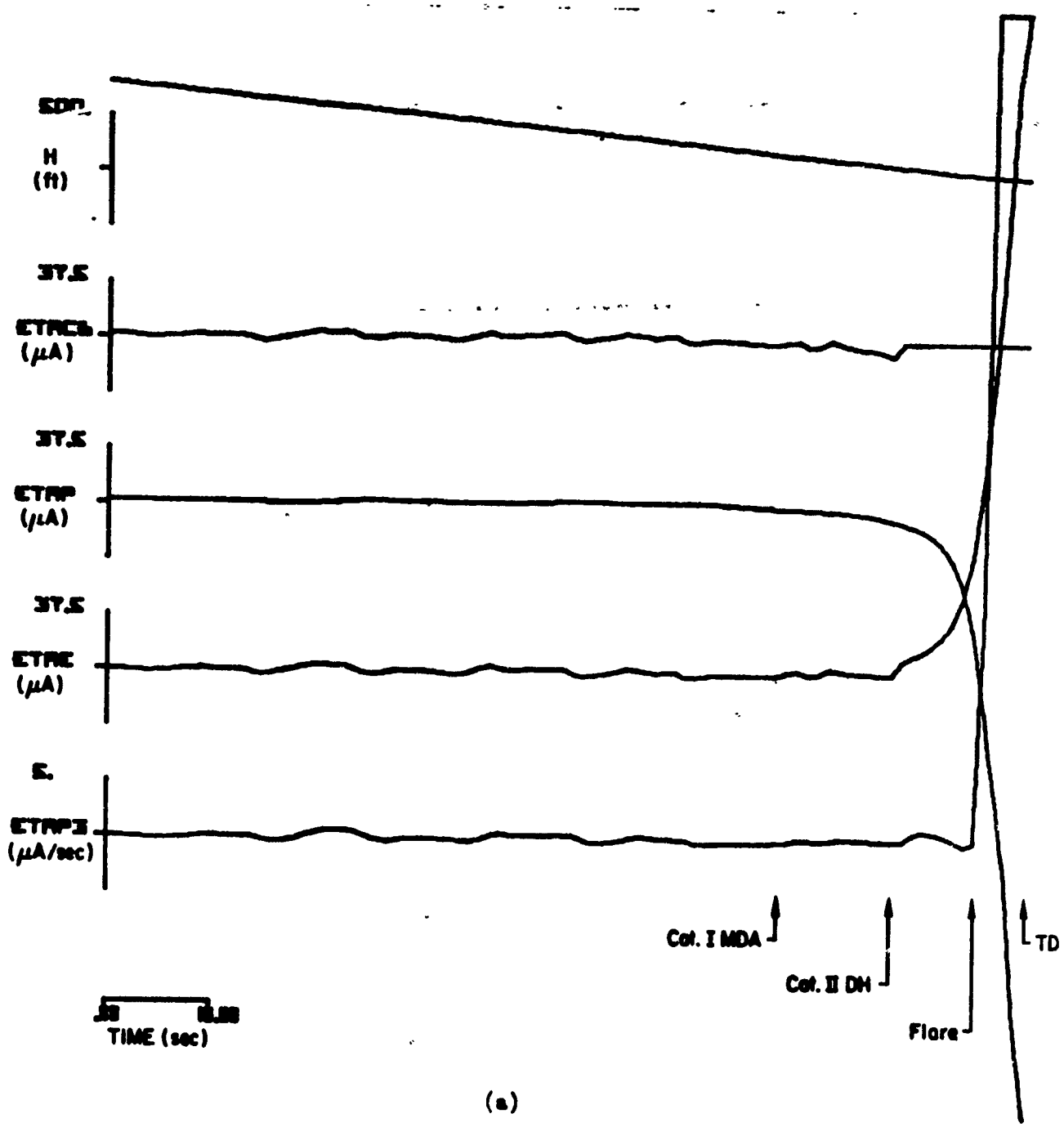

(a)

Figure B-15. Responses of the Piper PA-30 Aircraft with Invented Flight Control System and Conventional Glide Slope Coupling to Glide Slope Flight Inspection Record No. 3. Category II M Utilization Simulated

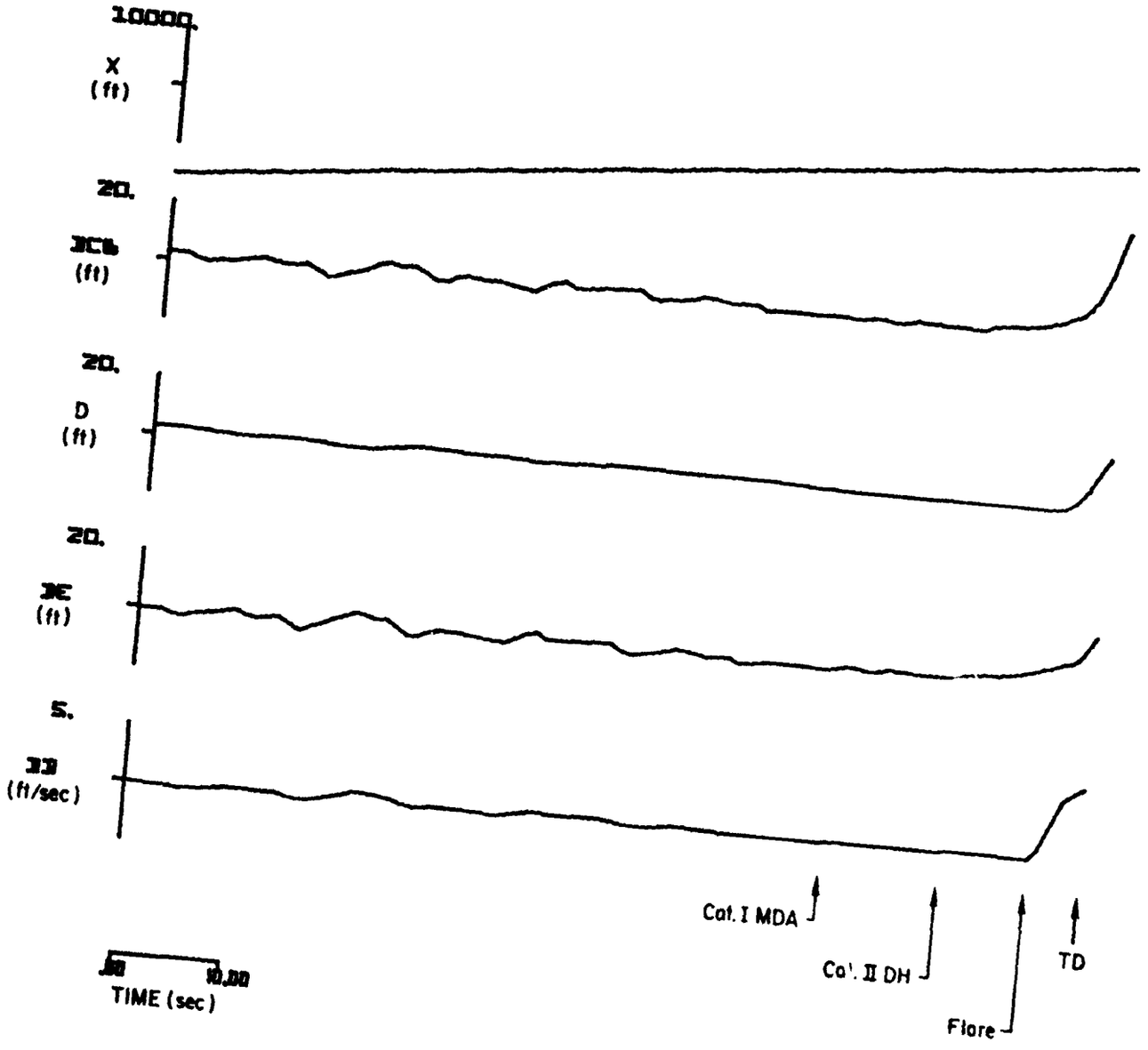

(b)

Figure B-15. (Continued)

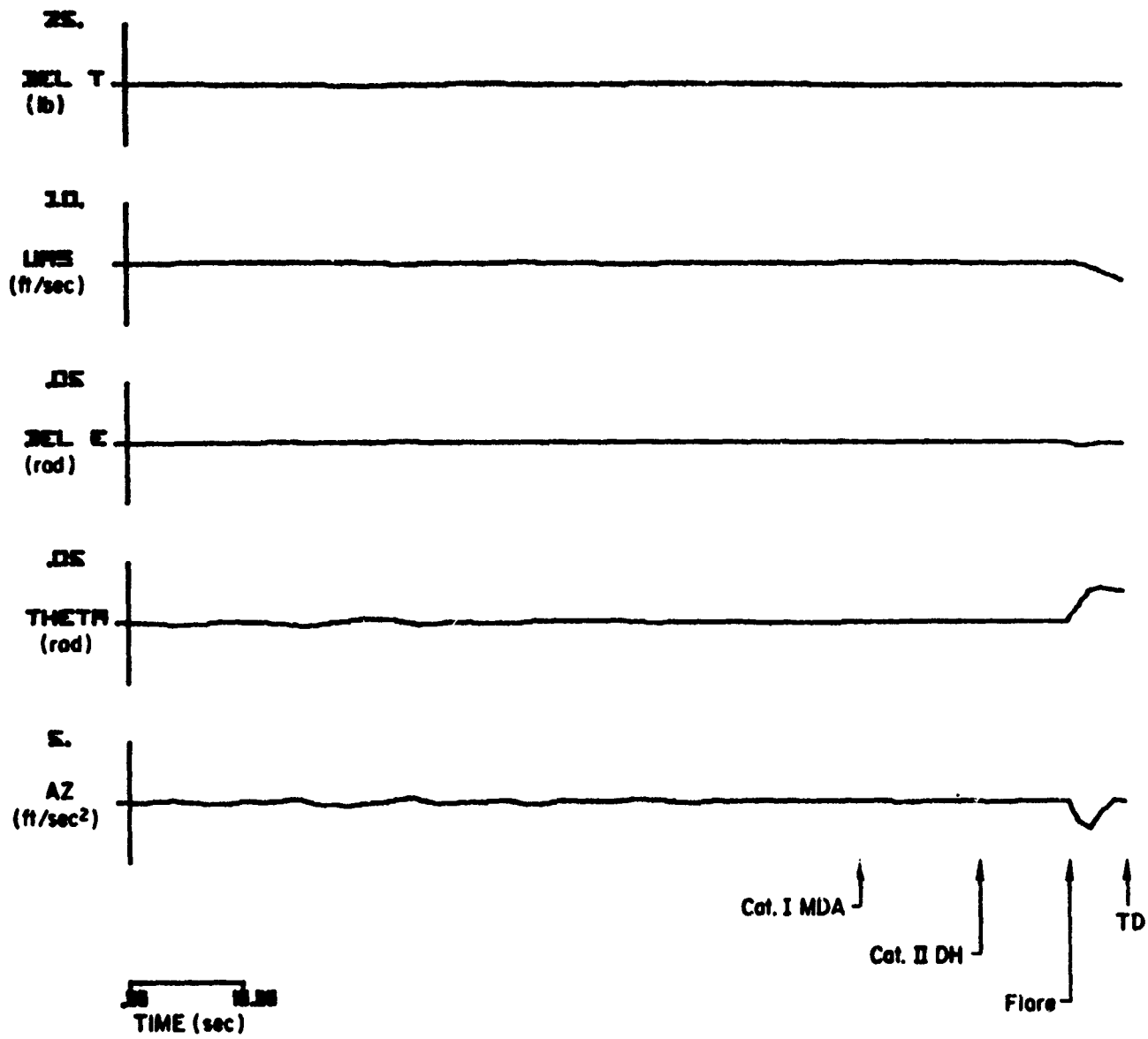

(c)

Figure B-1. (Concluded)

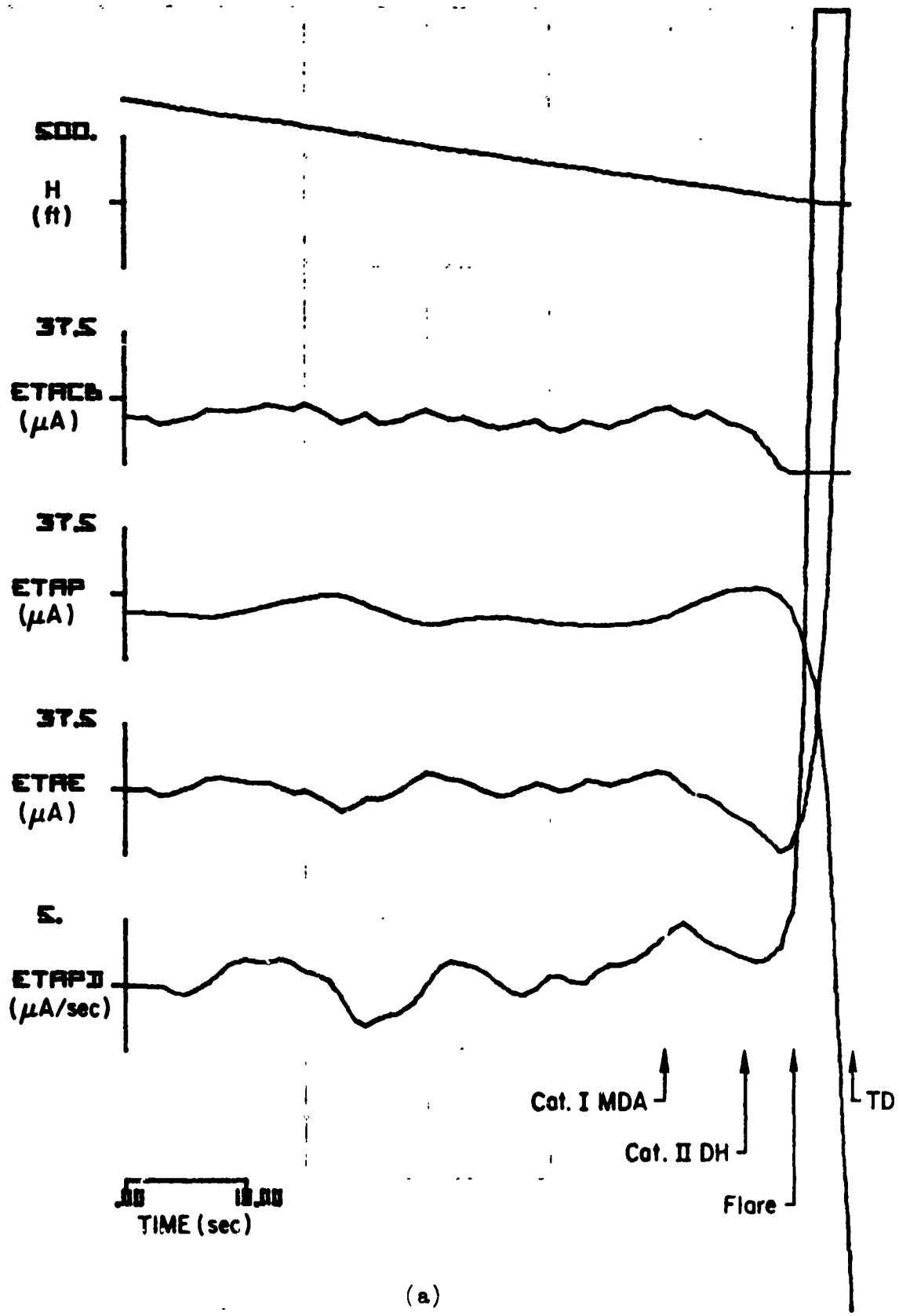

(a)

Figure B-16. Responses of the CV-880 Aircraft with LSI Automatic Landing System and Conventional Glide Slope Coupling to Glide Slope Flight Inspection Record No. 4. Category II-III Utilization Simulated

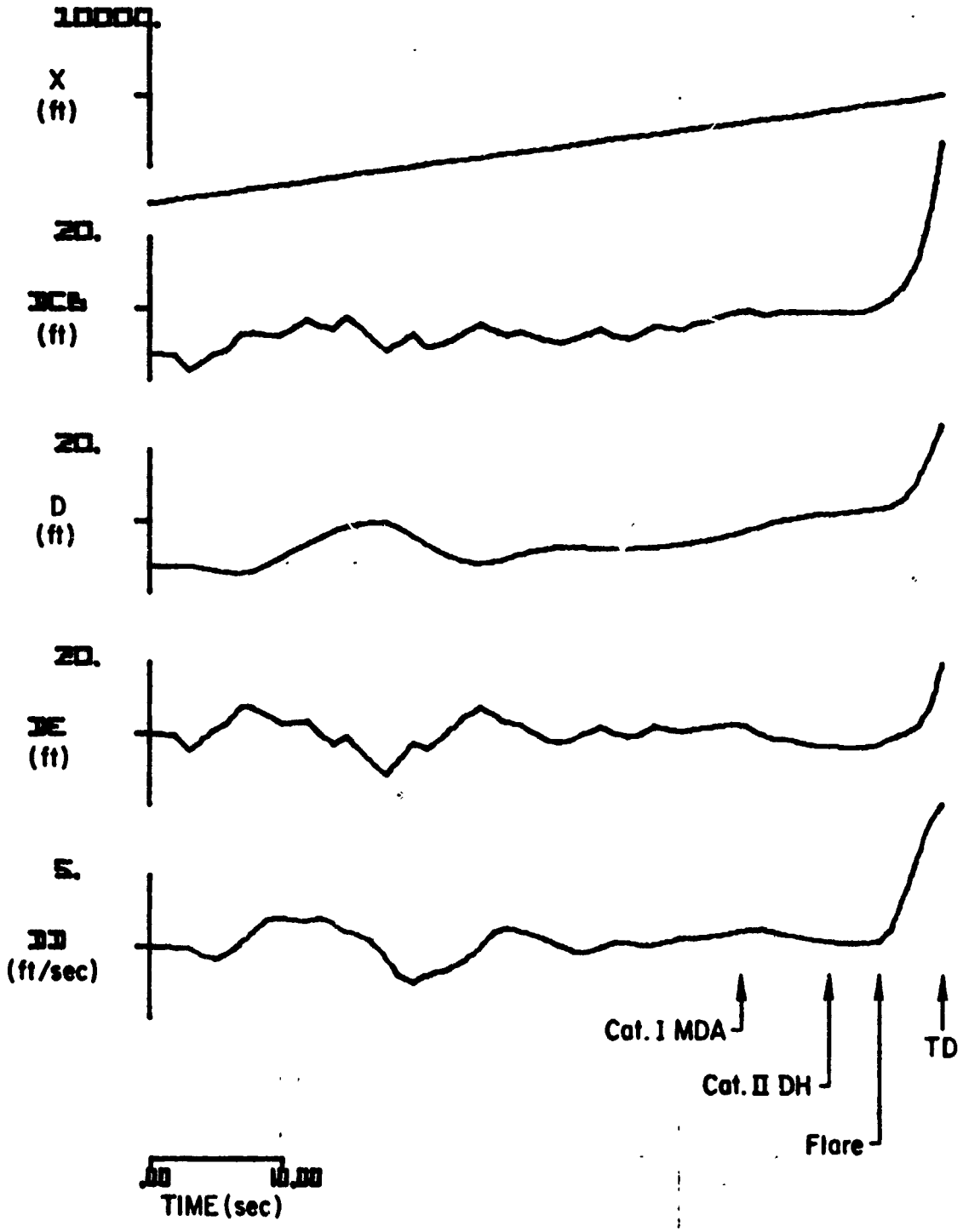

(b)

Figure B-16. (Continued)

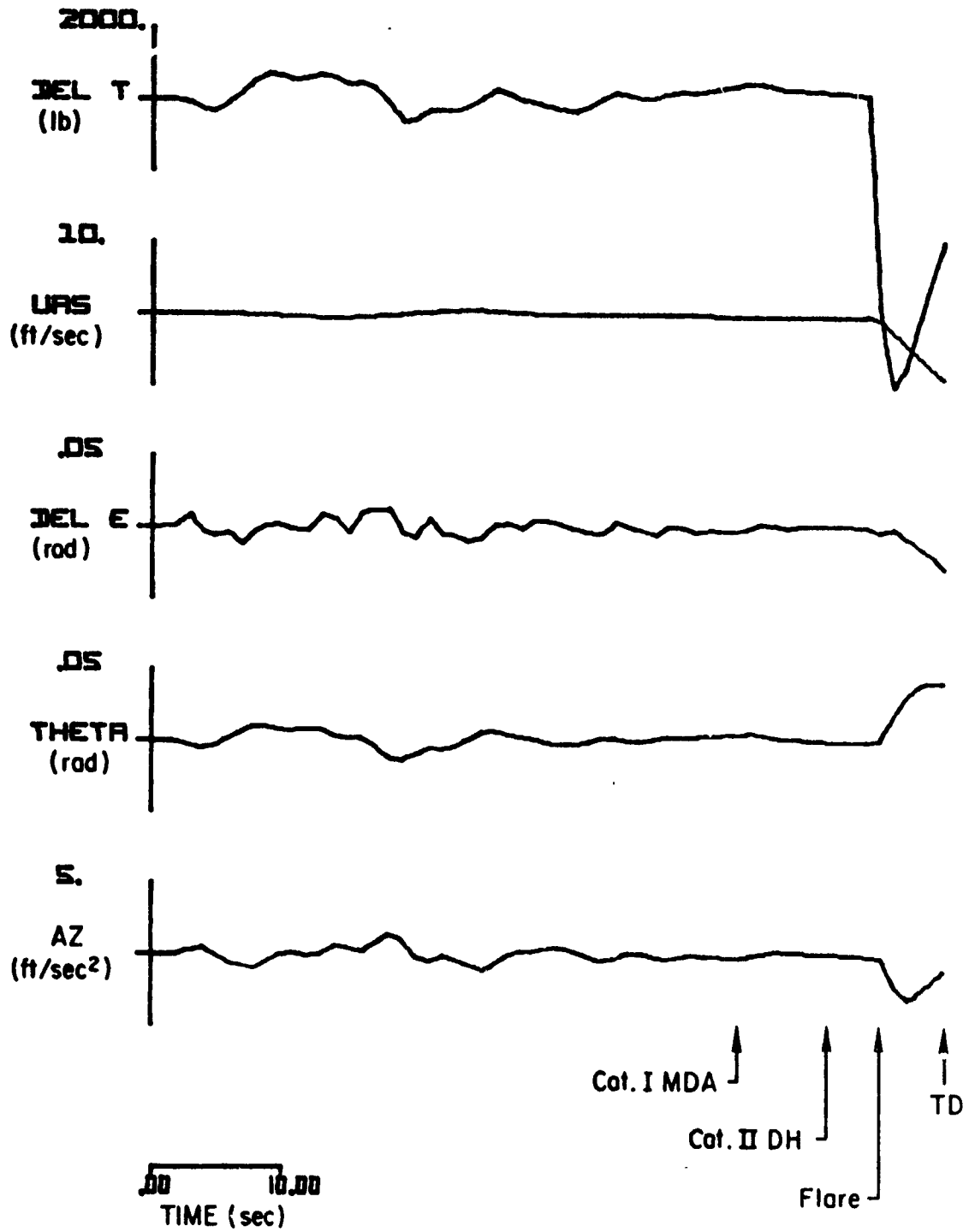

(c)

Figure B-16. (Concluded)

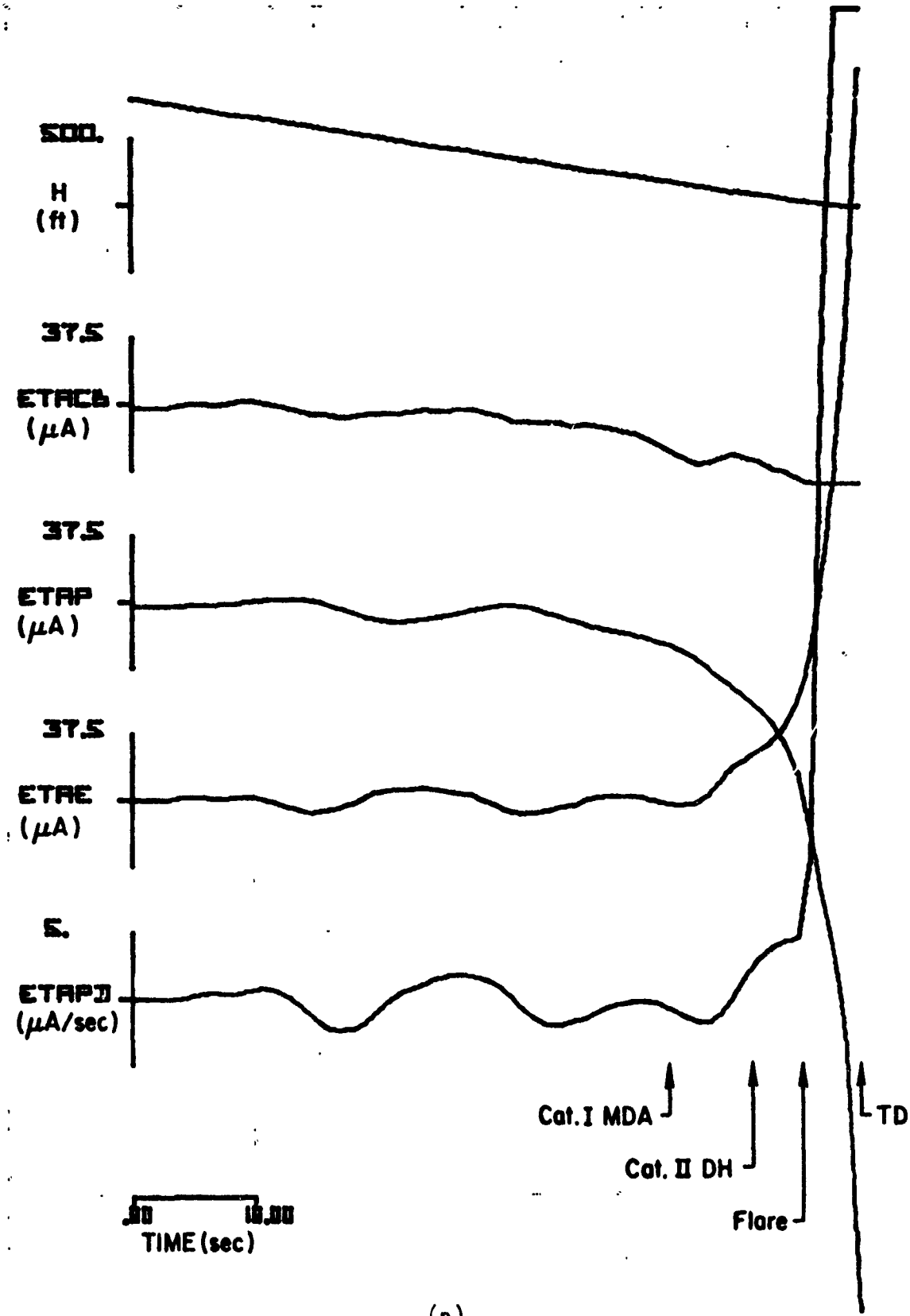

(a)

Figure B-17. Responses of the CV-880 Aircraft with ILSI Automatic Landing System and Conventional Glide Slope Coupling to Glide Slope Flight Inspection Record No. 5. Category II-III Utilization Simulated

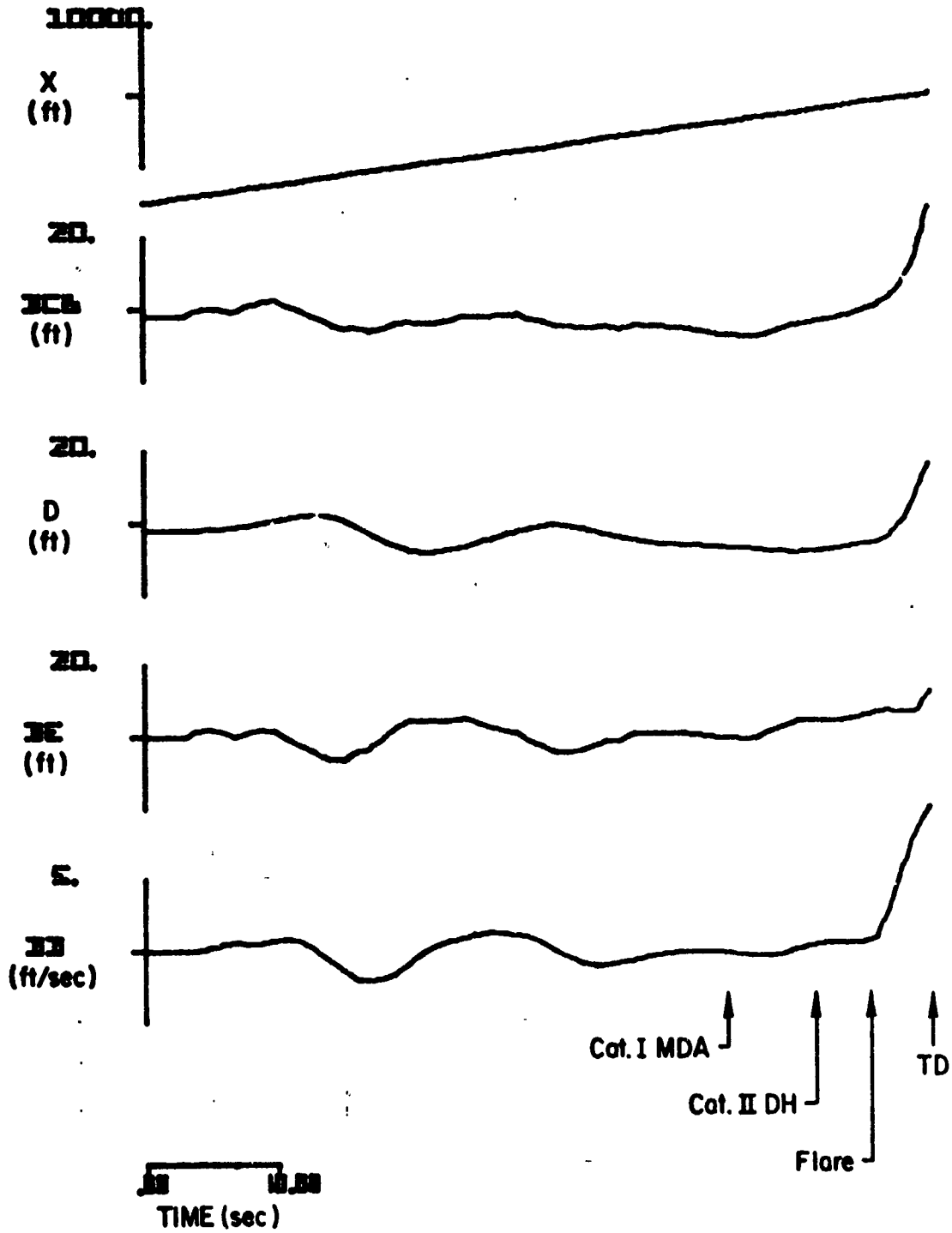

(b)

Figure B-17. (Continued)

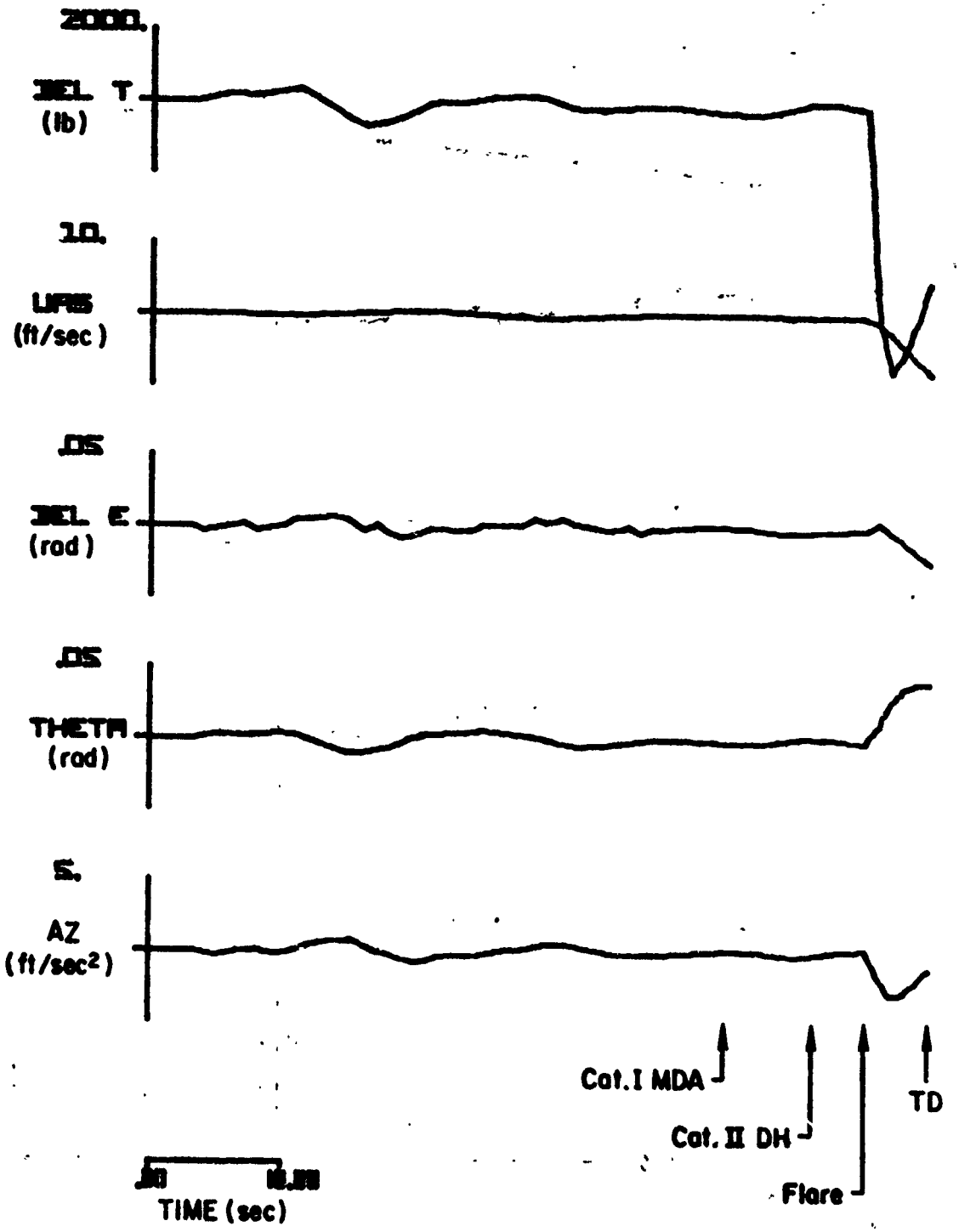

(c)

Figure B-17. (Concluded)

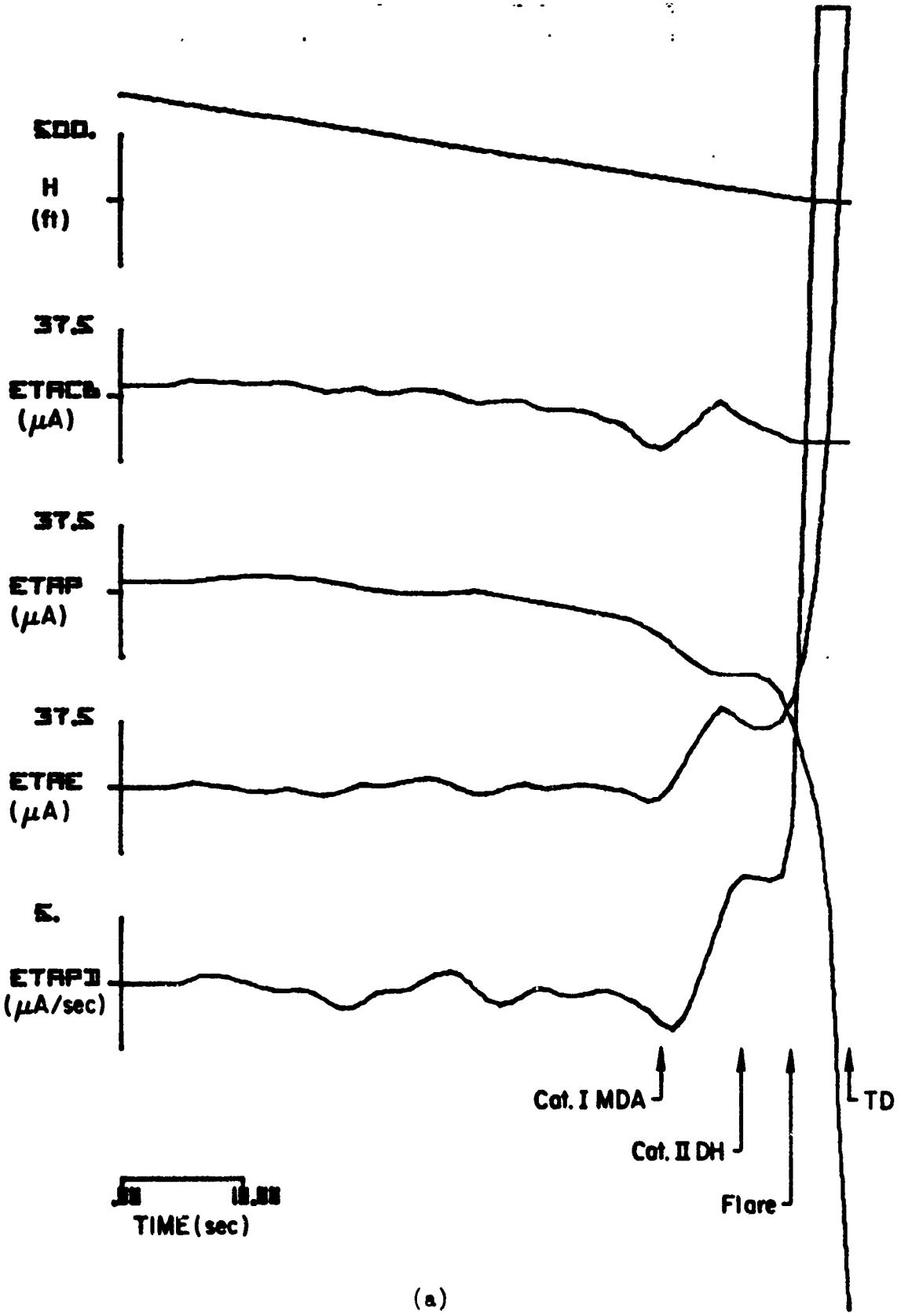

(a)

Figure B-18. Responses of the CV-880 Aircraft with LSI Automatic Landing System and Conventional Glide Slope Coupling to Glide Slope Flight Inspection Record No. 6. Category II-III Utilization Simulated

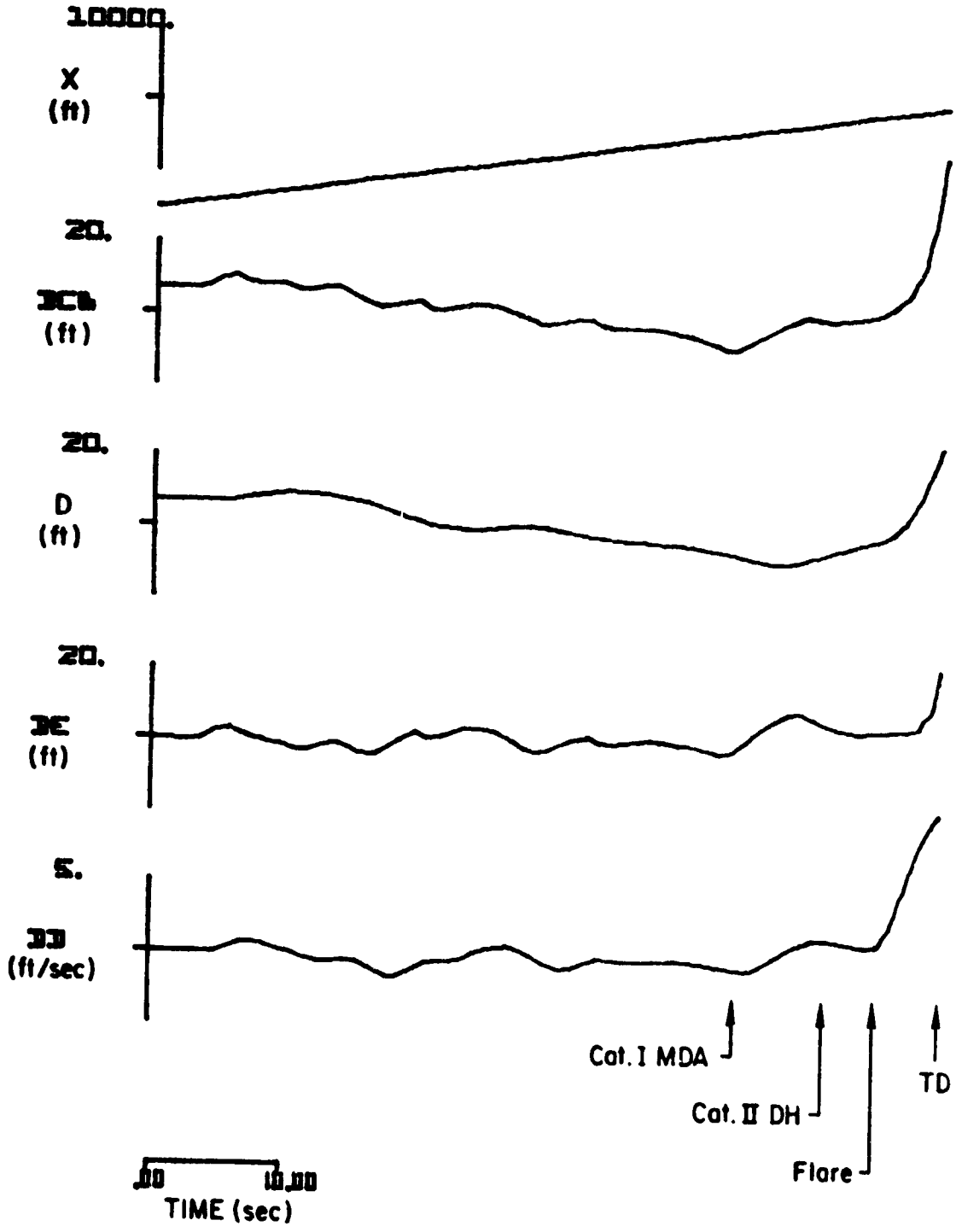

(b)

Figure B-18. (Continued)

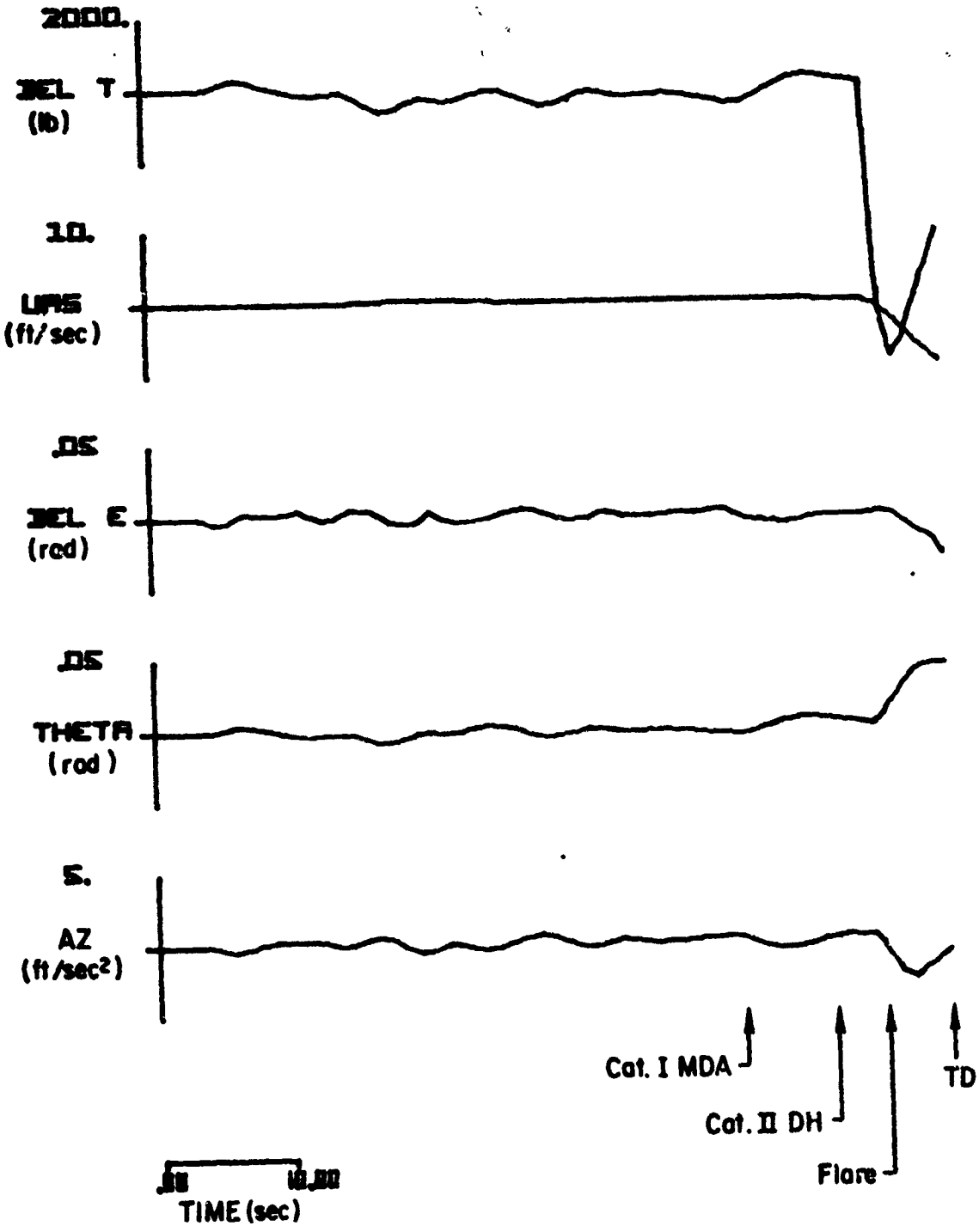

(c)

Figure B-18. (Concluded)

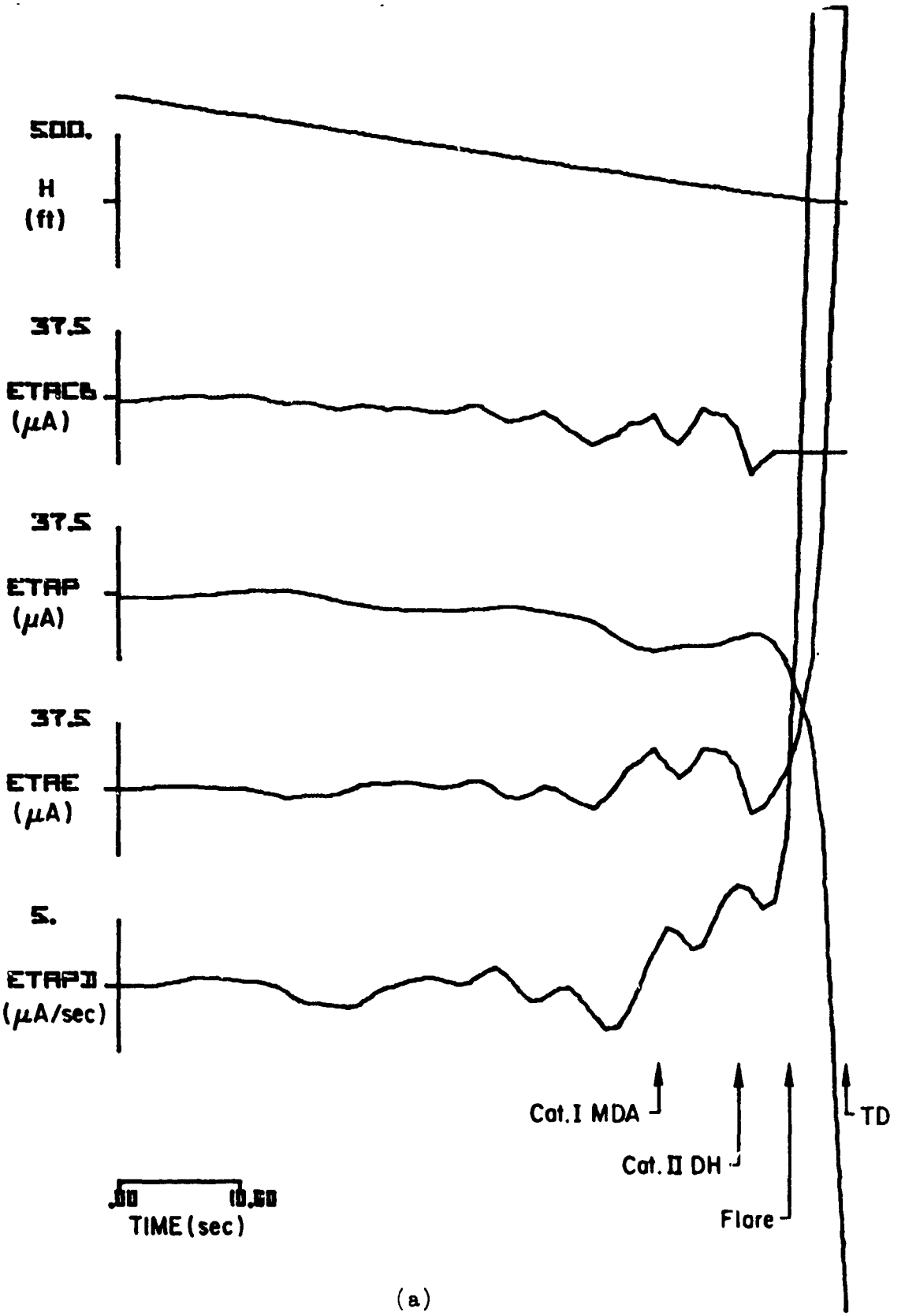

(a)

Figure B-19. Responses of the CV-880 Aircraft with LSI Automatic Landing System and Conventional Glide Slope Coupling to Glide Slope Flight Inspection Record No. 7. Category II-III Utilization Simulated

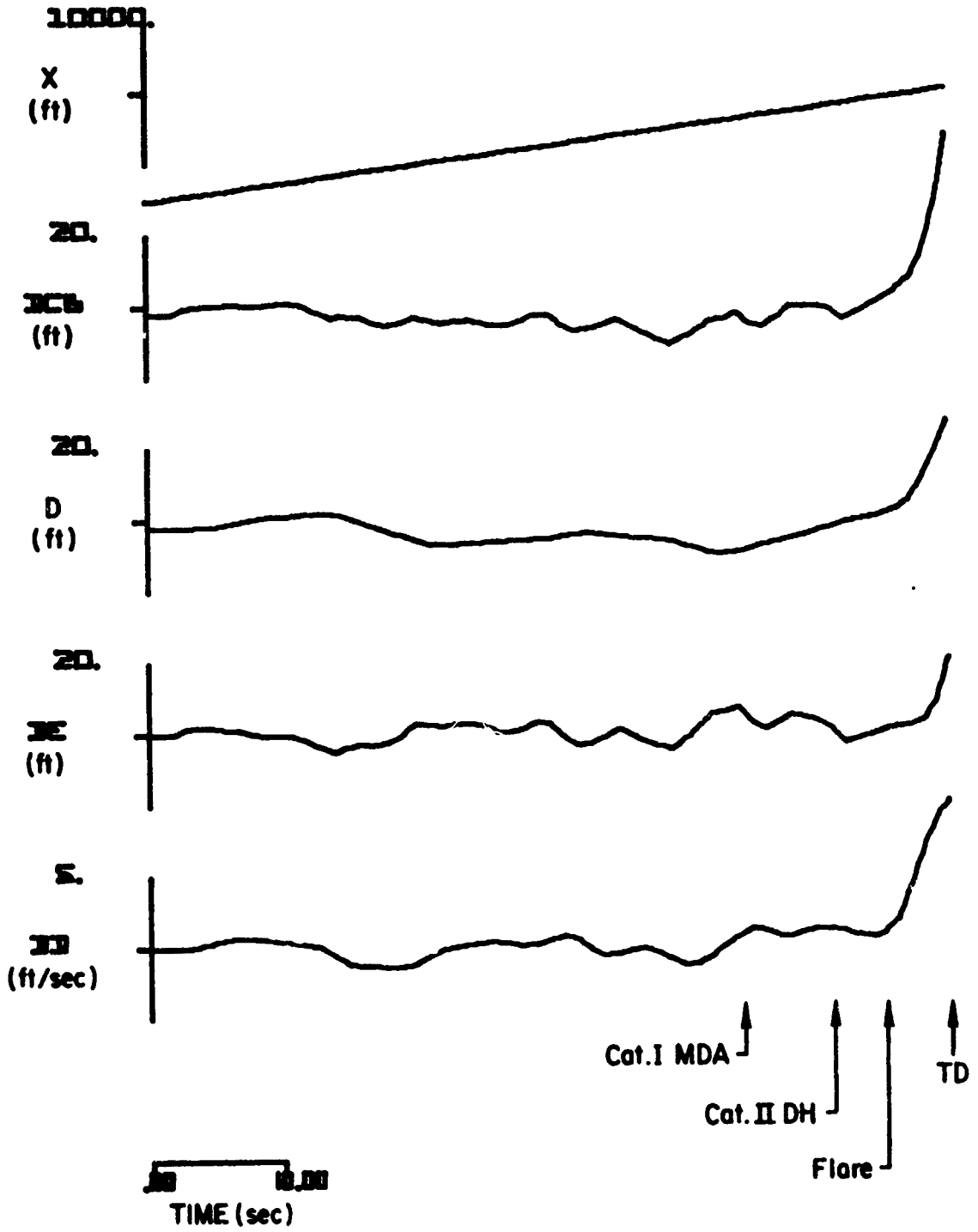

(b)

Figure B-19. (Continued)

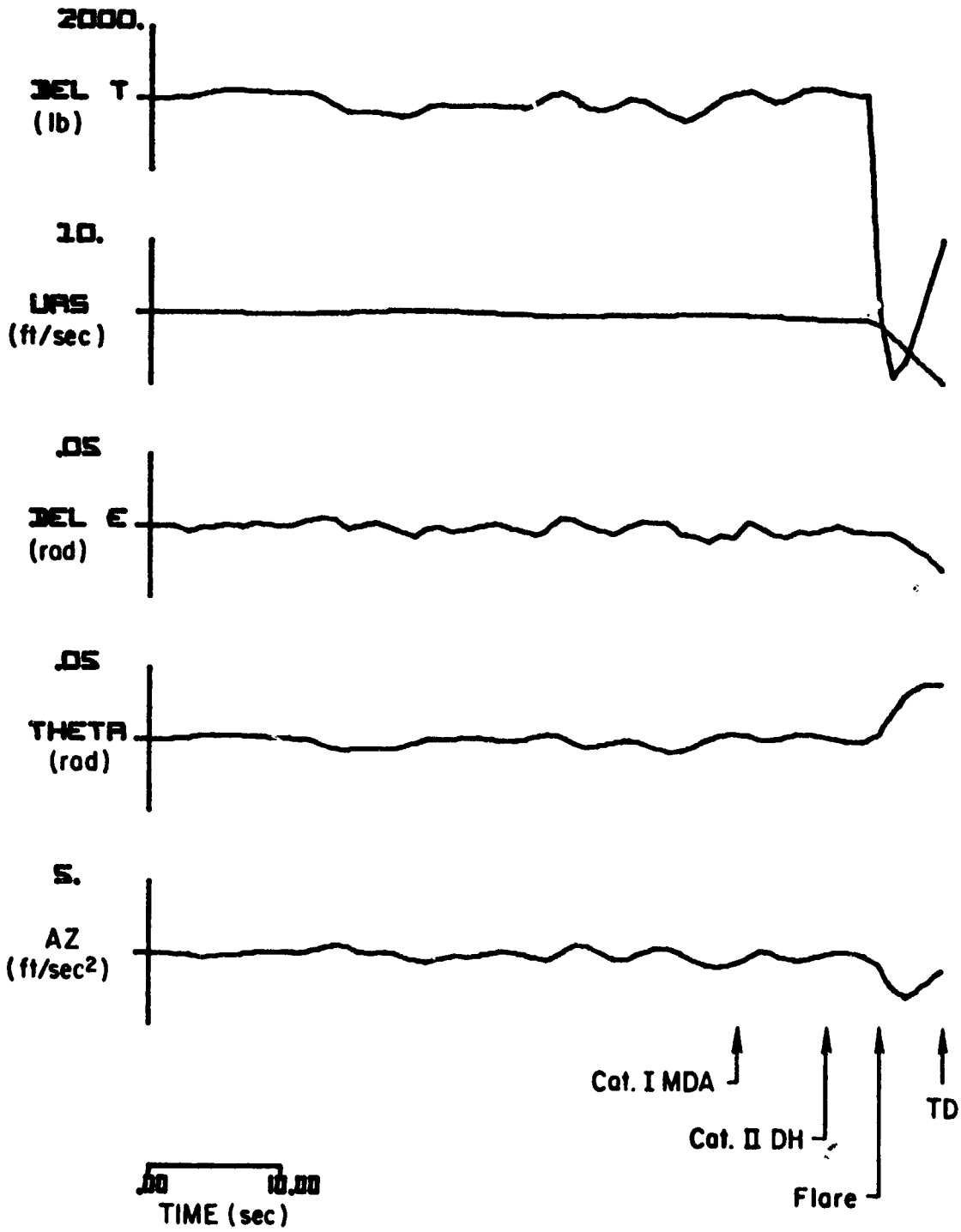

(c)

Figure B-19. (Concluded)

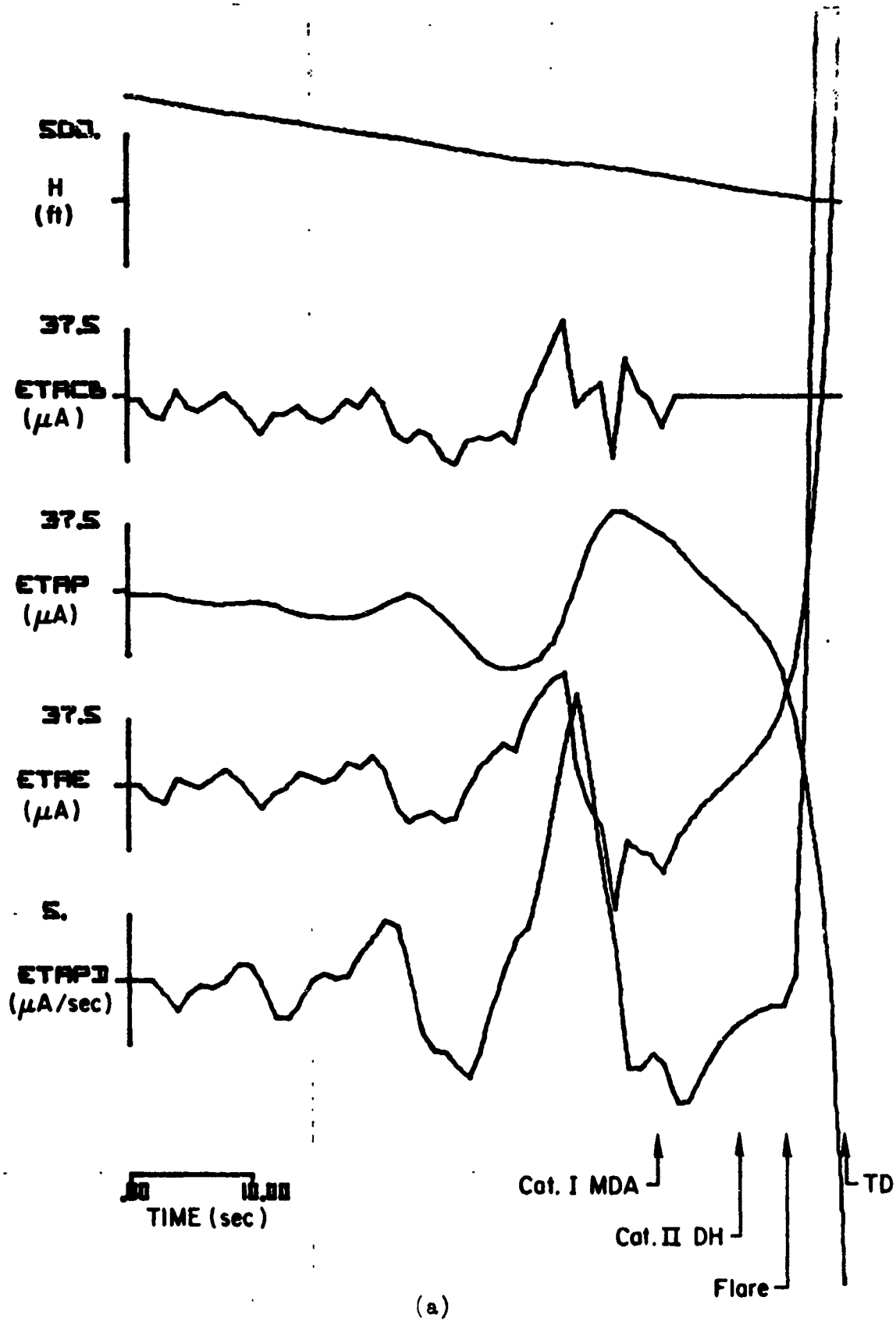

(a)

Figure B-20. Responses of the CV-880 Aircraft with LSI Automatic Landing System and Conventional Glide Slope Coupling to Glide Slope Flight Inspection Record No. 9. Category I Utilization Simulated

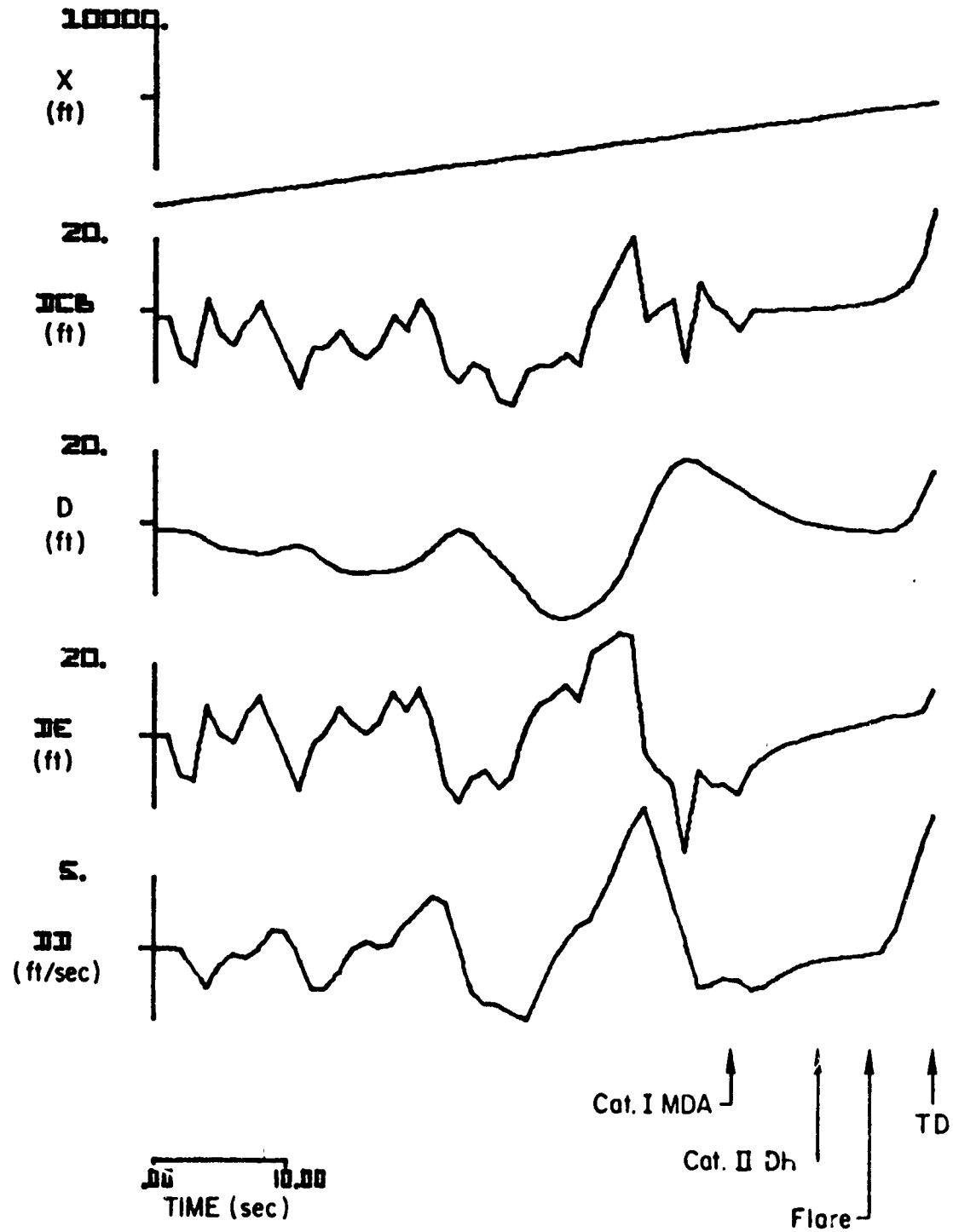

(b)

Figure B-20. (Continued)

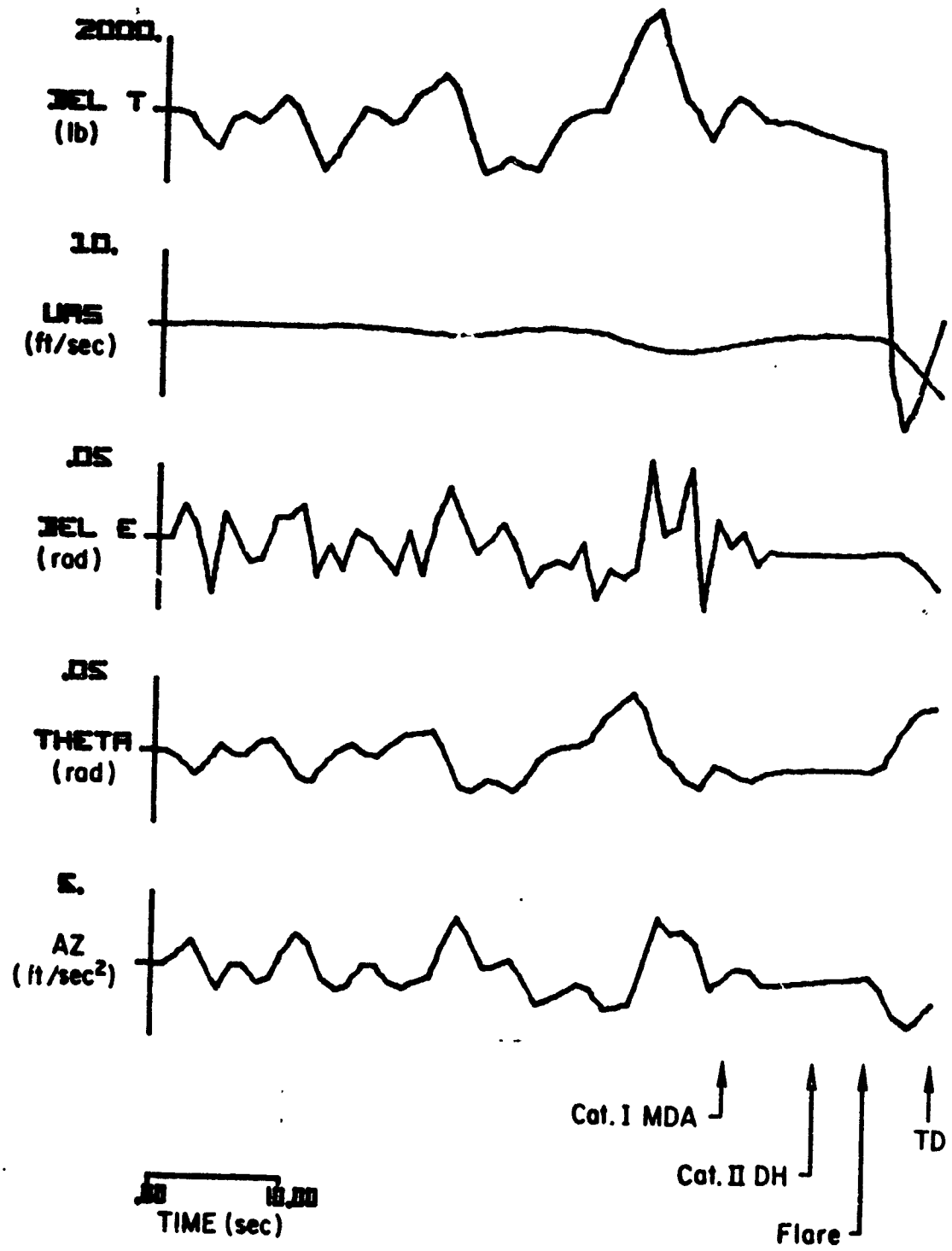

(c)

Figure B-20. (Concluded)

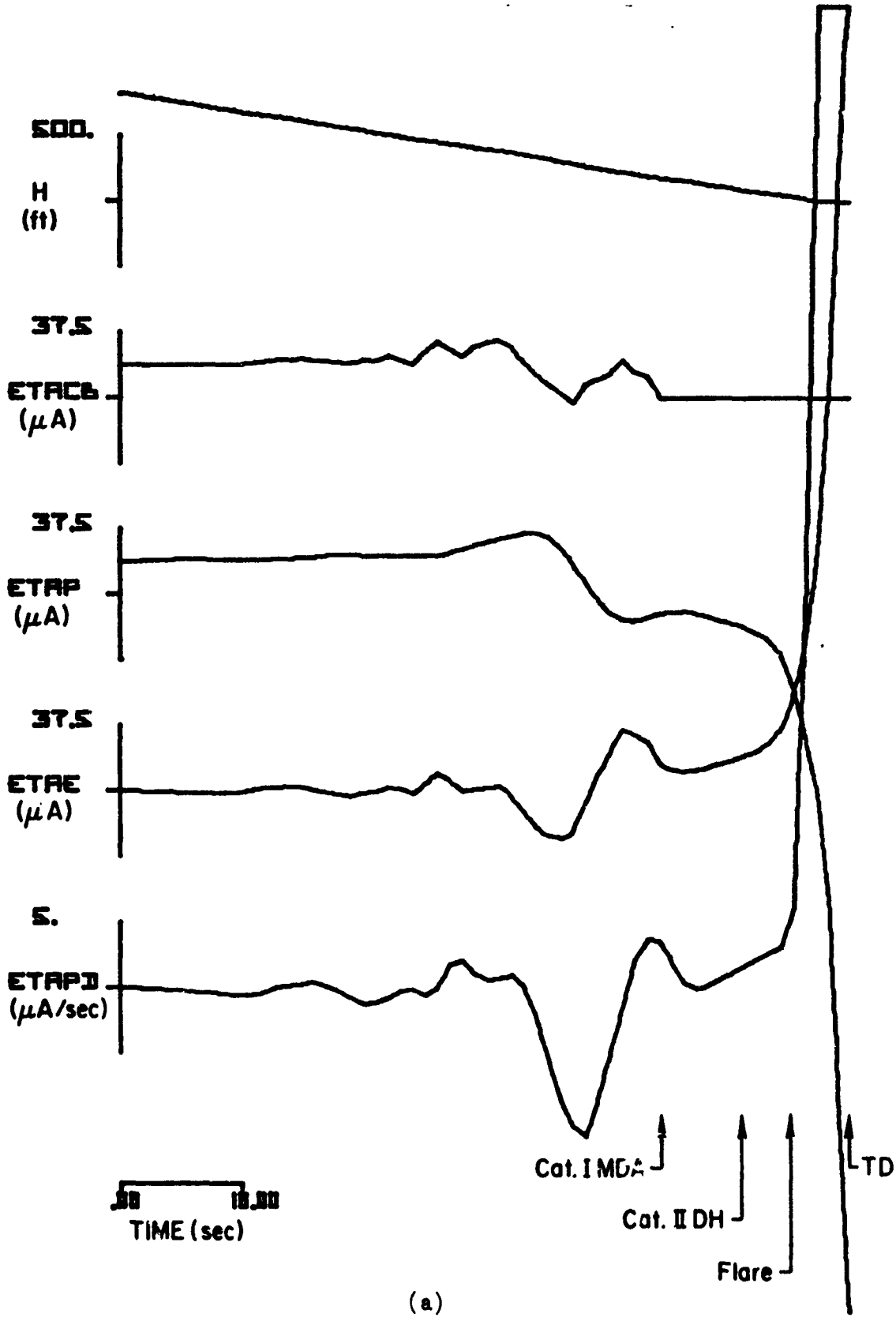

(a)

Figure B-21. Responses of the CV-880 Aircraft with LSI Automatic Landing System and Conventional Glide Slope Coupling to Glide Slope Flight Inspection Record No. 11. Category I Utilization Simulated

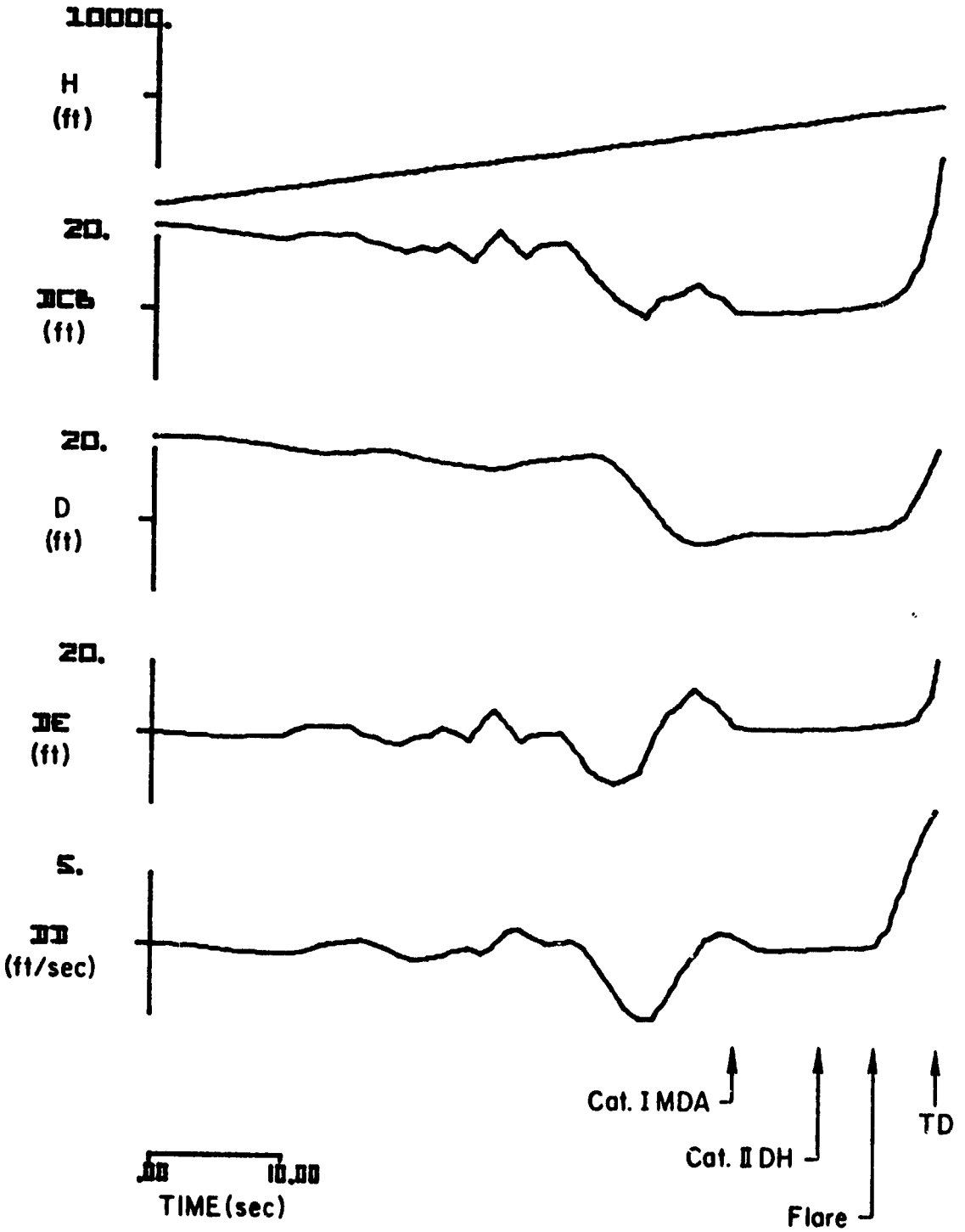

(b)

Figure B-21. (Continued)

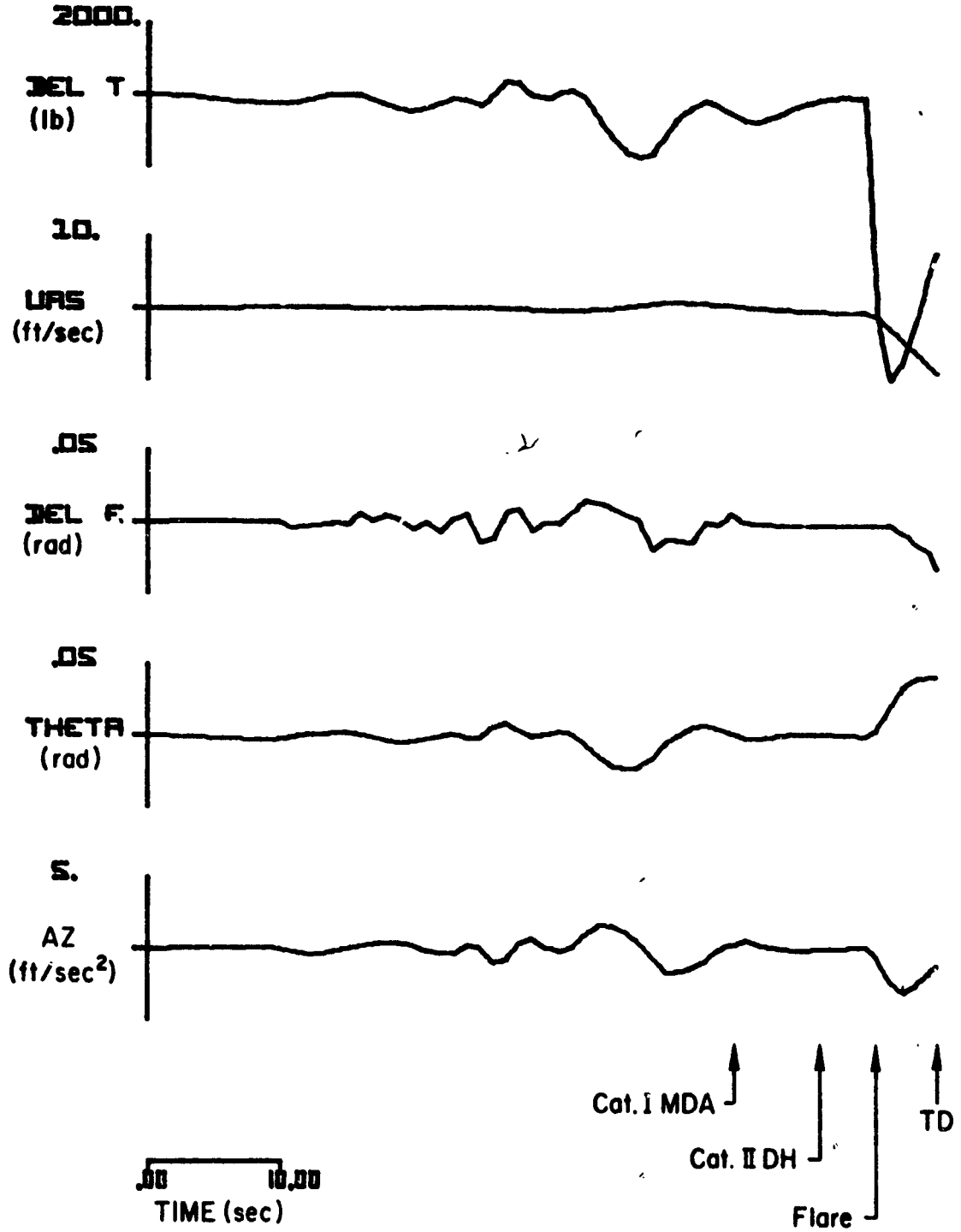

(c)

Figure B-21. (Concluded)

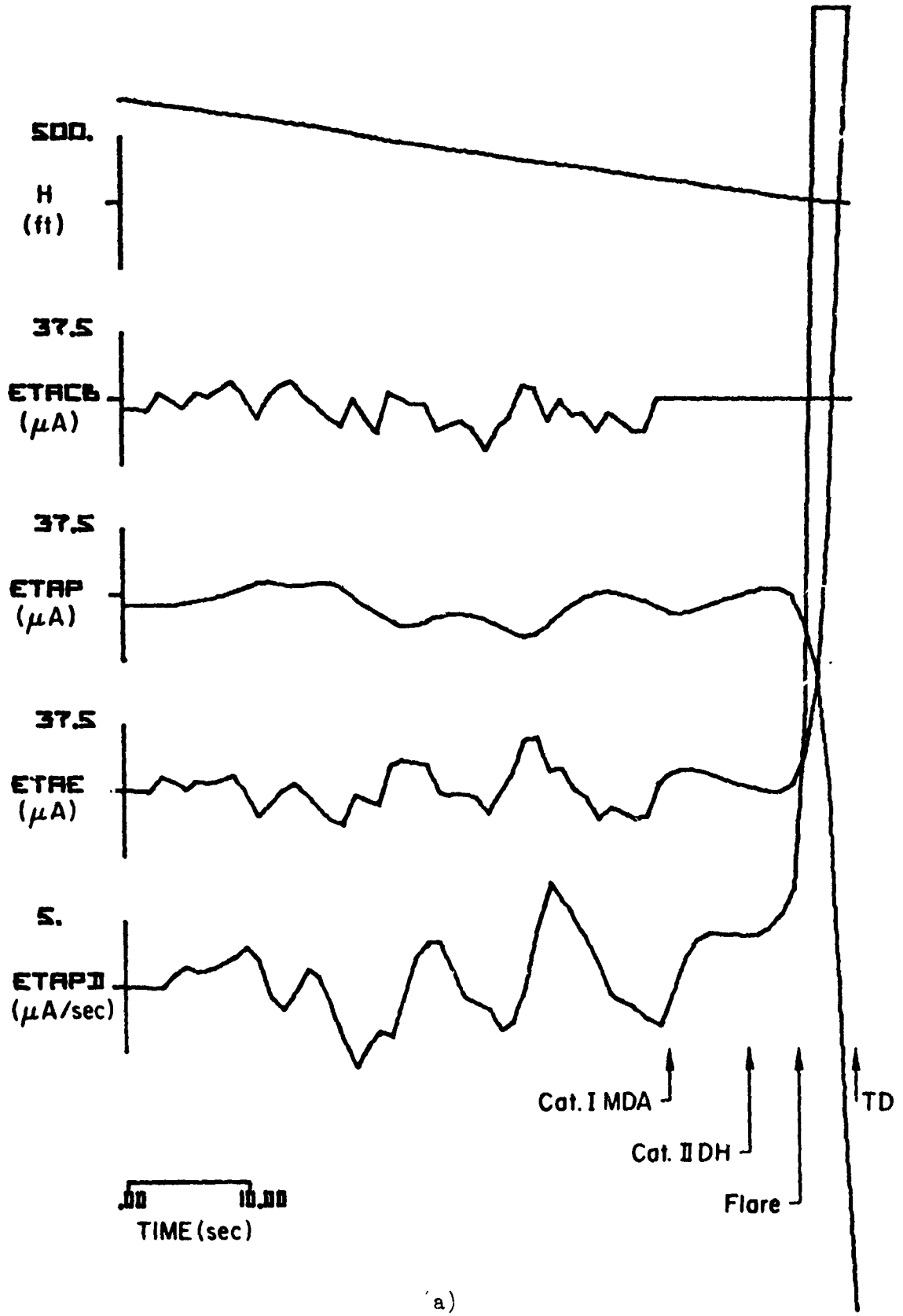

(a)

Figure B-22. Responses of the CV-880 Aircraft with LSI Automatic Landing System and Conventional Glide Slope Coupling to Glide Slope Flight Inspection Record No. 12. Category I Utilization Simulated

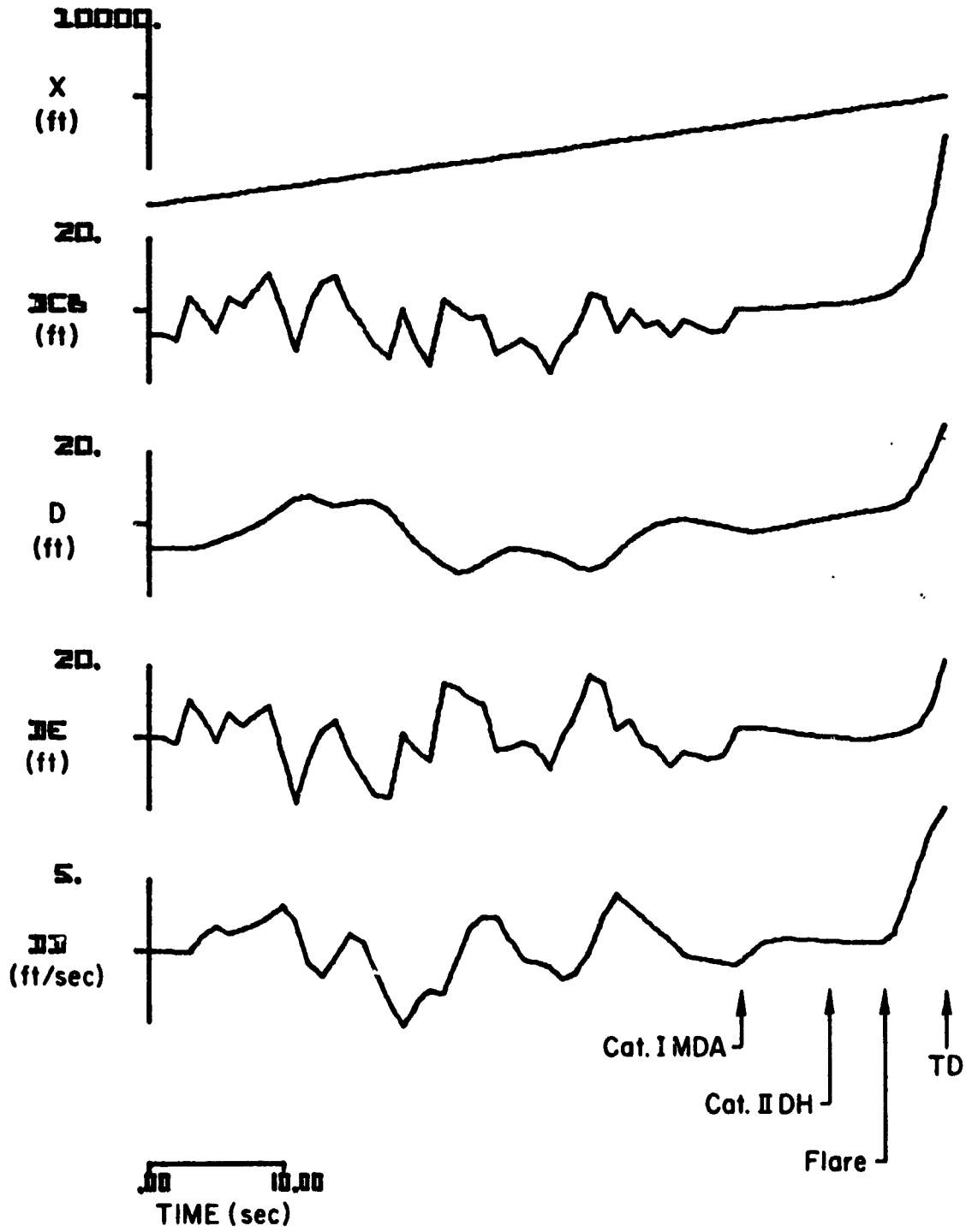

(b)

Figure B-22. (Continued)

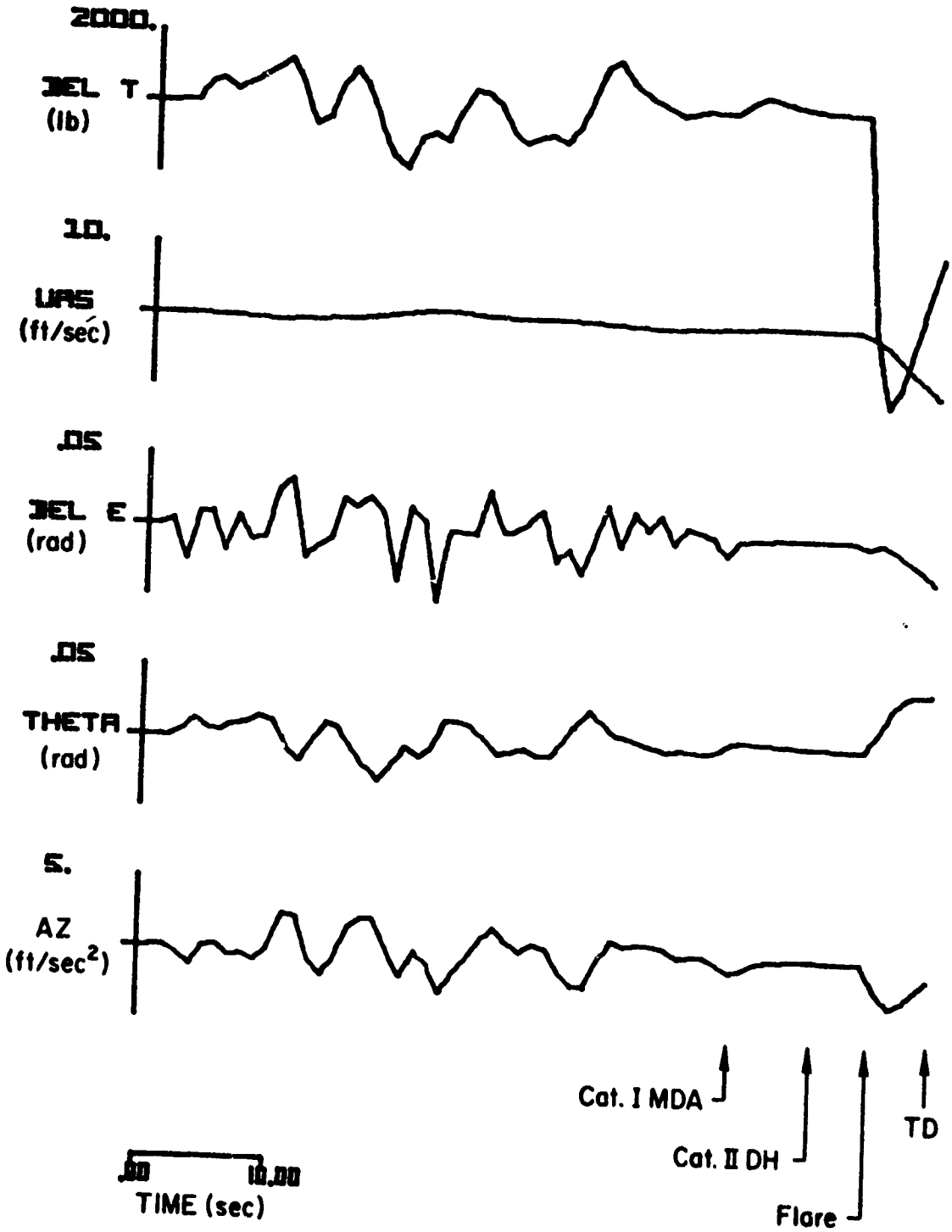

(c)

Figure B-22. (Concluded)

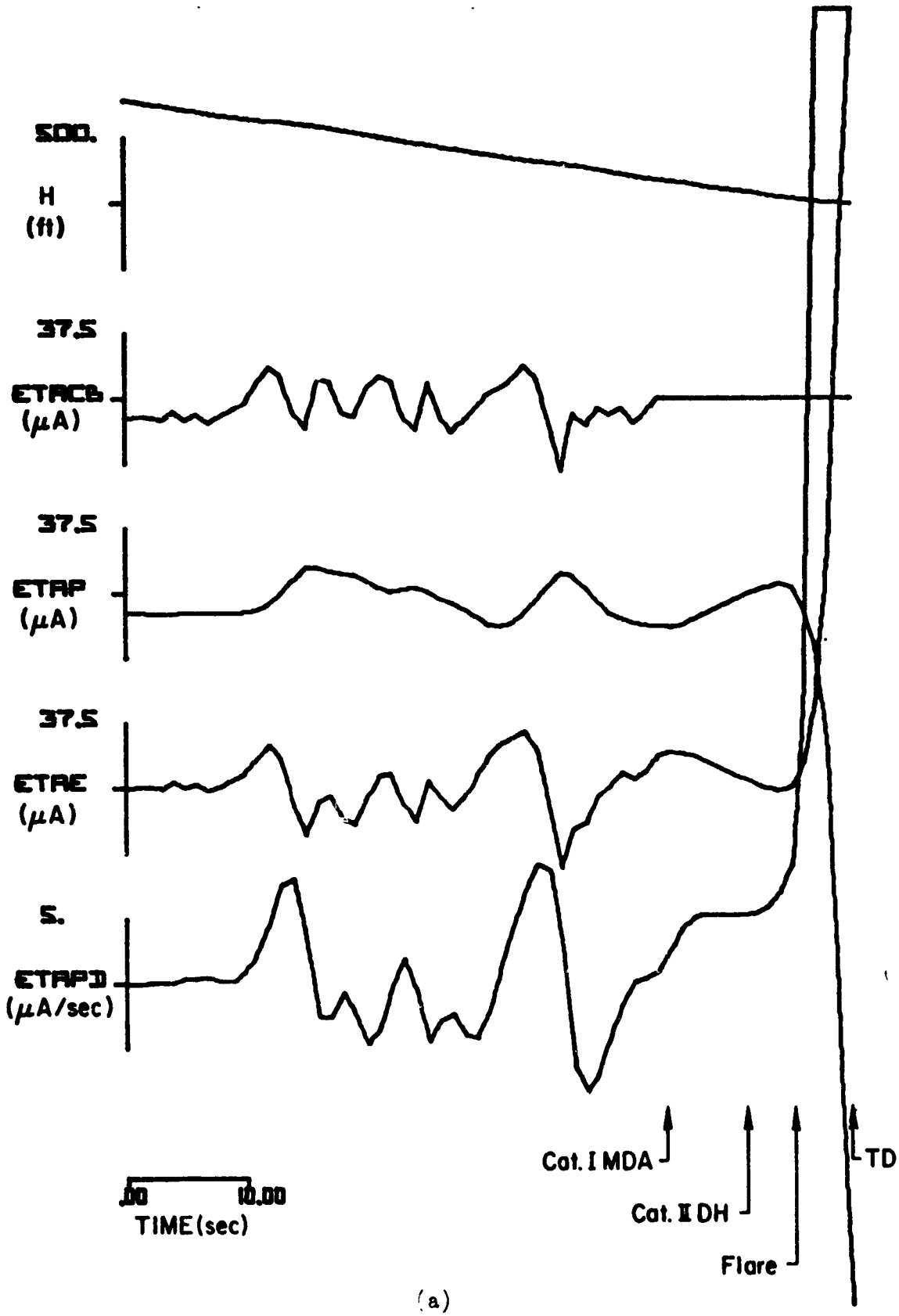

(a)

Figure B-23. Responses of the CV-880 Aircraft with LSI Automatic Landing System and Conventional Glide Slope Coupling to Glide Slope Flight Inspection Record No. 13. Category I Utilization Simulated

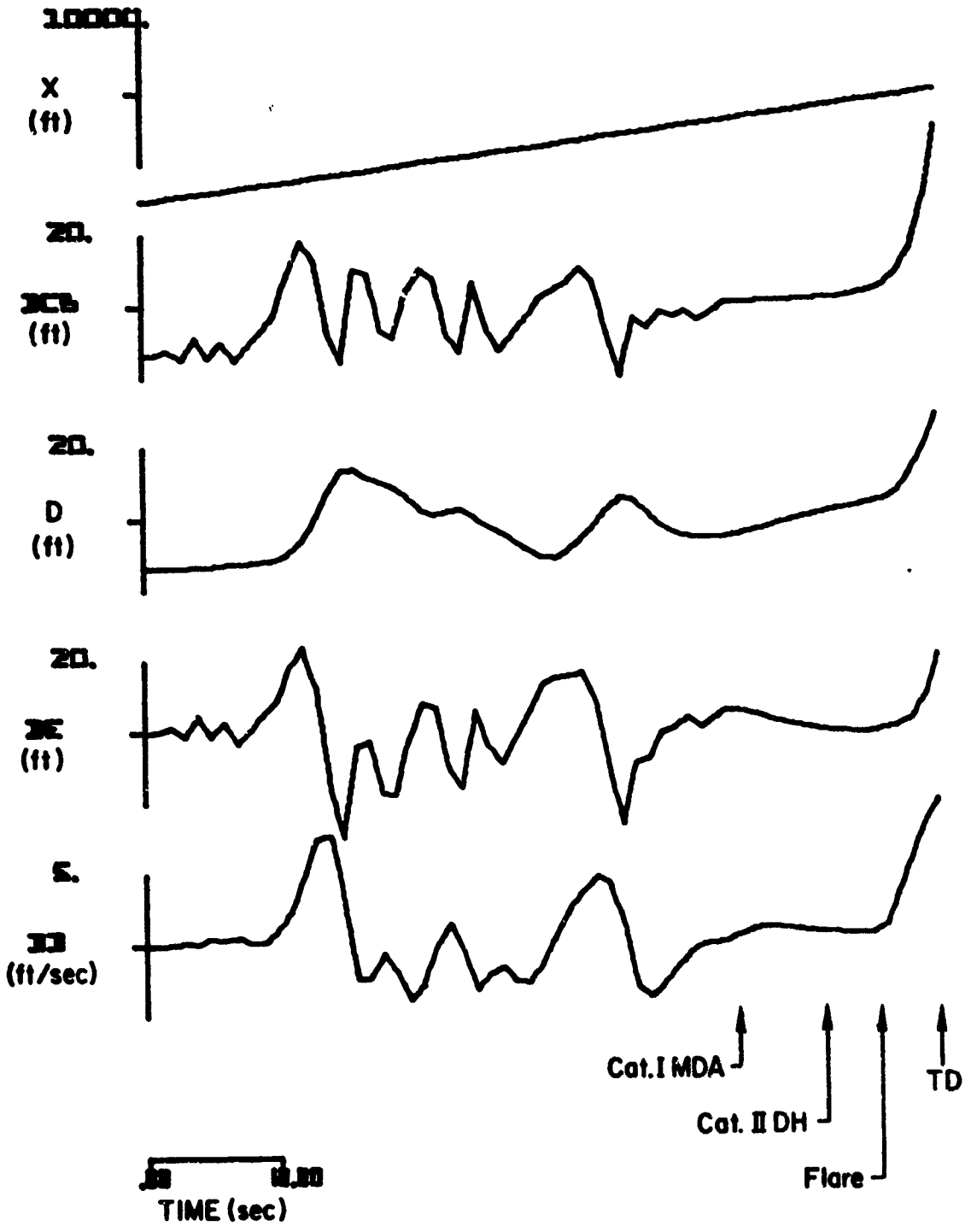

(b)

Figure B-23. (Continued)

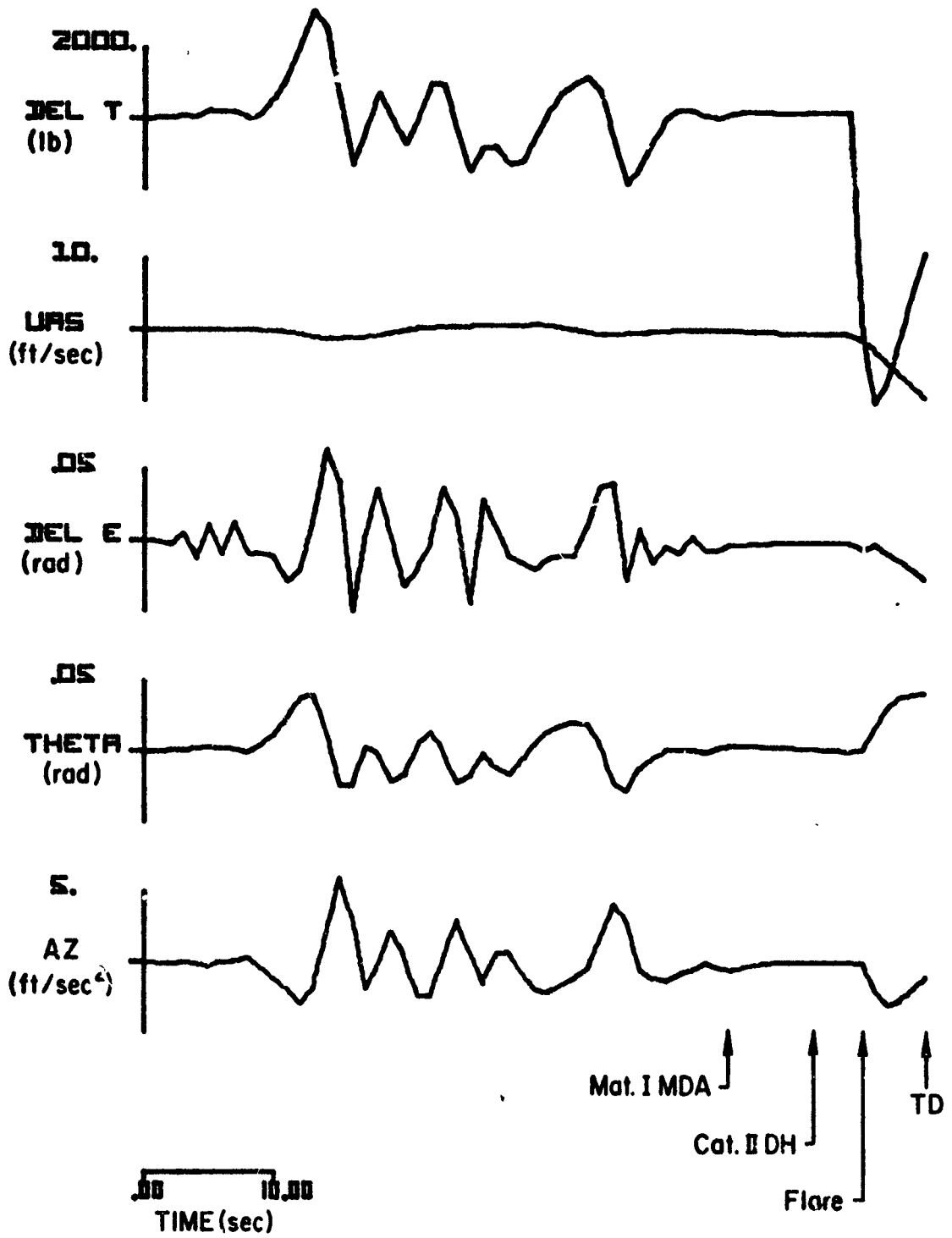

(c)

Figure B-23. (Concluded)

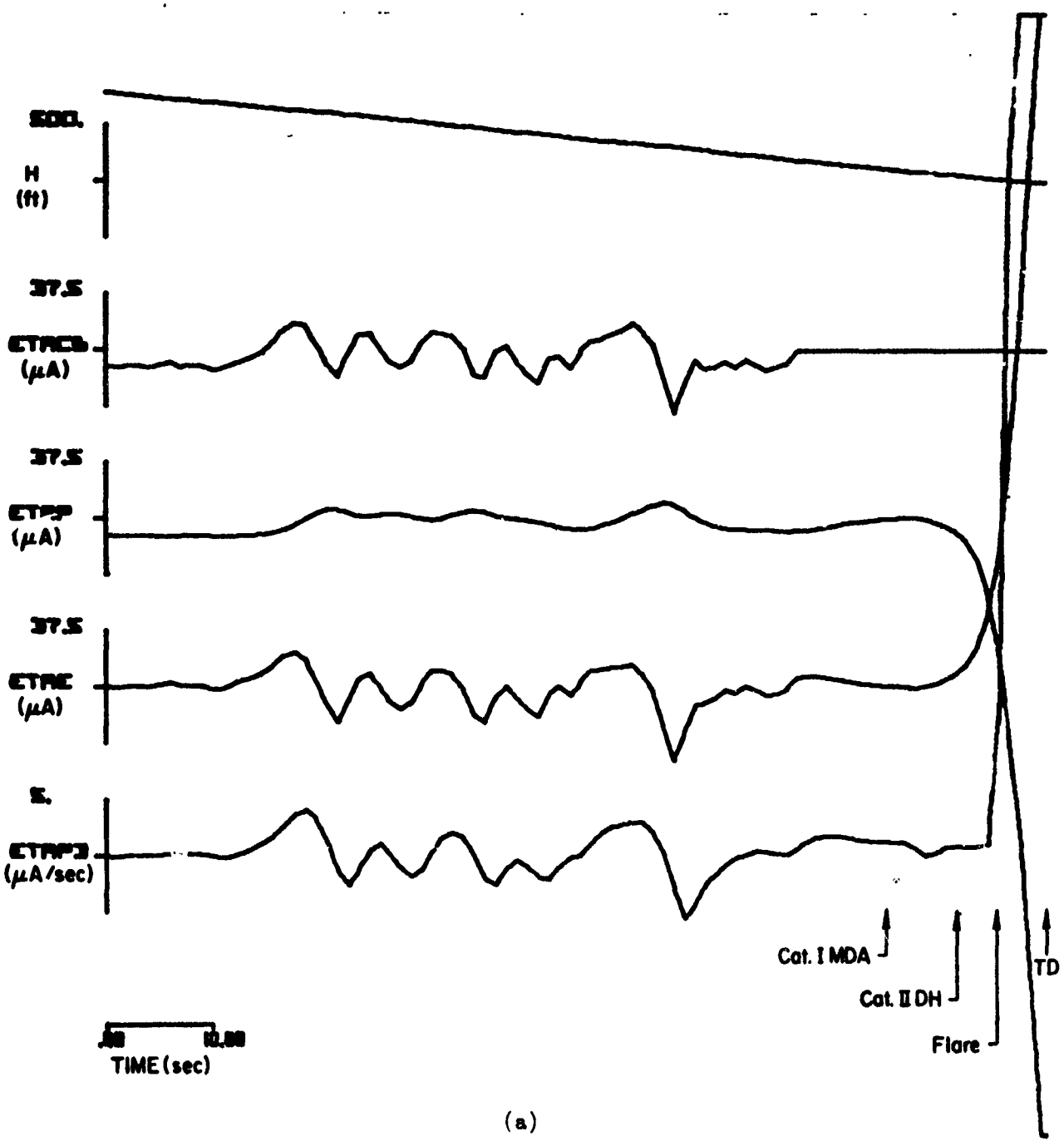

(a)

Figure B-24. Responses of the Piper PA-30 Aircraft with Invented Flight Control System and Conventional Glide Slope Coupling to Glide Slope Flight Inspection Record No. 13. Category I Utilization Simulated

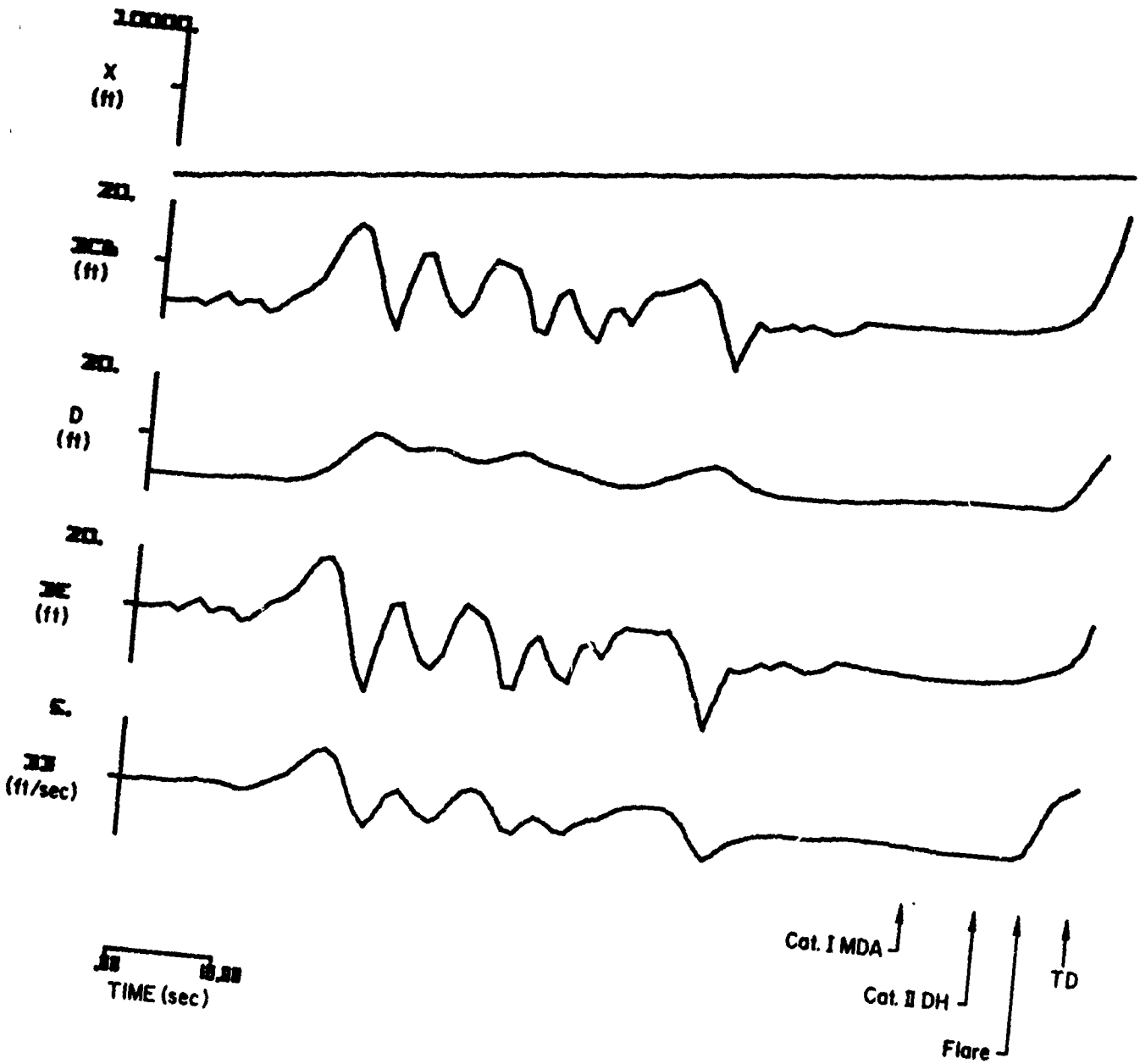

(b)

Figure B-24. (Continued)

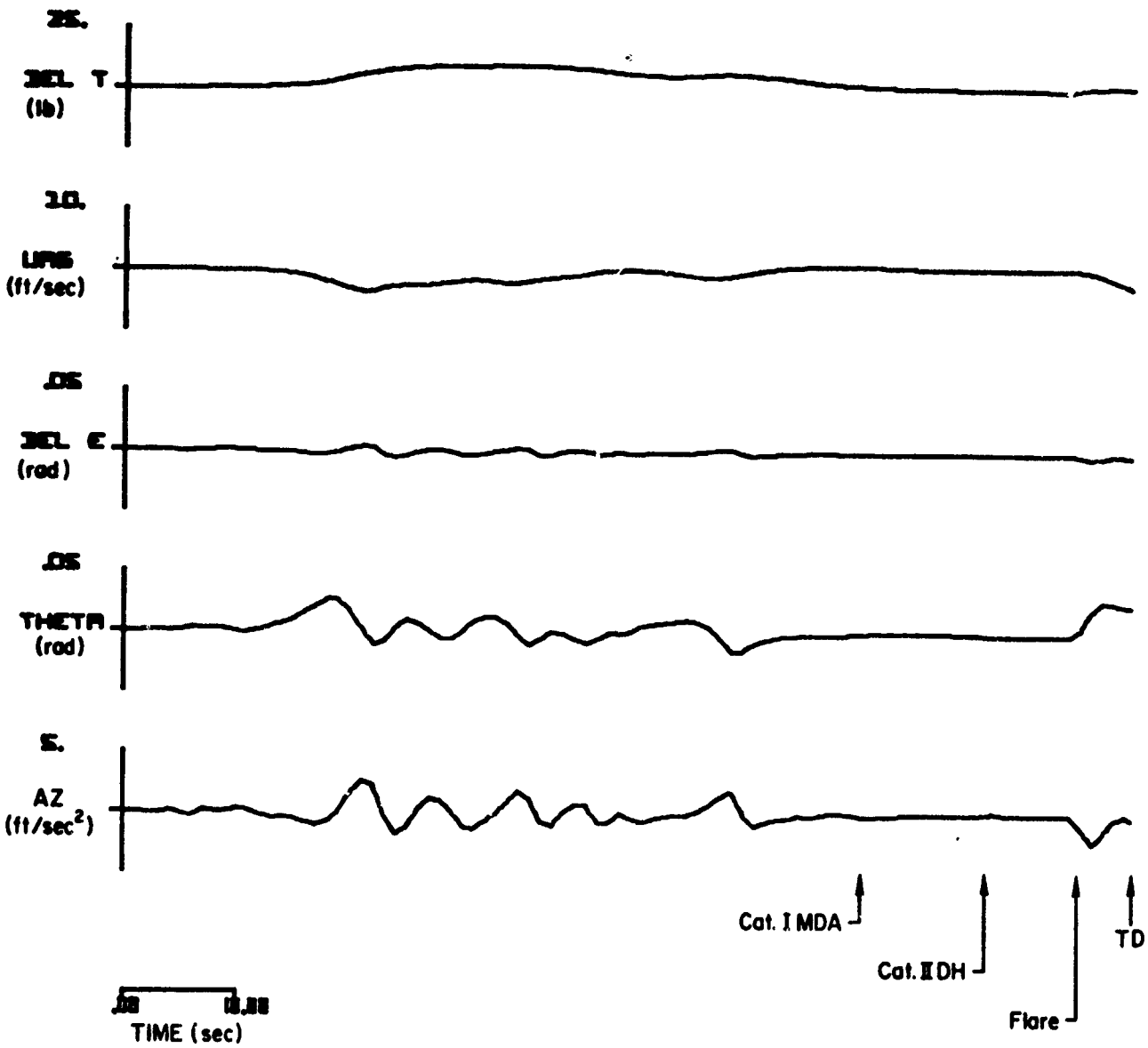

(c)

Figure B-24. (Concluded)

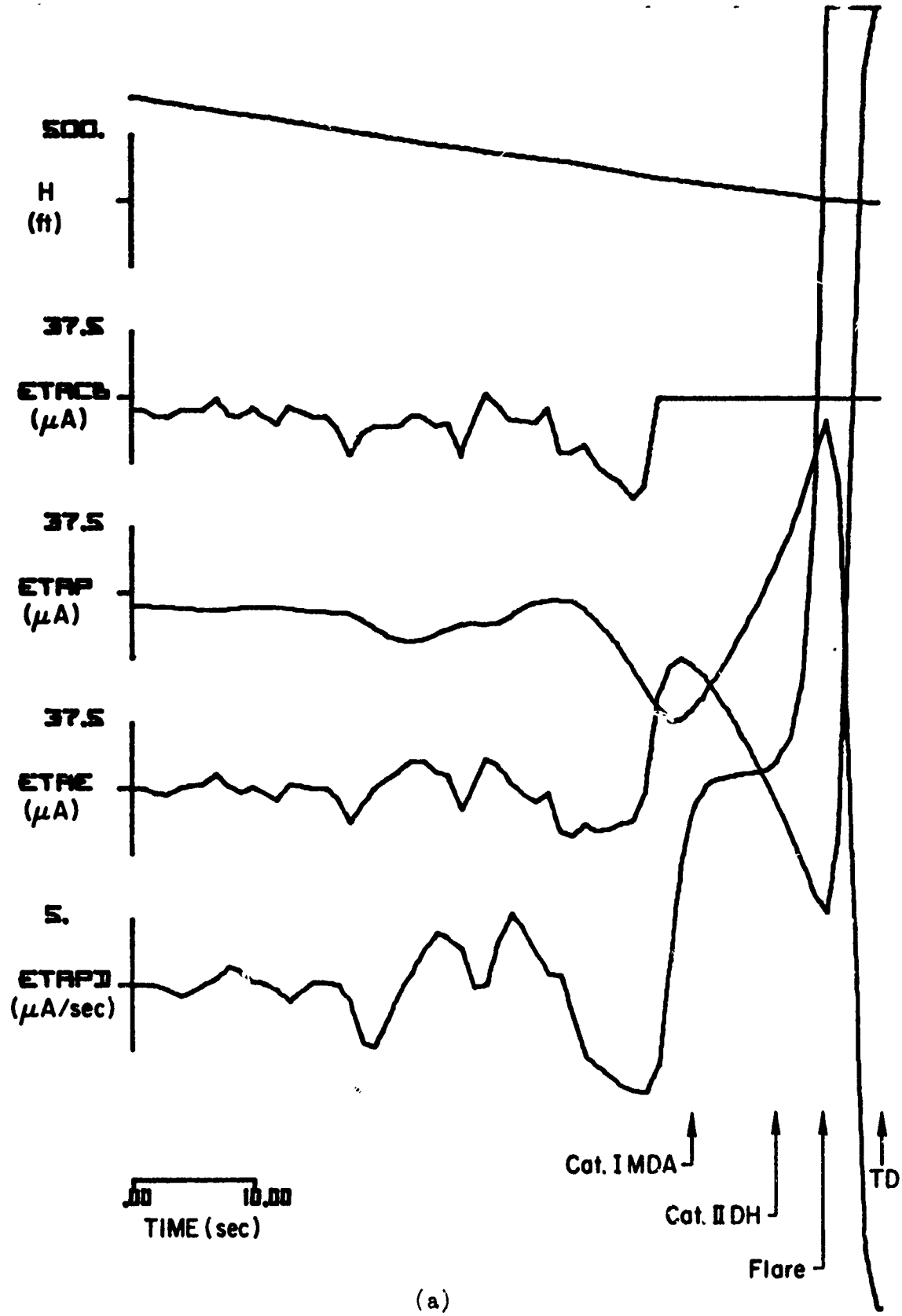

(a)

Figure B-25. Responses of the CV-880 Aircraft with LSI Automatic Landing System and Conventional Glide Slope Coupling to Glide Slope Flight Inspection Record No. 14. Category I Utilization Simulated

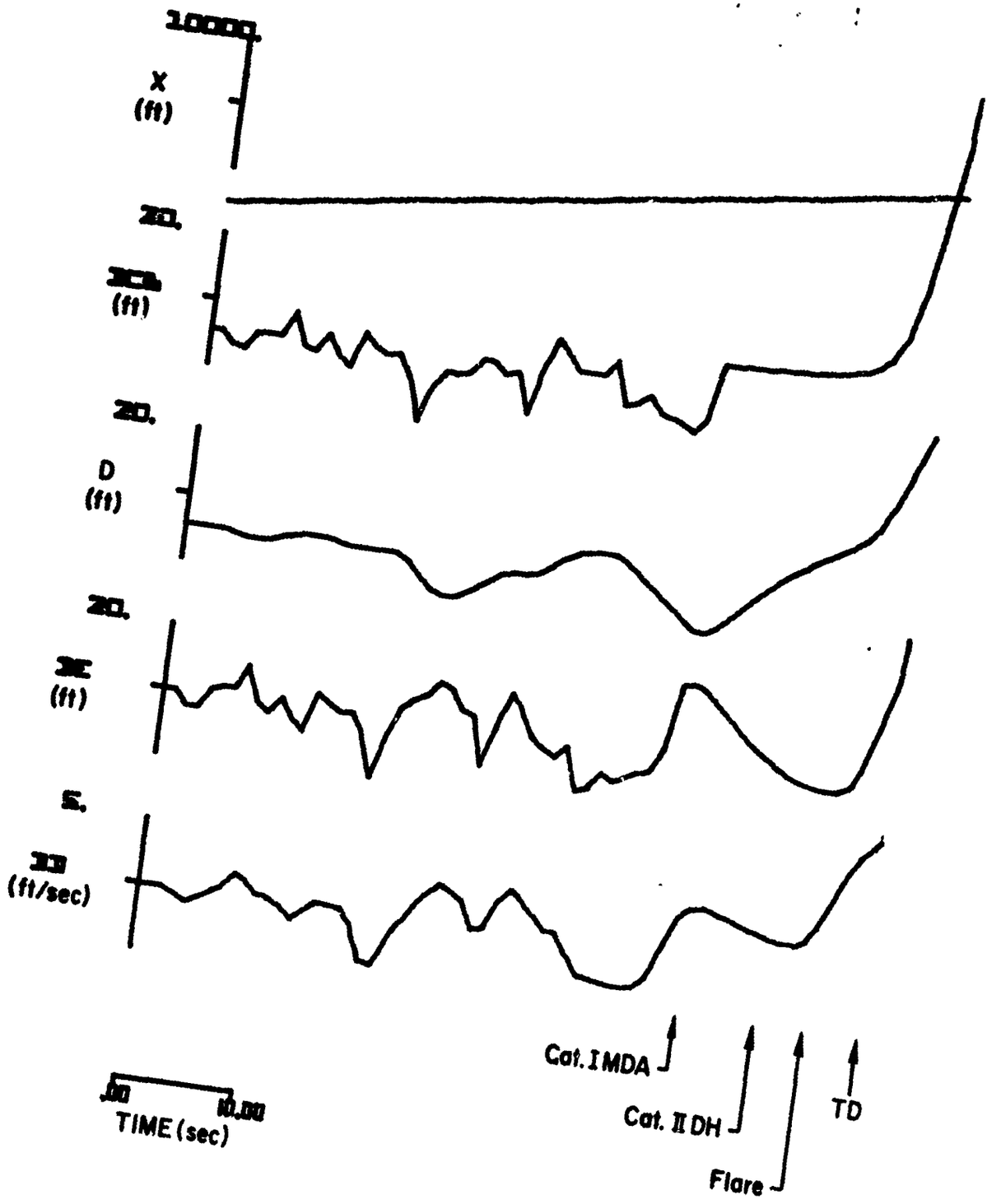

(b)

Figure B-25. (Continued)

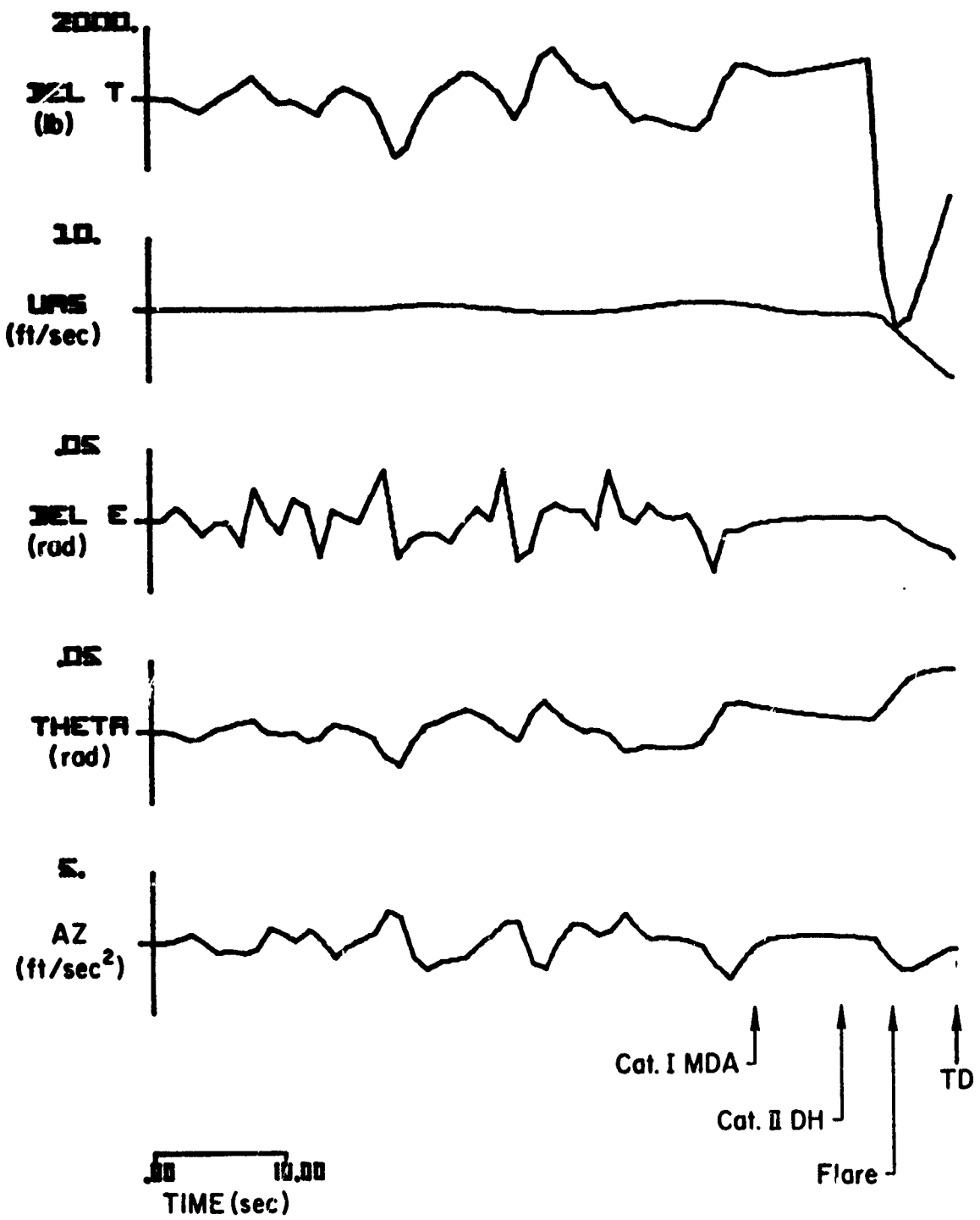

(c)

Figure B-25. (Concluded)

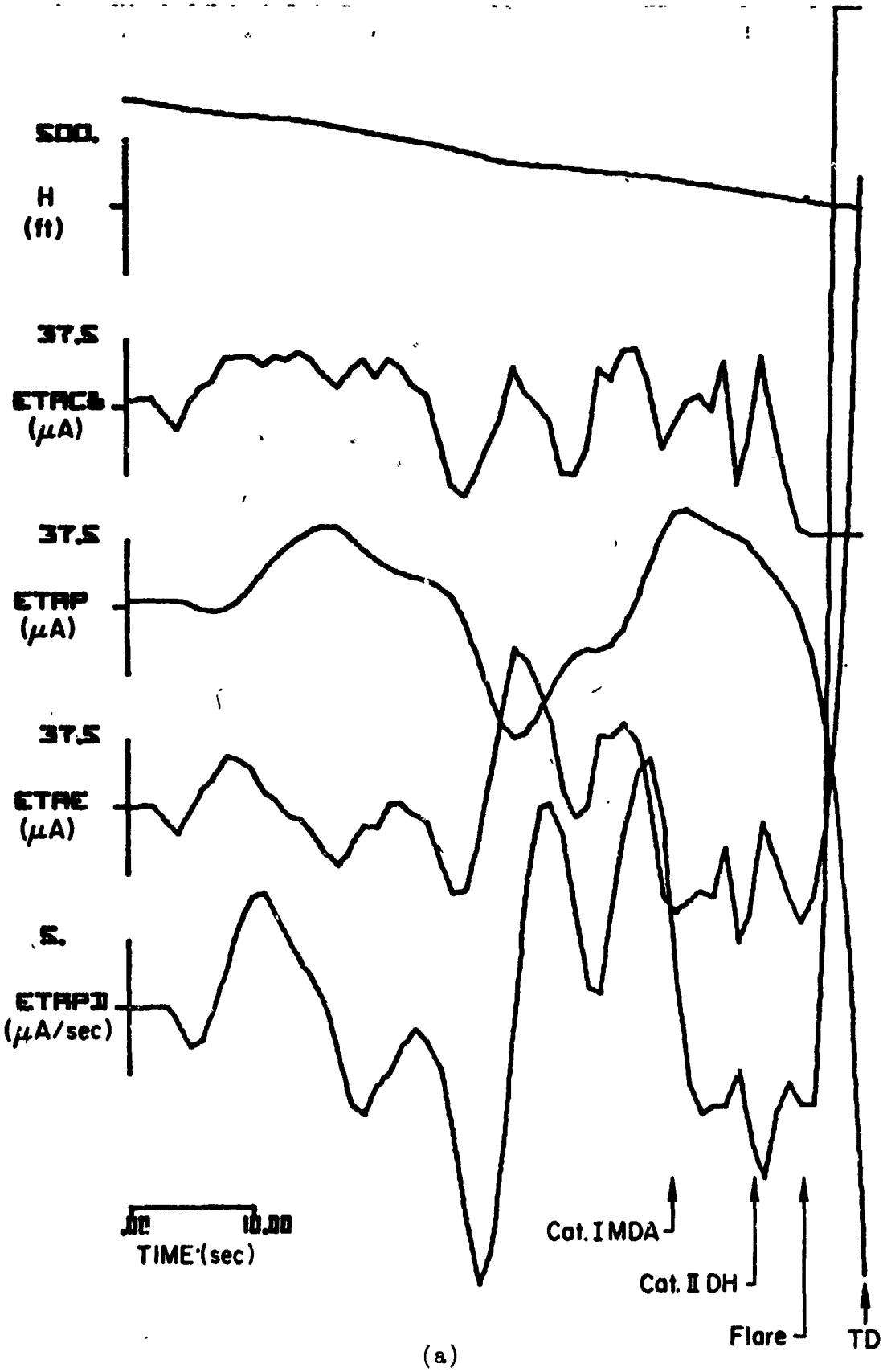

(a)

Figure B-26. Responses of the CV-880 Aircraft with LSI Automatic Landing System and Conventional Glide Slope Coupling to Glide Slope Flight Inspection Record No. 15. Category II-III Utilization Simulated

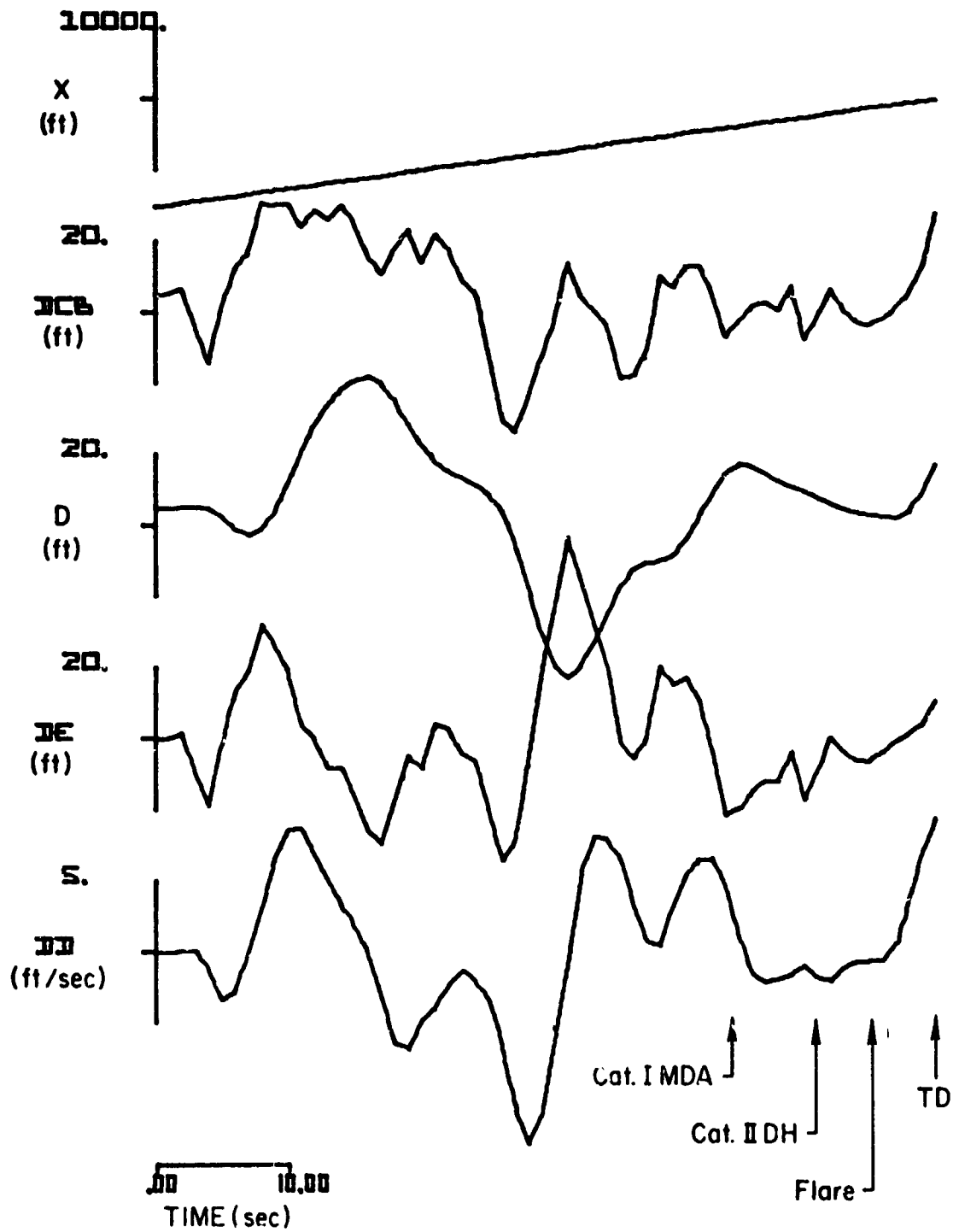

(b)

Figure B-26. (Continued)

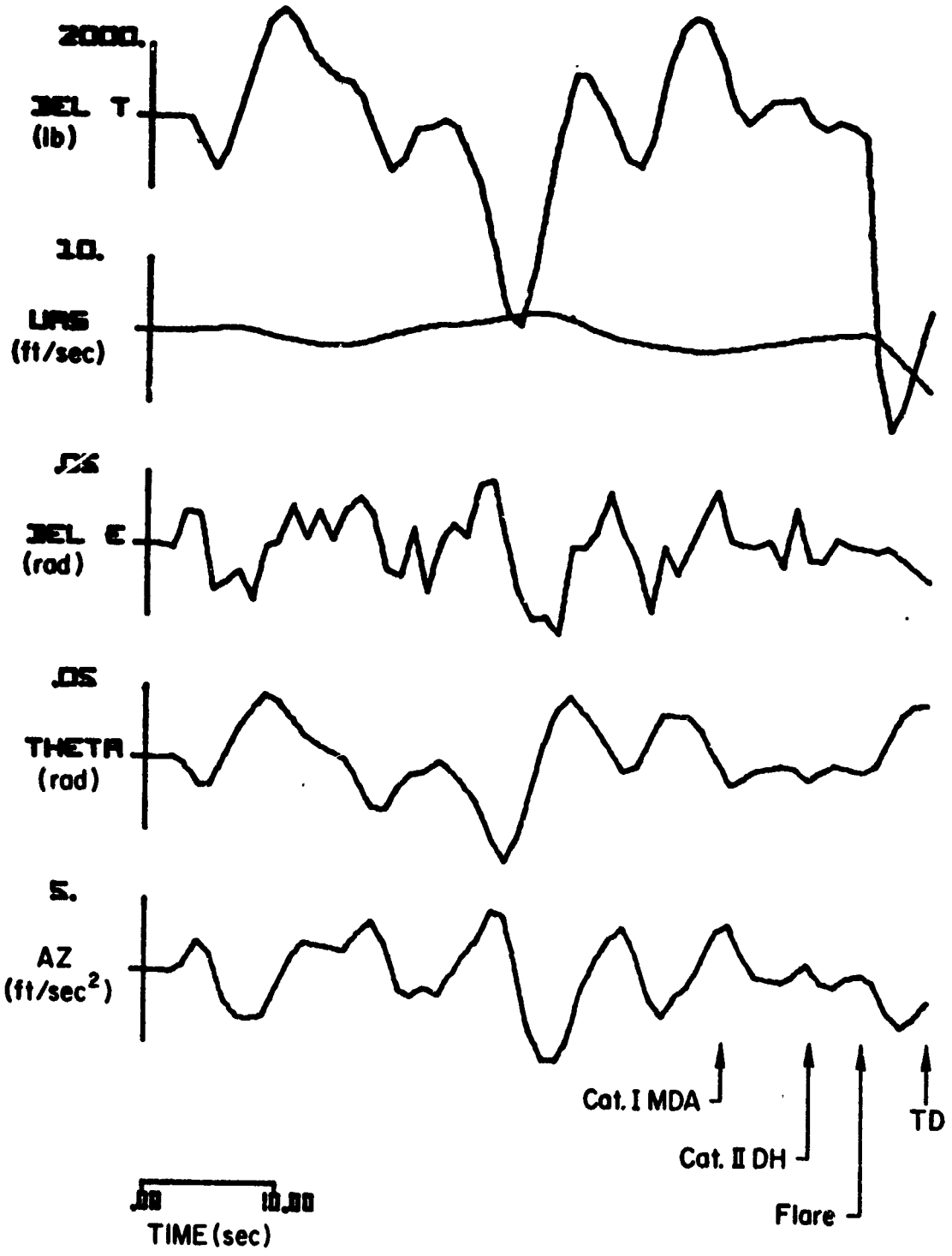

(c)

Figure B-26. (Concluded)

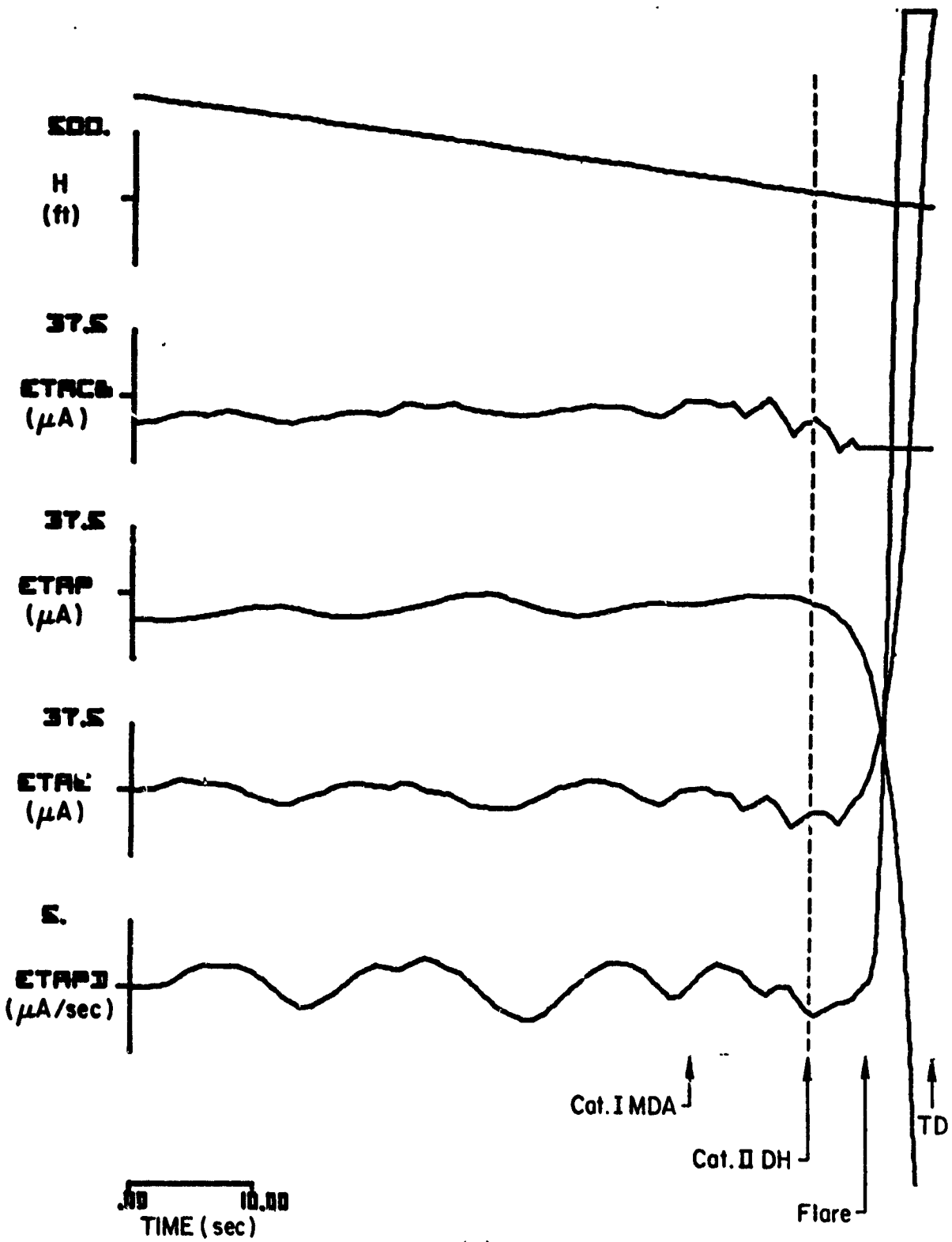

(a)

Figure B-27. Responses of the CV-880 Aircraft with LSI Automatic Landing System and Conventional Glide Slope Coupling to Glide Slope Flight Inspection Record No. 2. Category II-III Utilization Simulated

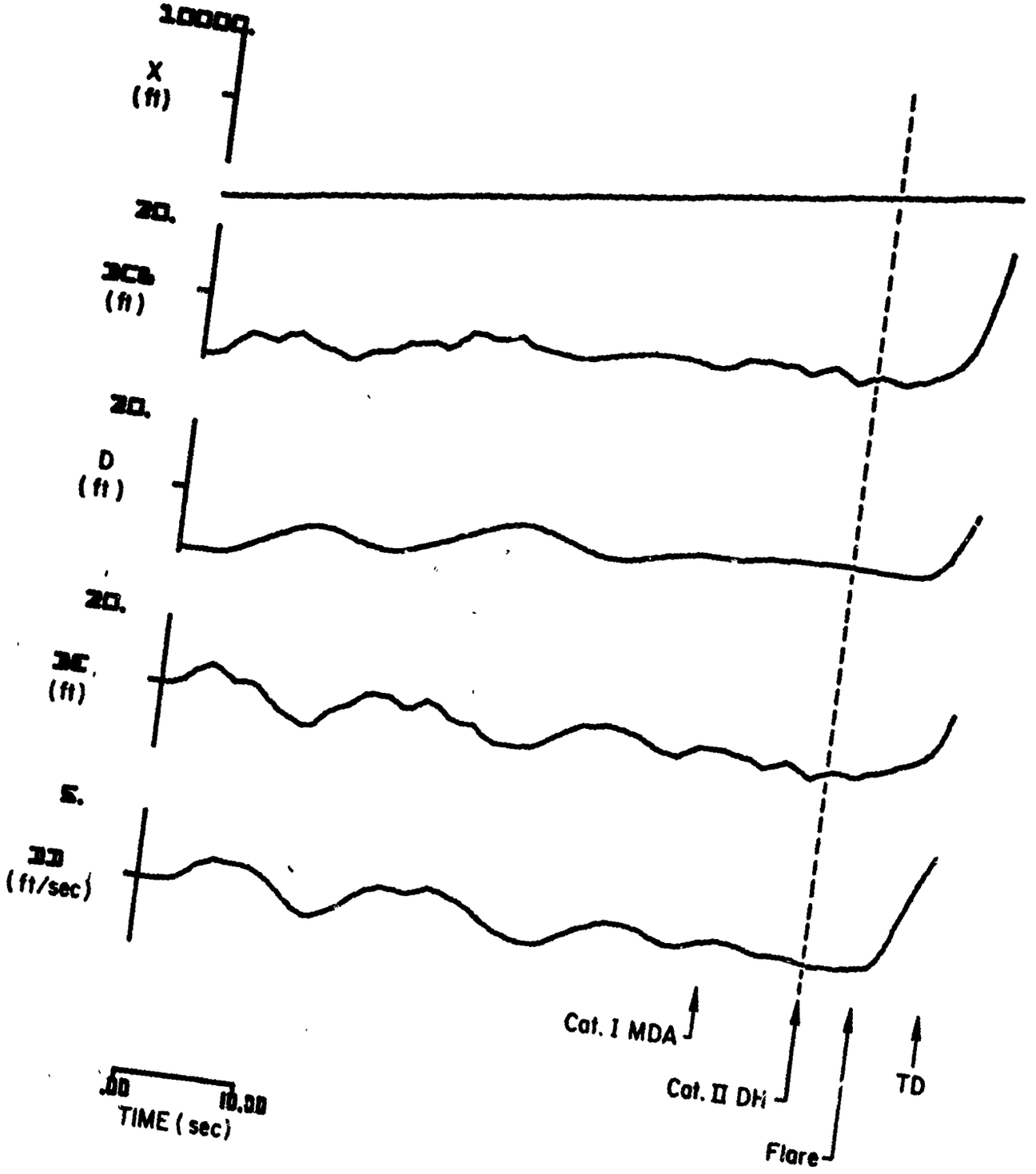

(b)

Figure B-27. (Continued)

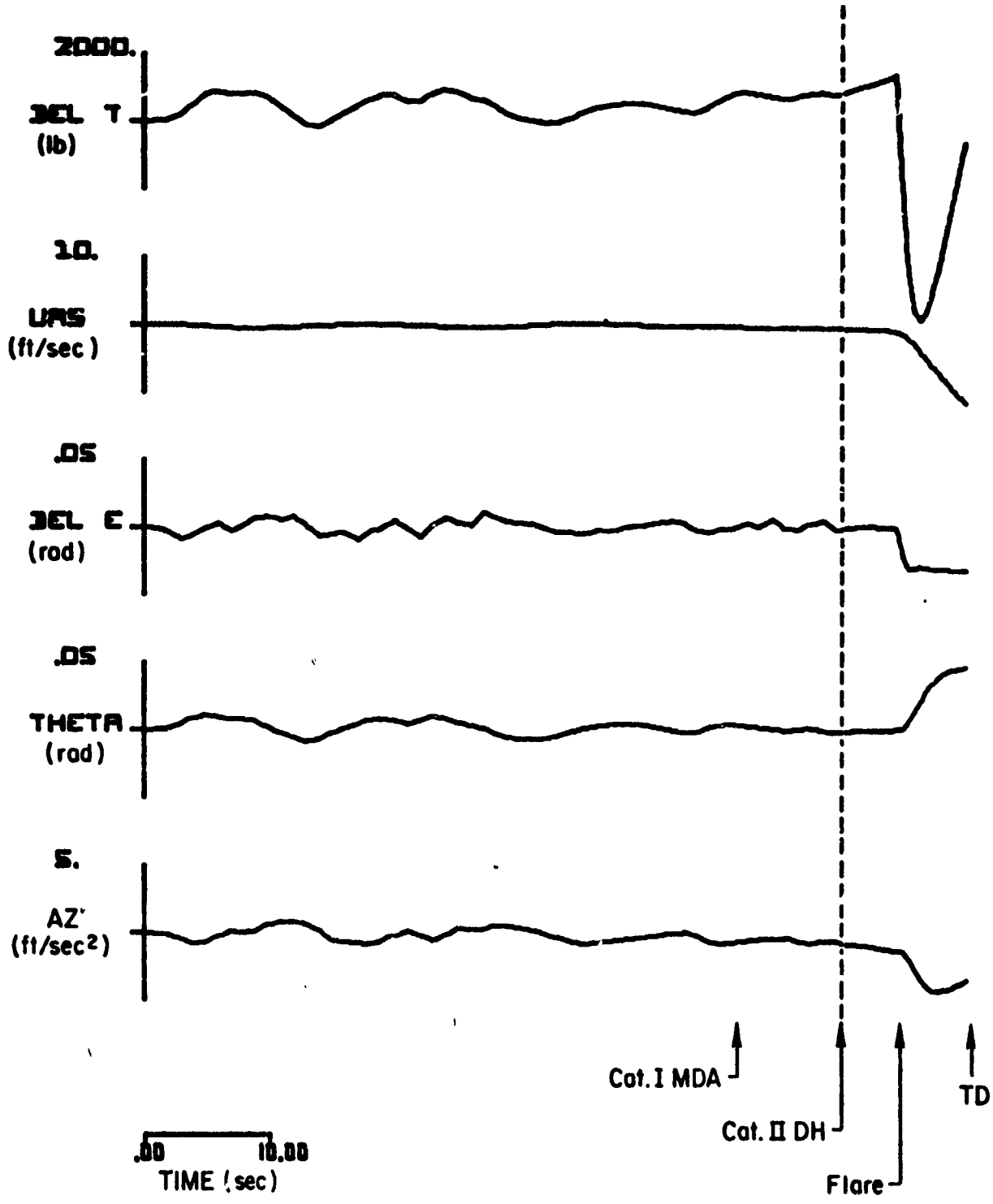

(c)

Figure B-27. (Continued)

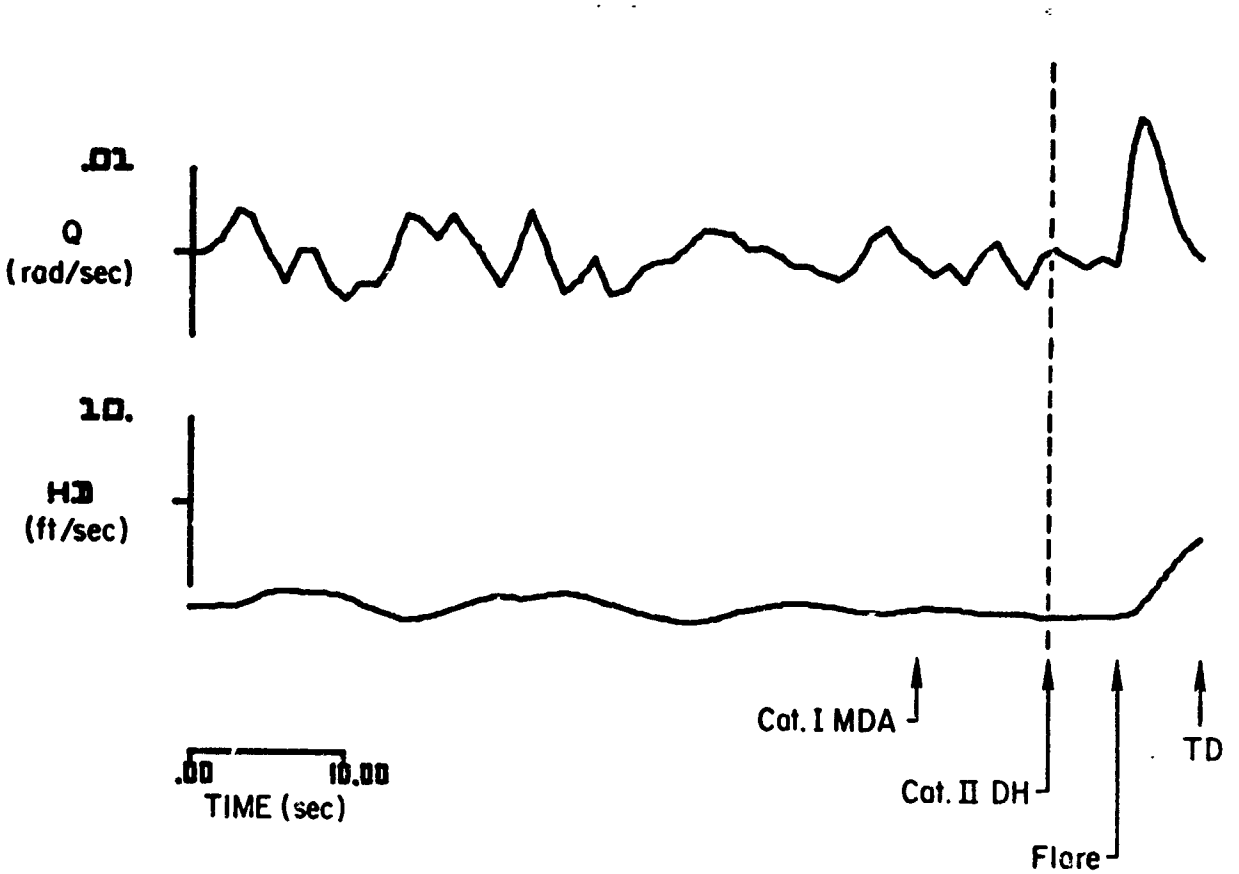

(d)

Figure B-27. (Concluded)

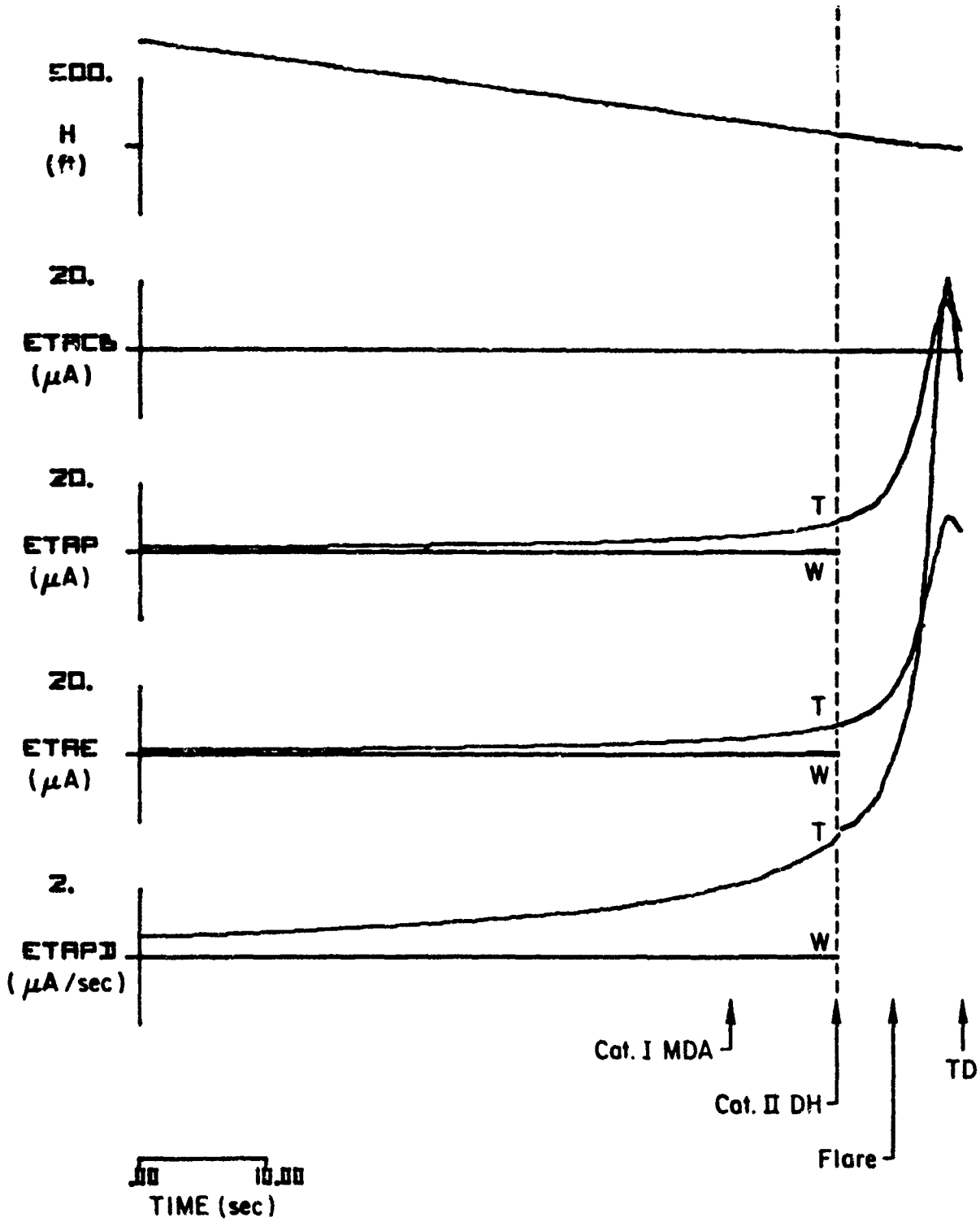

(a)

Figure B-28. Standard Deviation Responses to Wind, Wind Shear, and Turbulence for the CV-880 Aircraft with LSI Automatic Landing System and Conventional Glide Slope Coupling to Glide Slope Flight Inspection Record No. 2. Category II-III Utilization Simulated

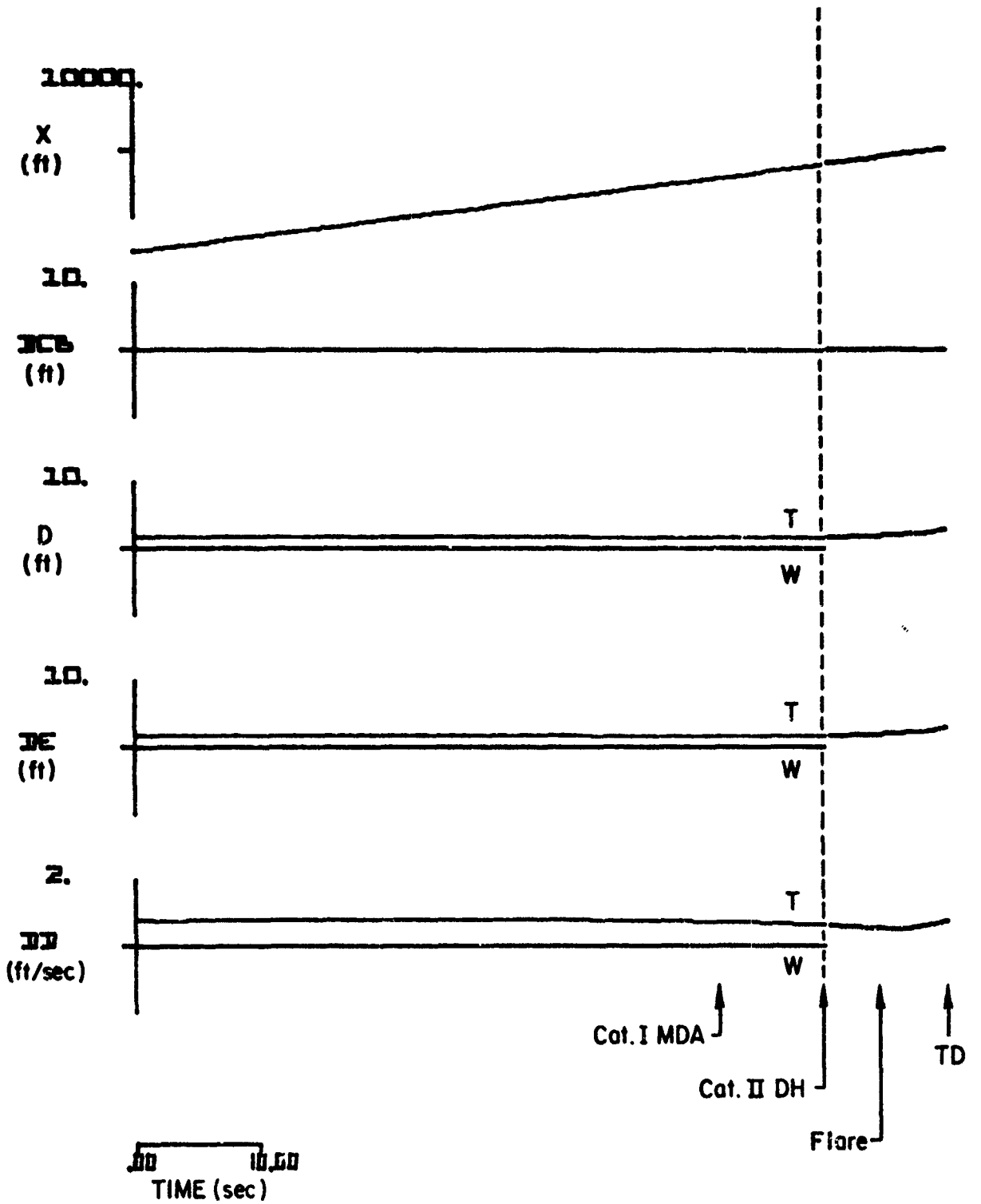

(b)

Figure B-28. (Continued)

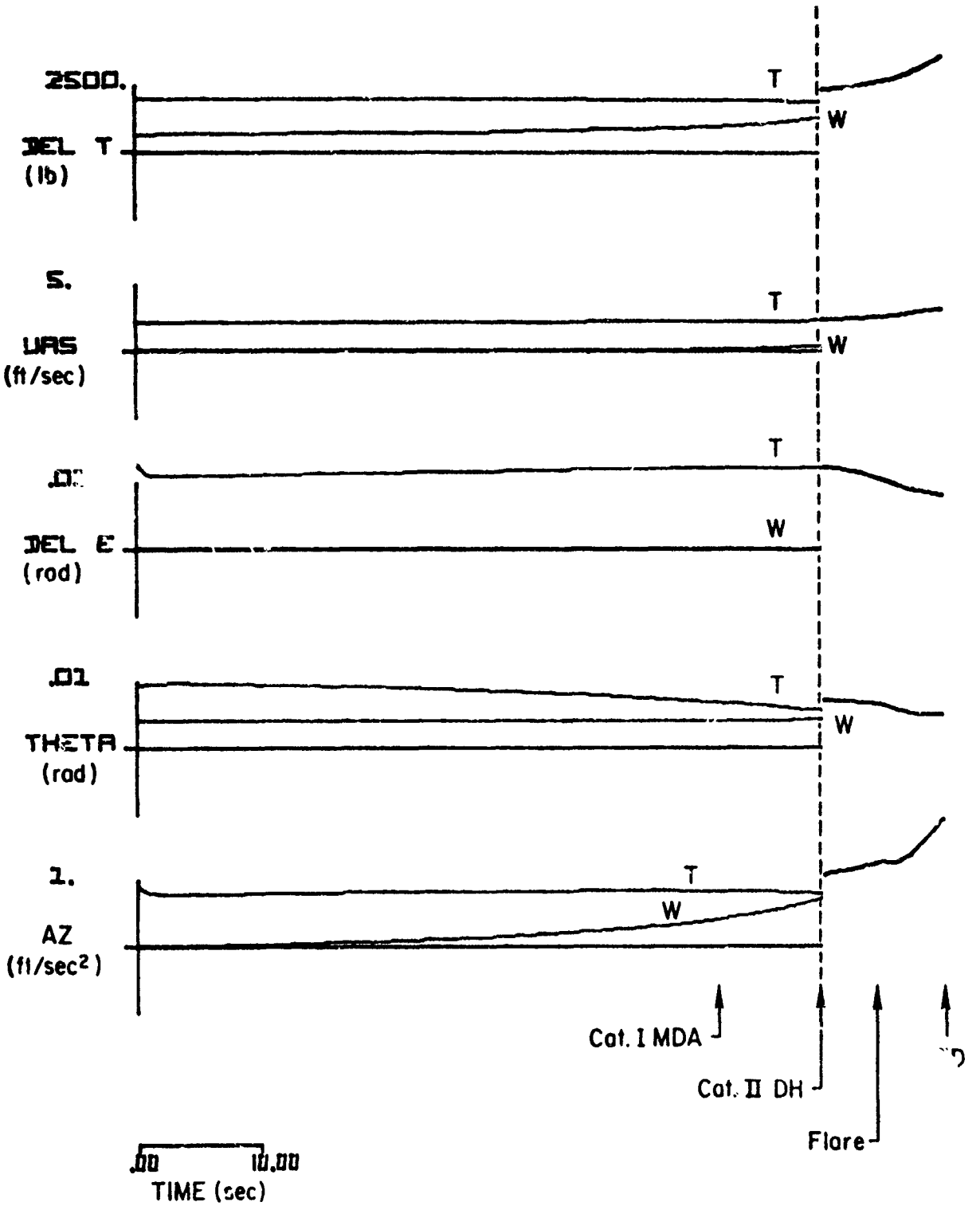

(c)

Figure B-28. (Continued)

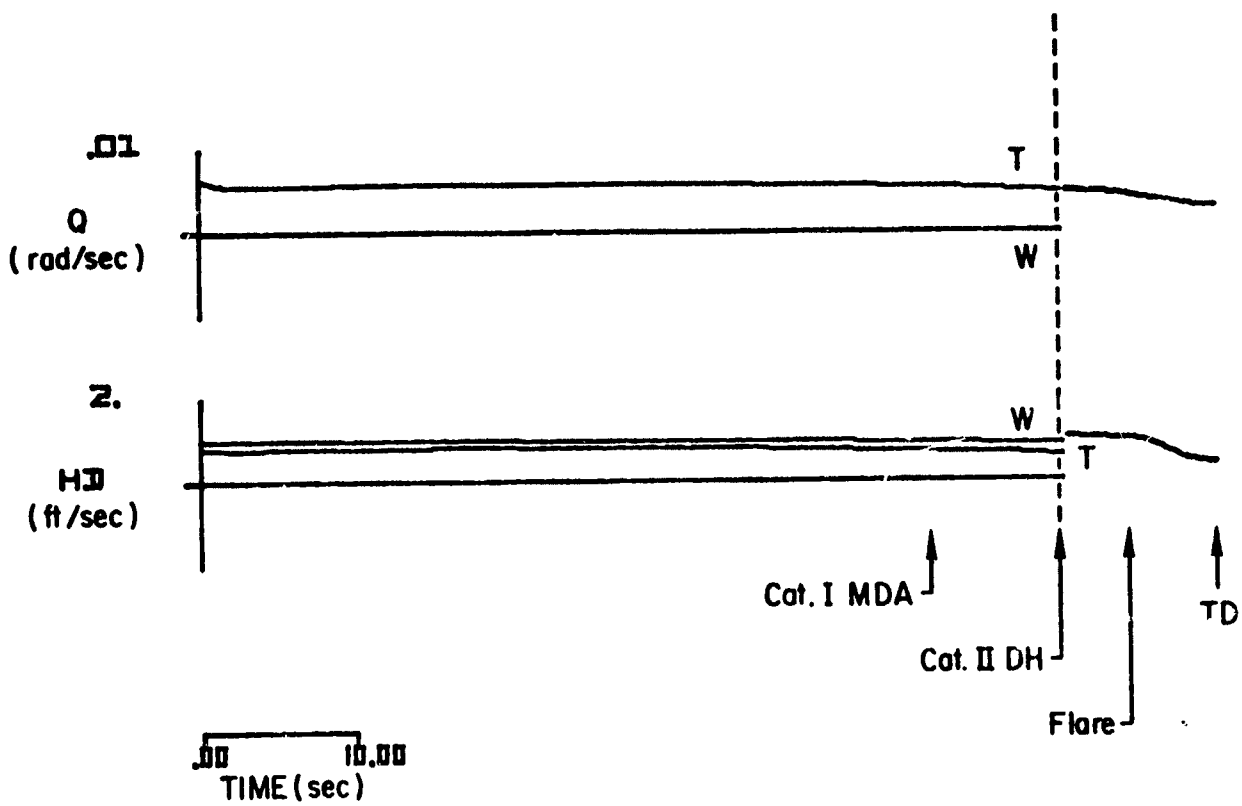

(d)

Figure B-28. (Concluded)

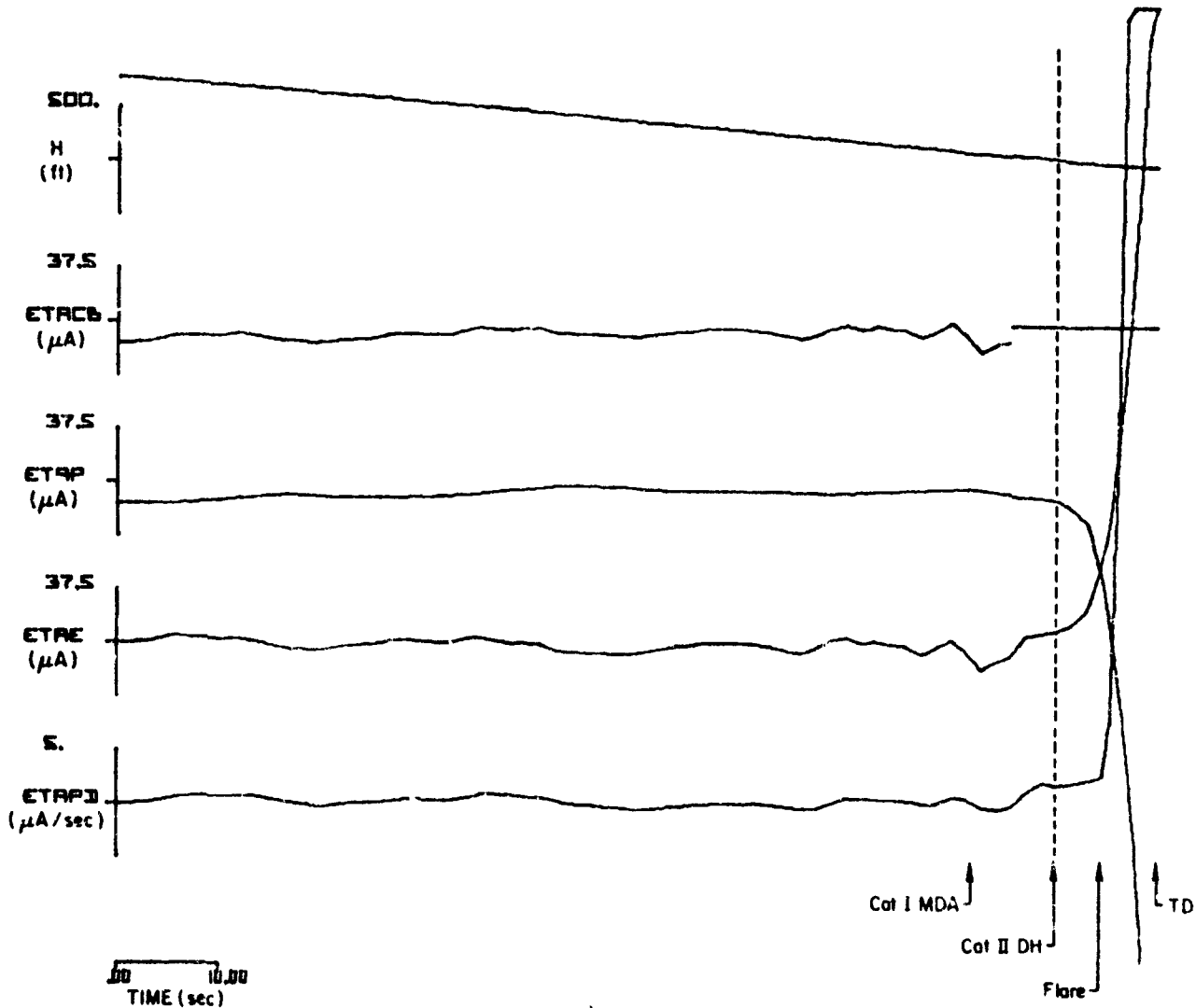

a)

Figure B-29. Responses of the Piper PA-30 Aircraft with Inverted Flight Control System and Conventional Glide Slope Coupling to Glide Slope Flight Inspection Record No. . . Category II M Utilization Simulated

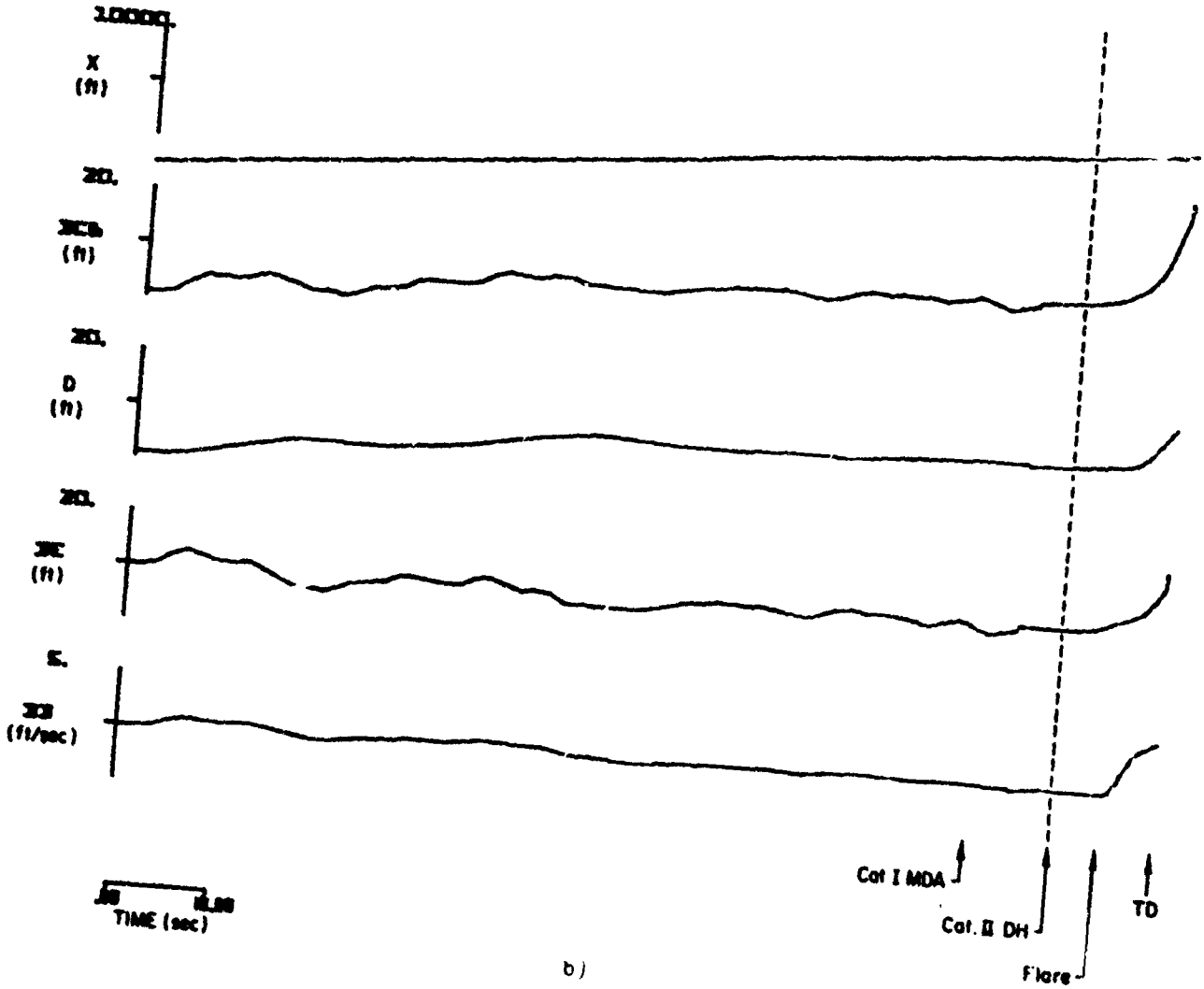

b)

Figure B-29. (Continued)

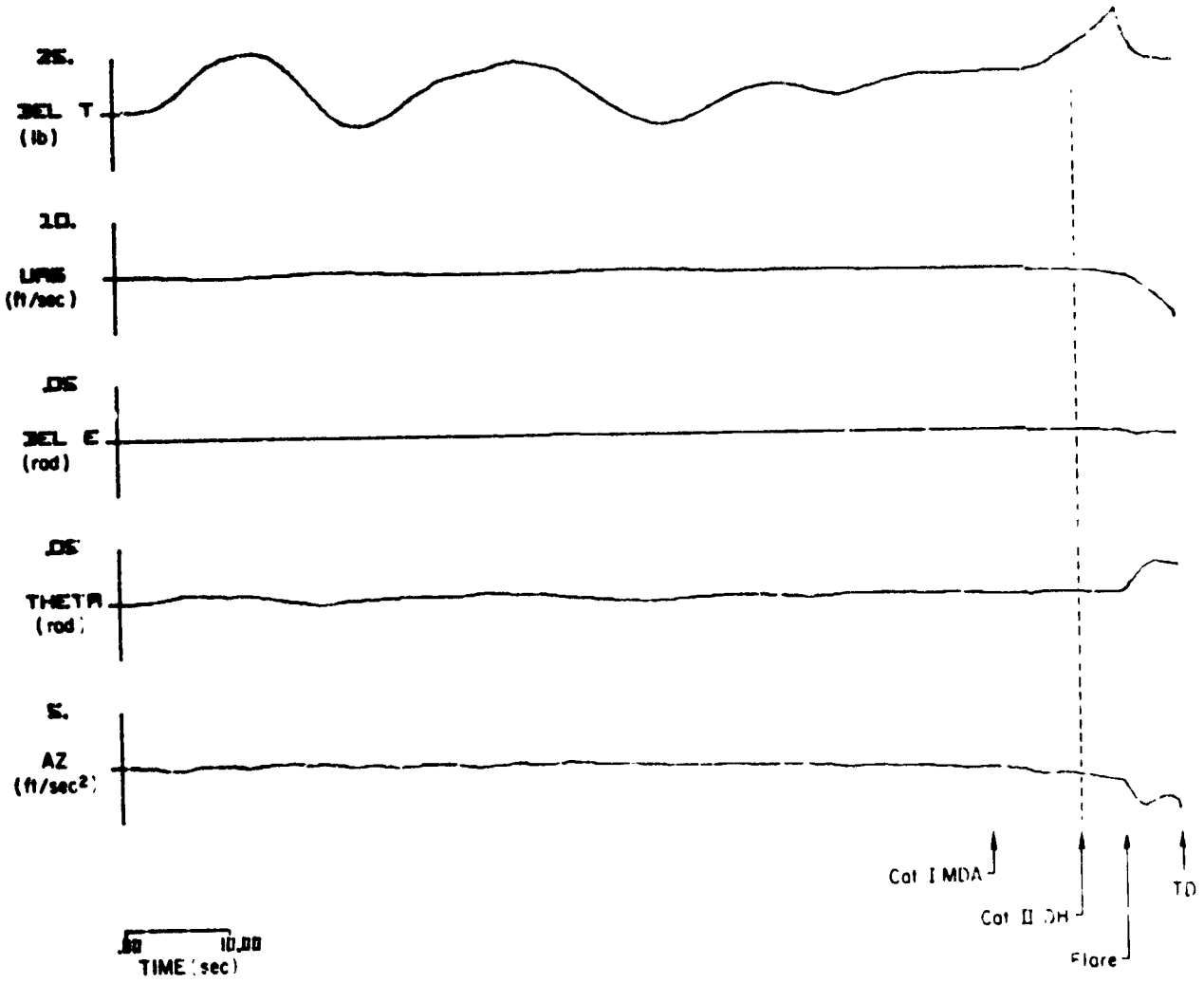

(c)

Figure B-9. Continued

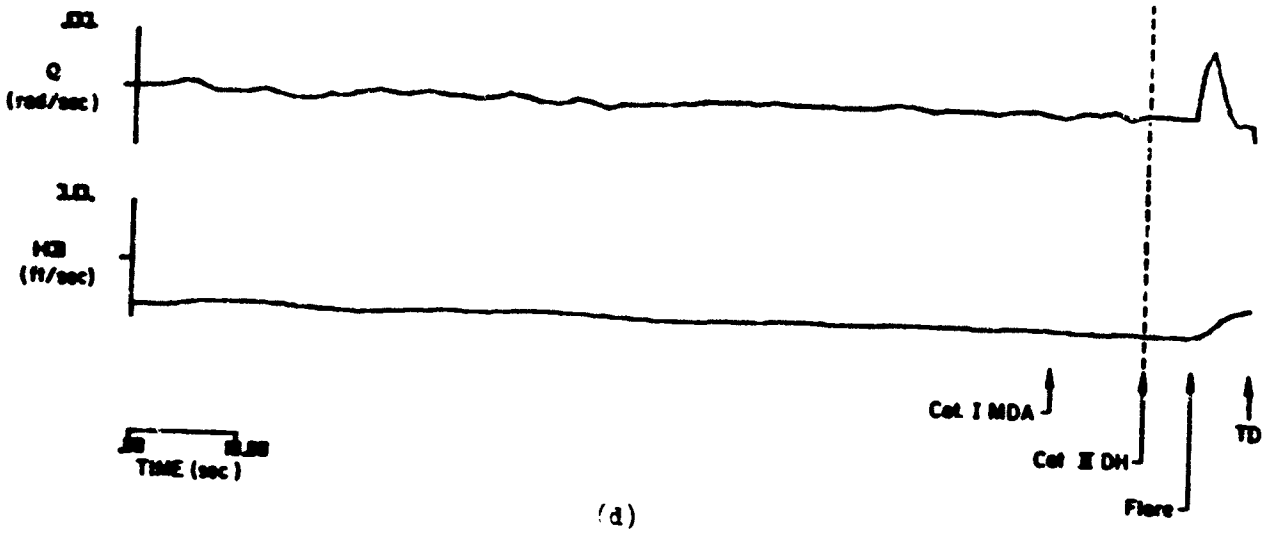

(d)

Figure B-29. (Concluded)

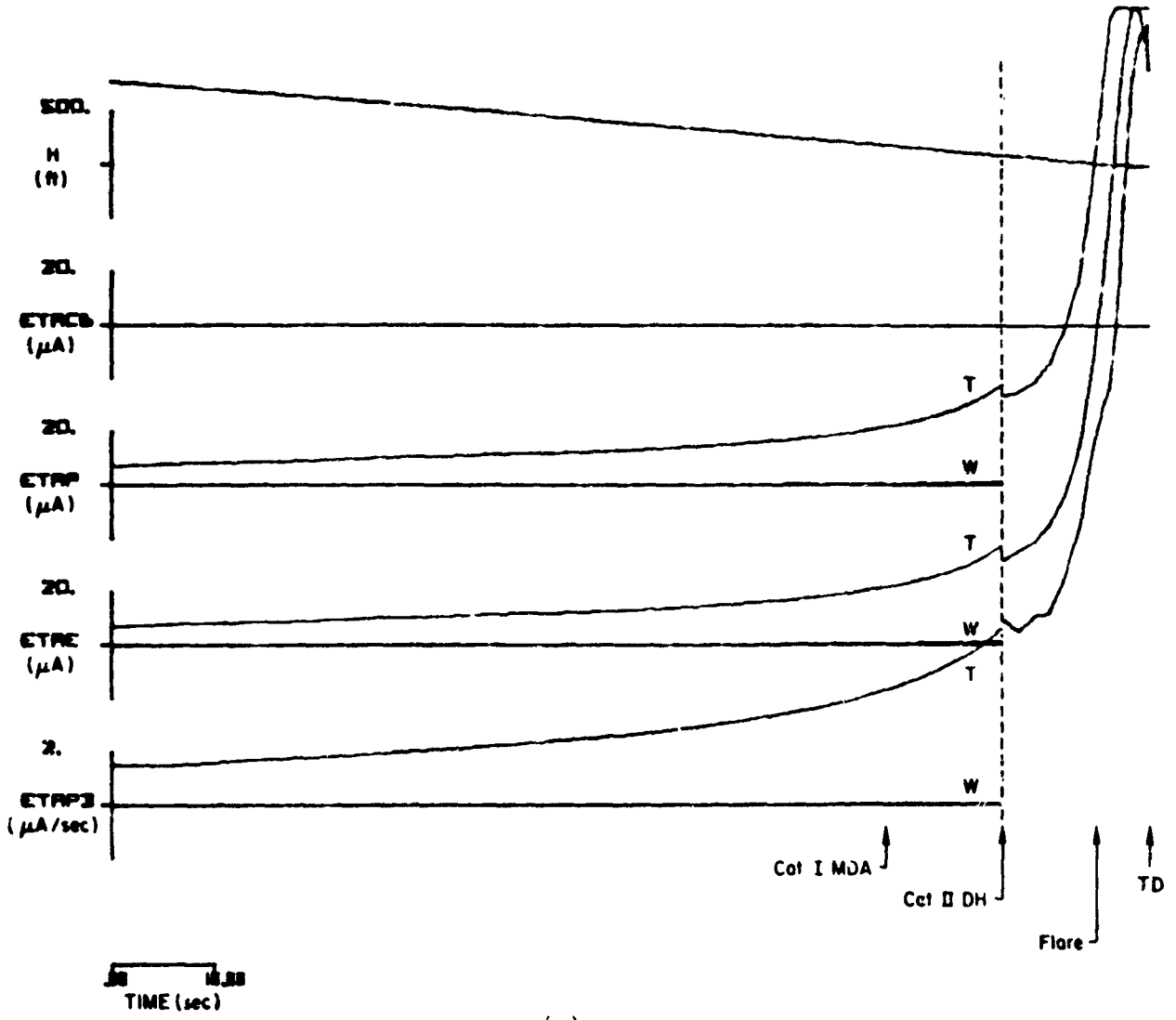

(a)

Figure 5-3). Standard Deviation Responses to Wind, Wind Shear, and Turbulence for the Piper PA-31 Aircraft with Inverted Flight Control System and Conventional Glide Slope Coupling to Glide Slope Flight Inspection Record No. 1 Category II Configuration Simulated

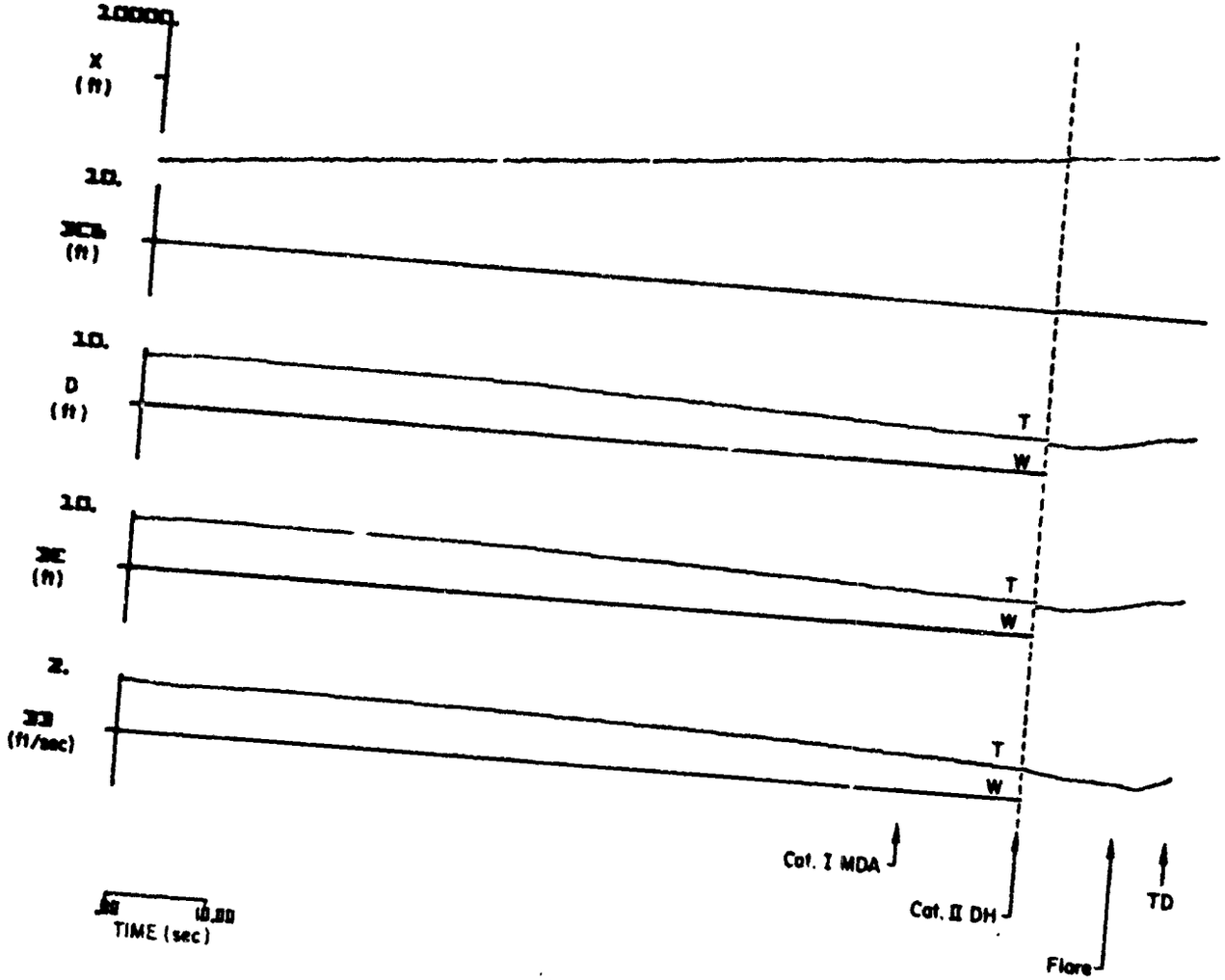

Figure B-30. (Continued)

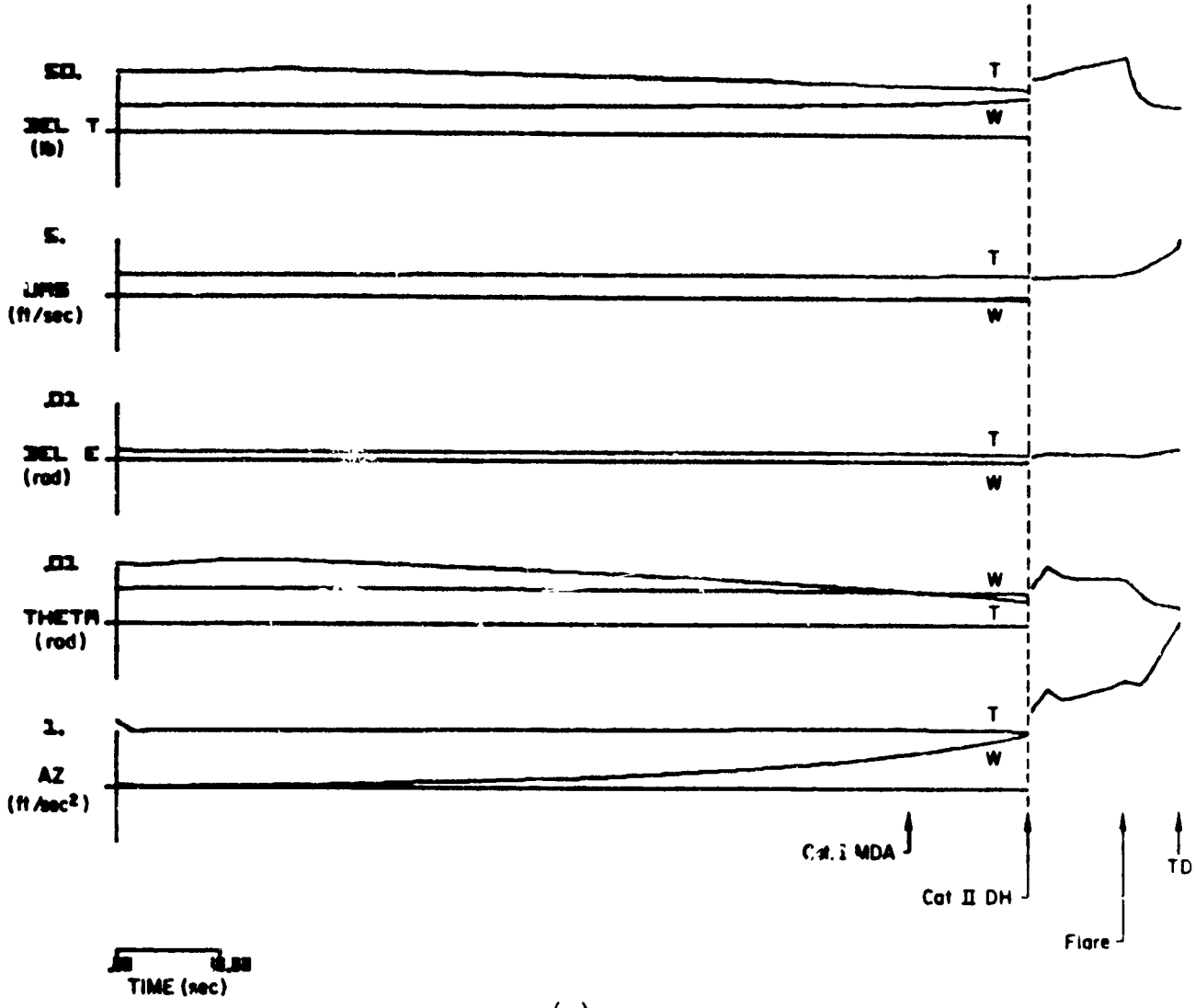

(c)

Figure B-30. (Continued)

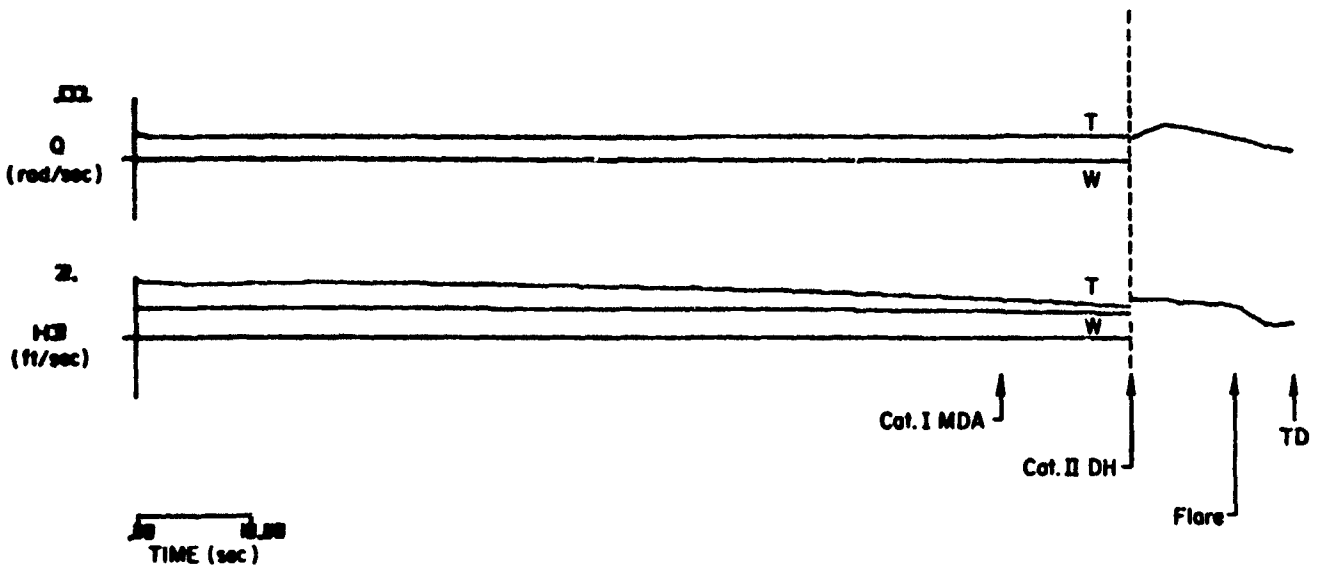

(d)

Figure B-30. (Concluded)

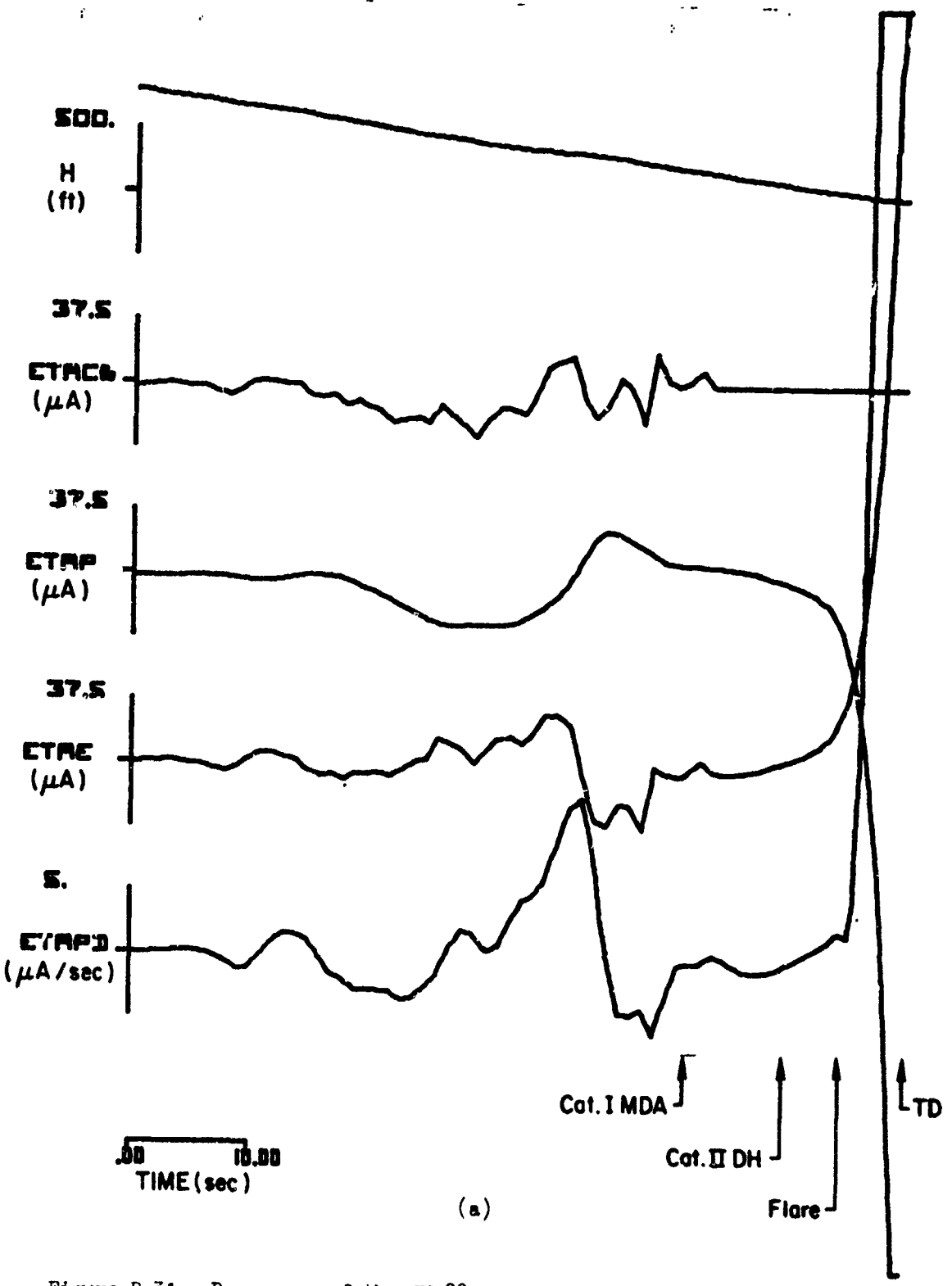

Figure B-31. Responses of the CV-880 Aircraft with LSI Automatic Landing System and Conventional Glide Slope Coupling to Glide Slope Flight Inspection Record No. 10. Category I Utilization Simulated

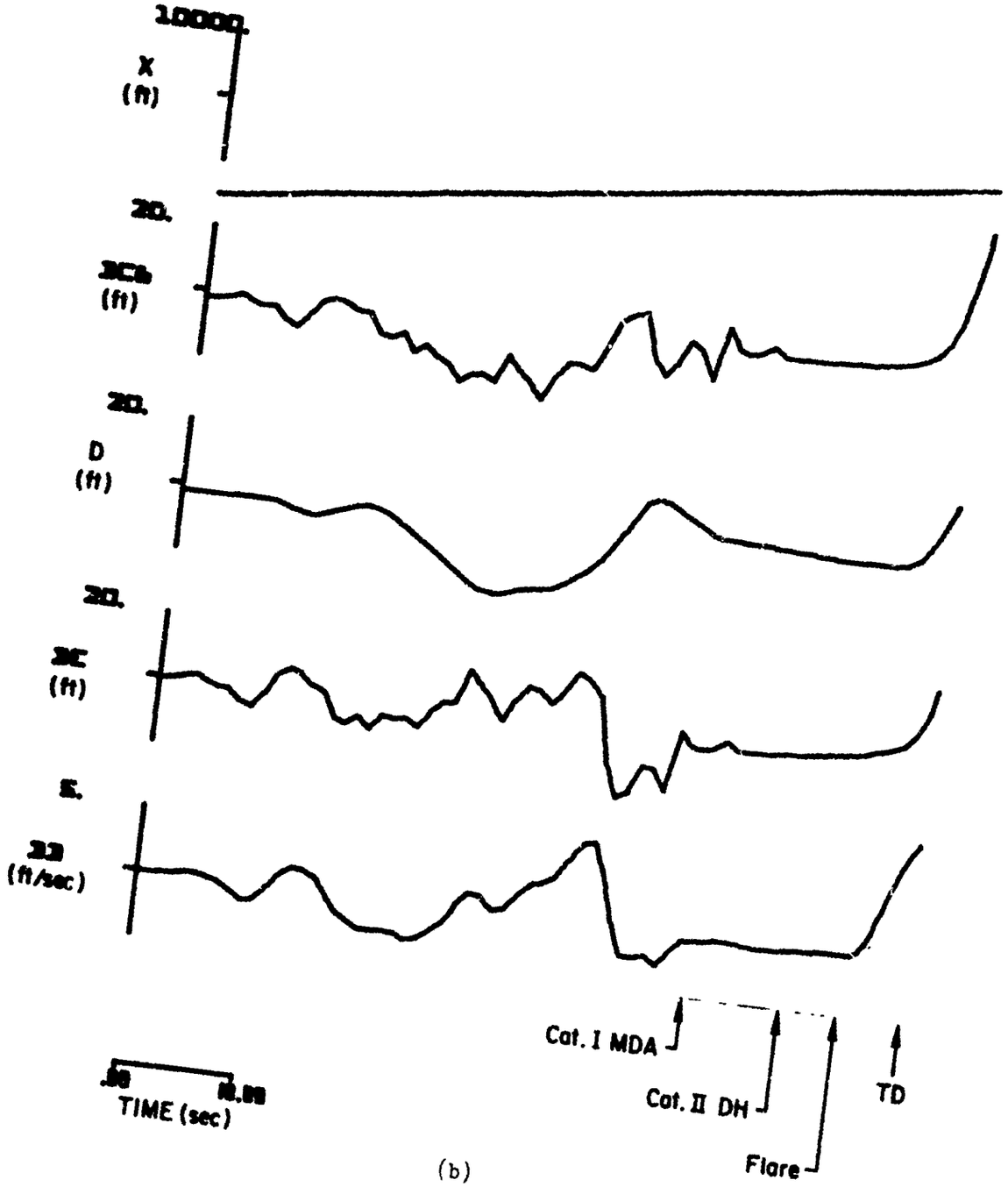

(b)

Figure B-31. (Continued)

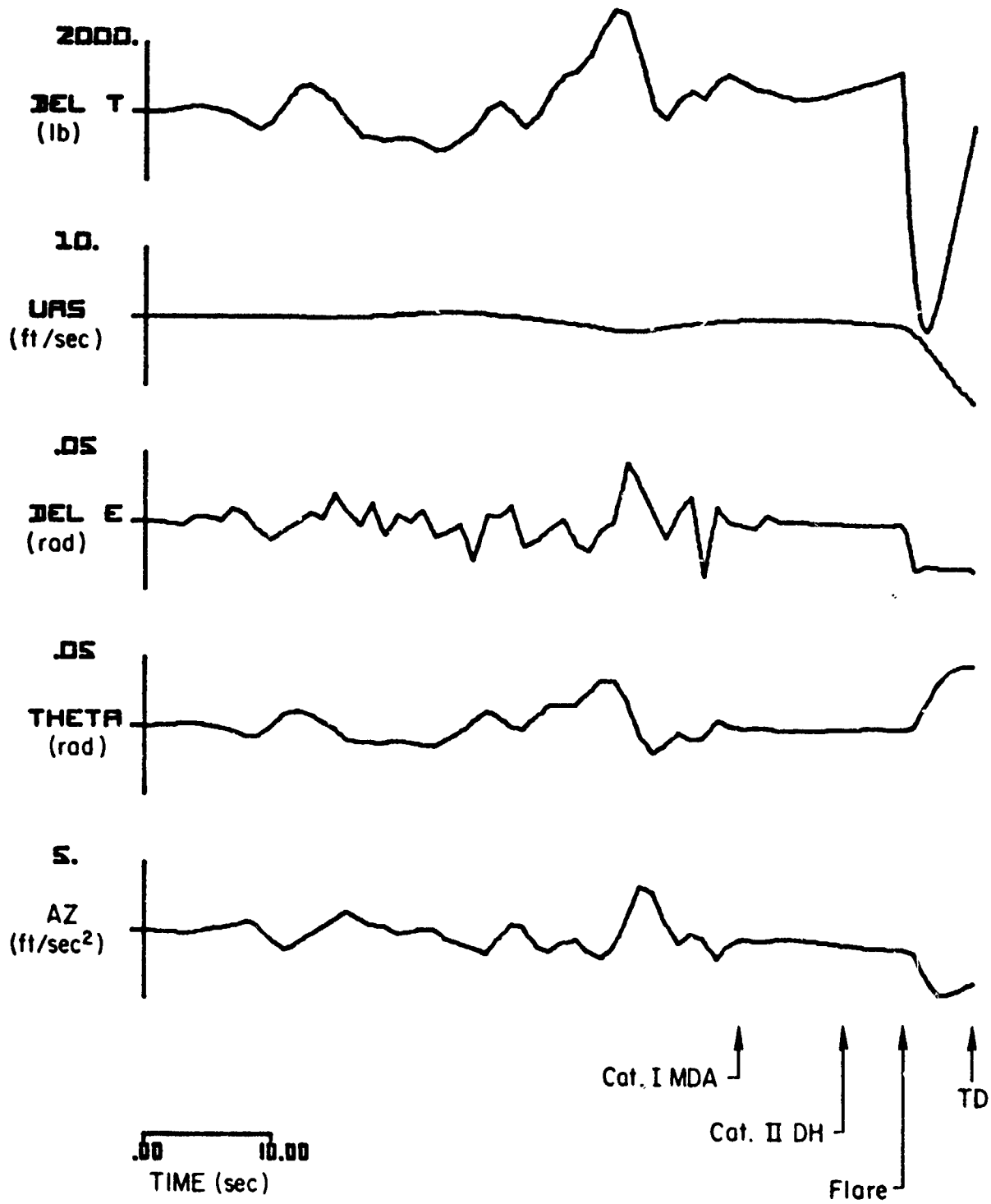

(c)

Figure B-31. (Continued)

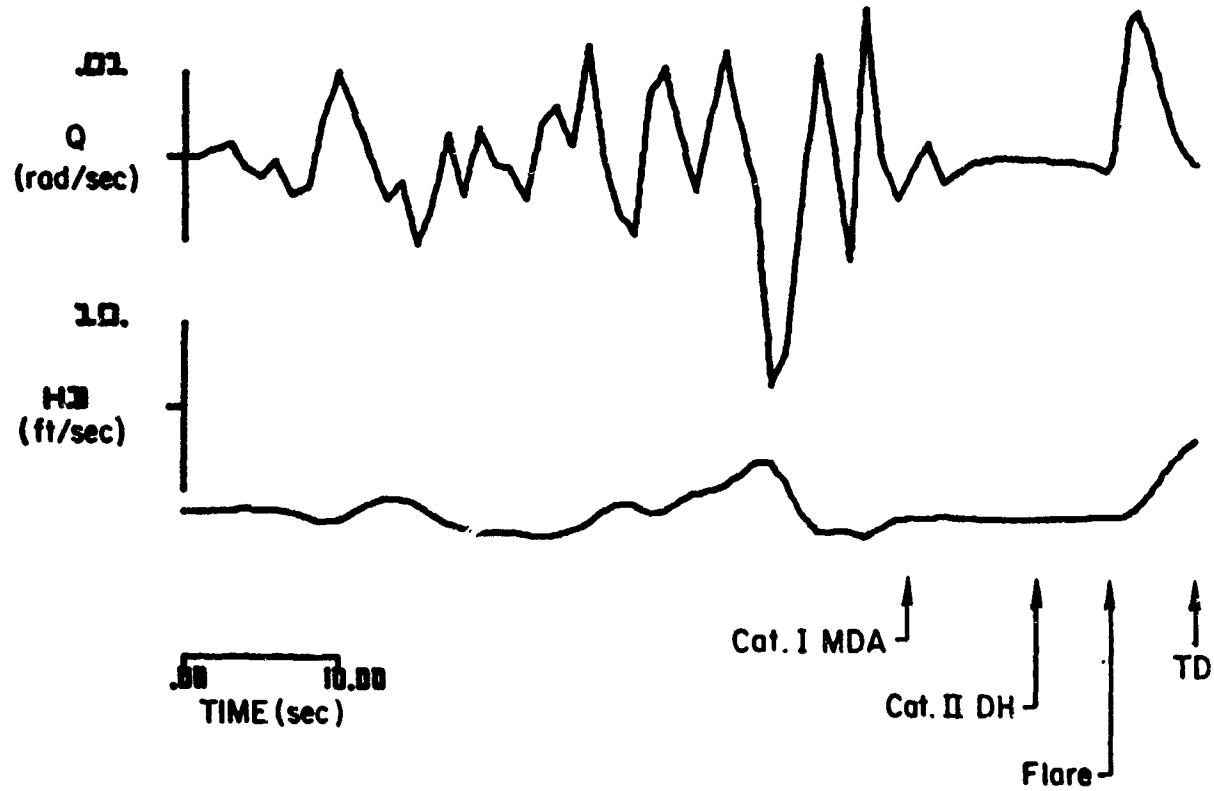

(d)

Figure B-31. (Concluded)

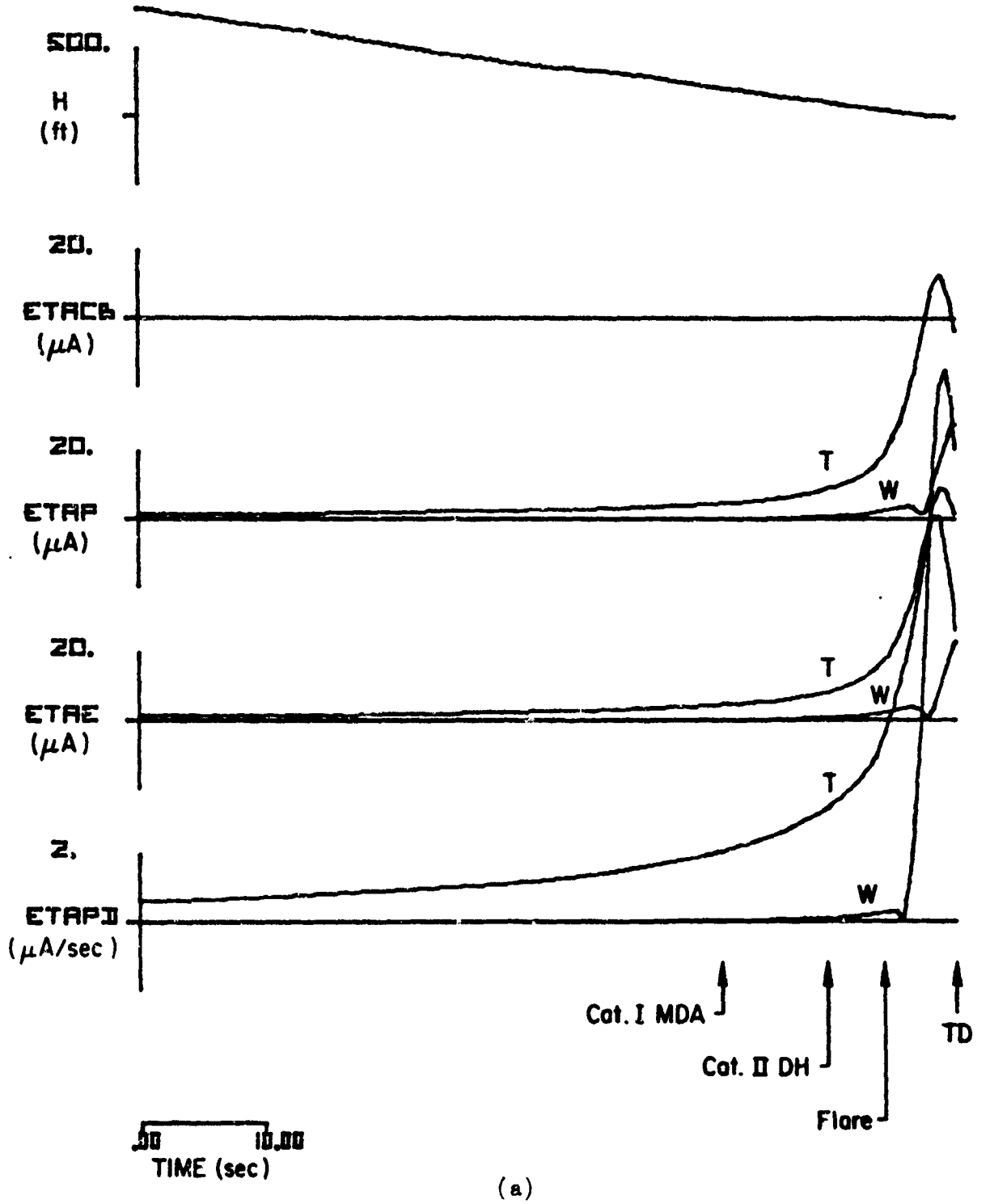

(a)

Figure B-32. Standard Deviation Responses to Wind, Wind Shear, and Turbulence for the CV-880 Aircraft with LSI Automatic Landing System and Conventional Glide Slope Coupling to Glide Slope Flight Inspection Record No. 10. Category I Utilization Simulated

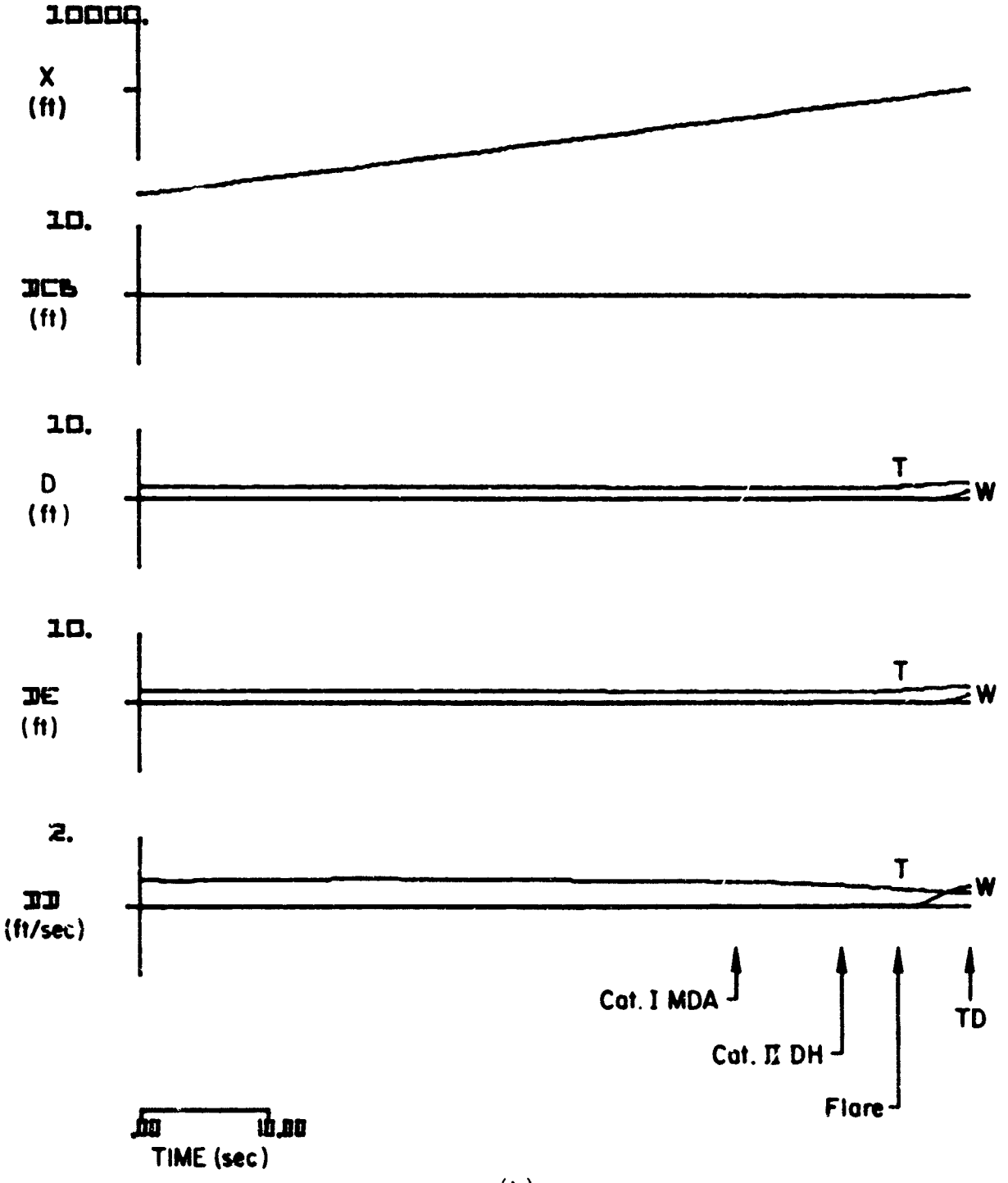

(b)

Figure B-32. (Continued)

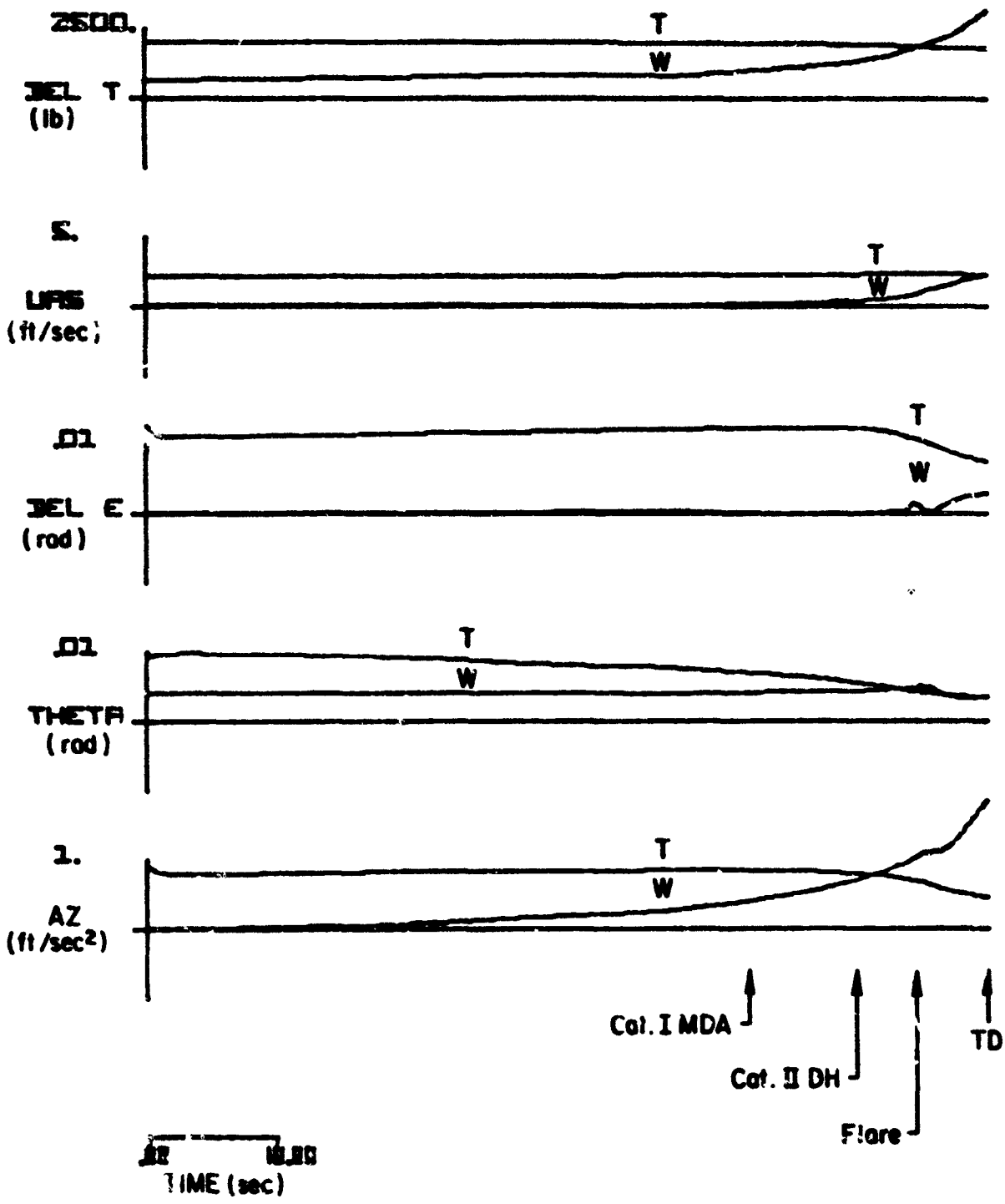

(c)

Figure A-32. (Continued)

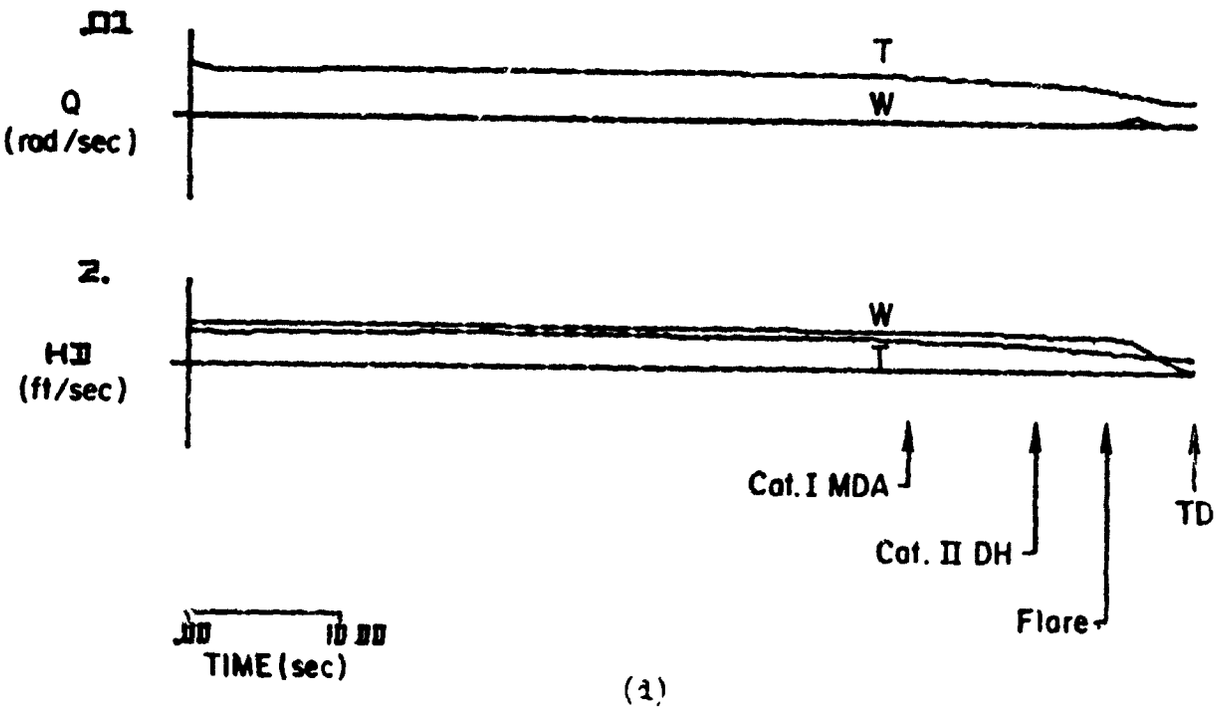

(i)

Figure B-32. (Concluded)

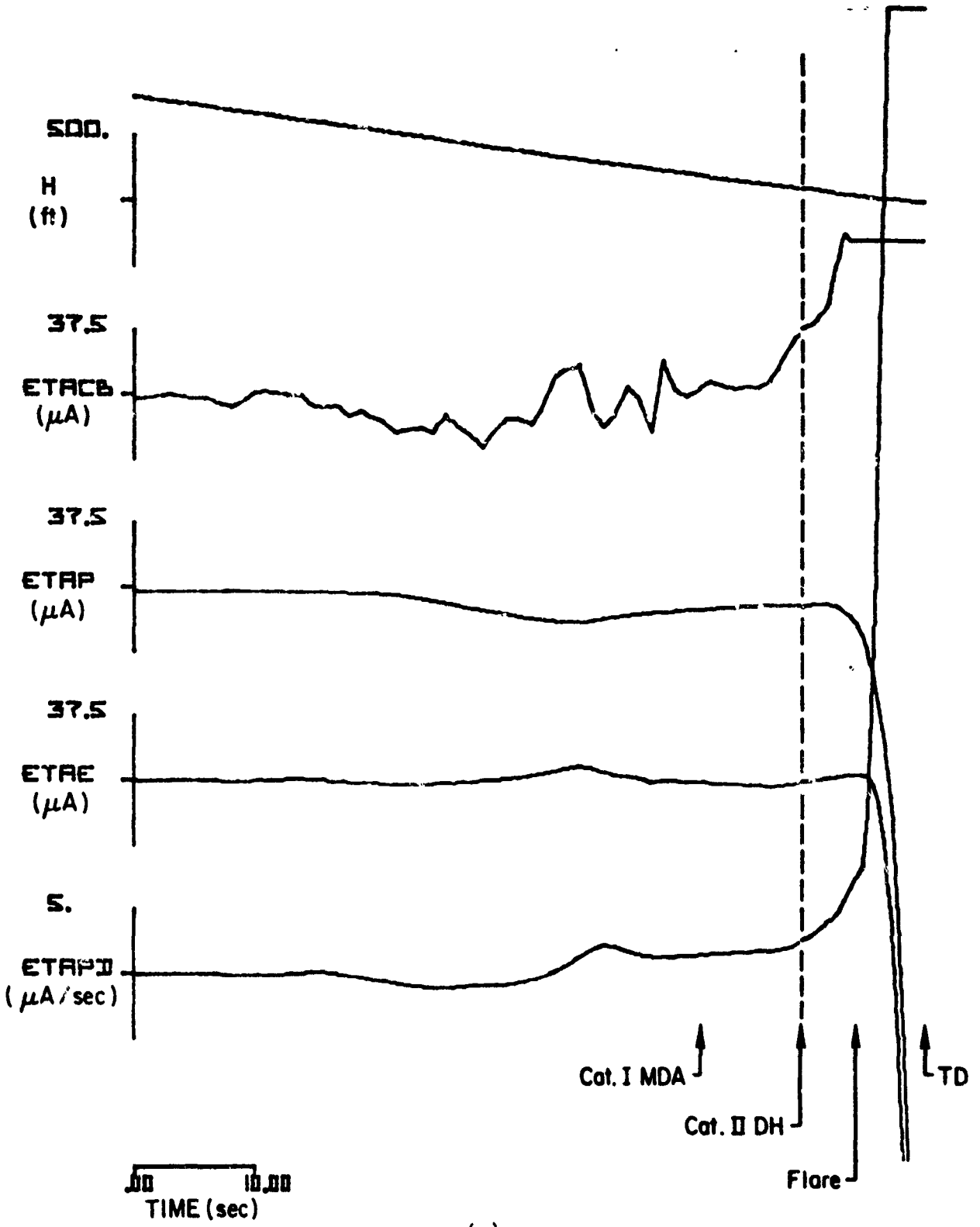

(a)

Figure B-33. Responses of the CV-880 Aircraft with LSI Automatic Landing System and Inertially Augmented Glide Slope Coupling to Glide Slope Flight Inspection Record No. 10. Category II-III Utilization Simulated

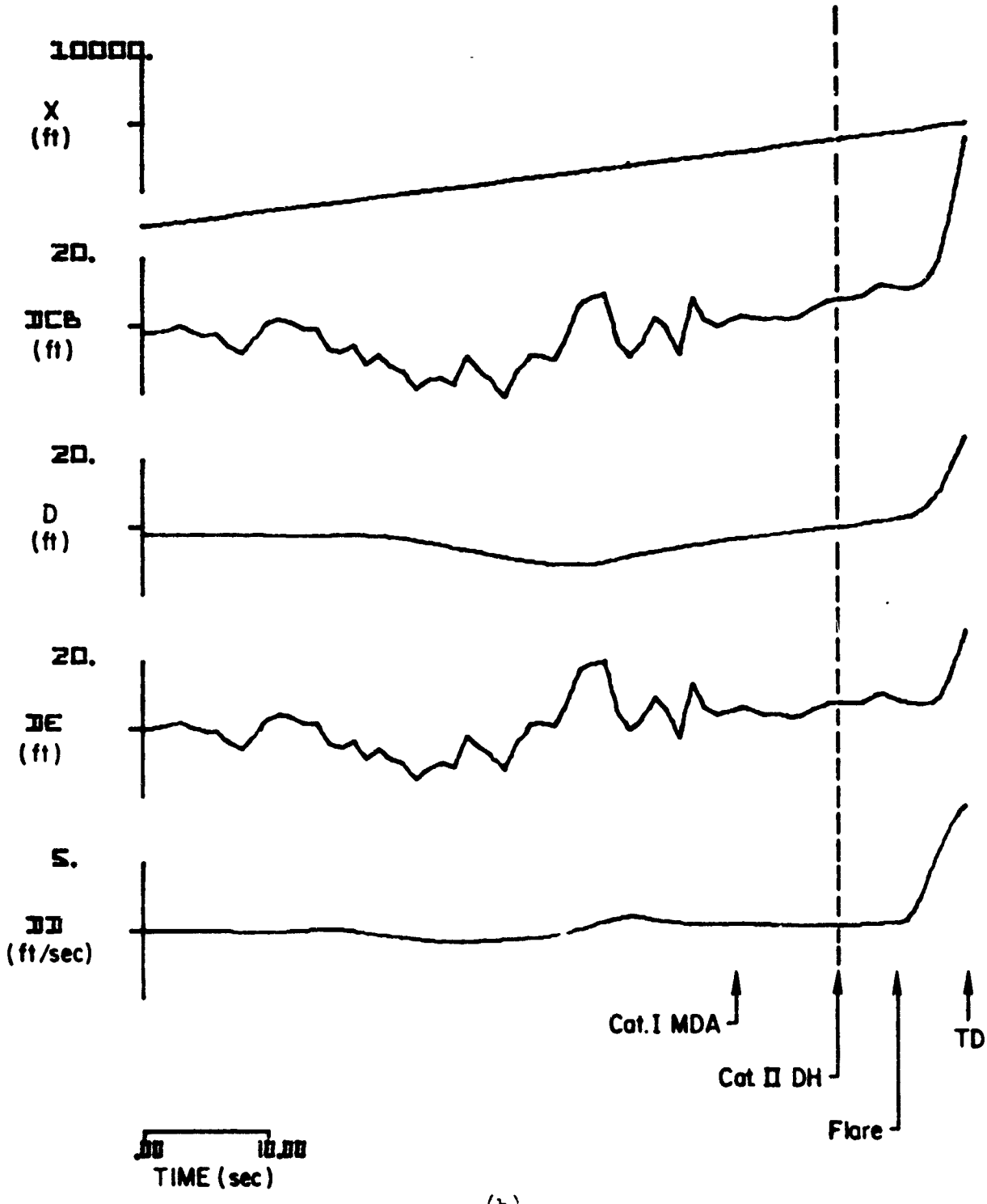

(b)

Figure B-33. (Continued)

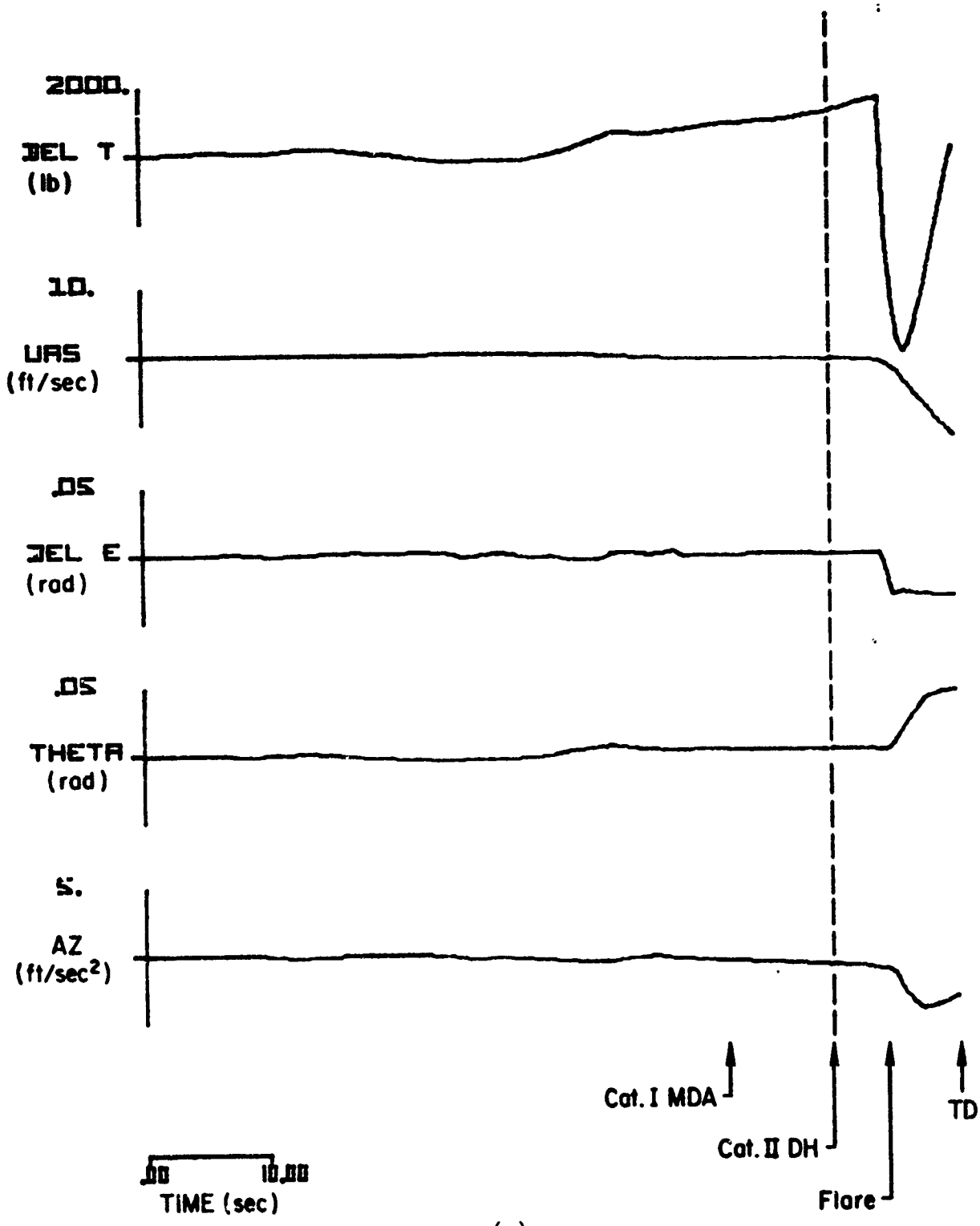

(c)

Figure B-33. (Continued)

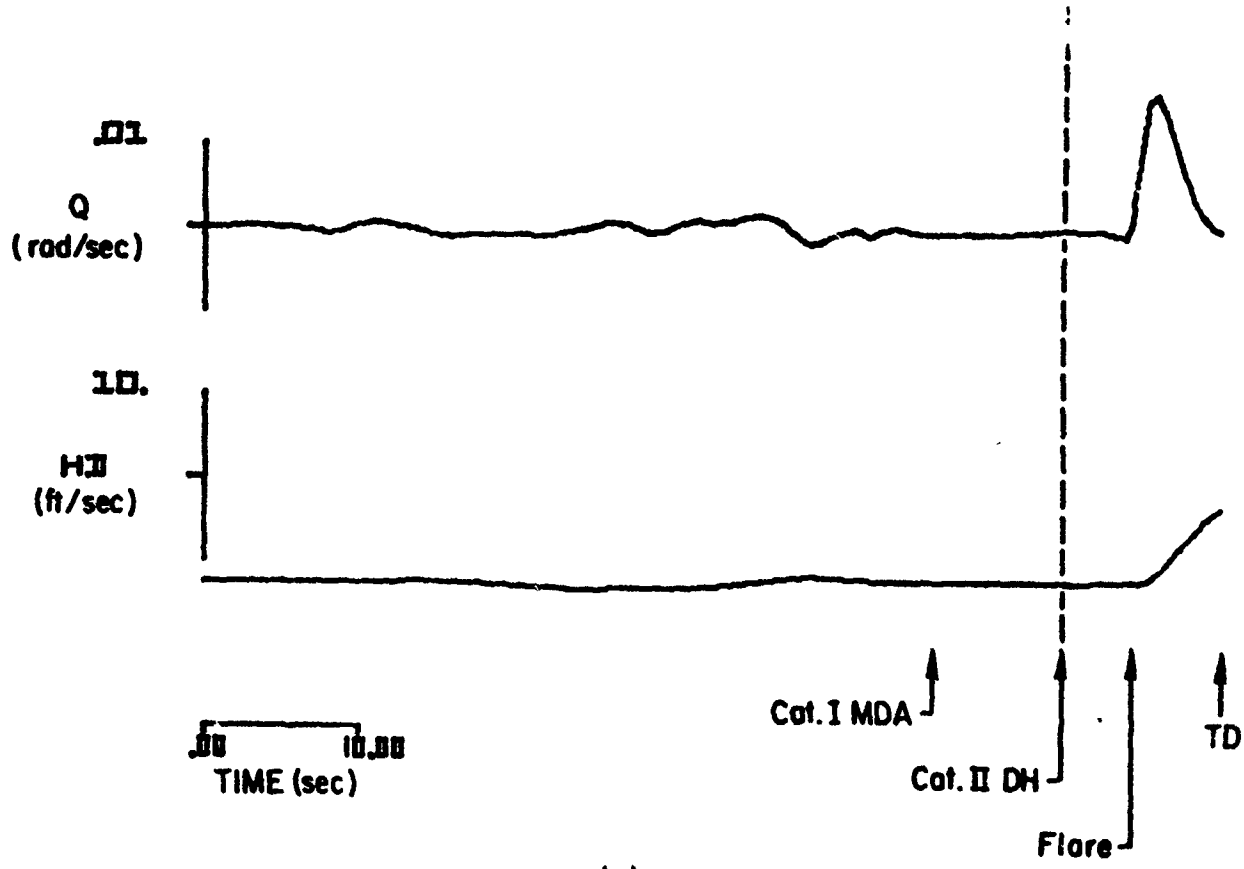

(d)

Figure B-33. (Concluded)

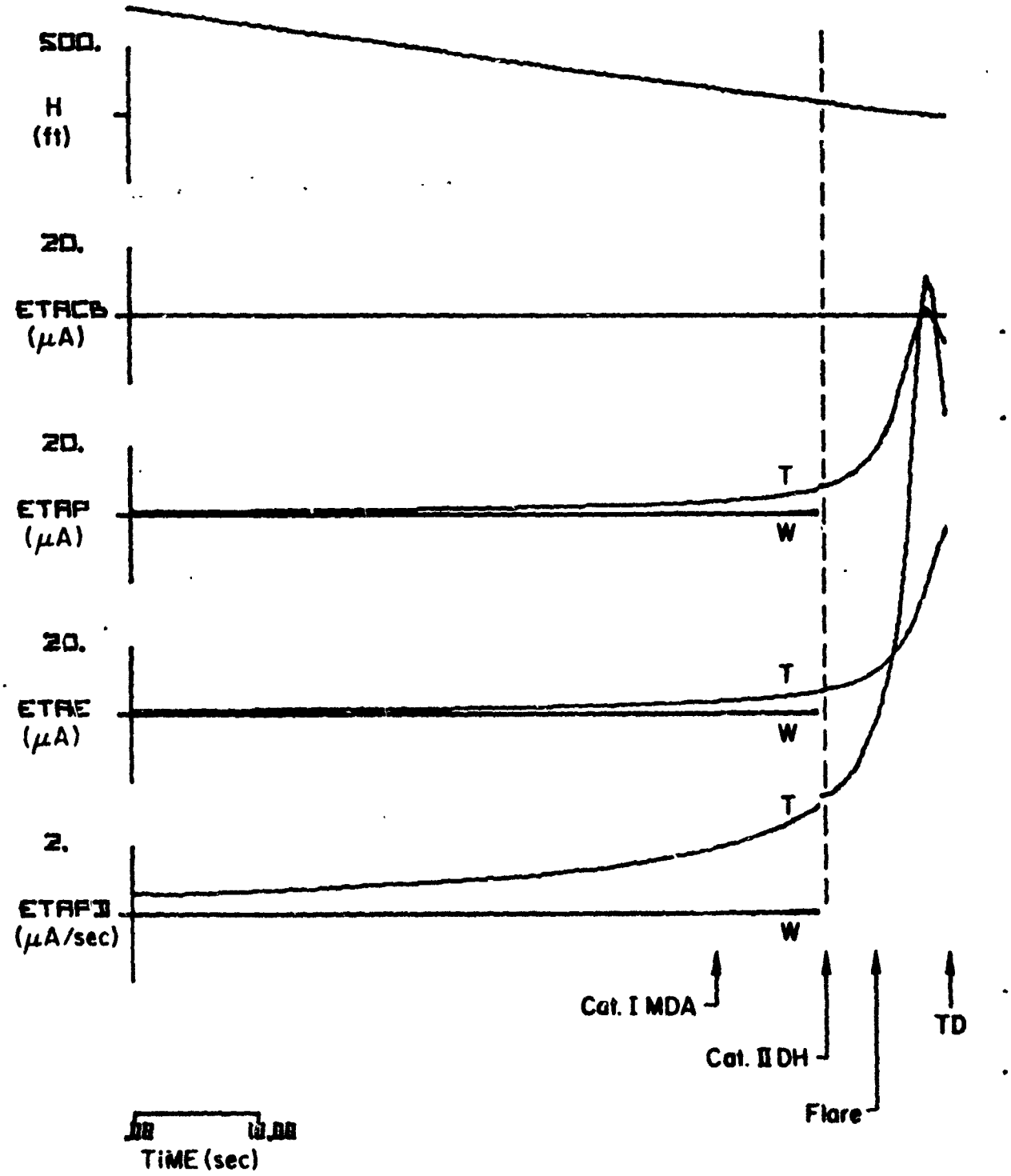

(a)

Figure B-34. Standard Deviation Responses to Wind, Wind Shear, and Turbulence for the CV-880 Aircraft with LSI Automatic Landing System and Inertially Augmented Glide Slope Coupling to Glide Slope Flight Inspection Record No. 10. Category II-III Utilization Simulated

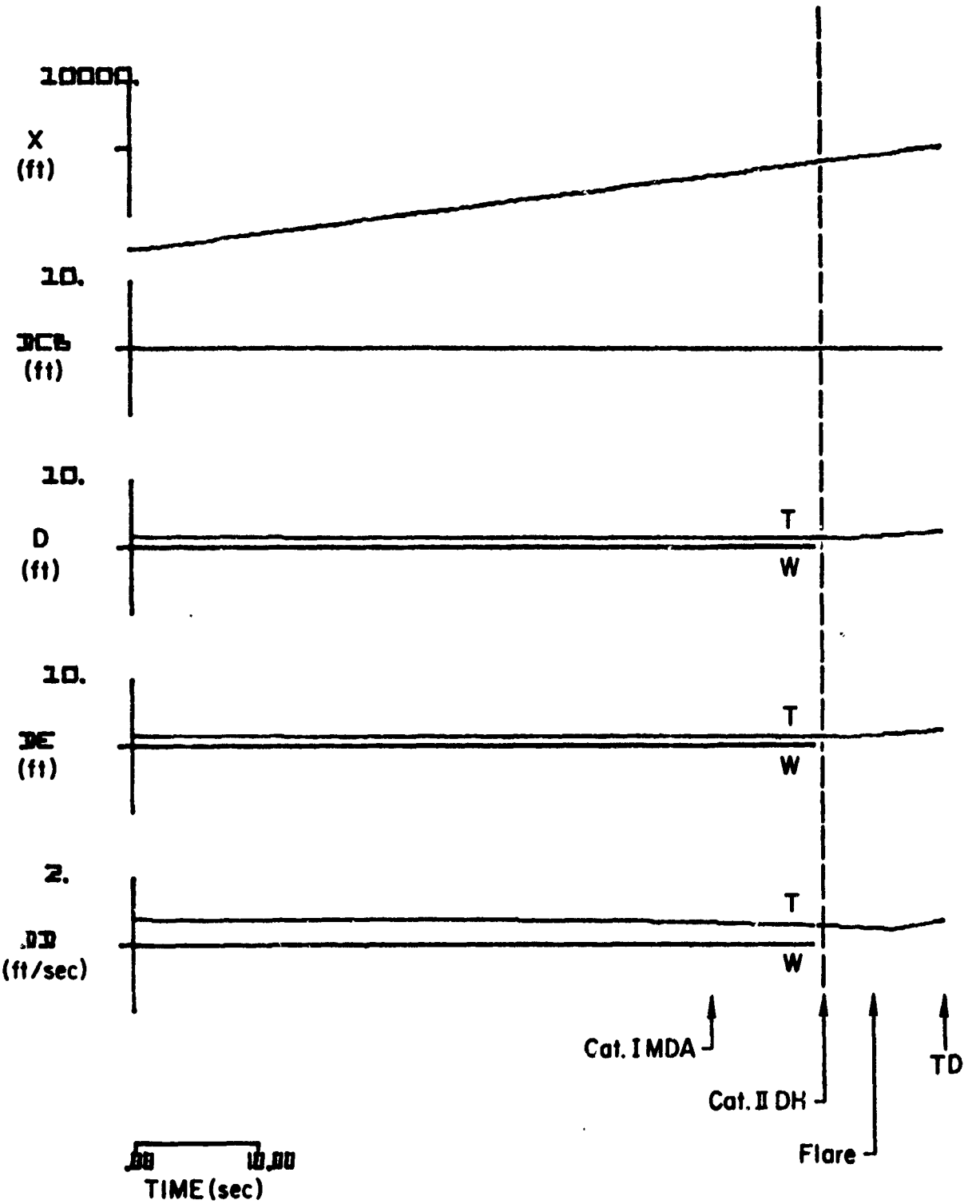

(b)

Figure B-34. (Continued)

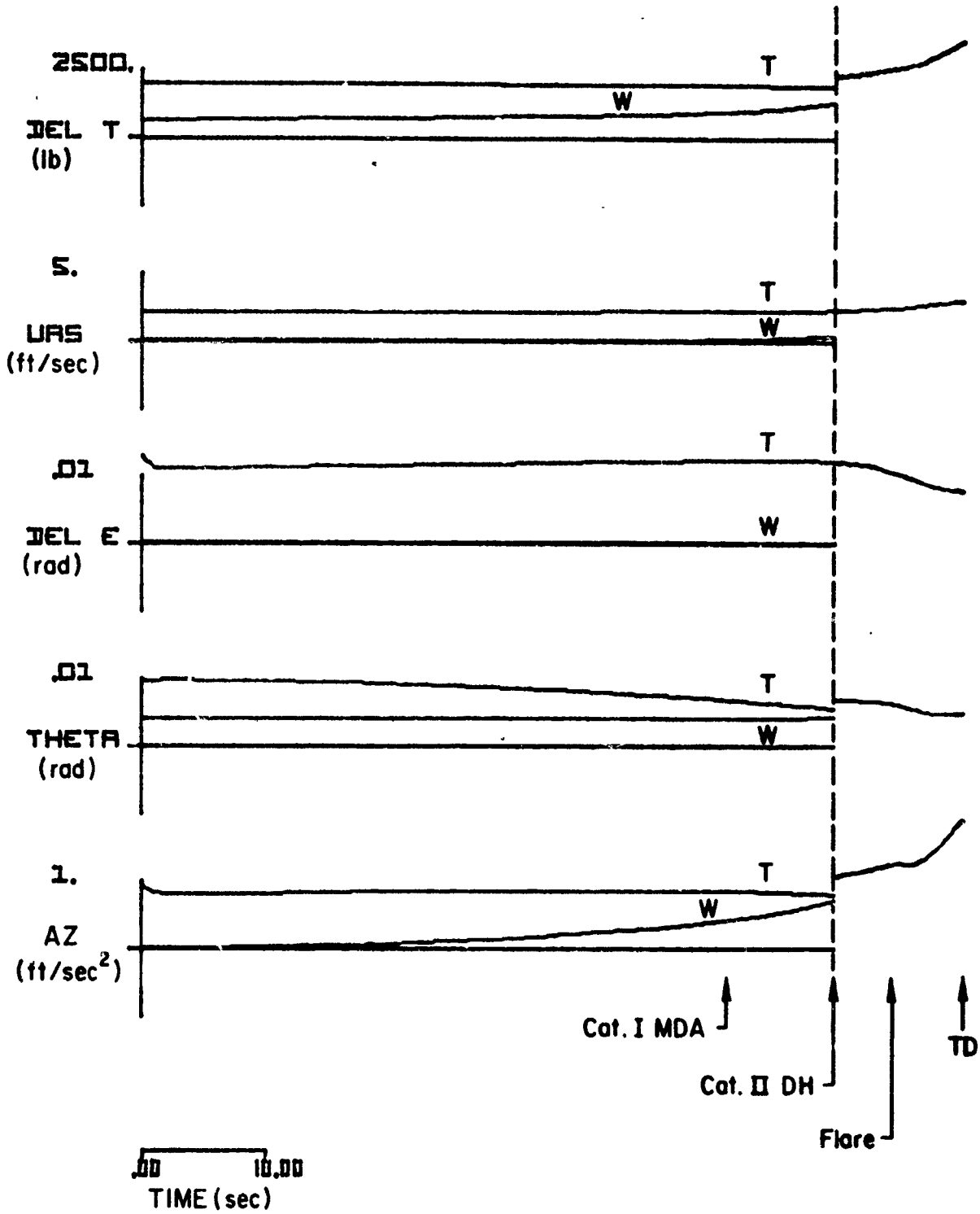

(c)

Figure B-34. (Continued)

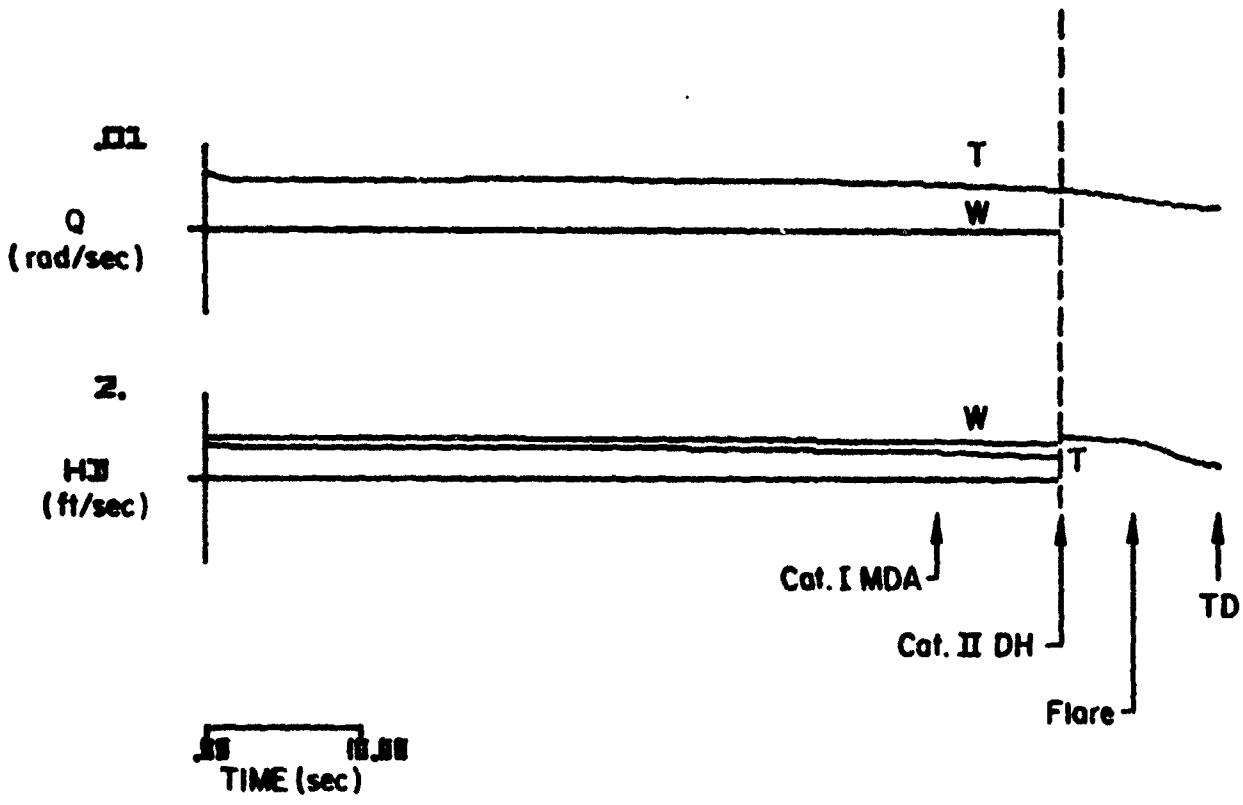

(d)

Figure B-34. (Concluded)

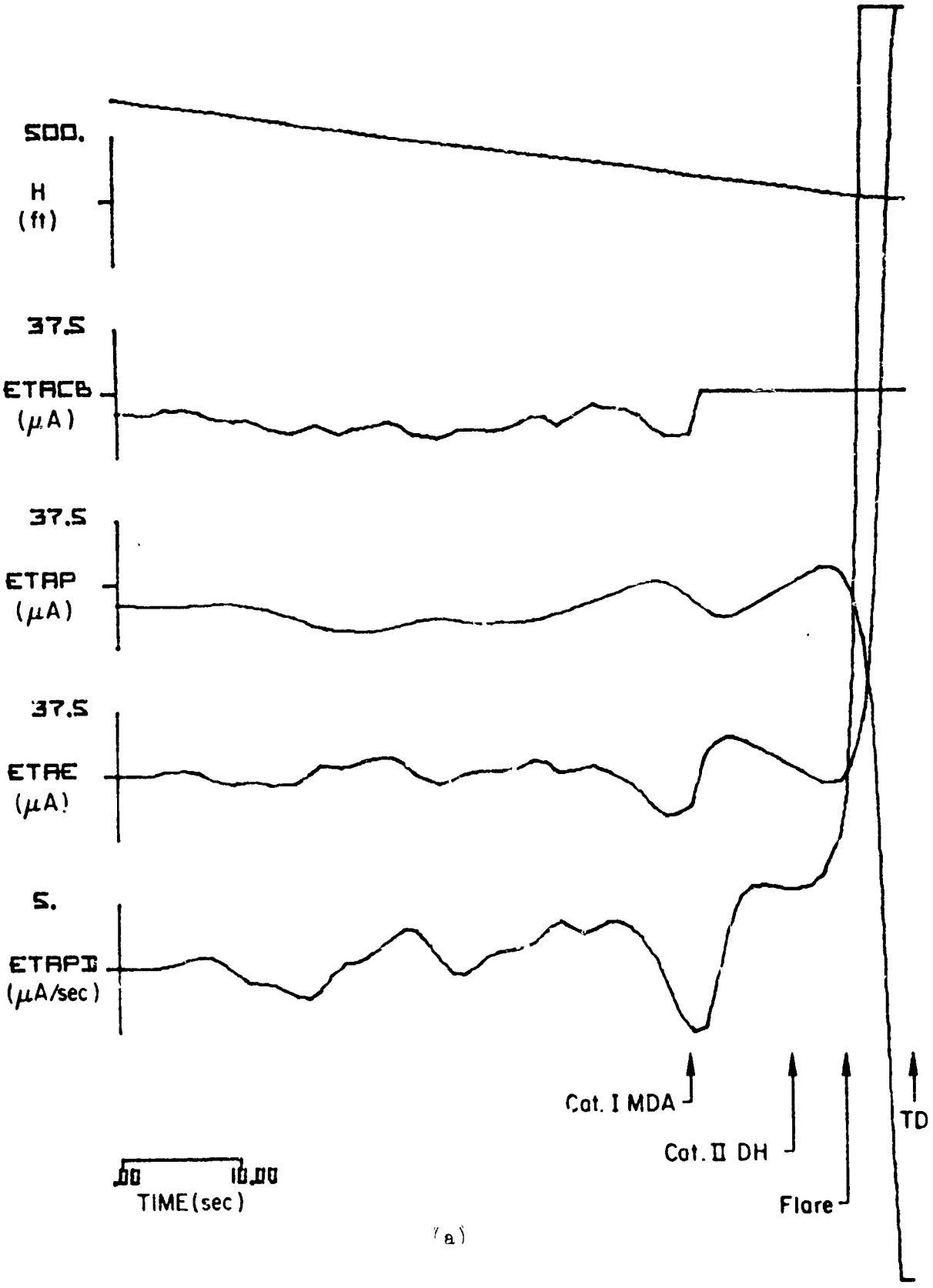

(a)

Figure B-35. Responses of the CV-880 Aircraft with LSI Automatic Landing System and Conventional Glide Slope Coupling to Glide Slope Flight Inspection Record No. 15. Category I Utilization Simulated

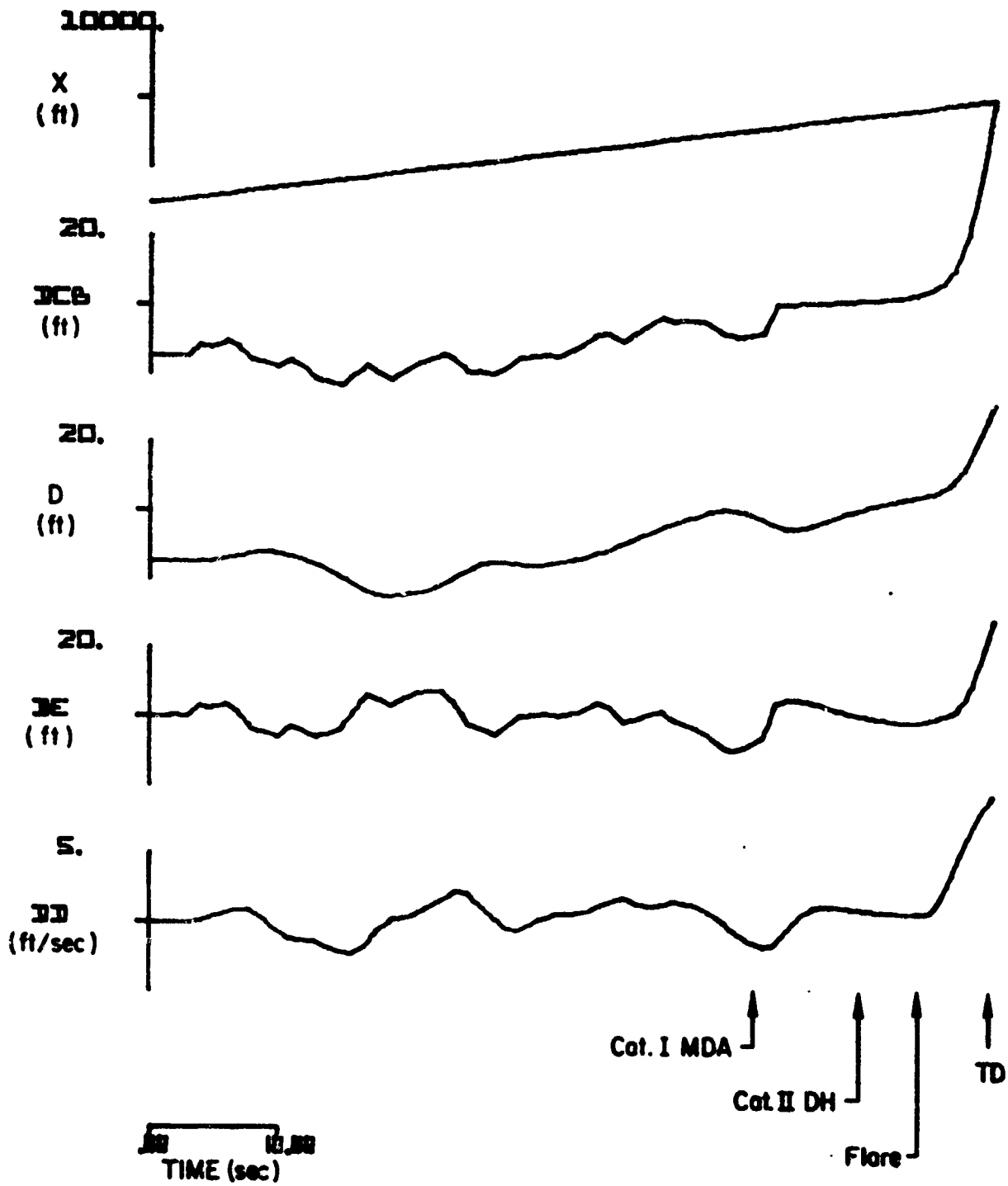

(b)

Figure B-35. (Continued)

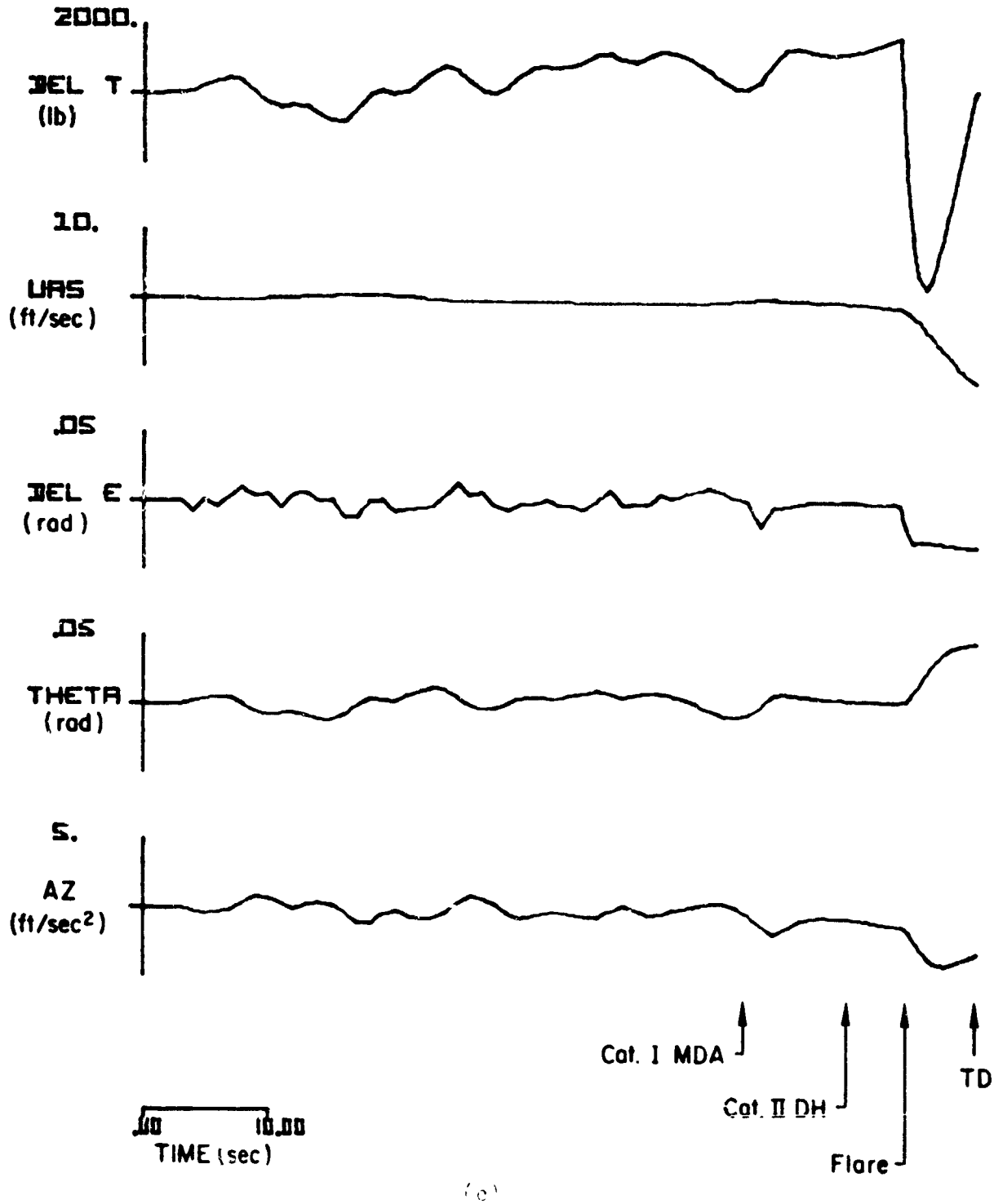

(c)

Figure B-3. (Continued)

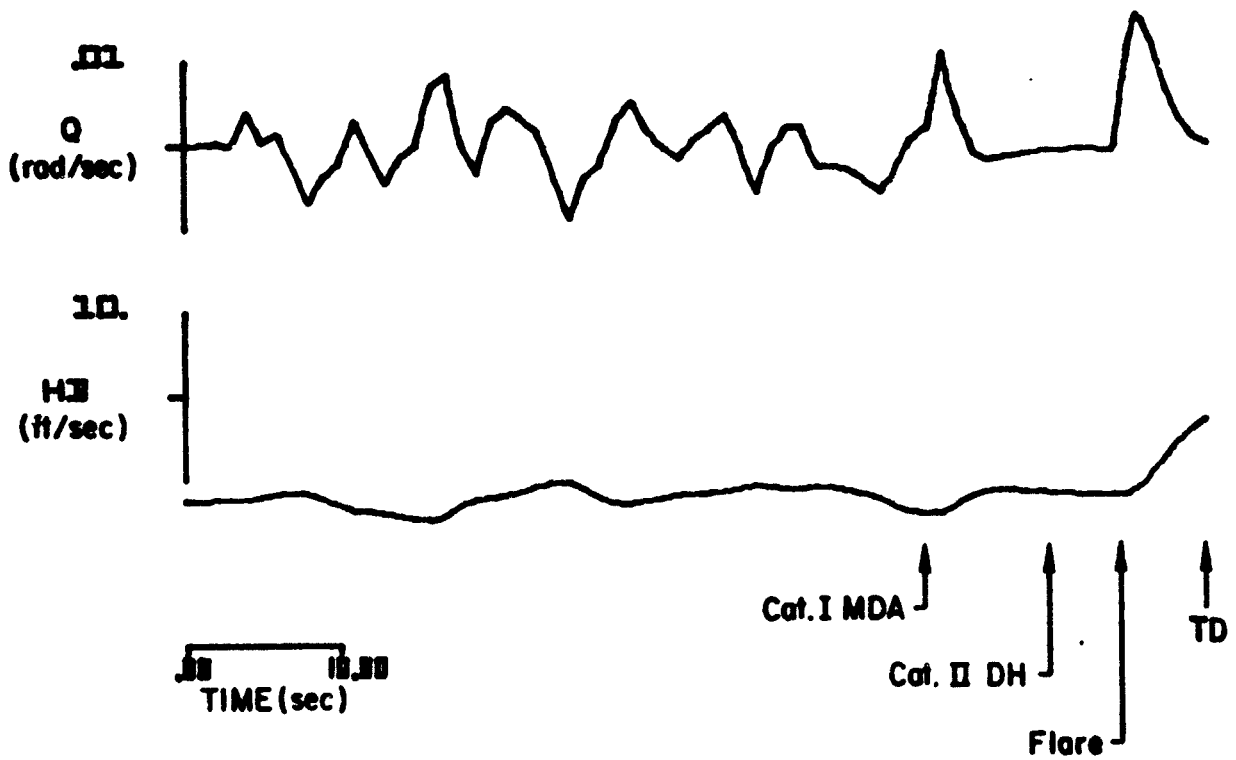

(d)

Figure B-35. (Concluded)

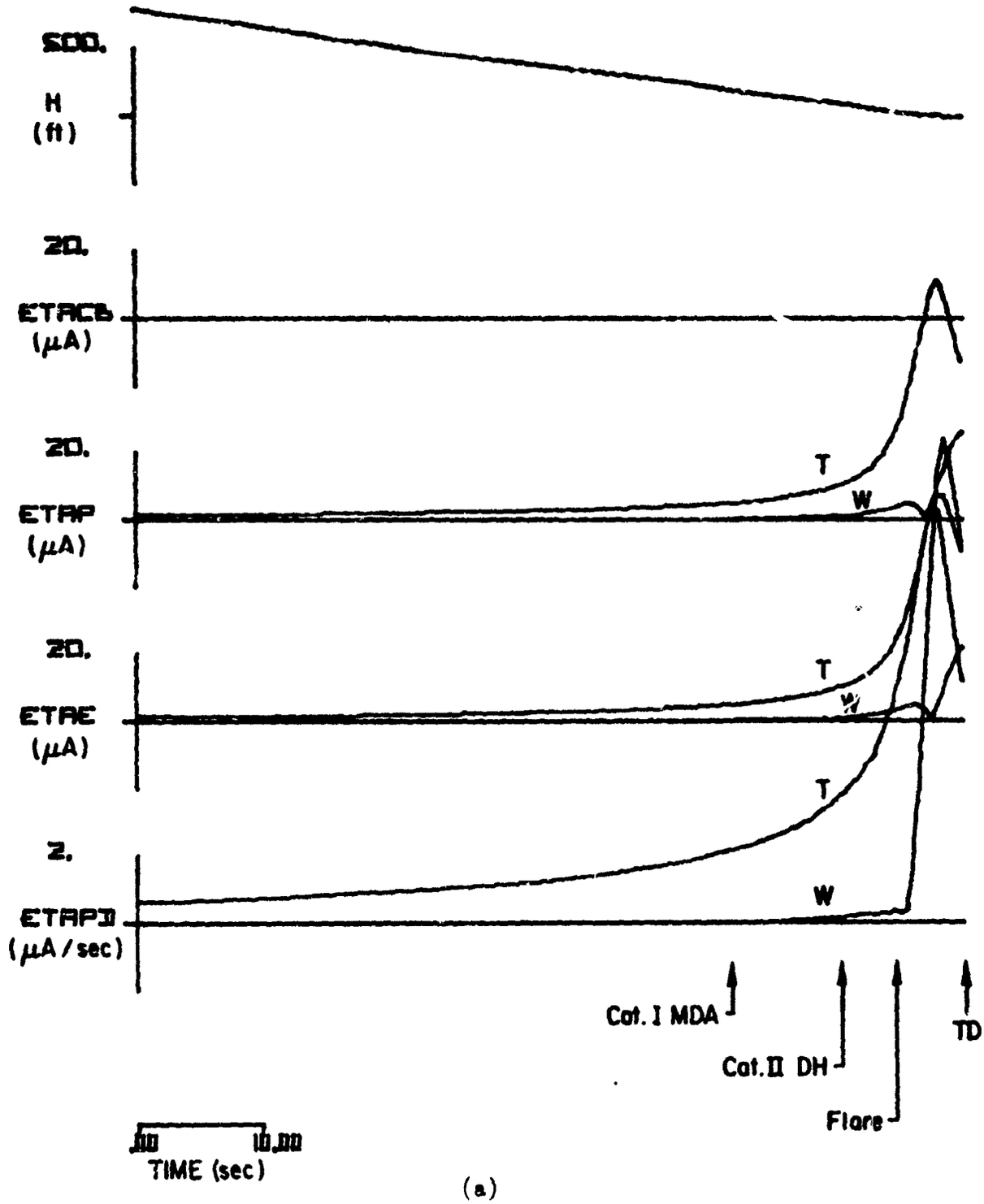

(a)

Figure B-36. Standard Deviation Responses to Wind, Wind Shear, and Turbulence for the CV-880 Aircraft with LSI Automatic Landing System and Conventional Glide Slope Coupling to Glide Slope Flight Inspection Record No. 16. Category I Utilization Simulated

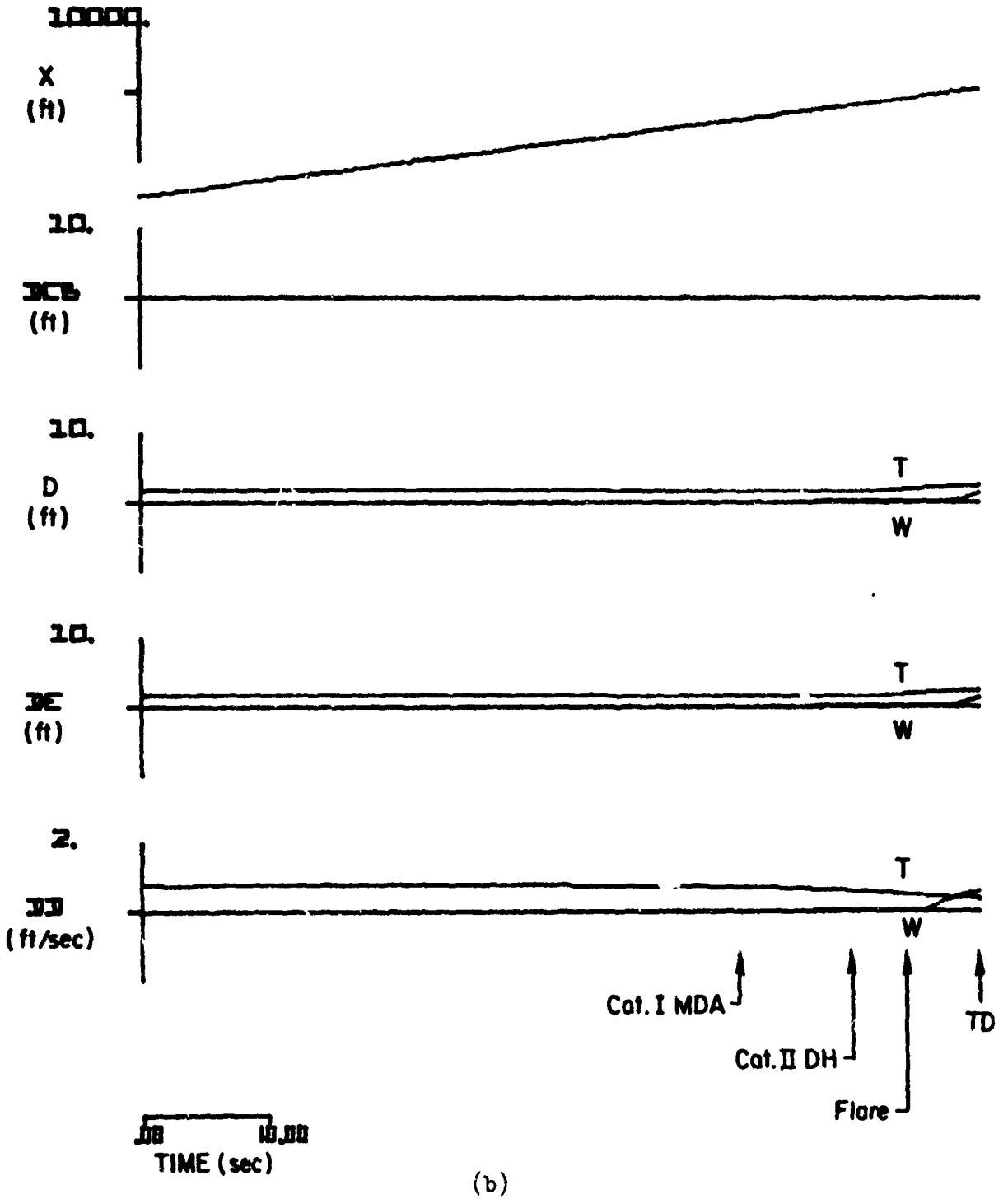

(b)

Figure B-36. (Continued)

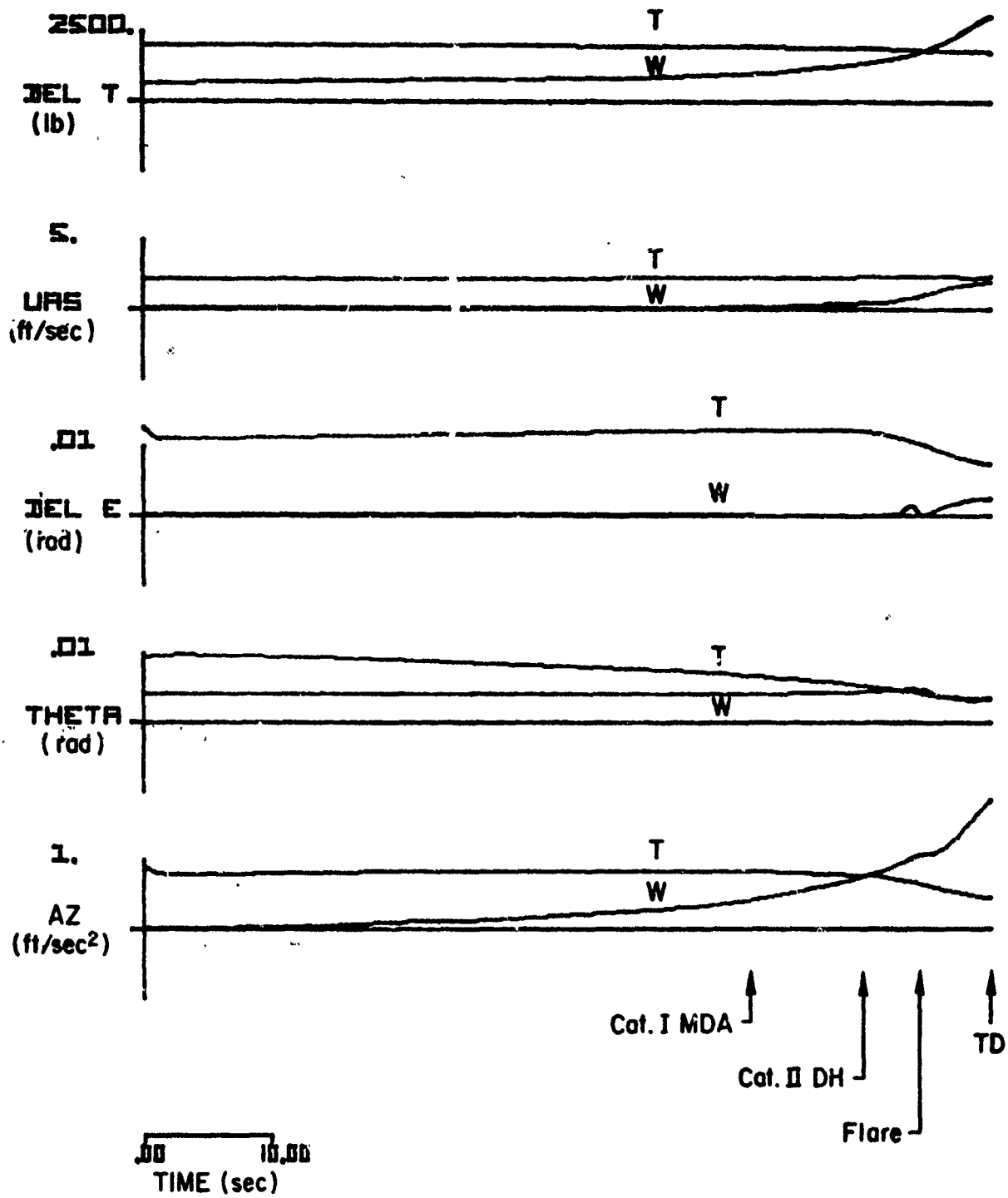

(c)

Figure B-36. (Continued)

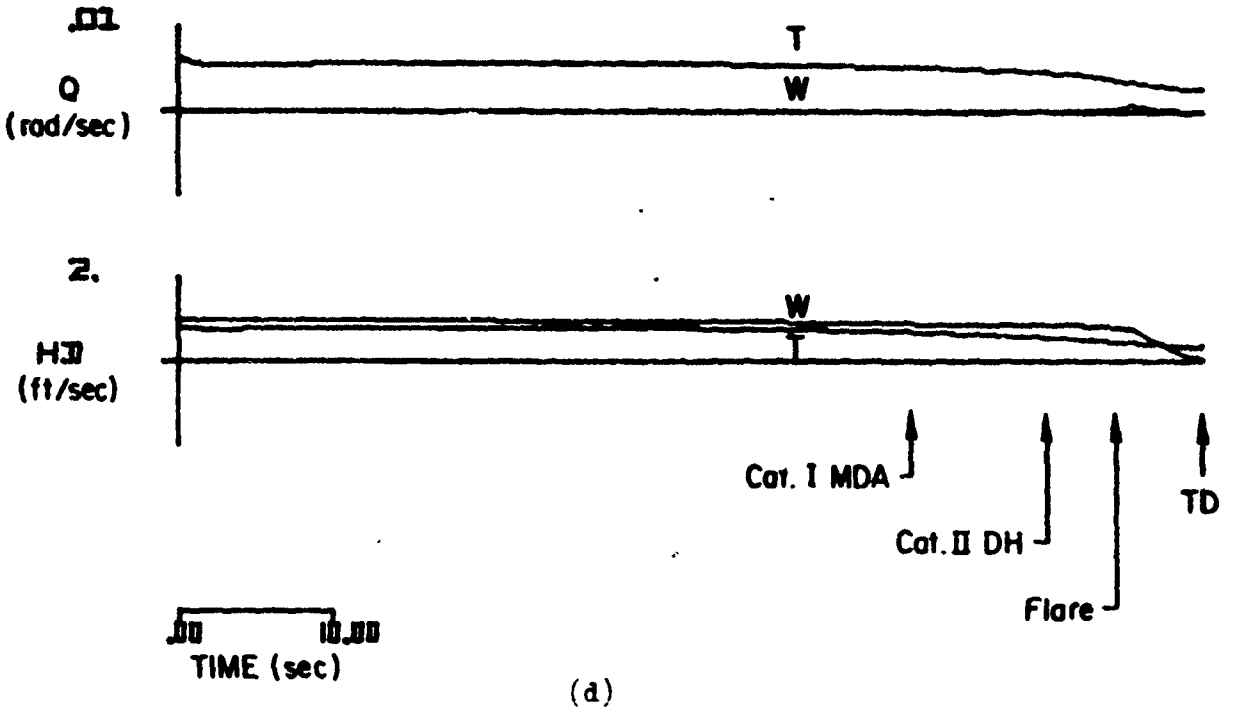

(d)

Figure B-36. (Concluded)

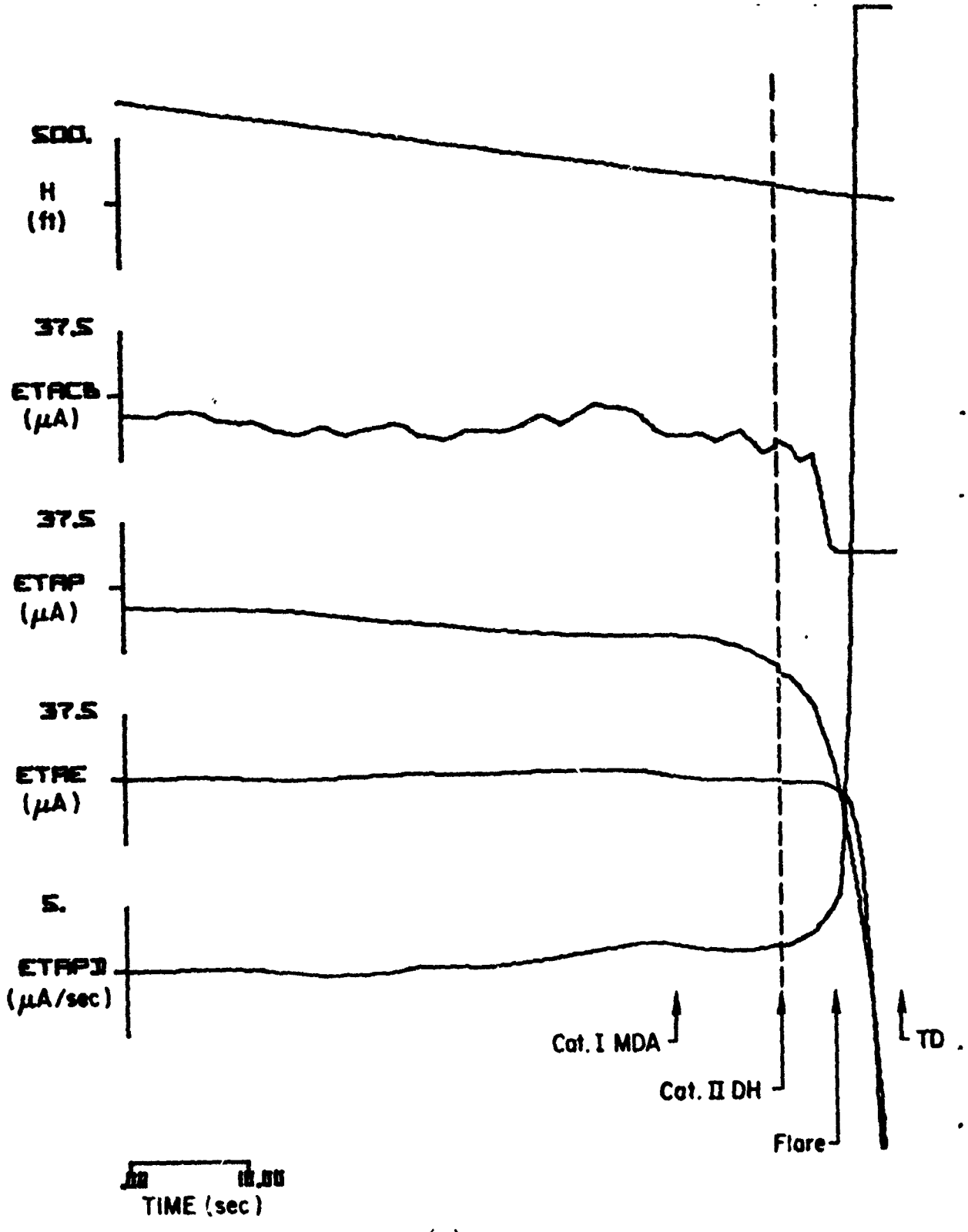

(a)

Figure B-37. Responses of the CV-880 Aircraft with LSI Automatic Landing System and Inertially Augmented Glide Slope Coupling to Glide Slope Flight Inspection Record No. 16. Category II-III Utilization Simulated

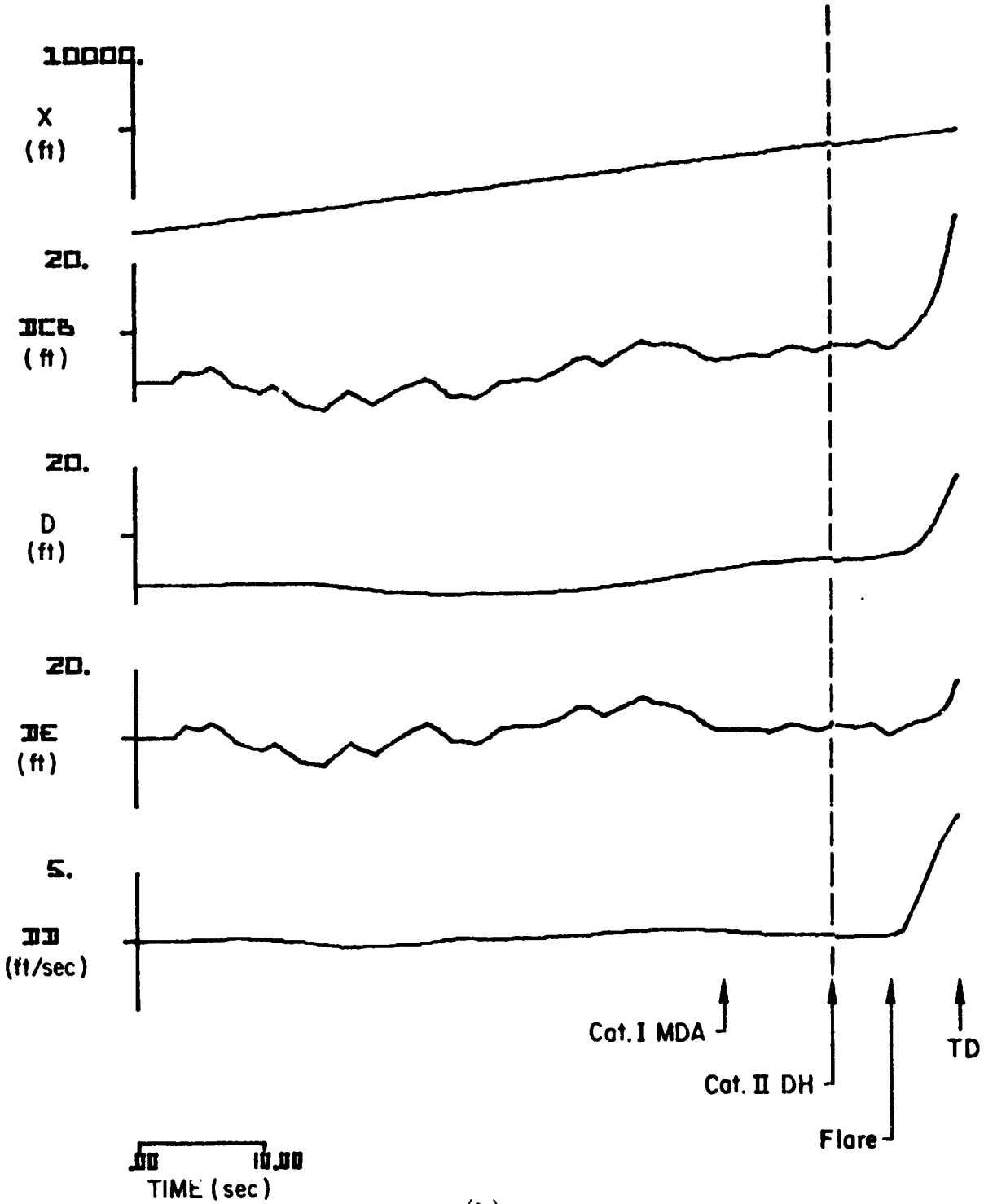

(b)

Figure B-37. (Continued)

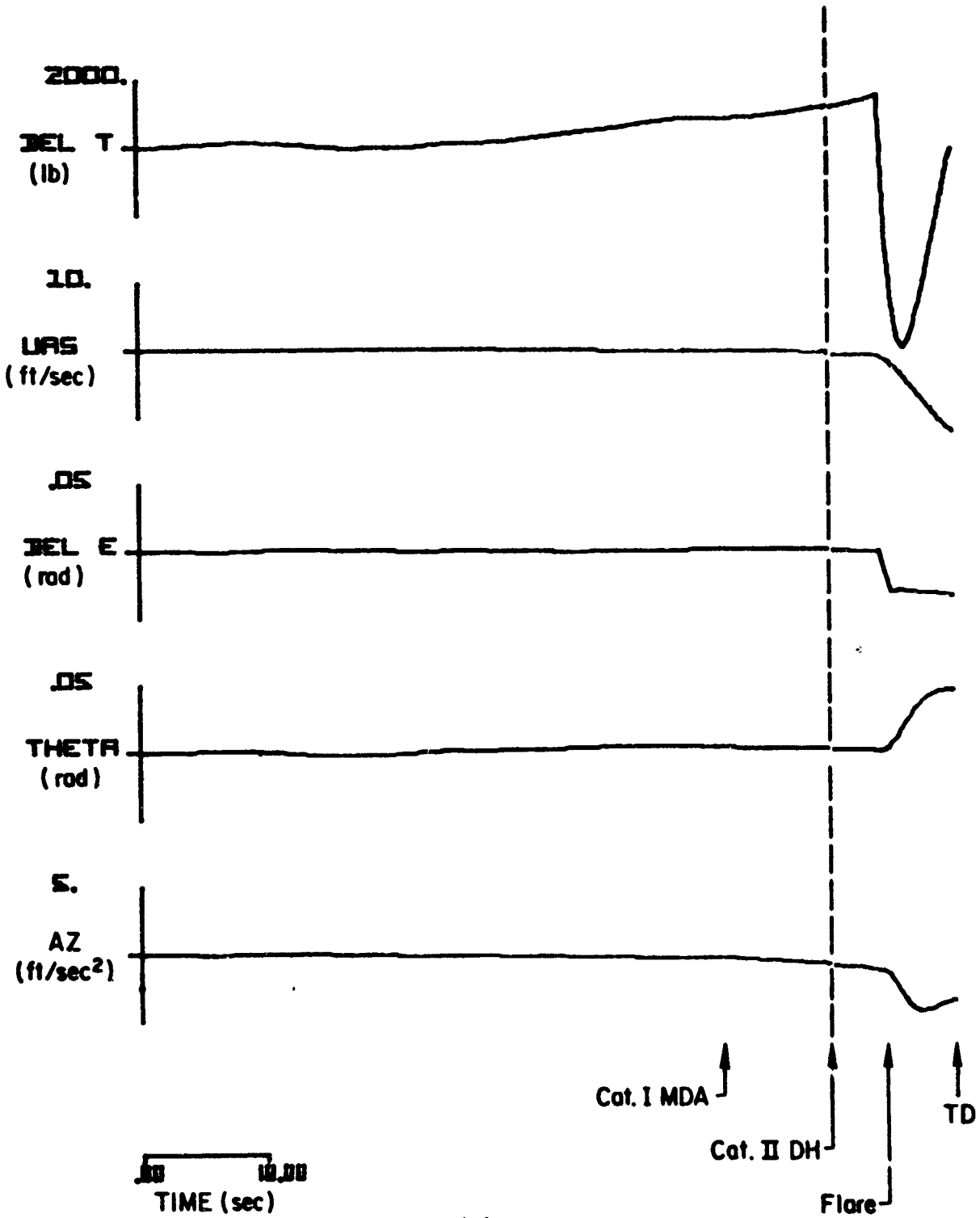

(c)

Figure B-37. (Continued)

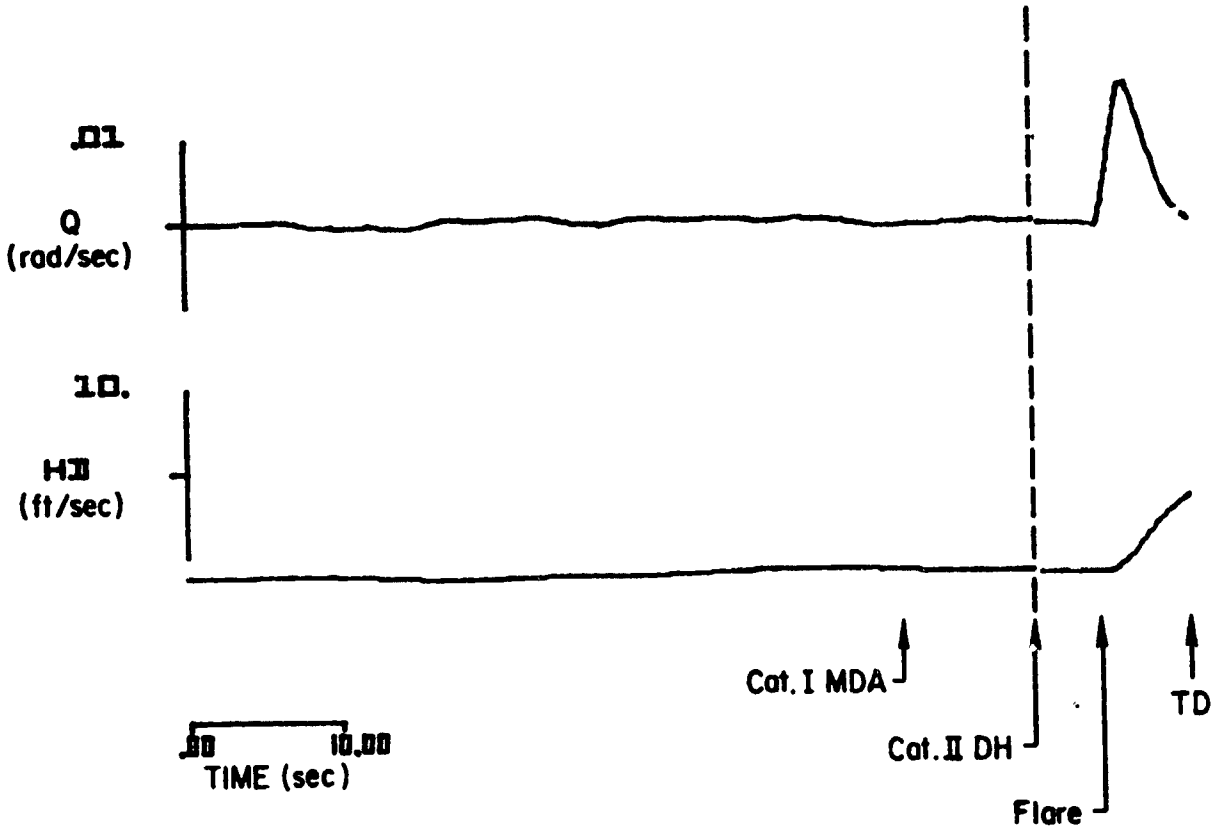

(d)

Figure B-37. (Concluded)

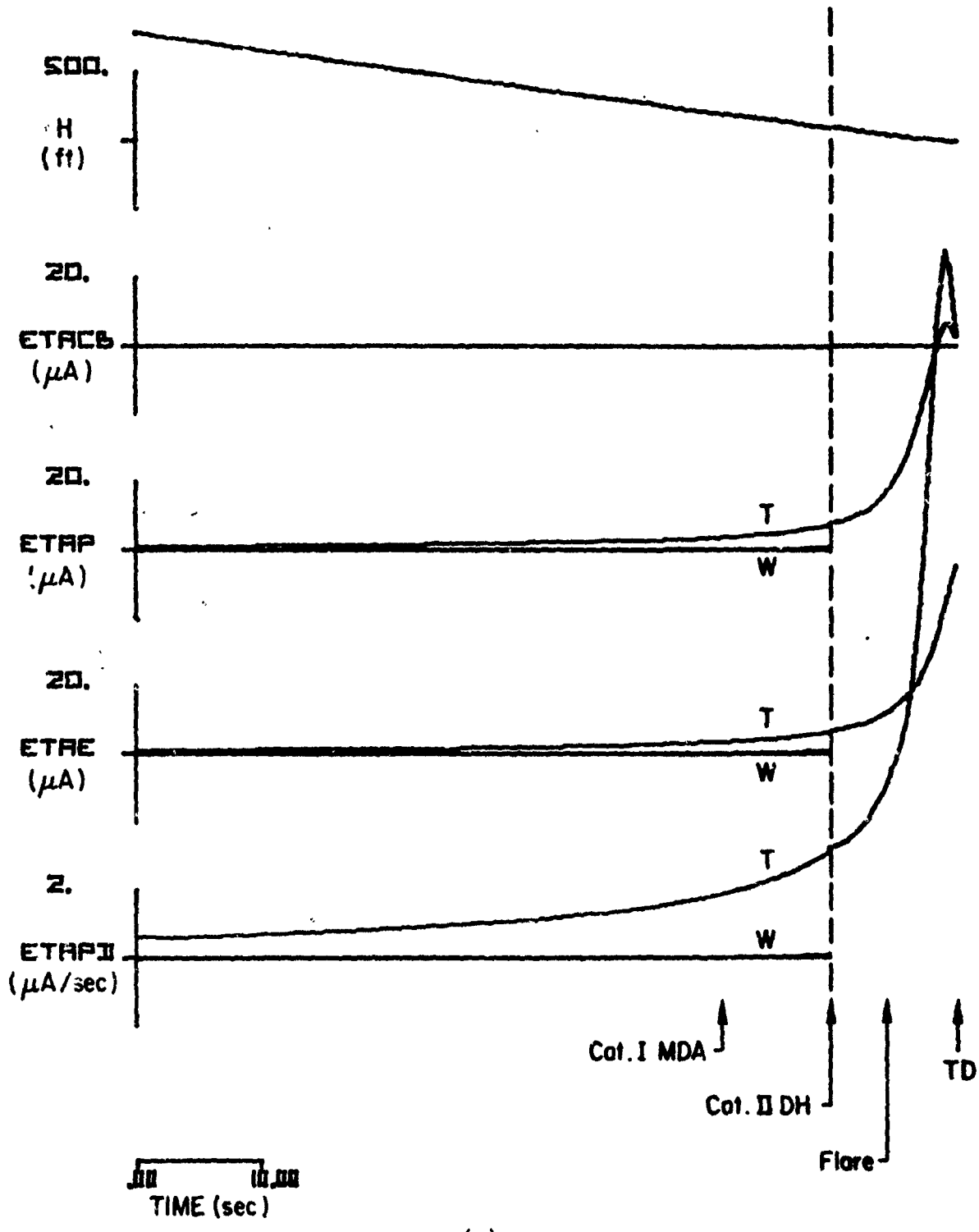

(a)

Figure B-38. Standard Deviation Responses to Wind, Wind Shear, and Turbulence for the CV-880 Aircraft with LSI Automatic Landing System and Inertially Augmented Glide Slope Coupling to Glide Slope Flight Inspection Record No. 16. Category II-III Utilization Simulated

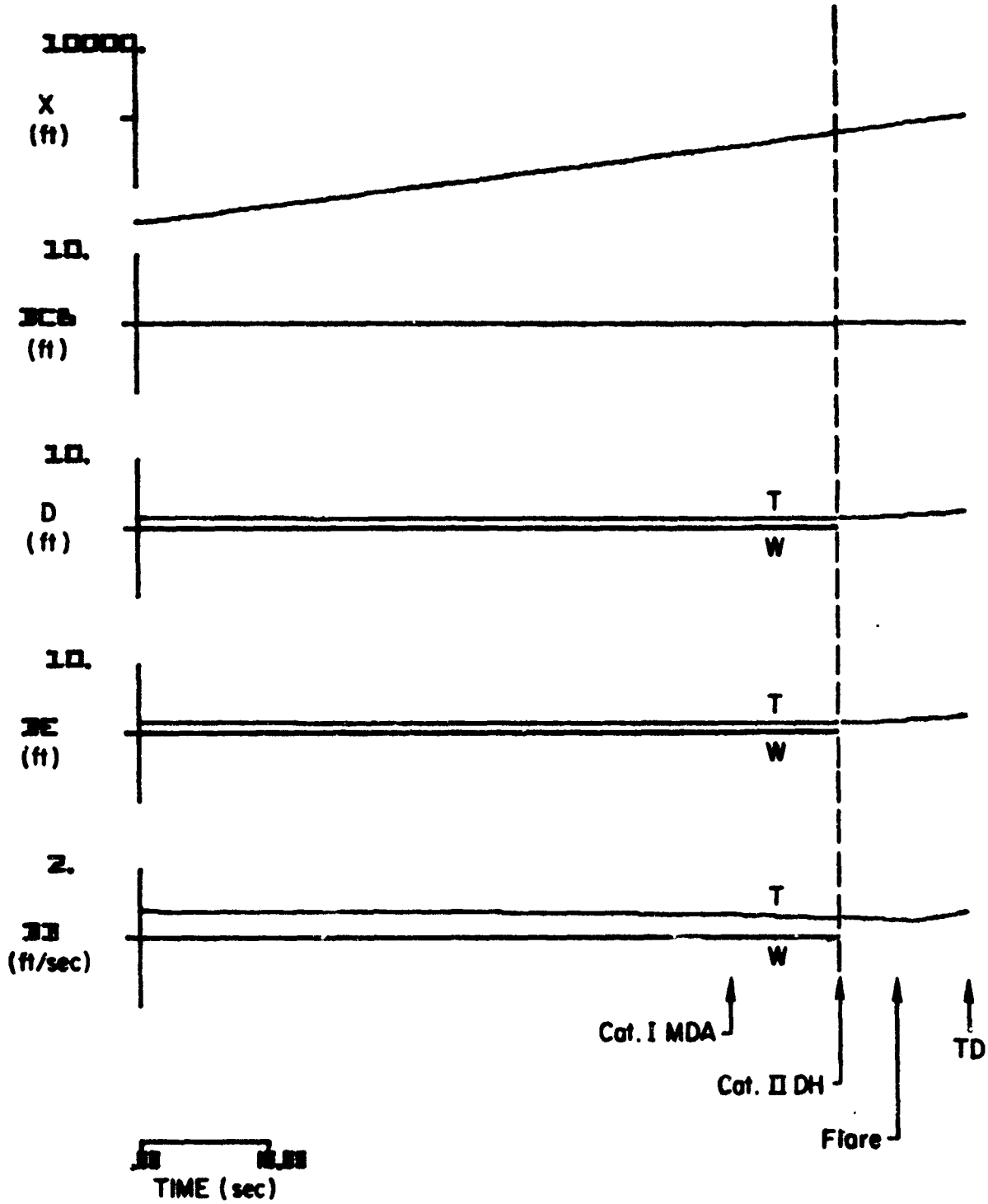

(b)

Figure B-38. (Continued)

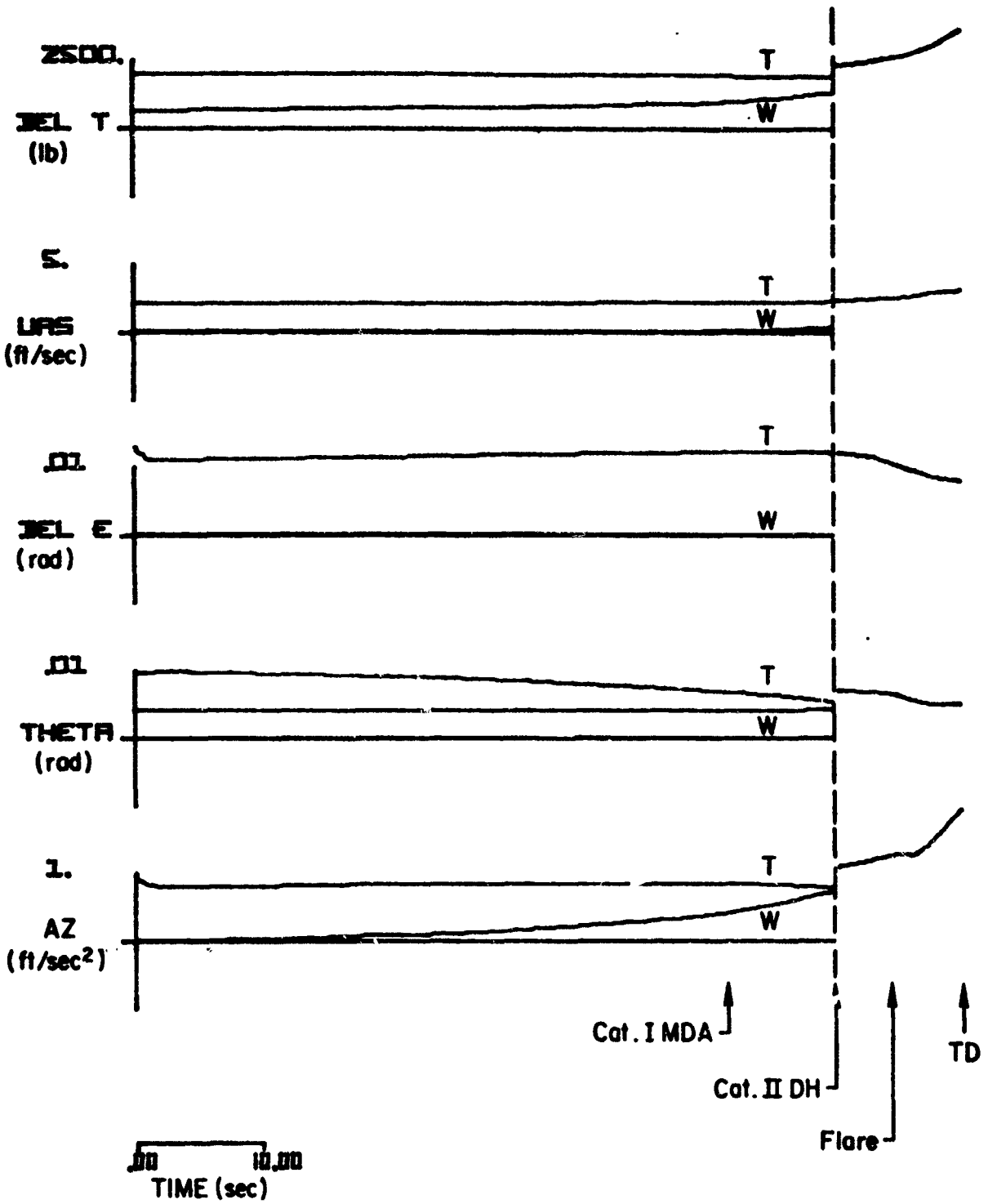

(c)

Figure B-38. (Continued)

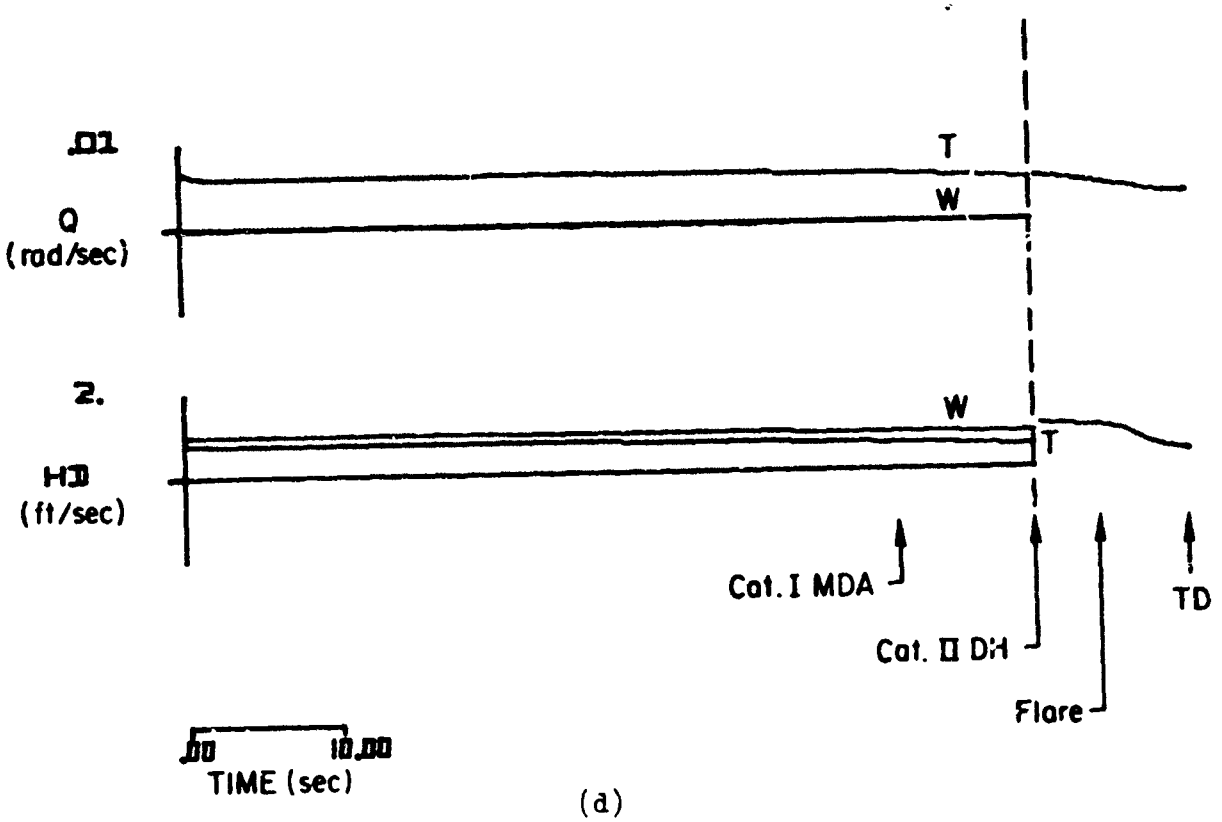

(d)

Figure B-39. (Concluded)

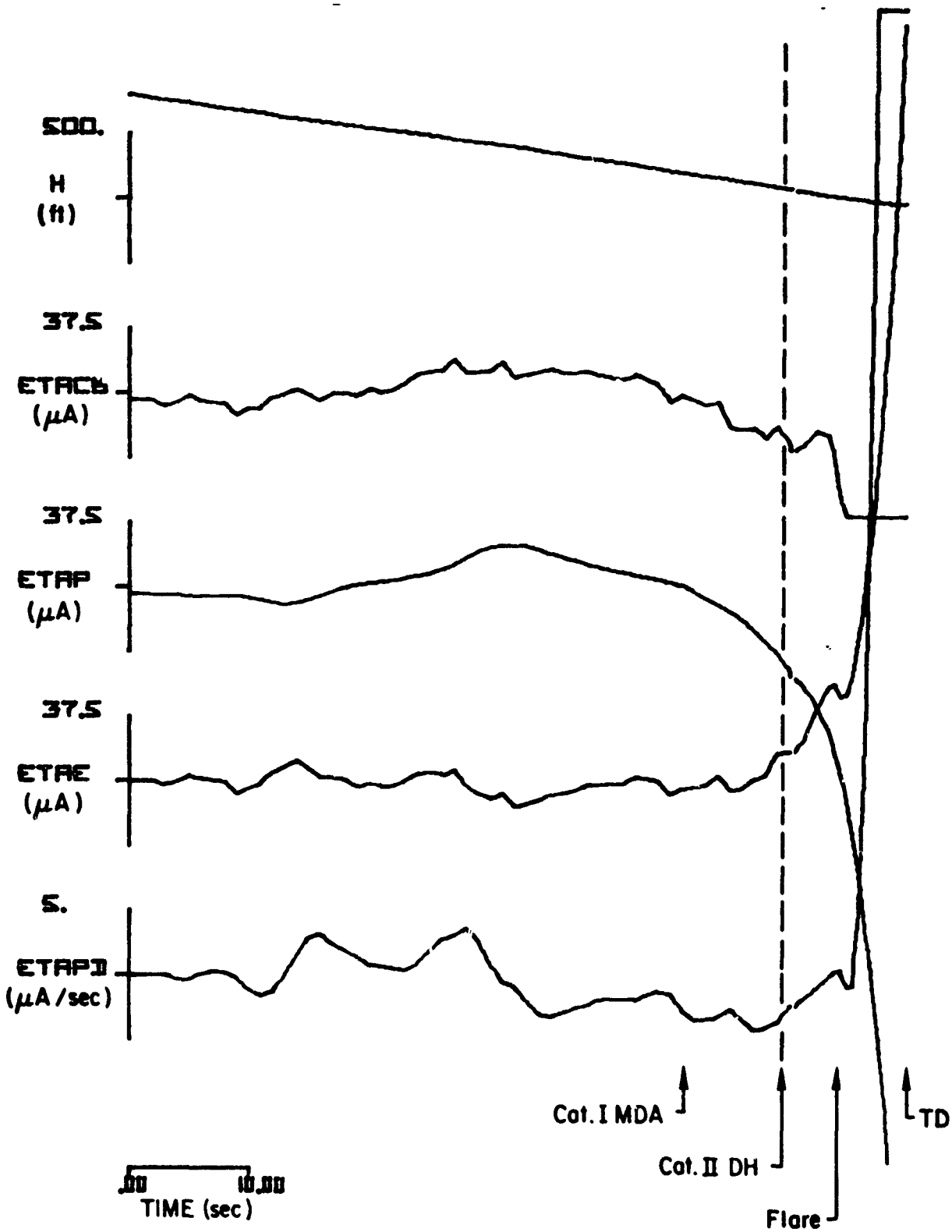

(a)

Figure B-39. Responses of the CV-880 Aircraft with LSI Automatic Landing System and Inertially Augmented Glide Slope Coupling to Glide Slope Flight Inspection Record No. 24. Category II-III Utilization Simulated

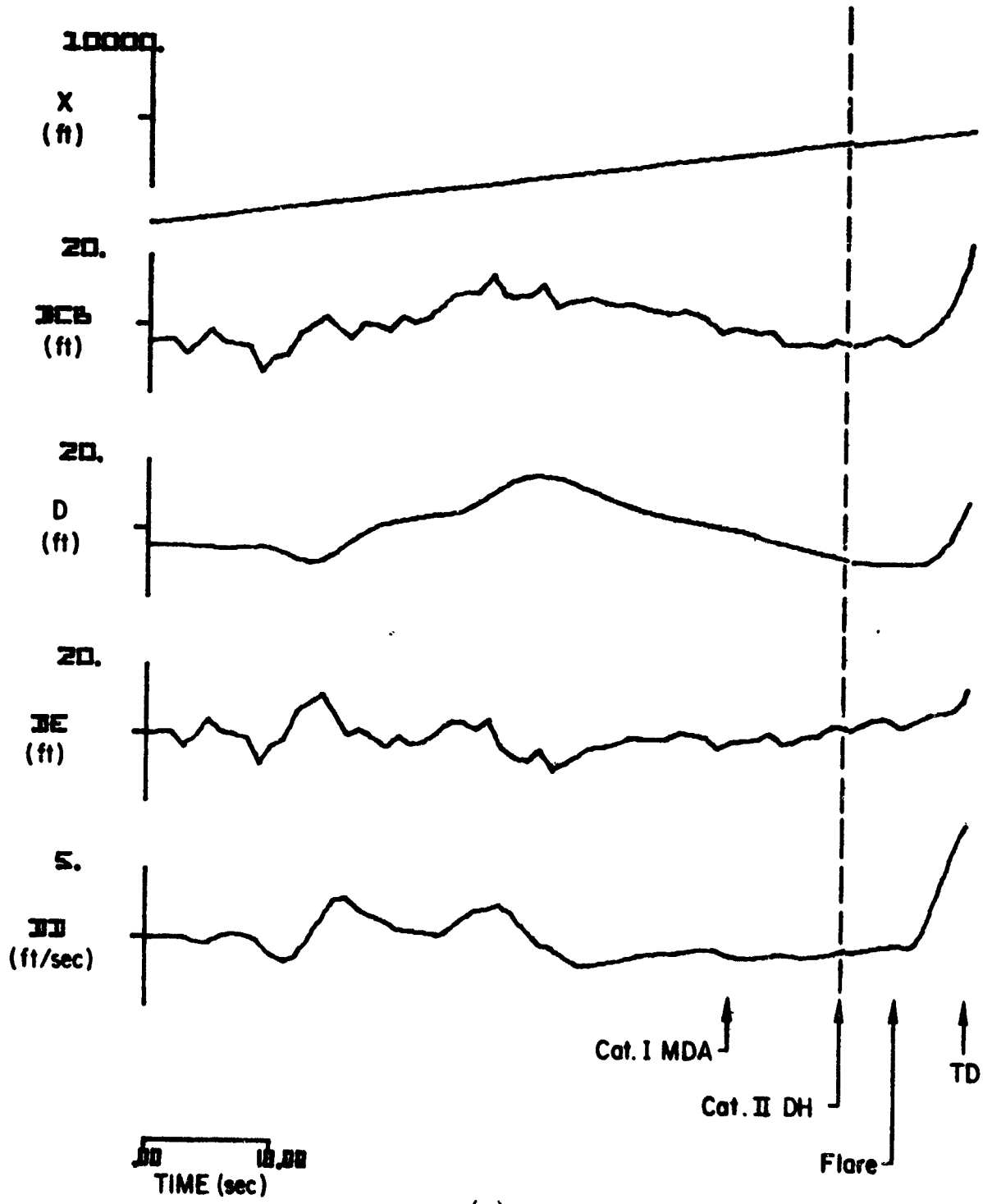

(b)

Figure B-39. (Continued)

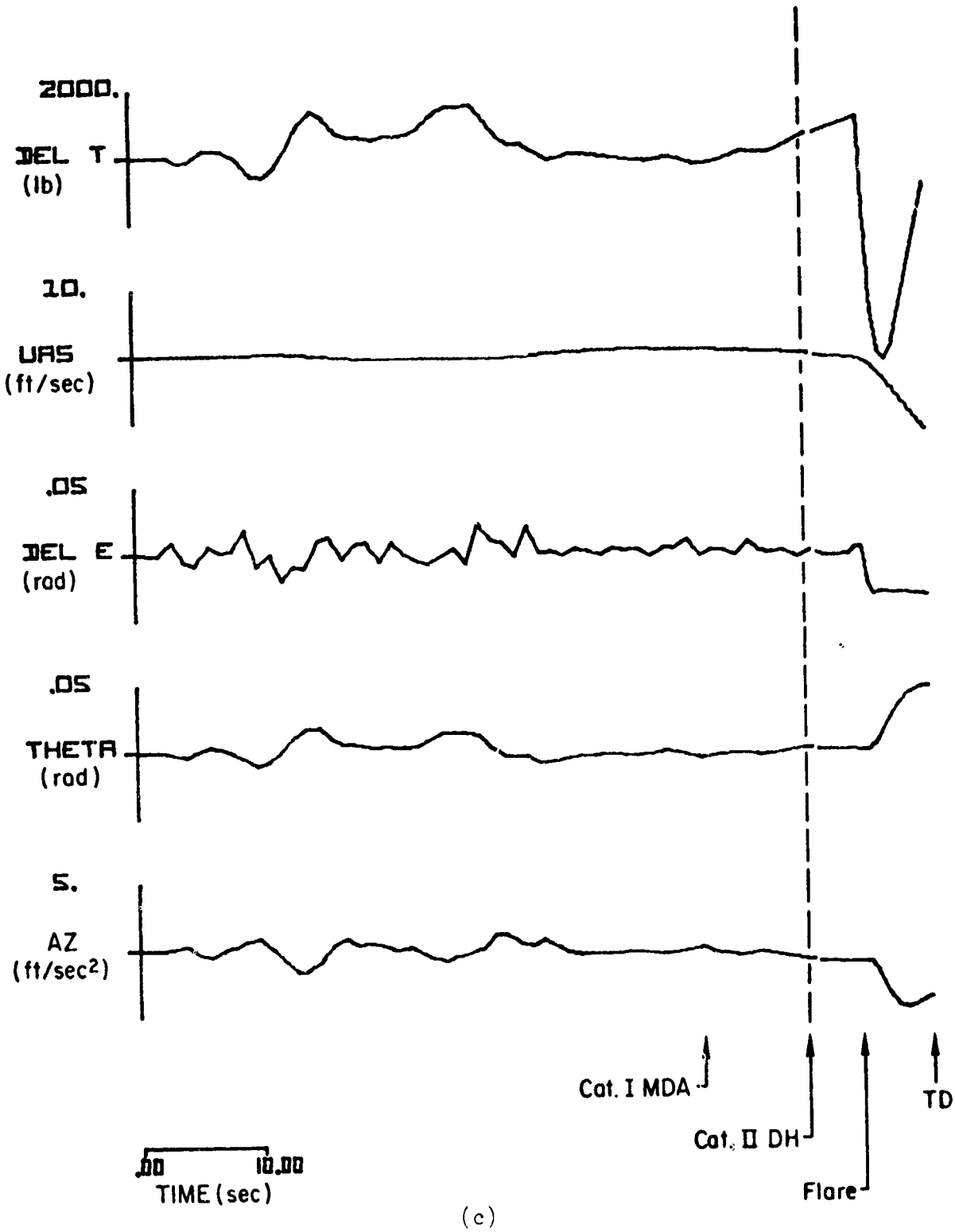

(c)

Figure B-39. (Continued)

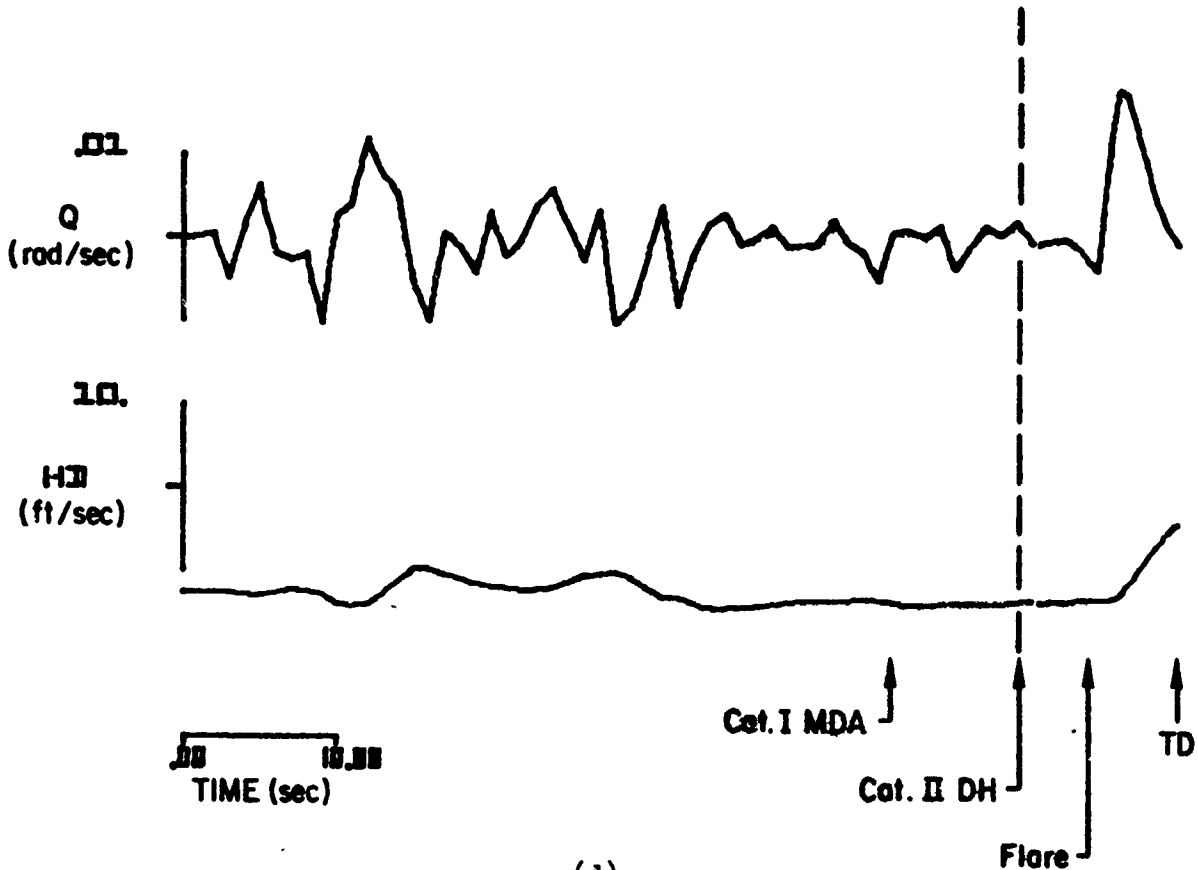

(d)

Figure B-39. (Concluded)

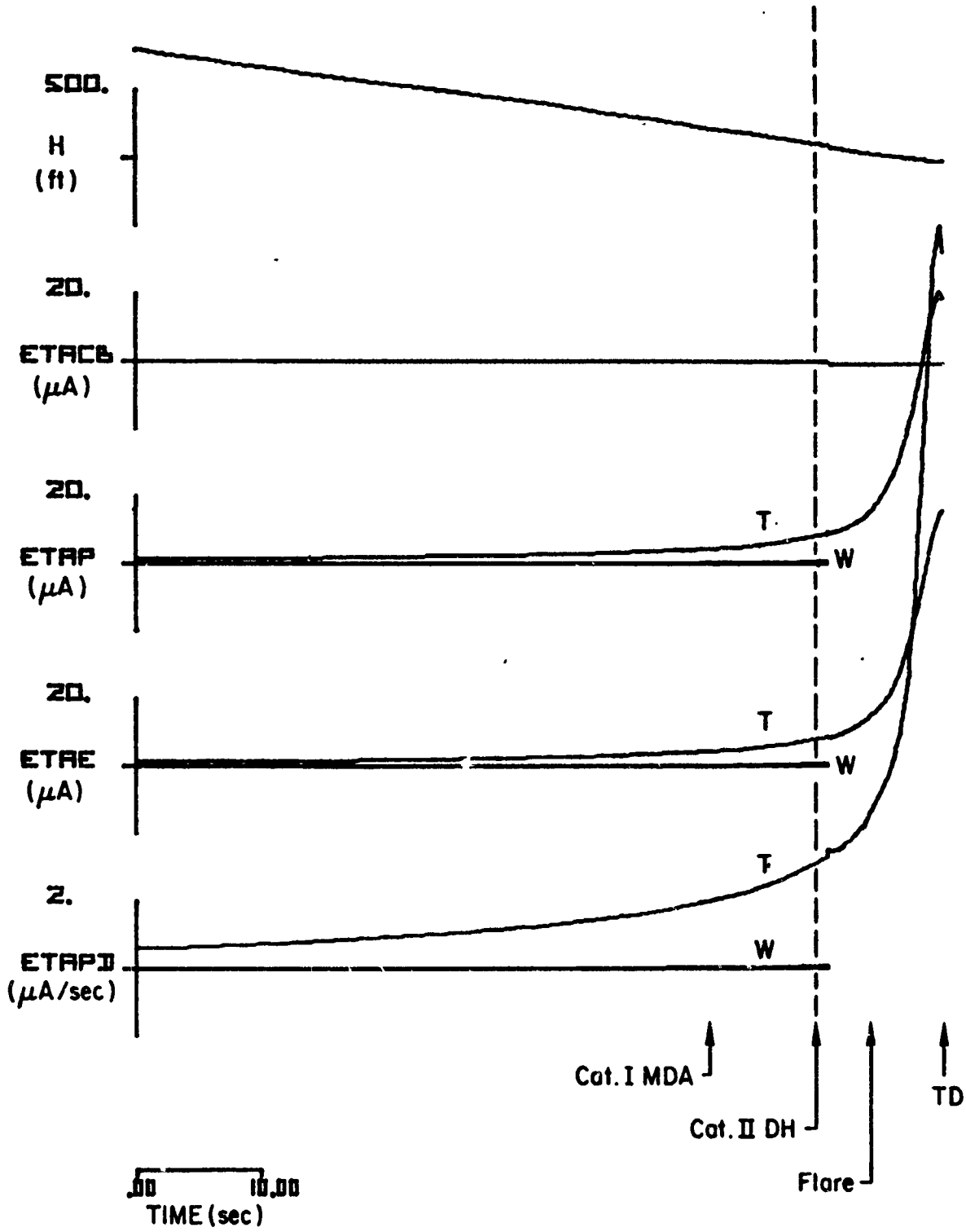

(a)

Figure B-40. Standard Deviation Responses to Wind, Wind Shear, and Turbulence for the CV-880 Aircraft with LSI Automatic Landing System and Conventional Glide Slope Coupling to Glide Slope Flight Inspection Record No. 24. Category II-III Utilization Simulated

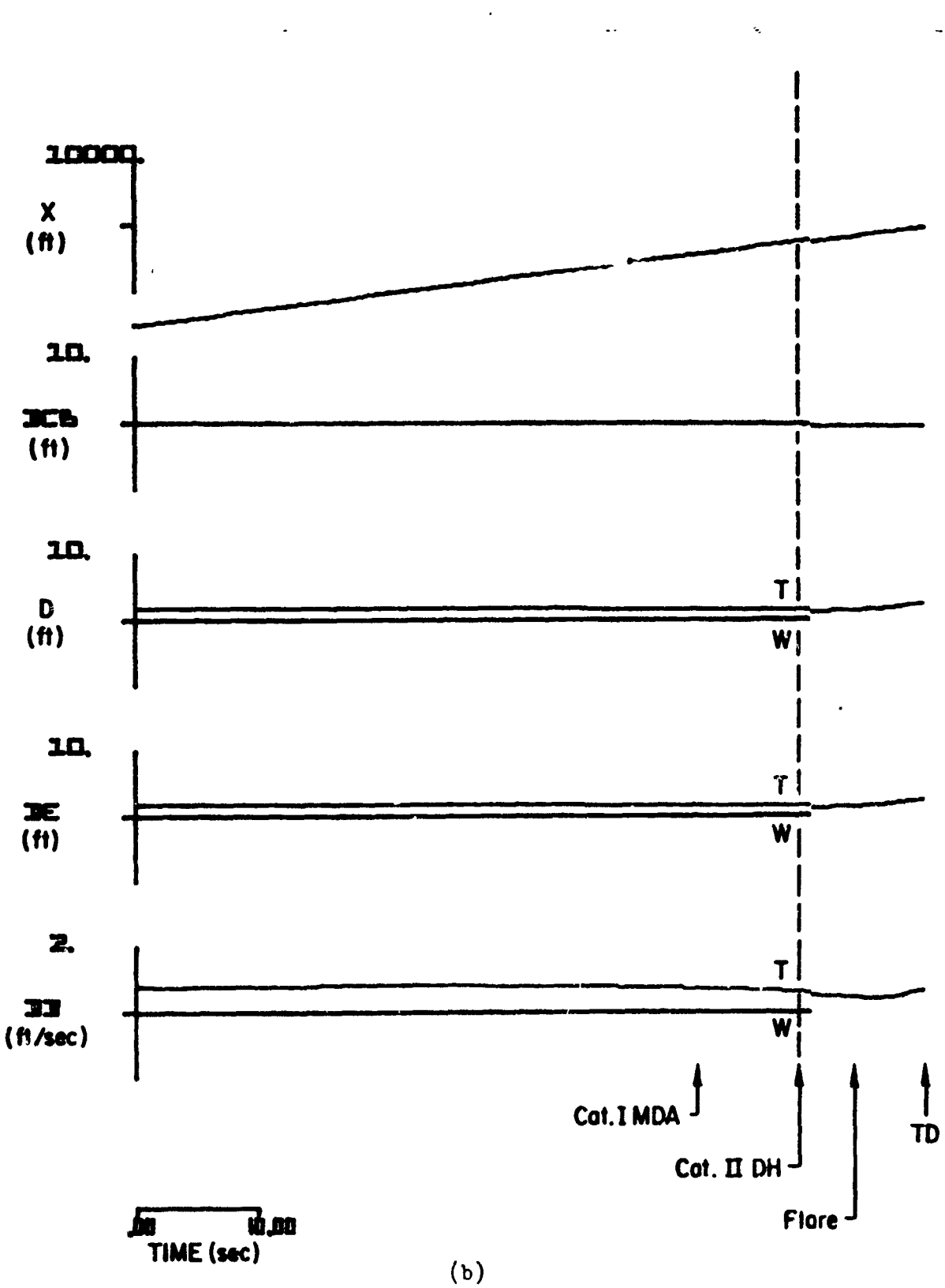

(b)

Figure B-40. (Continued)

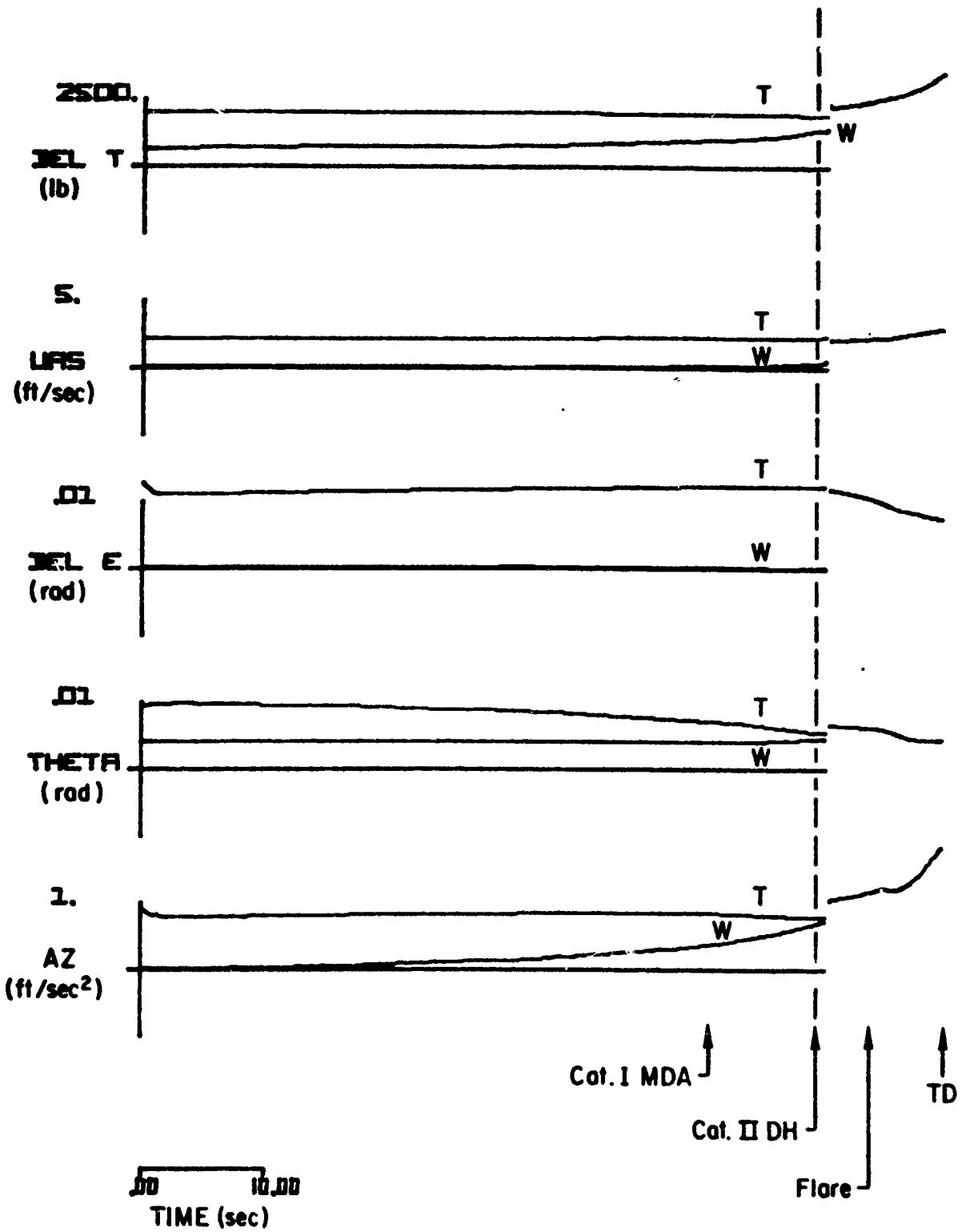

(c)

Figure B-40. (Continued)

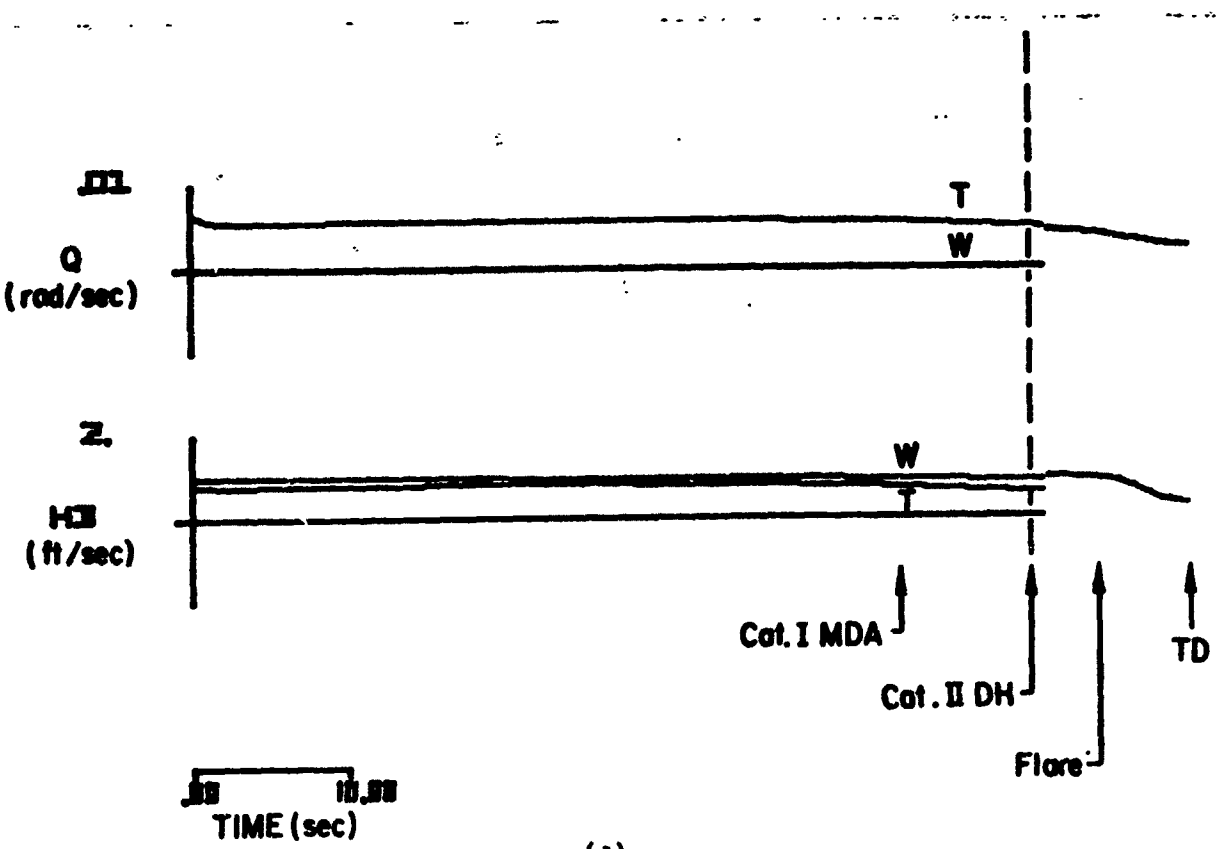

(d)

Figure B-40. (Concluded)

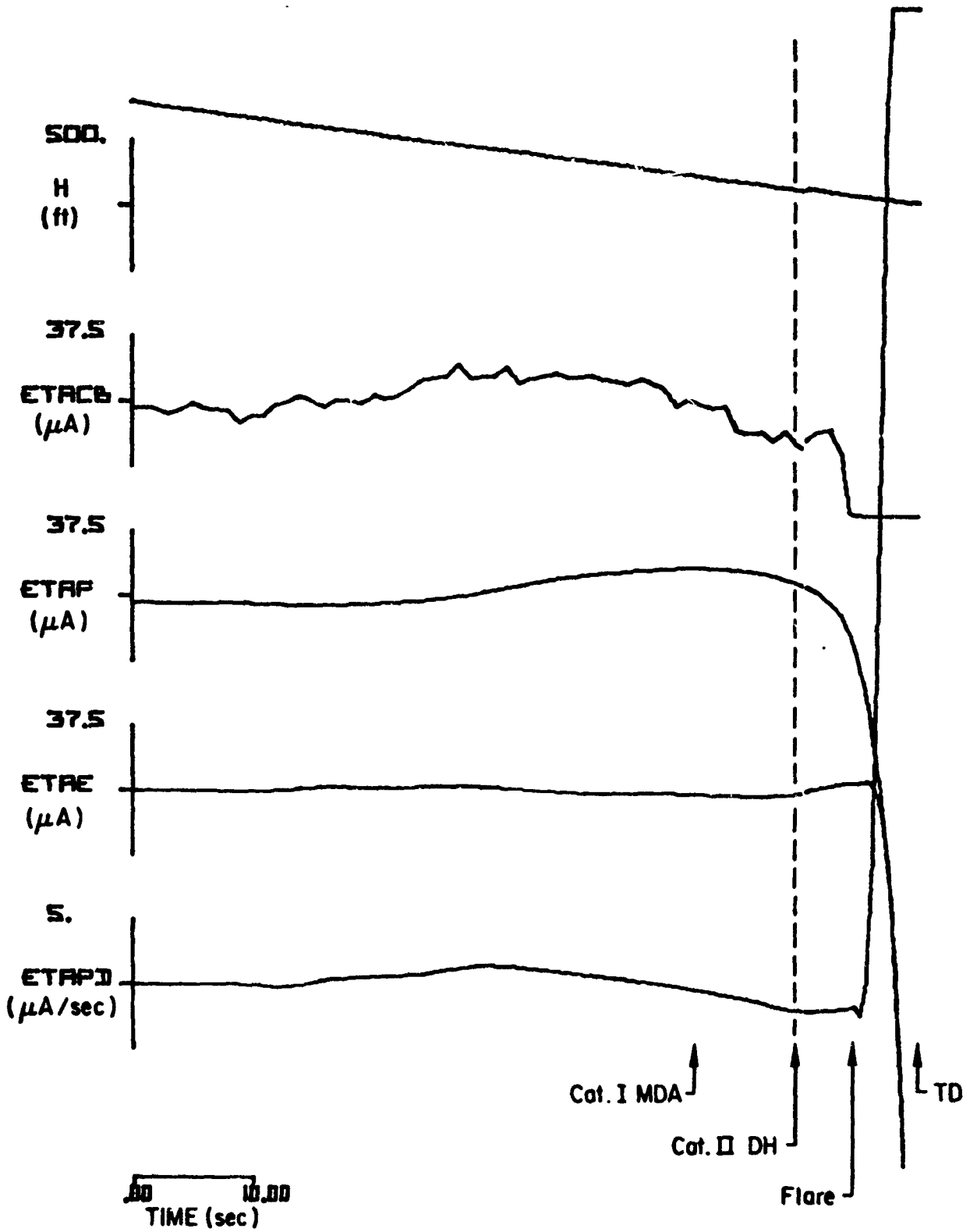

(a)

Figure B-41 Responses of the CV-880 Aircraft with LSI Automatic Landing System and Inertially Augmented Glide Slope Coupling to Glide Slope Flight Inspection Record No. 24. Category II-III Utilization Simulated

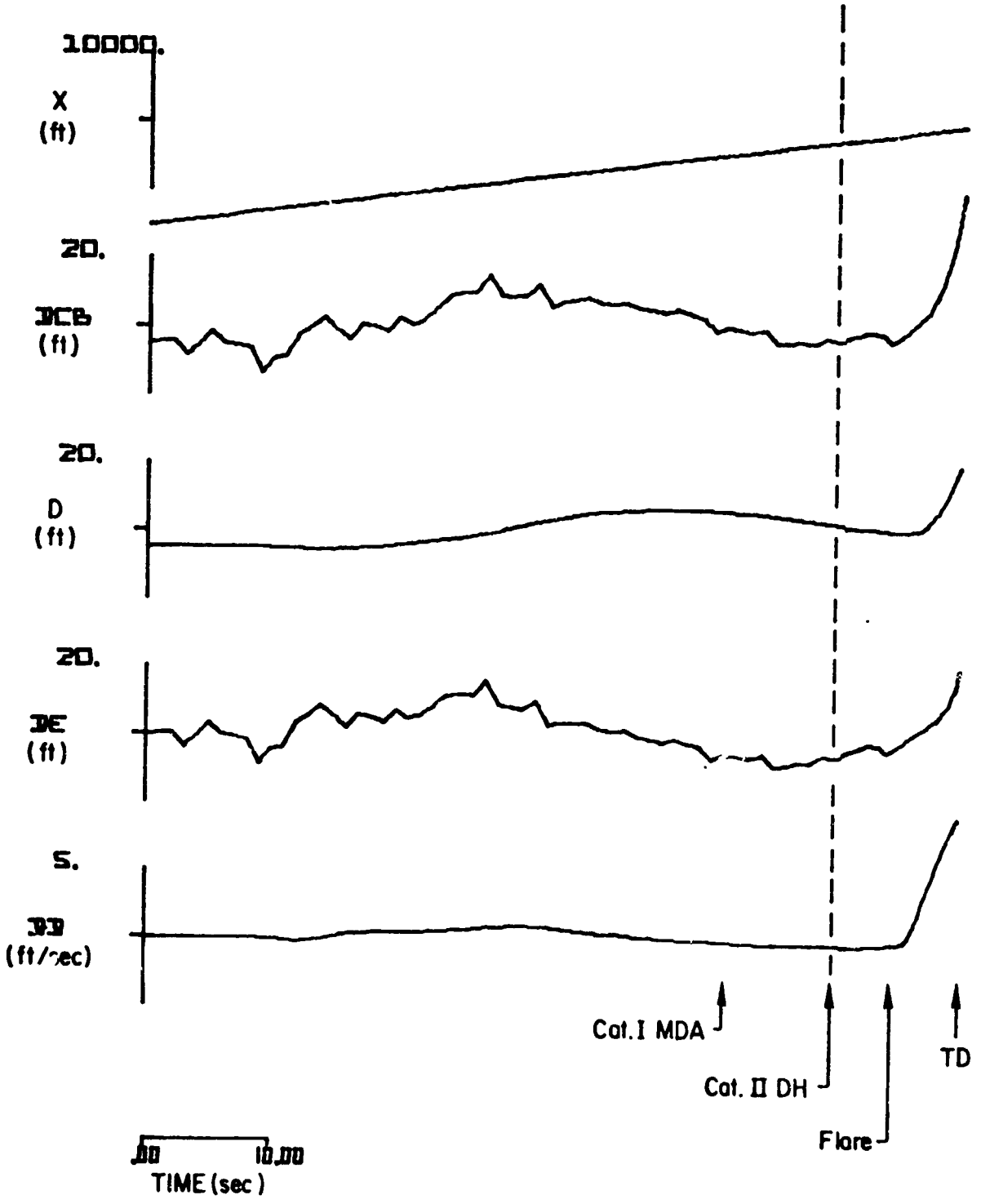

(b)

Figure B-41. (Continued)

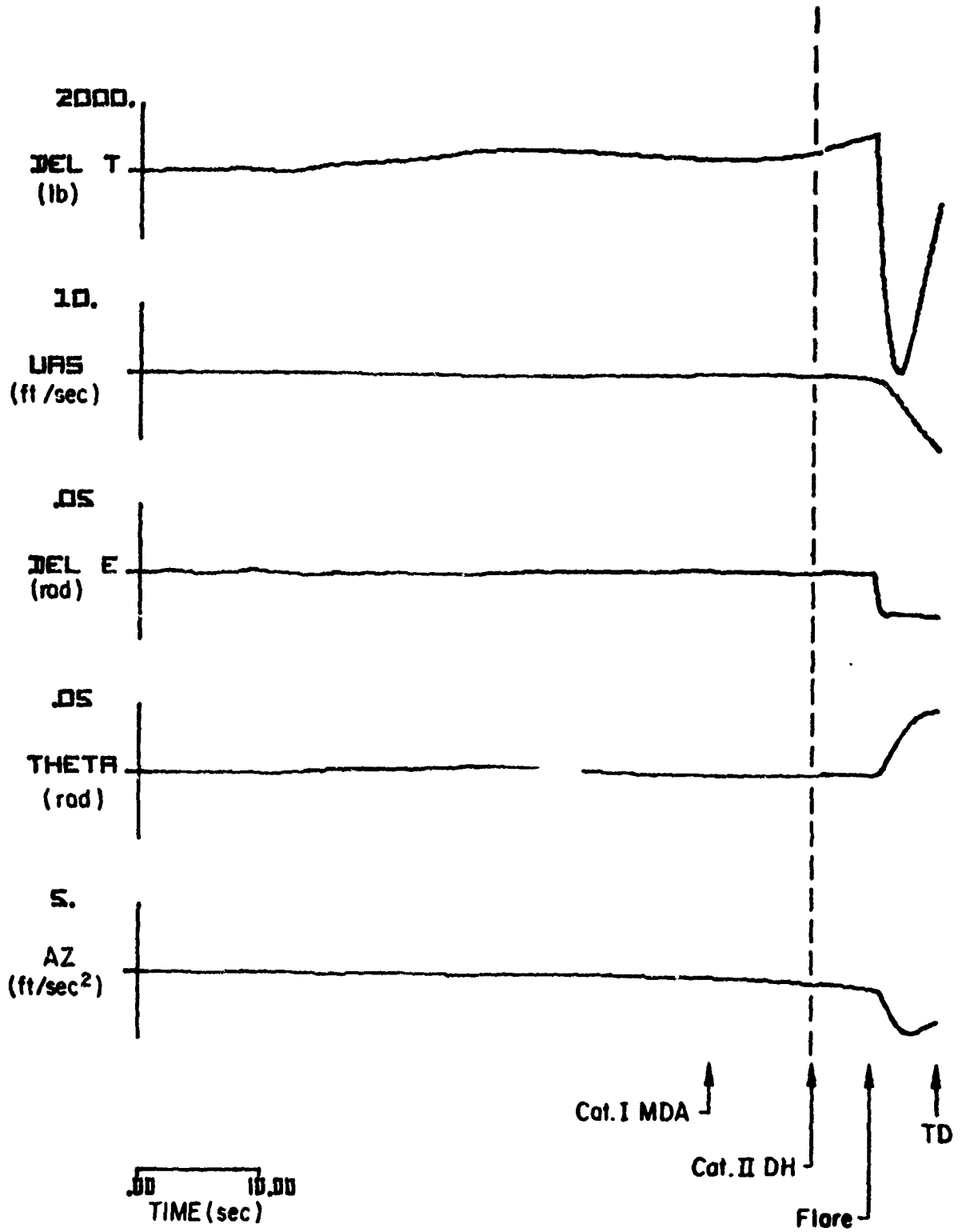

(c)

Figure B-41. (Continued)

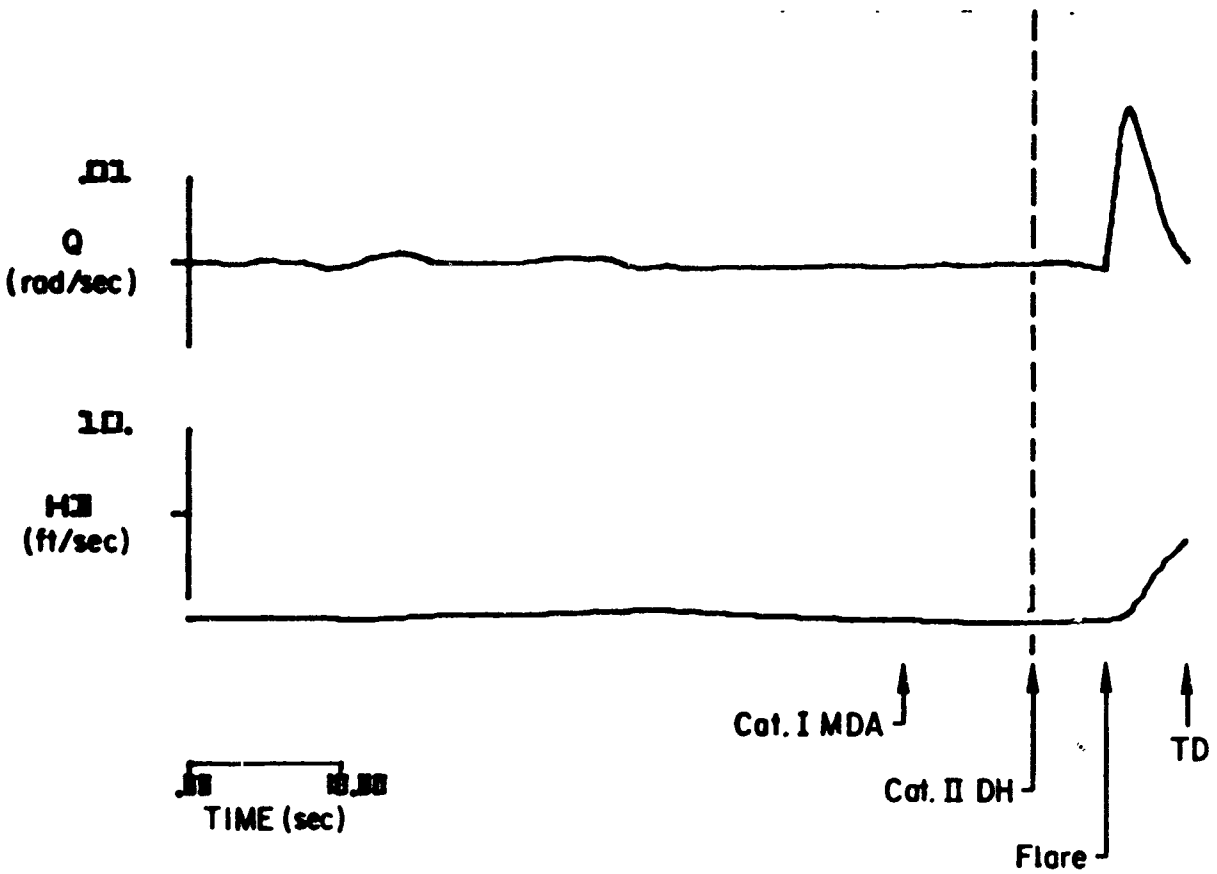

(d)

Figure B-41. (Concluded)

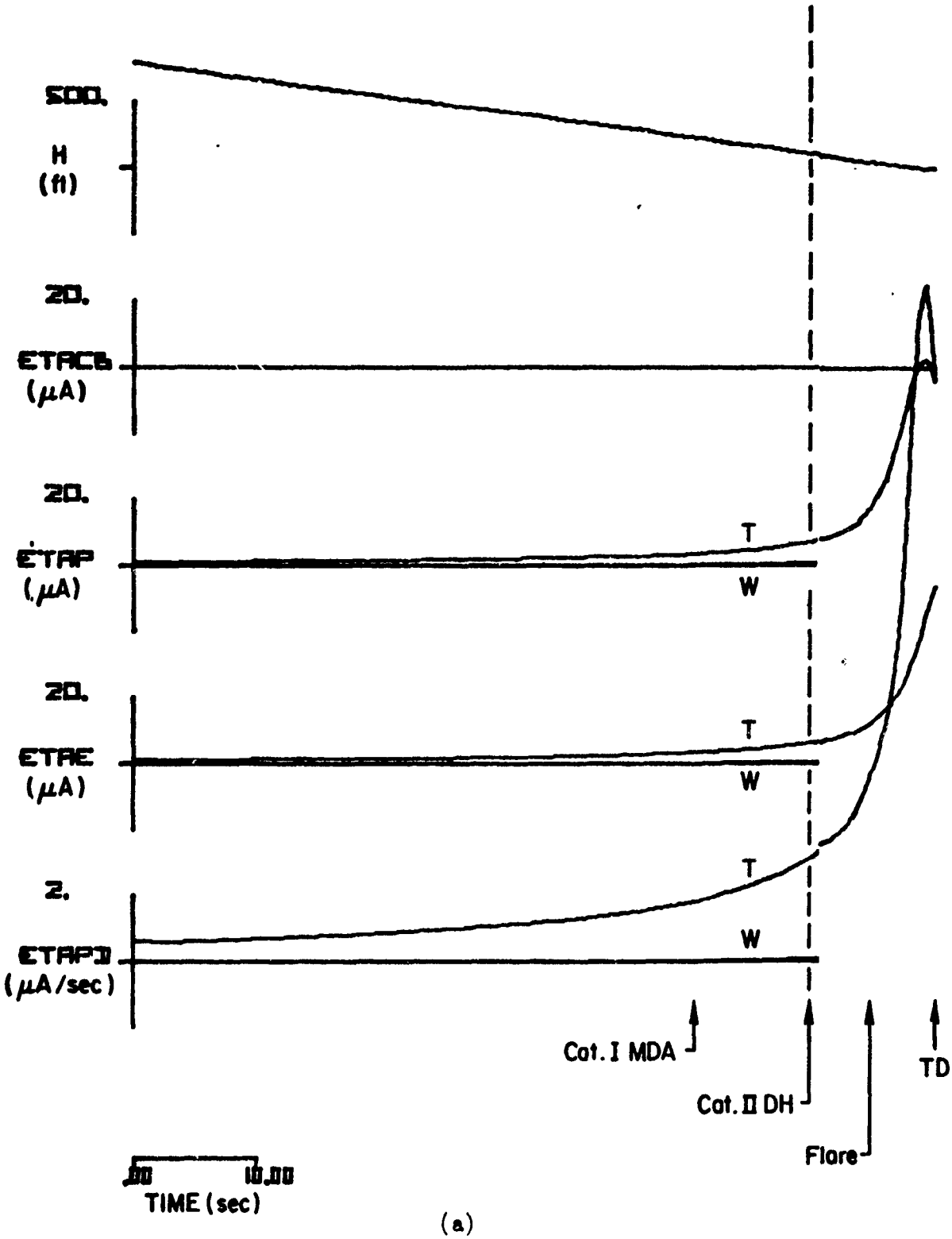

(a)

Figure B-42. Standard Deviation Responses to Wind, Wind Shear, and Turbulence for the CV-880 Aircraft with LSI Automatic Landing System and Inertially Augmented Glide Slope Coupling to Glide Slope Flight Inspection Record No. 24. Category II-III Utilization Simulated

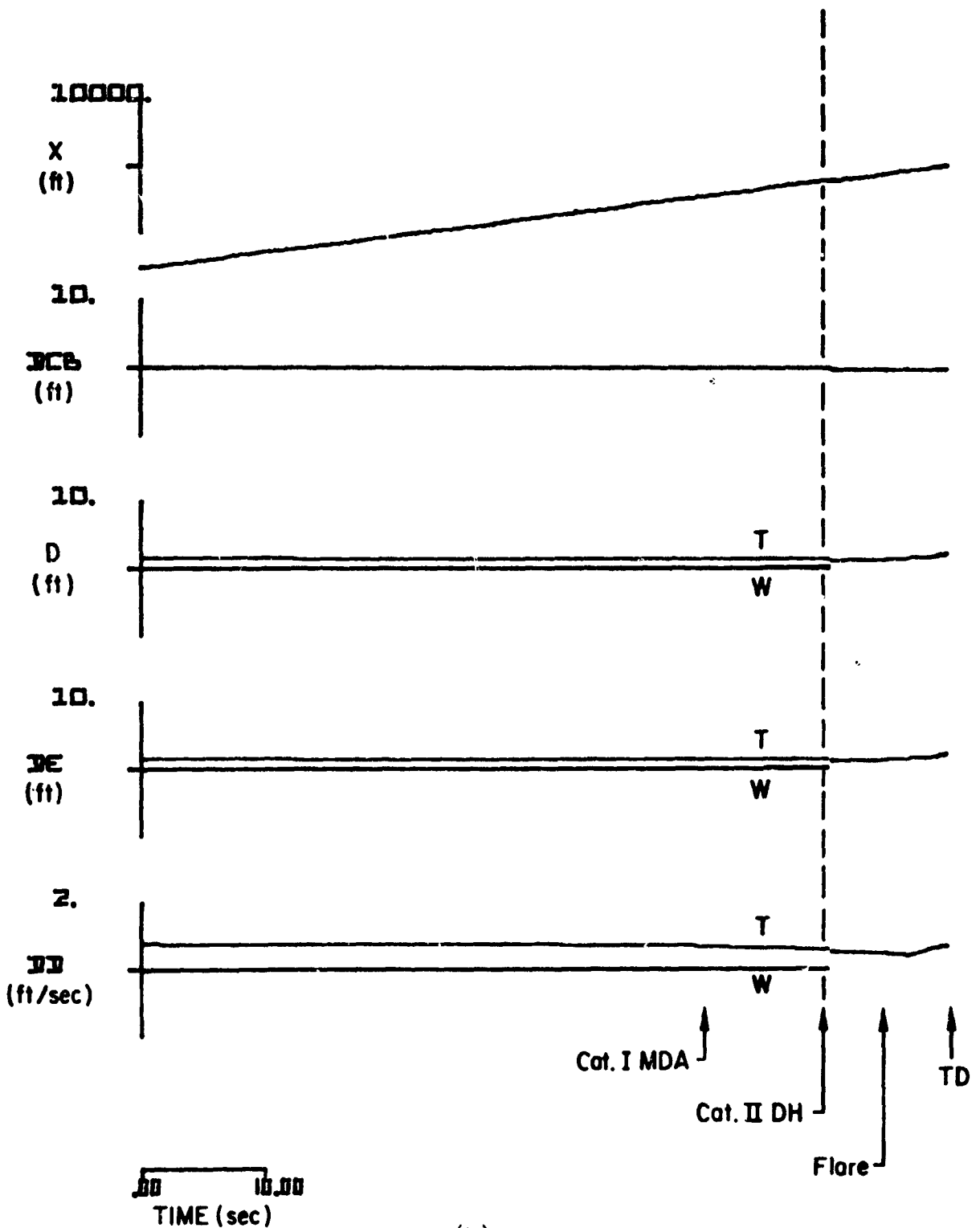

(b)

Figure B-42. (Continued)

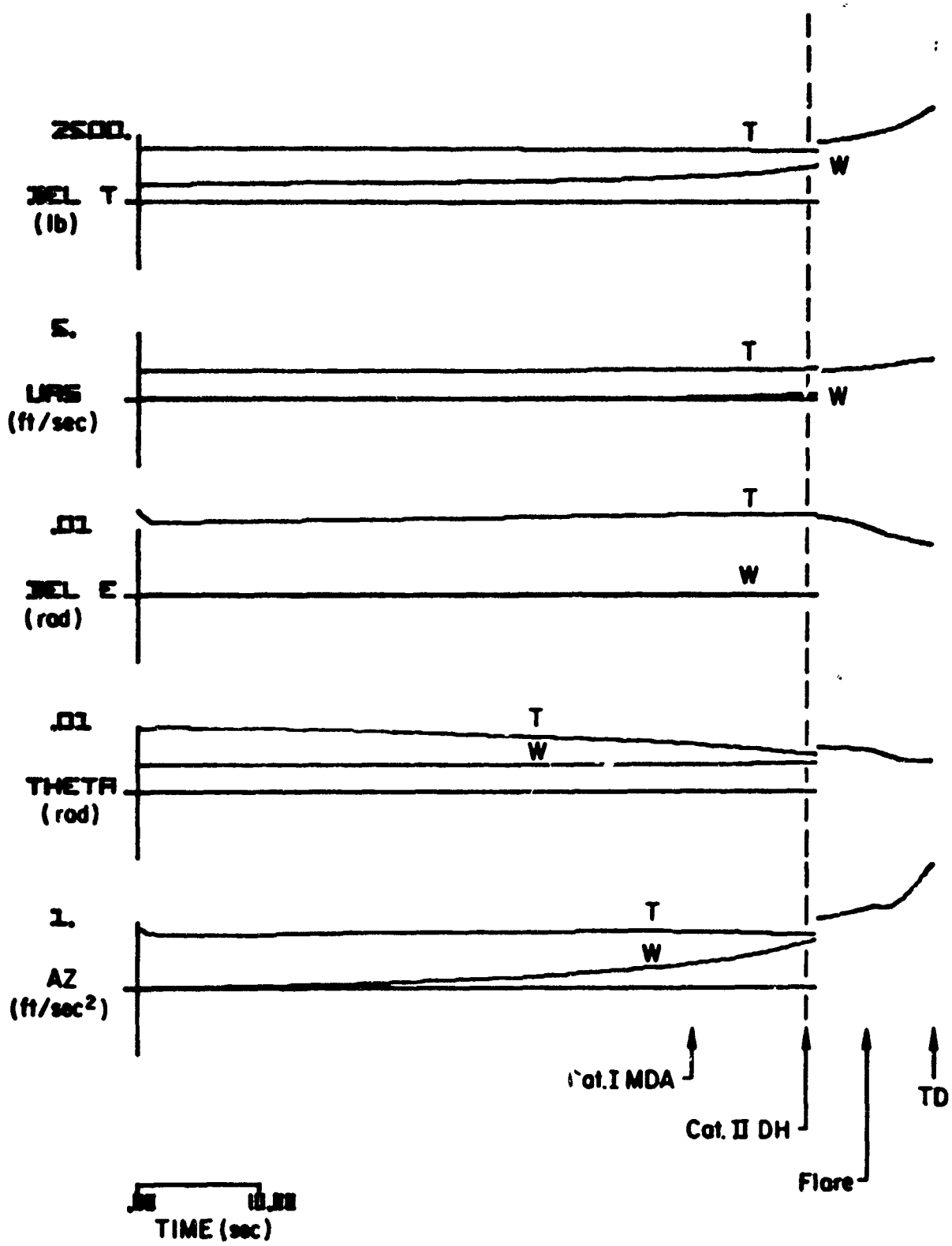

(c)

Figure B-42. (Continued)

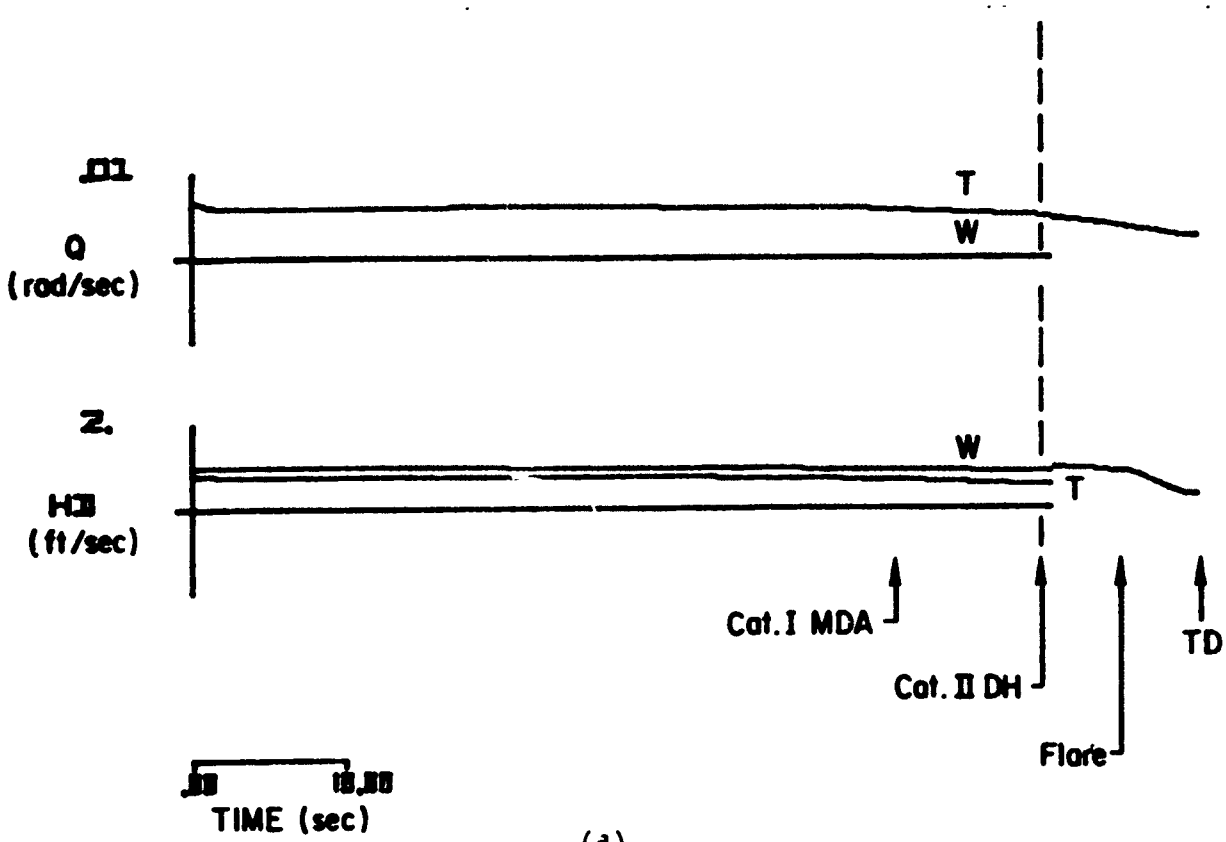

(d)

Figure B-42. (Concluded)